ABSTRACT

Title of Document:

ENGINEERING BIODEGRADABLE
VASCULAR SCAFFOLDS FOR
CONGENITAL HEART DISEASE

Anthony J Melchiorri, Doctor of
Philosophy, 2015

Directed by:

John P. Fisher, Ph.D., Fischell
Family Distinguished Professor
Fischell Department of Bioengineering

The most common birth defects worldwide are congenital heart defects. To treat these malformations in a child's cardiovascular system, synthetic grafts have been used as a primary intervention. However, current grafts suffer from deficiencies such as minimal biological compatibility, inability to grow and adapt, and high failure rates. Additionally, the grafts are not customized to the patient, which may lead to graft failure given that defects may vary significantly from patient to patient. The work presented here aims to adapt tissue engineering paradigms to develop customizable vascular grafts for congenital heart defects using to reduce the long-term risk and the number of surgeries experienced by patients.

The first component of this research focuses on solvent-cast vascular grafts. This system of fabrication was used to explore how various strategies and graft modifications affect the graft's performance *in vivo*. Grafts were fabricated with the mechanical properties necessary to withstand the stresses

of a physiological environment and support neotissue formation. To improve tissue formation, the grafts were modified with bioactive molecules to improve vascular tissue growth. In addition, the grafts were combined with a tissue perfusion bioreactor. The bioreactor applied fluid flow to support cell seeding, differentiation, and growth of endothelial progenitor cells on the grafts, demonstrating a robust strategy for tissue formation prior to implantation.

The second component of this research centers on the development of a biomaterial for 3D printing. 3D printing offers unparalleled customizability, as a graft can be designed based on medical images of a patient, tested via computer modeling, and then printed for implantation. A resin was developed consisting to produce grafts that were mechanically compatible with native blood vessels and maintained patency and tissue formation six months after implantation. The library of 3D printed vascular graft materials was also expanded by creating a novel copolymer resins, which varied in mechanical properties and degradation profiles. In addition, the concepts and strategies of biofunctionalization developed in the solvent-cast vascular grafts can be combined with the 3D printed graft strategies. Grafts designed, printed, and modified using these combinatorial approaches can greatly improve the long-term outcomes of treating congenital heart disease.

ENGINEERING BIODEGRADABLE VASCULAR SCAFFOLDS FOR CONGENITAL
HEART DISEASE

By

Anthony John Melchiorri

Dissertation submitted to the Faculty of the Graduate School of the
University of Maryland, College Park, in partial fulfillment
of the requirements for the degree of
Doctor of Philosophy
2015

Advisory Committee:
Professor John Fisher, Chair
Professor David Mosser
Professor Steven Jay
Professor Adam Hsieh
Professor Axel Krieger

Acknowledgements

I would like to thank Dr. John Fisher for his support, advice, and encouragement in this project. I'm especially grateful for the opportunity to pursue this particular avenue of research in the Tissue Engineering & Biomaterials lab. I would also like to extend my appreciation to all the other lab members, past and present, who have shared many science and non-science conversations, helpful feedback and advice, and friendship. Thank you to Chelsea Kraynak, Lucas Kimerer, and Zachary Brandes for all their hard work and contributions within the various facets of the vascular graft project. Thanks to Katarina for her unwavering love and support. A huge thank you to my parents, brother, and sister for their love and encouragement.

Table of Contents

Contents

List of Tables

List of Figures

Chapter 1: Introduction

Congenital heart disease (CHD) is the most common birth defect, affecting nearly 1% of all live births.[1] CHD remains the leading cause of death due to congenital anomalies in the newborn period, despite advances in surgical procedures and treatments.[2] These challenges are a result of several factors affecting patients with CHD.

For example, CHD presents over a wide range of structural malformations. Two patients may present a condition with the same name, but possess striking differences. One such disease set is single ventricle anomalies (SVA). SVAs are one of the largest groups of cardiac anomalies and result in debilitating, life-threatening conditions. SVAs share a common feature in that only one of two ventricles is of an adequate size to function, but each cardiac structure may still be vastly different in size and geometry. Regardless of these factors, SVAs introduce the mixing of deoxygenated and oxygenated blood, leading to chronic hypoxia and volume overload to the ventricle. If neglected, SVAs can lead to total heart failure. Untreated SVAs are associated with a 70% mortality rate in the first year of life.[3]

Treatment of conditions such as SVAs often requires surgical reconstruction with artificial or biological grafts. In SVAs, such a graft would be utilized as an extracardiac conduit to enable blood flow from the inferior vena cava (IVC) to the pulmonary artery. However, artificial grafts introduce a host of problems including lack of growth potential, increased susceptibility to

infection, degeneration due to progressive obstruction, and thromboembolitic complications.[4,5] Biological grafts, such as homografts or heterografts, may lead to significantly lower thromboembolotic complications compared to artificial grafts, but they also are associated with a lack of growth potential and poor durability due to accelerated calcification and secondary graft failure.[6–8] Thus, overall graft failure rates range between 70-100% within 10-15 years.[6,8,9] The risk of failure is also increased in grafts with small diameters (<6 mm). As such, it is assumed that all grafts will eventually need to be replaced, especially in growing patients.[10]

To reduce these complications associated with current clinically used grafts, tissue engineering offers a promising alternative. A tissue engineered vascular graft (TEVG) would provide a biodegradable scaffold that supports the growth of the patient's own tissue. As the patient's tissue grows into and over the scaffold, the scaffold degrades and is replaced by the patient's healthy tissue. This could significantly reduce the multiple surgeries needed throughout a patient's life necessary to replace and remove permanent grafts. In addition, thromboembolitic and calcification risks would be greatly reduced due to the growth and natural regulation provided by healthy tissues.

As mentioned previously, the prevalent issue of diverse CHD malformations necessitates that grafts must be shaped specifically for each patient. Currently, this requires that surgeons construct these complex structures with a limited choice of available grafts on the market under demanding time constraints during an operation. Achieving proper graft

orientation and shape is critical to the long term success of these surgeries.[11,12]

Fortunately, recent advances in medical imaging approaches have enabled high-quality, detailed computer reconstructions of complex cardiovascular anatomies.[13,14] These 3D models offer tremendous opportunity for surgical pre-planning, which is greatly augmented by the advent of 3D printing.[15–17] 3D printing not only allows surgeons to gain a first-hand perspective of the patient's anatomy, but it also introduces the possibility of fabricating patient-specific cardiovascular devices.

An ideal solution to the challenges presented by CHD would consist of a patient-specific TEVG. However, in order to utilize a 3D printed TEVG, several challenges remain. One of the most crucial elements of a successful, patient-specific TEVG is also a critical problem in adult vascular grafts: endothelialization of implanted materials. In addition, a 3D printed material must encompass mechanical compatibility, biocompatibility, and biodegradation properties. The research presented here aims to achieve these goals. In order to accomplish this, the objectives of the research are divided into two overall categories:

1. Development and use of established vascular graft fabrication method to study endothelialization phenomena
    a. Characterize the mechanical properties of solvent-cast grafts and assess their implantability *in vivo*

b. Develop a biofuncationalization strategy that supports endothelial cell and endothelial progenitor cell attachment, proliferation, and differentiation

c. Utilize a bioreactor system to examine the neotissue formation of EPCs on solvent-cast grafts in venous flow conditions

2. Development and assessment of novel 3D printing method for vascular graft fabrication

a. Establish and assess a polymeric resin and 3D printing platform for the fabrication of vascular graft-suitable materials

b. Examine the feasibility and surface characteristics of 3D-printed grafts modified with biofunctional molecules

c. Expand the 3D printing platform via the use of copolymers and characterize these novel printing resins to elucidate their effects on 3D printed scaffolds

The presented objectives will advance the understanding of endothelialization on biodegradable vascular grafts, while providing a novel platform to fabricate patient-specific prosthetics. Achieving these goals may offer a new paradigm for the fabrication of vascular grafts and offer the improved long-term benefits of custom-designed TEVGs for patients.

Chapter 2: *In Situ* Endothelialization of Tissue-Engineered Vascular Grafts[1]

Coronary artery disease is a leading cause of mortality and morbidity worldwide.[1] In cases where the vessel is occlusion is limited, angioplasty and stenting procedures are used. More occluded vessels require bypass surgery, occurring in approximately 250,000 patients per year.[1] Autologous transplantation of conduits such as saphenous veins and mammary arteries are often used in cases necessitating arterial bypass. Patients requiring bypass surgery, however, may not have vessels available due to disease or previous surgery. Synthetic, non-degradable vessels have been used in such cases. Success rates in large diameter grafts (> 6 mm) have been satisfactory with patency rates of 95% after five years.[19] Conversely, the patency rate of small-diameter grafts (<6mm) was reported to be only 30% in the same study.[19] Other studies demonstrated patency rates such as 0% to 25 % after only weeks or months of implantation in various animal models.[20–22] Complications resulting from noncompliance, thrombogenicity, intimal hyperplasia, aneurysms, and calcium deposition contribute to these low patency rates.[23–25] While much graft research has focused on coronary artery bypass procedures, the need for small-diameter vascular grafts extends far beyond coronary artery disease. Each year, over 500,000 patients are

---

diagnosed with end-stage renal disease and 8 million with peripheral artery disease,[1] prompting research into small-diameter grafts for hemodialysis access and peripheral artery bypass.[26,27]

To improve the long-term patency and functionality of vascular grafts, biodegradable grafts have emerged over the years as a chief solution to the complications associated with commonly-used biologically stable materials such as polytetrafluoroethylene (PTFE) or Dacron. The focus of biodegradable grafts is to promote native tissue ingrowth and replacement of the graft while the scaffold material degrades over a sustained period of time necessary for adequate vessel repair and growth. Tissue engineering approaches to the problem of developing small-diameter, biodegradable vascular grafts have been numerous. Approaches aim to achieve acceptable patency rates through the development of grafts that best mimic or promote the extra-cellular environment and mechanical properties of native blood vessels. A tissue engineered, small-diameter vascular graft is based on three basic principles:

1.) Base scaffold matrix;

2.) Biofunctional molecules;

3.) Cells (seeded or recruited *in vivo*).

In order to promote fully-functional, native tissue replacement, grafts must promote the establishment of cellular and tissue organization similar to a native vessel. A blood vessel contains three identifiable layers called the tunica intima, the tunica media, and the tunica adventitia, from the lumen outwards. Endothelial cells (ECs) make up the monolayer intimal lining, often called the

endothelial layer or endothelium. Smooth muscle cells (SMCs) are predominately located in the media, while the adventitia primarily consists of fibroblasts.[23] Of these vessel layers, establishment of the endothelium on a graft has been a primary focus due to the endothelial layer's crucial role in vascular biology. The endothelial layer provides dynamic control of interactions with blood flowing through the vessel, maintaining hemostasis by regulating inflammation, permeability, thrombosis, and fibrinolysis.[28,29] Establishment of a healthy endothelium on an implanted graft is thought to be crucial in the prevention of complications such as reduced patency due to intimal hyperplasia and thrombogenicity. The endothelium plays a direct role in the regulation of the coagulation cascade and, thus, thrombosis.[30] While intimal hyperplasia is caused by the ingrowth of SMCs, the endothelium plays a crucial role in regulating SMC growth from the media layer. Inflammation and thrombosis, both regulated by the endothelium, can trigger intimal hyperplasia. A healthy endothelium also has the capability to inhibit excess SMC proliferation and migration, thus preventing intimal hyperplasia.[31] In a reciprocal effect, the medial layer plays an integral role in endothelialization. Mechanical stability provided by the medial layer can prevent anastomosis, while extra cellular matrix production and remodeling can further promote the development of neovessel tissue and support endothelial growth.[32,33]

Many strategies for seeding cells on vascular grafts have been developed to establish a complete endothelium before implantation. Even when these strategies are successful, the hurdles of cell seeding may limit clinical

applicability, drastically increase graft costs, and/or require a lengthy amount of time.[34,35] Obtaining adequate number of mature ECs for proper cell seeding may be difficult without causing donor site morbidity.[36] Instead of relying on autologous or allogous cell seeding for the production and implantation of vascular grafts, many current small-diameter, vascular graft strategies incorporate biofunctional molecules or components to mobilize autologous cells within the vasculature to the graft post-implantation.[37,38]

This chapter will focus on current and developing strategies to promote the adhesion, differentiation, and proliferation of endothelial cells (ECs) and endothelial progenitor cells (EPCs) to form a complete endothelium on biodegradable, small-diameter, vascular grafts *in situ*. We have chosen to focus on polymeric grafts due to their relative ease of production, ability to be tuned for mechanical properties, and availability of surface modification techniques. Techniques of surface modification will be reviewed, examining chemical and topographical factors that contribute to successful endothelialization and how such strategies have or can be applied to biodegradable, small-diameter grafts. In addition, alternative strategies, treatments and concepts will be covered that can be applied to promote endothelialization of such grafts. This chapter will attempt to provide a framework useful for combining these approaches in the ultimate development of a biodegradable, small-diameter vascular graft that can effectively enhance and expedite the endothelialization process post-implantation.

2.1 Targeted Cells for *In Situ* Endothelialization

2.1.1 Endothelial Cells (ECs)

EC adhesion and proliferation is vital to the establishment of a thromboresistant cellular layer and the prevention of intimal hyperplasia by inhibiting SMC growth into the inner lumen of a vascular graft.[39,40] If endothelial cells are not seeded on the graft, migration and adhesion of endothelial cells occurs in one, or a combination, of several manners. ECs may migrate over the anastomosis site of the graft from the neighboring vessel structure. ECs may also migrate through pores in the graft via ingrowth of capillaries.[41] However, EC ingrowth beyond the anastomosis site into the graft is often restricted to 1-2 cm.[23] Thus, relying on the passive migration of neighboring ECs may be insufficient for expedited endothelialization of an implanted graft.

2.1.2 Endothelial Progenitor Cells (EPCs)

Circulating EPCs may also contribute to the endothelialization of the graft via adhesion, proliferation, and differentiation into ECs. EPCs were first identified in 1997 as a population of cells capable of neovascularization derived from the bone marrow.[42] EPCs appear to play a significant role in vascular homeostasis and blood vessel formation.[43–45] They are capable of expressing various EC characteristics and markers such as CD31, VE-cadherin, vascular endothelial growth factor receptor-2 (VEGFR2), and von Willebrand factor (vWF).[42,46,47] These markers contribute to vascular permeability, cell-cell adhesion, and controlling other cellular responses during neovascularization. It has been suggested that EPCs migrate to ischemic

tissues and sites of vascular injury to promote neovascularization and vessel healing, responding to hemodynamics and chemical stimuli to differentiate into mature endothelial phenotype cells.[48–50] Endothelial injury coagulation activation and platelet response provides mobilization and homing of EPCs. Amongst EPCs, distinct populations have been identified: Early-outgrowth and late-outgrowth cells. The early-outgrowth EPCs, though exhibiting several endothelial markers, are unable to form vascular structures, though they have been found to impact homeostasis and neo-angiogenesis.[51,52] Late-outgrowth EPCs display endothelial markers and have been found to form vessel structures.[51] Despite their differences when cultured alone, these two populations of EPCs have been found to interact synergistically to promote neovascularization.[53] While the nature of neighboring ECs versus EPCs in endothelial repair remains unclear, research still suggests that administration of EPCs can lead to enhanced vascular function.[54] Besides contributing to the endothelium through proliferation and differentiation, EPCs also release soluble factors that enhance the migration of ECs.[55] A basic schematic demonstrating these pathways of EPC and EC migration can be observed in Figure 2.1. Optimal endothelialization of a small-diameter vascular graft may be achieved through utilization of EPC mobilization, homing, adhesion, and differentiation into ECs.
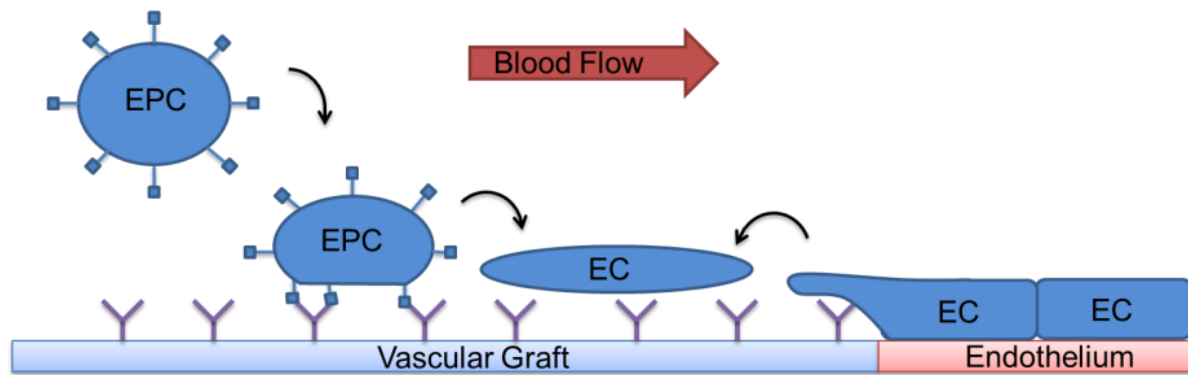
Figure 2.1. Paradigms of endothelialization of vascular grafts. ECs migrate from neighboring tissues over the anastomosis, while EPCs respond to functionalized vascular graft surfaces. EPCs adopt a EC phenotype, under influence of shear stress, growth factors, and immobilization to the graft surface.

2.2 EPC Homing, Mobilization, and Migration

EPCs circulate the bloodstream in relatively low abundance in normal, physiological conditions, so graft designs utilizing the accelerated endothelialization potential of these cells must incorporate methods of increased mobilization of EPCs.[56]

2.2.1 Growth Factor Incorporation

Growth factors such as VEGF,[42] stromal cell-derived factor-1 (SDF-1),[58] and granulocyte colony-stimulating factor (G-CSF)[59] have been found to increase mobilization of EPCs from the bone marrow and used in vascular graft applications. Nerve growth factor (NGF) has also been found to promote EPC migration *in vitro* and mobilization and homing *in vivo* to a collagen-modified decellularized blood vessel matrix.[60] NGF was bound to the blood vessels, resulting in significantly increased endothelialization and patency rates in a mouse model.[60] Recently, brain-derived neurotrophic factor (BDNF) has been

found to enhance graft patency rates in rats when bound to small-diameter tissue engineered blood vessels.[61] BDNF was found to increase EPC mobilization and capture *in vitro* and *in vivo*. VEGF production was found to have been increased 2-fold in BDNF-treated cultures with EPCs, demonstrated the paracrine effects that contribute to the enhanced mobilization and migration of EPCs due to BDNF. *In vivo*, EPC migration to BDNF-modified grafts experienced a 5-fold increase over control grafts.

While not studying biodegradable grafts, improved endothelialization and reduced thrombosis were demonstrated for two commercially available polyester grafts (Gelsoft™ from Vacutek® and POLYMAILLE® C from Perouse Medical).[58] Grafts were coated with fibronectin and, subsequently, homing factor SDF-1α to promote homing and adhesion of hematopoietic stem cells and EPCs. Significantly less thrombotic material accumulated on both grafts after coating and EC coverage of the grafts was almost doubled compared to the uncoated controls. In addition, tests demonstrated the increased proliferation, differentiation, and homing of EPCs due to BDNF. Star poly(ethylene glycol) (PEG)-heparin hydrogels were modified by immobilizing a novel, biased-like SDF-1 derivative to mobilize EPCs.[62] Research into the use of growth factors for EPC homing, mobilization, and migration has been increasingly robust. Future work may include tuning the presentation of these growth factors by combining several factors immobilized on a graft, controlling their release in the case of soluble factors, and varying local concentrations of the factors on the graft's surface.

2.3 **Adhesion and Proliferation**

2.3.1 Biofunctional Molecules

Adhesion and supported proliferation of ECs and EPCs is essential to graft endothelialization. As previously mentioned, ECs may migrate from neighboring tissues to the graft. EPC adhesion may be a more complex process. A current model of EPC recruitment involves EPC rolling and adhesion, similar to leukocytes, followed by migration and differentiation. Adhesion of EPCs to ECs involves adhesive bonds formed by a variety of adhesive molecule interactions, dependent on the substrate stiffness and shear flow in the vascular environment.[63] Incorporating molecules into a graft to simulate these effects has proven to be an effective method of increasing EC and EPC adhesion and subsequent proliferation.

2.3.1.1 Antibodies

Immobilization of antibodies has been pursued in a variety of cardiovascular implant applications. Antibodies targeting markers for ECs and EPCs have been explored for increasing the adhesion of cells to the inner lumen of vascular grafts. For EPCs, two identified surface markers have been utilized in graft applications: CD34 and kinase insert domain receptor (KDR).[37,64] KDR, also known as VEGFR-2, and CD34 are present in circulating EPCs. CD31 antibodies and VEGFR-2 antibodies have been used to target ECs.[65,66]

Coating poly(caprolactone) (PCL) grafts with anti-CD31 antibodies has been shown to induce EC-specific binding, promoting attachment and long-term adhesion of ECs.[65] Human umbilical vein endothelial cell (HUVEC) adhesion to the modified graft was found to be 14.9-fold higher than adhesion to bare PCL films. Cell viability was also higher over a five day experiment. CD31 is also expressed on platelets, granulocytes, lymphocytes, and monocytes,[67–69] which could cause deleterious immune and inflammation responses when implanted *in vivo*.

Anti-CD34 antibodies have been used in a variety of applications to aid in the endothelialization of vascular stents.[70–73] Anti-CD34 end-grafted to covalently immobilized PEG on titanium stents to enhance EPC migration and proliferation to improve endothelialization.[72] Similarly, anti-CD34 antibodies have been immobilized on a heparin/collagen coating for a stent, accelerating the attachment of cells and expediting endothelialization.[71]

While CD34 antibodies bind to EPCs, some debate remains asserting that solely recruiting CD34 cells can be detrimental to long-term graft patency. CD34$^+$ cells can differentiate into other cell types including cardiomyocytes, endothelial cells, and vascular smooth muscle cells.[74] Non-specific adhesion of all CD34$^+$ cells can lead to problems such as restenosis due to smooth muscle cell proliferation from the captured CD34$^+$ population. Because it is thought a small percent of circulating CD34+ cells are EPCs,[75] recruitment of non-EPC cells to a graft relying on CD34$^+$ capture raises the potential for undesired cell attachment and graft patency rates.

VEGF receptors are located on both EC and EPC cell membranes. A VEGFR-2 (or anti-Flk-1) antibody for the VEGF receptor has been utilized through surface immobilization.[66] The group found a 2.5-fold increase in HUVEC capture with the molecule by orienting it with a G-protein rather than through passive coating. The anti-FLk-1 antibody was utilized in an attempt to capture circulating EPCs and ECs.[76] The group used a radial flow chamber with three regions coated with fibronectin, VEGF, or anti-Flk-1 antibody. Cell spreading was greatest with fibronectin, followed by VEGF and anti-Flk-1 antibody. Cell adhesion was independent of the bound protein. However, the group did not orient the anti-Flk-1 antibody binding like the strategy utilized in the previously mentioned study.[66] Passive absorption could lead to a lower quantity of available antigen-specific binding sites. It is possible that orienting the anti-Flk-1 antibody could lead to more promising results for cell adhesion via VEGFR binding in ECs and EPCs. For example, protection of the antigen-binding site of an antibody led to an almost 10 fold increase in number of active sites available for binding compared to non-protected, randomly immobilized antibodies in one study.[77] Another study utilized hydrophilic spacer arms for antibody attachment to increase the activity of antibodies.[78] Employing techniques such as these in the immobilization of antibodies could increase binding activity and efficiency on graft surfaces, resulting in better endothelialization rates over randomly immobilized antibody applications.

Besides the orientation of antibodies, it is also important to consider an appropriate combination of antibodies or other factors that will better uniquely

encourage EPC attachment. As described, the incorporation of solely antibodies for CD34 may encourage the attachment of cells inappropriate for expedited endothelialization. It may be necessary to include other antibodies or biofunctional molecules to better isolate and encourage the attachment of EPCs and ECs.

2.3.1.2 Peptides

Extracellular matrix (ECM) proteins have been a popular addition to vascular grafts, permanent and biodegradable, in order to mimic native vessel architecture and achieve enhanced endothelialization.[38] Significant evidence exists supporting the notion that the ECM regulates EC and EPC function through integrin interactions.[79–82] Laminin type 1 has been utilized in ePTFE grafts, demonstrating enhanced endothelialization over unmodified grafts.[83] While laminin-derived RGD continues to be one of the more popular ECM-derived peptides to enhance endothelialization,[84] a variety of other peptide sequences derived from fibronectin, laminin, and collagen type I have been incorporated into vascular grafts..

EC adhesion to polyurethane (PU) surfaces was improved via the cross-linking of elastin-like polypeptide 4 macromolecules.[85] In addition to the favorable cell morphology and increased expression of endothelial nitric oxide synthase, platelet adhesion and activation were reduced compared to control PU surfaces. ECs and EPCs were shown to have adhered well to L-selectin and vascular endothelial (VE)-cadherin chimera proteins that were coated on titanium surfaces.[86] Compared to single protein coated and uncoated

surfaces, a 50:50 ratio of the proteins on a coated surface showed the highest HUVEC and EPC adherence, viability, and proliferation. One group described 2.2mm diameter, electrospun PCL grafts modified with Nap-FFGRGD via dip coating.[87] Surface modification of the PCL films was accomplished by self-assembly of the Nap-FFGRGD utilizing a hydrogelator (Nap-FF).[88] After 2 and 4 weeks of implantation in rabbits, a 3-fold increase in EC coverage of the luminal side of the grafts was observed compared to unmodified grafts.[87]

Besides modifying the surface, an alternative approach is to incorporate isolated adhesion peptide sequences into the scaffold material. In a rat model, the accelerated endothelialization of a graft that incorporated the peptide cysteine-alanine-glycine (CAG) into PCL fibers was demonstrated.[89] CAG peptide was shown to selectively enhance attachment of ECs while rejecting SMC adhesion.[90] CAG was mixed with PCL and electrospun into fibers used to form a graft with an inner diameter of .7 mm. The area of endothelialization of the CAG-PCL grafts compared with PCL grafts was higher at 1, 2 and 6 weeks after implantation.[89]

An inherent weakness of peptide modification is the unselective nature of peptide-promoted cell adhesion. Sequences, such as RGD, allow for the adhesion of a variety of cell types.[84] In one study, CAG was chosen for incorporation into the graft design based on results from an array-based peptide-cell interaction assay methodology.[89,91] Approaches, like this one, to identify EC- and EPC-selective adhesion peptides or peptide combinations should be employed to improve small-diameter vascular graft success. Since

most adhesive peptide sequences are non-specific, it may be appropriate to include other, more specific biofunctional molecules, such as antibodies or aptamers, to better encourage EPC and EC adhesion.

In addition to being used for its direct cellular adhesion interactions, recent research has examined the effectiveness of biomimetic proteins and peptides to immobilize other functional molecules to graft surfaces. For example, dopamine is a key functional group in mussels which allows the animals to attach to virtually any material. Researchers have developed a method of mimicking this behavior through co-polypeptides containing 3,4-dihydroxyphenylalinine and L-lysine.[92] PCL grafts were also coated with poly(dopamine) (PDA).[93] The PDA coated PCL nanofibers demonstrated highly enhanced HUVEC adhesion and viability compared to unmodified PCL nanofibers. In another study, 3,4-dihydroxyphenylalinine and L-lysine co-polypeptide was used to immobilize CD34 antibodies on a PCL substrate, enhancing EC and EPC attachment, growth, and adhesion.[73] VEGF was also immobilized through a simple dipping methodology after PDA was deposited on the surface of a poly(L-lactide-co-ε-caprolactone) (PLCL) film.[94] VEGF-dopamine coatings demonstrated accelerated HUVEC migration and proliferation compared to dopamine-coated or uncoated PLCL films. The group also was able to immobilize basic fibroblast growth factor, demonstrating the versatility of the PDA immobilization techniques. The technology appears promising for *in situ* endothelialization. *In vivo* studies will be informative to determine the feasibility of this technology in the future of vascular grafts.

2.4.2 Topography and Physical Properties

Cells are influenced by mechanical cues in their environment. These cues can affect cellular adhesion, proliferation, differentiation, and morphology.[95] As such, surface topography of materials has been an important topic in various cardiovascular prosthetics. To improve stent designs, the topography of stent surfaces has been examined to expedite endothelialization.[96] Such insights and strategies have been adapted to vascular grafts. One study examined the effects of nano-structured PLGA surfaces.[97] Nano-structured surface features were found to significantly enhance EC densities compared to micro-structured and untreated PLGA surfaces. Substrate rigidity has been found to affect cellular differentiation, as well. For example, one group enhanced the differentiation and proliferation of endothelial cells from cardiosphere-derived cells (CDCs) by testing polyacrylamide gels coated with fibronectin with Young's modulus values ranging from 8 to 21 kPa.[98] When matching the rigidity of native tissue, greater numbers of CD31$^+$ cells were present on the substrates after initial seeding of CDCs. Substrate rigidity appeared to influence the expression of p190RhoGAP which promotes VEGFR expression. This caused a cascade of events known to control endothelial differentiation.

2.4.2.1 Fiber Alignment

With the popularity of electrospun fiber designs in vascular grafts, it is crucial to examine the architecture of such grafts and the resulting effects on endothelialization. It has been thought that the architecture of the nanofibers

can influence cell proliferation, migration, and differentiation.[99–101] In native vessels, fiber architecture varies by layer. The medial layer consists of a circumferential orientation, while the intimal layer of endothelial cells are aligned longitudinally with the direction of the blood vessel.[99] Creating a vascular graft with distinctly oriented fiber layers could be crucial to better endothelialization and long-term graft outcomes. Recently, electrospun tubular scaffolds with an inner layer of aligned poly(lactic acid) (PLA) fibers and an outer layer of random PCL and PLA fibers were fabricated, in an attempt to replicate native architecture.[102] HUVECs and SMCs were co-cultured on the grafts. HUVECs were oriented in the direction of the fibers and SMCs proliferated and spread throughout the random fibers. Another group fabricated oriented nanofibrous PCL scaffolds that were aminolyzed to promote the immobilization of HA for endothelial cell attachment.[103] On aligned nanofiber scaffolds, investigations revealed that nanofiber alignment influenced the pattern of f-actin organization in HUVECs. Spindle-shaped morphology and bipolar extension of HUVECs were more significantly facilitated with aligned nanofibers. Combining aligned nanofibers with the hyaluronic acid surface modification promoted a confluent HUVEC monolayer and greater expression levels of vWF compared to random-oriented unmodified scaffolds and scaffolds with only hyaluronic acid modification or aligned fibers. Simply put, it is certainly advantageous to mimic the cellular orientation present in native tissue via electrospun fibers to help ensure EPC and EC orientation, proliferation, migration, and differentiation.

2.4.2.2 Surface roughness and features

It was found that nanometer scale roughness, even at 10-100nm, could enhance HUVEC adhesion and growth.[104] Endothelial and smooth muscle cell densities were found to be increased on nano-structured poly(lactic-co-glycolic acid) (PLGA) surfaces.[97] Spherical features of 200 nm proved more beneficial for fibronectin spreading and both SMC and EC adhesion and growth on a PLGA surface.[105] On polydimethylsiloxane (PDMS) films, grooves and ridges (500 nm in depth) were created in alternating nano- and micron roughness regions in linear patterns for one study.[106] The space between these grooves ranged from 22 to 80 μm created via electron beam physical vapor deposition method on a flat titanium surface preceding polymer casting. Rat aortic EC adhesion was most adherent on patterned films with the greatest spacing in the sample group. Elongation of these cells was about twice as great as those on non-patterned films. According to the results, the optimal adhesion and elongation can be tuned on a 45 μm spacing micron-rough and 80 μm spacing nano-rough patterned PDMS film.[106]

In a recent study, one group modified PDMS with an array of micropillars.[107] They found that using 1 μm high micropillars of fibronectin allowed HUVEC adhesion and promoted cell alignment when testing a variety of heights and diameters of pillars. Endothelial colony forming cells (ECFCs), a subset of EPCs, and HUVECs were seeded on the substrates, showing much greater viability with micropillars of heights 1 and 3 μm than those 6 or 8 μm in height.   Cell spreading was best achieved on micropillars of height 1 μm.

Next, diameters and spacing between pillars were tested ranging from 1 to .56μm and .6 to 15 μm, respectively. It was reported that fewer HUVEC extensions were observed in larger pillars with small spacing (diameters of 2.8 μm with spacing of .8 μm, for example), while smaller diameter micropillars with wider spacing yielded more pronounced adhesive protrusions (diameters of 2 μm with spacing of 4 μm). Otherwise, HUVEC adhesion and alignment occurred on most other substrates. ECFC adhesion and elongation was optimum on 1-2 μm diameter pillars. Finally, EC elongation and alignment was also found to be greater on PDMS with micropillar arrangements than a stiff SiO_2 substrate with similar topography.

In summary, it is crucial to consider the surface roughness and features of the vascular graft. It would appear that patterns with spaces on the scale of ~45-80 μm spacing with features of heights no more than 1-2 μm may be optimal for EC and EPC adhesion, proliferation, and spreading.

2.4.2.3 Porosity

Porosity has long been an important factor in vascular graft design. Inflammatory reactions can be instigated by grafts with pore sizes below the so-called "critical porosity size." Example sizes include 1.0 μm for PTFE, 0.8μm for cellulose acetate and acrylic copolymer, and 1.2 μm for mixed esters cellulose.[108] Additionally, it has been shown that the ideal pore size is between 10 and 45 μm to support EC coverage and reduce fibrous tissue infiltration. Endothelial cells could not bridge pores greater than cell-sized diameters.[109] In another study, PU grafts were prepared with an average

pore size between 5 and 30 µm. They found the highest rate of endothelialization with grafts of pore size 30 µm in the abdominal aortas of rats.[110] It was thought that ingrowth of perigraft collagenous tissues aided in the establishment of the endothelium by presenting an ECM suitable for establishment of an endothelial layer. The most significant impact of porosity on the rate of endothelialization may be the establishment of these subendothelium tissues that are crucial to native tissue replacement of a biodegradable graft. While most strategies for endothelialization techniques are focused on surface features, it is vital to consider the effect porosity has on cell migration through the graft.

2.4.2.3 Micropatterning of Molecules

Combining the advantages of physical and chemical modifications of graft surfaces is an important step to induce expedited endothelialization. For example, it is well-established that the spatial arrangement and organization of RGD is crucial to promoting cell adhesion and impacting the strength of cell adhesion, including in ECs.[111–113] In one study, the effects of nanotopography modification were compared to RGD-binding to a silicon surface. Varying the size of nano- and micro-scale pyramids on the material surface appeared to better control the initial adherence of ECs to the silicon film. However, RGD density better controlled EC spreading and length of focal adhesions.[114] As the authors indicate, this data points to the possibility that endothelialization may follow a two-step process. It can be inferred that surface features guide the initial adhesion of cells and the immobilized

molecules predominately influence cell spreading. Thus, controlling spatial presentation of molecules and surface features may be crucial to optimizing endothelialization of a vascular graft. One group used micropatterned lanes with selective collagen type I deposition to control EC and EPC adhesion, encouraging cells to form either elongated or cobblestone morphologies.[115] Elongated EPCs and ECs experienced good ECM deposition and maintained aligned actin skeletal formation. EC deposition of ECM was largely dependent on morphology; cobblestone patterns produced more collagen type IV and fibronectin. Elongated EPCs were found to deposit and remodel significantly more than the elongated ECs. Another study demonstrated that the patterning of fibronectin supported EPC elongation and subsequent tube formation.[116] Patterning of HUVECs has also been achieved with micropatterned-immobilized VEGF.[117] Through micropatterning, EC and EPC adhesion, elongation, and growth can be more precisely controlled. Optimization of micropatterns can lead to a geometrically, chemically, and mechanically functional graft that better replicates native blood vessel architecture and biological cues for endothelialization.

2.5 Surface Modification and Graft Fabrication Techniques

Surface modification and control of small-diameter vascular grafts is vital to influencing cellular response, hemocompatibility, and overall success of the graft once implanted. The modifications influencing cellular responses to the graft can be broken down into two categories: Chemical and physical surface

modifications. Such modifications can be controlled via biofunctionalization or through graft fabrication to control surface architecture.

2.5.1 Biofunctional Surface Modification

Biofunctionalization surface modification involves immobilizing molecules via methods such as surface coatings and covalent linking. These techniques involve a chemical change in the interface between the cells and the material surfaces in order to induce adhesion, proliferation, and differentiation.

2.5.1.1. Passive coating

In one attempt to modify material surfaces passively, hydrophobins were utilized to modify PDMS.[118] Hydrophobins are a family of fungal proteins with the ability to self-assemble into amphiphilic membranes.[119,120] The molecules self-assembled on the surface of the PDMS, significantly increasing the hyophilicity of the surface.[118] Hydrophobins alone have been found to improve cell adhesion to materials used for vascular grafts. In one study, improved cell adhesion was demonstrated on PLGA scaffolds modified with hydrophobins.[121] In addition, the group demonstrated that collagen immobilization could be improved on PLGA surfaces modified with hydrophobins. A technique was recently developed for the immobilization of anti-CD31 antibodies on electrospun PCL scaffolds by utilizing hydrophobins. Hydrophobin coating improved the hydrophilicity of the hydrophobic PCL surface, along with providing immobilization of the anti-CD31 antibody in a simple and efficient immersion technique. HUVEC adhesion to the hydrophobin-antibody-modified PCL films was 14.9-fold higher than uncoated

PCL films.[65] Hydrophobins provide a backbone for surface modification that
not only allows the mobilization of cell-specific bind molecules, but also
improves cell adhesion to the surface of the material on its own. This
technology could be promising in the development of *in situ* endothelializing
grafts. However, studies have not yet encompassed *in vivo* studies which
would be highly informational regarding the clinical potential of this surface
modification technique.

2.5.1.2 Covalently linked

Covalent binding of molecules for surface modification offers the ability
to more uniformly distribute bioactive molecules and functional groups on graft
surfaces. Plasma surface modification has been utilized significantly in
vascular graft engineering to aid in the development of hemocompatible,
bioactive, and biomimetic graft surfaces, especially on permanent polymeric
grafts.[122] However, it is vital to consider a covalent immobilization
technique's effect on biodegradable polymeric grafts. Modification can affect
the surface chemistry and ageing of polymers, as well as the effective function
of the attached biomolecule and the stability of their attachment.[123] Vapor
phase grafting has been demonstrated to initiate covalent VEGF
functionalization of grafts on PLLA and PCL in a non-destructive manner.[57]
One group covalently immobilized sulfated silk fibroin to PLGA scaffolds using
γ irradiation, supporting *in vitro* hemocompatibility and endothelialization.[124]
Another study examined the effectiveness of various strategies for
biofunctionalizing   PCL   using   ammonia   plasma,   oxygen

plasma/aminopropyltriethoxysilane (APTESI), and 4,4'-methylenebis(phenyl isocyanate)/water to add terminal amino groups to the PCL.[125] An anti-inflammatory and antithrombogenic drug, acetylsalicylic acid (ASA), and VEGF were immobilized via a N,N-disucciniidyl carbonate (DSC) crosslinker. Highest functionality was observed in the APTESI group and immobilization of ASA and VEGF was greatly improved with the DSC crosslinker compared to passive adsorption. NH_3 plasma-activated PCL had the highest ASA loading, while APTES modification provided the highest attachment of VEGF. This study makes it clear that choosing the proper methodology of immobilizing molecules for biofunctionalization of a graft can be just as important as the choice of biomolecule. Many covalent techniques have been proven to be effective for modifying the surface of graft materials and immobilizing functional molecules to encourage cell homing and binding. Covalent binding offers good control over the orientation of the ligands, but it is important to consider the impacts of covalent modification on the biodegradable graft material, so as to avoid deleterious side effects.

2.5.2 Methods of Graft Fabrication to Control Graft Architecture

As described, physical surface modification allows the manipulation of surface characteristics like roughness, patterns, features, and overall topography of the material surface that still consist of the bulk graft material. Methods of fabricating grafts to utilize the effects outlined in section 4.2 on topography and physical properties are outlined below.

2.5.2.1 Solvent Casting

To solvent cast a graft, a polymer is dissolved in a solvent. A porogen may be added to the solution and then the solution is added to a 3D mold. After the solvent is evaporated, the porogen may be leached, resulting in somewhat controlled porosity. The configuration of the mold enables some control over surface topography. Porous PU scaffolds were developed by one group using solvent casting and subsequent salt leaching. Porosity uniformity was controlled via centrifugation.[126] While solvent casting is not the most prevalent method of graft fabrication and physical surface control, it is a simple and relatively easy method of fabrication. Still, other methods, such as electrospinning and even stereolitheography may enable more precise control over fabricating grafts to mimic the native architecture of vascular ECM.

2.5.2.2 Electrospinning

Fabrication of electrospun grafts to mimic the native ECM is an important consideration in small-diameter vascular grafts. An increasingly investigated area of graft fabrication is the control of nanofiber orientation. Nanofibrous PCL scaffolds were fabricated in aligned and random orientations, followed by surface modification with hyaluronic acid.[103] Importantly, to align the PCL nanofibers, the rotating drum for collecting the fibers was operated at a high speed of rotation (2000 rpm) to generate well-aligned fibers. A low speed of rotation (20 rpm) produced random PCL nanofibers. Another study demonstrated the feasibility of controlling nanofiber layers in a PCL vascular graft by altering the rotation of the nanofiber collector and the electric

field during the electrospinning process.[127] This enabled the fabrication of interspaced layers aligned circumferentially, axially, and as a controlled mixture of orientations. Such studies demonstrate the expanding capabilities of electrospun vascular grafts. Electrospinning offers robust material selection, low cost, simplicity, high surface-to-volume ratios, and favorable, controllable porosity.[128–131] With these advantages, electrospinning is a proven framework allowing for the improved endothelialization of vascular grafts through precise fiber alignment and organization.

2.5.2.3 Stereolithography and 3D Printing

While elecrospinning has dominated the present direction of vascular graft production, there has been some investigation into controlling graft fabrication and surface characteristics via techniques like stereolithography and 3D printing. As previously mentioned, architecture of a graft should resemble native vessel conditions. The nature of electrospun fiber fabrication necessitates porosity in grafts, which increases surface area for cell attachment and allows cell invasion. However, 3D scaffold architecture and porosity can also be controlled via freeform fabrication techniques as demonstrated by one group.[132] Using microstereolithography, they studied internal pore and architecture relationship of a poly(propylene fumarate) graft intended for bone scaffolding. More recently, the feasibility of controlling graft architecture through a 3D computer-aided design was translated for vascular grafts. 3D microarchitectural features were created using a new stereo-biofabrication method on PEG diacrylate and gelatin methacrylate.[133] Another group

printed positive molds for the grafts and poured the graft material into the molds.[134]   All materials used were photocrosslinkable polymers based on urethane diacrylate monomers. UV light was applied to the filled molds to activate crosslinking of the materials. Currently, these techniques are not being widely pursued in the field of vascular grafts, presumably due to the difficulty of adapting such technologies to graft applications and the relative ease and low cost of electrospinning. Advances in the technology may also enable more precise control of graft architecture over electrospinning, allowing further investigating into better control of graft surfaces to encourage EC and EPC adhesion, differentiation, and proliferation.

2.5.2.4 Chemical Vapor Deposition

Vapor deposition can be used to deposit small particles onto graft material surfaces to create micro- and nano-scale patterns and structures. One group studied plasma modified nanostructures on a variety of polymeric and metallic surfaces.[135]   The process altered the nano-roughness and surface energy of the materials, affecting EC adhesion. E-beam evaporation has been used to generate surface features on a titanium substrate.[136] In addition, vapor deposition was used to modify surfaces used in a mold for polymer casting.[106]

Chemical vapor deposition can also be used to allow for functionalization of graft surfaces. Surface chemistry can be altered or reactive groups can be added to allow for covalent immobilization of biomolecules to material surfaces.[137]   One study demonstrated plasma modification to modify a

biodegradable graft material for enhanced endothelialization.[138] The group introduced poly(vinylacetic acid) groups to the PLLA substrate in order to immobilize fibronectin. Cell adhesion and proliferation were improved, along with increased cell retention under shear stress. Chemical vapor deposition has been more extensively researched in permanent materials, and this study offers a glimpse of the potential application in biodegradable, small-diameter grafts.

2.6 Controlling EPC Differentiation into EC-like Cells

2.6.1 Shear Stress

In mature blood vessels, ECs are exposed to shear stress resulting from blood flow. This shear stress affects a variety of mechanotransduction pathways including cell alignment and biochemical functions.[139] Shear stress has been found to induce EPC differentiation into adhesive ECs.[140] Recent research indicates that shear stress affects EPCs through VEGF-R2 and PI3K/Akt/mTOR signal transduction pathways, increasing adhesion, differentiation, migration, and proliferation of circulating EPCs.[141] While shear stress is innately applied due to blood flow, it is important to ensure that graft designs preserve hemodynamics similar to native vessels. Fluid dynamic analyses of novel graft architectural structures or surface patterns should not be neglected.

2.6.2 Chemokines, Cytokines, and Growth Factors

Besides assisting in homing and mobilizing of EPCs, growth factors, are also integral to the differentiation of EPCs into EC-like cells. SDF-1,[142,143] matrix metallopeptidase (MMP9),[142] VEGF,[144,145] erythropoietin,[146] and interleukin-8[147] have been identified for their roles in vascular remodeling, neovasculogenesis, and EPC differentiation. Research is ongoing to determine other factors that influence EPC differentiation into EC-like phenotypes and inclusion of these factors in graft applications. For example, BDNF has been found to support EC viability and neoangiogenesis and thought to have a significant regulatory role in EC development.[148] BDNF was found to improve the patency rate of grafts fabricated from decellularized rat carotid arteries when incorporated on the inner lumen.[61] Improved isolation and immobilization of factors could greatly increase the effectiveness of EPC homing, recruitment, and, most importantly, differentiation to EC-like phenotypes. Additionally, continued research into the biology of EPCs is necessary to better understand these pathways and how these chemokines, cytokines, and growth factors interact with EPCs to better control EPC response *in vivo*.

It is important to consider the effects of chemokines, cytokines, and growth factors in environments more similar to *in vivo* environments, as well. Static culture studies may not be representative of the actual effects on EPCs. Exposure to shear stress has been found to augment EPC differentiation into EC-like cells on fibronectin and VEGF-bound surfaces, compared to modified

surfaces in static cultures or shear stress alone. An increase in VEGFR2 and VE-cadherin expression indicative of EC differentiation of EPCs augmented was found on fibronectin-coated surfaces when shear stress was applied.[149] Furthermore, another study demonstrated that EPC expression of vWF, CD31, and ephribB2 signals, markers for arterial ECs, were significantly increased on VEGF-bound surfaces when shear stress was applied.[150] Comparing marker expression in these two studies, VEGF-bound surfaces appeared to better support EPC differentiation under shear stress conditions than fibronectin-bound surfaces.[150] Evaluation of prototype grafts should include shear stress conditions to better understand EPC differentiation under the influence of various immobilized biofunctional molecules.

2.6.3 Material and Surface Properties

Material and topographical properties alone have been found to influence the differentiation of EPCs into EC-like cells. Recently, it was demonstrated that growth of EPCs on fibrin display significantly increased levels of cytokine release associated with angiogenesis compared to EPCs grown on fibronectin, though EC marker expression was similar between both groups.[151] It was recently demonstrated that EPCs produced varying levels of markers influencing EC function depending on the surfaces on which the cells were seeded.[152] The group modified titanium surfaces for the following experimental groups: acid-etched, sand-blasted and acid-etched, hydrophilic acid-etched, and hydrophilic acid-etched and sand-blasted. These groups were compared to cell-culture compatible plastic and fibronectin-coated plastic

controls. Lower levels of VEGF expression were measured on acid-etched titanium while the highest VEGF expression was found in hydrophilic acid-etched and sand-blasted. The highest EC endothelial nitric oxide synthetase expression was also found on hydrophilic acid-etched and sand-blasted titanium.[153] Combining the material properties encountered by the EPCs along with controlling surface textures could work to selectively promote EPC growth. A recent study demonstrated the differentiation of adipocyte-derived stem cells (ADSC) into ECs and subsequent EC marker expression has been found to be significantly upregulated by nanopographical modification on quartz substrates with 250 nm ridges and 500 nm grooves.[154] While ADSCs are not a cell type suitable for *in situ* endothelialization, this study demonstrates the importance of nanotopography of graft surfaces in differentiation of endothelial lineages. Further work into the effects of nanotopography on EPC differentiation could further elucidate this phenomenon to promote expedited EPC differentiation. Combining these material and surface property stimuli along with the presentation of appropriate growth factors can work to achieve optimal EPC growth and differentiation.

2.7 Future Directions of In Situ Endothelialization Techniques and Conclusions

Many strategies have been studied to support *in situ* endothelialization of small-diameter vascular grafts. Likely, the optimal vascular graft will

incorporate several strategies. The graft must effectively support EPC mobilizing and homing. This may be accomplished by presentation and release of a growth factor like VEGF or G-CSF. The graft surface will need to have molecules suitable for selective adhesion of EPCs and ECs, while maintaining thromboresistance and hemocompatibility. Nanotopography can also aid in adhesion of EPCs and ECs, while affecting cell geometry, growth, and differentiation. Porosity and hierarchical design of grafts incorporating various materials will also be necessarily optimized to allow for adequate cell infiltration to support subendothelial tissues to support EC and EPC growth and differentiation. After the graft degrades, establishment of these tissues will be crucial to long-term success of the graft and the new vessel.

Despite the increasing number of small-diameter graft strategies utilizing EPCs, there is still controversy surrounding the biological nature of these cells. There is no specific marker that uniquely identifies EPCs and, thus, a variety of EPC subpopulations have been identified under markers generally presented by EPCs.[155] This can make EPC-specific cell attachment difficult. One group has taken the stance of abandoning EPCs almost entirely for their endothelialization potential, instead urging research to focus on the paracrine effects of these cells.[156] They maintain that the endothelial cells are primarily responsible for arterial repair and regenerations, and EPC research has not yielded data sufficient for supporting the idea that EPCs contribute directly to endothelial regeneration. Still, other perspectives offer that a particular subset of cells that have been labeled EPCs may have a significant

role in vascular repair: Endothelial colony forming cells (ECFCs).[155,157] More research into the unique markers that identify these cells will be necessary to better take advantage of their endothelialization properties in a small-diameter graft.

Strategies to promote *in situ* endothelialization of a small-diameter, biodegradable vascular graft have been robust, but much work remains to make these techniques clinically viable. The biology behind *in situ* endothelialization techniques, especially those utilizing EPCs and, specifically, ECFCs, should be further investigated. In addition, combinatorial methods of graft coating, topography, porosity, and external treatments should be investigated to optimize graft environments that enable efficient and thorough endothelialization of graft surfaces.

Chapter 3: Bioprinting of Blood Vessels[2]

To transport nutrients, oxygen, and waste, the human body utilizes an intricate network of blood vessels, ranging from large arteries and veins with diameters on the scale of centimeters to microvasculature on the scale of micrometers. Such vessels are crucial to the growth of new tissue and to the sustenance and restoration of existing tissues. Due to the undeniable importance of mature and functional blood vessels in almost all tissues, there is an enormous demand for transplantable blood vessels. Transplantable vessels are necessary in a variety of clinical conditions. Annually, there are approximately 200,000 coronary artery bypass graft procedures performed in the United States.[1] Additionally, peripheral artery disease affects 8 million individuals and 500,000 patients suffer from end-stage renal disease. Such conditions often require the transplantation of autologous blood vessels. However, these vessels may be unavailable due to disease or prior operations. In addition, options for autologous vessels do not perform equivalently. For example, in coronary artery bypass grafts, autologous transplantation of the internal mammary artery may offer better outcomes and increased patency retention rates compared to transplantation of the saphenous vein.[158–160] Synthetic vessels have been used with moderate success in large-diameter applications (>6mm), though small-diameter applications (<6mm) often lead to

---

[2] Adapted from: Melchiorri AJ and Fisher JP. Bioprinting of Blood Vessels. In: Essentials of 3D Biofabrication and Translation. (Atala and Yoo, eds.) Academic Press—Winston-Salem, NC. 337-348 (2015).

failure rates upwards of 30% due primarily to complications such as restenosis and thrombosis.[19] Many of these inadequacies and unfavorable failure rates are linked to complications associated with blood-material interactions of these permanent synthetic vessels.

To address these challenges, researchers have pursued tissue engineering strategies to eliminate the need for a permanent synthetic scaffold within the vasculature. The traditional processes associated with tissue engineering requires the seeding and expansion of cells on a scaffold until populations are sufficient for harvest. Such a process can be slow, labor and time intensive, and clinically difficult.[34–36] Bioprinting offers a potential solution to these challenges. Printing patient or scaffold specific vascular grafts or blood vessels may improve outcomes in a variety of applications. For example, congenital heart diseases in pediatric patients may present vast anatomical differences between patients despite sharing a similar moniker. In single ventricle anomalies, as one case study, one of the two ventricles is of an inadequate size for normal cardiac function. These malformations in the ventricle and the surrounding anatomy may differ drastically between patients. Thus, each of these defects requires careful planning and attention from the patient's clinicians in order to restore function. Often, such defects require the use of vascular grafts, cut and adjusted to fit the patient during surgery. Using medical images to guide the design and fabrication of a custom vessel before surgery would help reduce some of the challenges associated with current

congenital heart disease corrective surgeries, potentially reducing the time necessary for surgery completion.

Besides macroscale vessels, researchers have also pursued tissue engineering strategies for the development of microvasculature networks for the vascularization of artificial organs and tissues. An enormous challenge in tissue engineering of these organs and tissues is a lack of vascularization. Vascularization is of course necessary for the transport of oxygen and other nutrients, along with the removal of waste byproducts. Without adequate vascularization, diffusion through a tissue engineered construct may be limited to a few hundred microns. Inadequate vascularization leads to tissue necrosis and increased tissue engineered construct morbidity.[161] In order for the fabrication of artificial organs to become a reality, researchers must first tackle the challenge of integrating a functional vascular network. Integration of a functional vascular network is a challenge faced by all manners of large-scale tissue engineering. One example is the bioprinting of patient-specific bone constructs for critical-sized bone defects.[162–164] Custom fabrication of a vessel or vessel network specifically designed to vascularize the bone construct may alleviate tissue morbidity by promoting healthy vascularization. Thus, vascular tissue engineering is not only crucial for macro-scale grafts, but also for encouraging vasculogensis and/or angiogenesis within other tissue engineered organs or tissues.

Bioprinting of blood vessels may be advantageous both to the improvement and customization of direct cardiovascular implants, as well as

the stepping stone necessary for achieving long-term clinical success in bulk

tissue and organ constructs through custom vascularization networks. Blood

vessel bioprinting has enabled the printing of functional vessels with capillary

sized diameters, suitable for nutrient and oxygen delivery and waste removal

along with vascular grafts that may be used for congenital heart diseases or

coronary artery bypass grafts. Researchers continue to develop a variety of

printing strategies involving printing hardware, bioinks, biopapers, new

materials, and software to explore the potential of blood vessel

bioprinting.[165–168] These fabrication technologies are designed with the

underlying goal of promoting healthy tissue growth to overcome current

barriers in prosthetic blood vessel technologies, especially when it comes to the

endothelium. While much research has been performed in developing materials

for vascular applications, no material matches the blood compatibility of the

natural endothelium.[169,170] The endothelium, consisting of a monolayer of

endothelial cells (ECs), is largely responsible for vascular homeostasis. ECs

release a variety of factors to help control and prevent platelet activation and

inhibition, thrombogensis, and fibrinolysis.[28,29] A healthy endothelial layer

also aids in preventing smooth muscle cells (SMCs) from spreading into the

inner lumen as it occurs in intimal hyperplasia, preventing complications such

as restenosis.[31] Thus, functional vessel tissue layers are critical to

supporting proper blood flow and maintaining vessel patency and an

understanding of blood vessel composition is necessary for effective vessel

bioprinting. Because of the functional performance of the hierarchically

Endothelium
(Tunica Intimate)

Internal Elastic
Tissue

Smooth Muscle
(Tunica Media)

External Elastic
Tissue

Fibrous Connective
Tissue
(Tunica Adventitia)
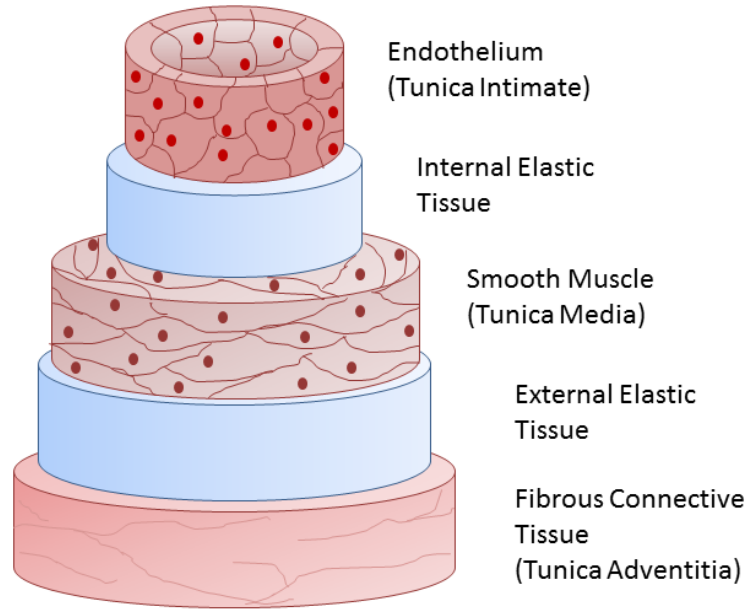
organized tissues that make up blood vessels, it is important to understand

native blood vessel composition and biology in order to achieve success in

blood vessel bioprinting.

Figure 3.1. Basic architecture of blood vessels in the human body.

3.1 Blood Vessel Composition

Generally, blood vessels are comprised of three layers identified, from the

inner lumen outward, as the endothelium or tunica intima, the medial layer or

tunica media, and the adventitia or tunic adventitia, as demonstrated in Figure

3.1. Not all blood vessels contain these three layers. Depending on the type

and size of a blood vessel, the thickness of these three layers may be drastically

different. For example, capillaries mediate nutrient delivery, waste removal,

and gas exchange by consisting of primarily an endothelial layer. This single

layer of cells lines an inner lumen with a diameter of only 5 to 10

micrometers.[171,172] The aorta, on the other hand, is the largest vessel in the human body and consists of the tunica adventitia, tunica media, and tunica intima. Because of its size, an array of vascular networks actually provides blood circulation to the outer layers of the aorta. The vessel walls may be generally characterized by three types of cells prominent to vessel architecture and organization: ECs, SMCs, and fibroblasts.[173,174] As previously mentioned, the ECs comprise the endothelium. The medial layer is primarily comprised of SMCs and the adventitia consists mostly of fibroblasts. The thrombo-resistant endothelium supports healthy vascular homeostasis, providing a selectively permeable barrier between the circulating blood, vessel, and surrounding tissues. Healthy ECs also help in regulating platelet activation, adhesion, and aggregation; leukocyte adhesion; and SMC proliferation and migration.[30,175–177] These functions of the endothelial layer are crucial to preventing complications such as thrombosis or emboli formation and restenosis of blood vessels due to intimal hypersplasia, or the ingrowth of SMCs. SMCs can influence mechanical adaptation of the blood vessels through extracellular matrix (ECM) production, while also possessing secretory capabilities.[178] The extracellular matrix components secreted by SMCs, such as collagen, elastic fibers, elastic lamellae, and proteoglycans, aid in the maintenance of the compliance and elasticity of the blood vessel. Successful vessel bioprinting must incorporate tissue and layer organization consistent with the intended vessel's size, function, and biology.

3.2 Challenges Associated with Vessel Bioprinting

Bioprinting blood vessels is not free from the challenges faced in the ongoing efforts to develop fully functional tissue engineered vascular grafts and blood vessels. Such vessels must conform to an extensive list of requirements associated with other vascular grafts: mechanical strength must be adequate to prevent complications such as aneurysm and withstand hemodynamic stresses while reducing complications associated with non-compliance; biocompatibility must be adequate to ensure cell attachment and proliferation of vascular cell populations, while retaining non-toxic and non-immunogenic inertness; materials need to be suturable and easily handled during surgery; vessels and grafts should resist inducing thrombosis and infection; host tissue must be able to be incorporated through proper healing and tissue formation; and, for pediatric patients, grafts must allow for, and adapt to, growth of the patient.[27]

Besides these requirements, bioprinting of vascular grafts and blood vessels introduces additional challenges due to limited material selection and varying printing techniques. For example, some bioprinted grafts may have insufficient mechanical properties after fabrication due to material or fabrication constraints. Many bioprinted vessel constructs rely on the use of biological or cell-infused hydrogels, which may not have the mechanical strength necessary to withstand hemodynamic forces after fabrication. It is only with long-term culturing that these constructs become strong via the ECM formation of the cultured cells. For example, a graft printed utilizing a layered

filament approach demonstrated that freshly bioprinted vessels demonstrated a burst pressure of only 6 mm Hg.[179] However, after the grafts were cultured, the vessels demonstrated burst pressures of 315 $\pm$ 81 mmHg at 3 days and 773 $\pm$ 78 mmHg at 21 days. Other materials, like polyurethanes, may be printed with adequate mechanical properties. However, these materials and the processes used to print them do not allow for the direct inclusion of vascular cells. Cells must be seeded after printing the constructs and these grafts may be limited in scale. Once a scaffold is successfully printed and the cells or tissues have matured, the fabricated vascular tissues must oftentimes be suturable to existing vessel networks to ensure immediate and effective blood perfusion. In these microvasulature networks, printing resolution must be adequate to print patent capillaries with diameters on the scale of micrometers. Even if vessels can be incorporated into an artificial organ, they must be manufactured to mimic natural vascular anatomy. Thus, vessels must be bifurcated over multiple scales to replicate the natural vascular trees that provide nutrient delivery, waste removal, and gas exchange in native organs.

Designing a proper vasculature tree for the purpose of blood vessel bioprinting involves more than just concerns over material and tissue compatibility. Researchers must also integrate computer models that effectively capture the anatomical formations of native vascular trees. Some efforts have been made in computer models that lead these efforts, though much research is still necessary to better mimic bifurcating and branching networks.[166,180,181] These designs must also be optimized so that shear

stress can be maintained within the networks. While the actual printing of microvasculature is important, computer-aided design of blood vessel structures is an integral component to the success of bioprinted blood vessels. One strategy involves the use of micro-computed tomography, which is used to generate 3D tissue structures. This approach has been utilized in the reconstruction of complex capillary beds. However, there is some difficulty in this regard due to the contrast agents used in microCT imaging. Such agents generally do not lend themselves to producing high-resolution images of small vessels. Without accurate imaging of these vessels, it can be difficult to accurately produce a computer aided design (CAD) model for printing of a capillary bed. To overcome these challenges, one group demonstrated the use of Batson's methylmethacrylate corrosion casting (BMCC) to create a vessel cast for acquiring high resolution microCT images.[180] Animals were sacrificed and heparinized normal saline solution was perfused through the vasculature. Following heparin perfusion, the vasculature was perfused with Batson's #17 solution modified with methyl methacrylate. The polymers cured to the animal's tissue and the tissues were corroded away. The BMCC produced more accurate and more complete models compared to a standard contrast agent method of microCT imaging. While such a method may produce better capillary bed models for 3D fabrication, BMCC modeling and imaging requires that the capillary bed specimen be sacrificed for the initial model reconstruction. However, this method of imaging and subsequent model

reconstruction avoids the blocking of microvascular and capillary vessels attributed to use of contrasting metals.

Instead of designing and fabricating the vascular tree, some researchers propose simply printing microfluidic channels within organs to mimic a vascular network.[165] Such a microfluidic network may allow for fluid perfusion throughout the construct and enable gas transfer. These channels would then be able to support the survival and maturation of the artificial tissue or organ.

3.3 Direct Vessel Printing

Bioprinting of blood vessels has primarily consisted of three main techniques: 1) Inkjet based, 2) laser based, and 3) extrusion based. Other methods of 3D printing, although not as widely used yet in vessel printing, have been investigated for vessel or graft fabrication including: 4) Digital stereolithography and 5) syringe based deposition. Each technique possesses unique advantages and disadvantages, which must be considered depending on the intended application.

3.3.1 Inkjet or Drop Dispensing

Inkjet technologies have been an historically popular method of bioprinting due to the availability and adaptability of commercial inkjet printers. Bioprinting of blood vessels are no exception. For example, one group modified a basic Hewlett-Packard Deskjet 500 thermal inkjet printer to enable printing ECs and fibrin simultaneously to form microvasculature patterns.[182]

The group fabricated micron-sized fibrin channels. When these channels were produced simultaneously with the ECs, ECs preferentially aligned themselves within the fibrin channels to form confluent linings similar to an endothelial monolayer found the vasculature. Another group investigated drop-on-demand printing via inkjet technology to selectively print protein solutions to control cellular attachment on substrates as early as 2003.[183] The group used two different sources of type 1 collagen for their printing solution: rat-tail and calf-skin collagen. These protein solutions were used in a modified Canon Bubble Jet for printing onto substrates. The substrates consisted of glass coverslips treated with type II agarose to prevent non-specific cell attachment. Following the printing of patterns, rat smooth muscle cells were seeded onto the coverslips. The group achieved successful patterning and subsequent attachment in features designed to be 350 μm or larger. Such two-dimensional structures can be important in the fabrication of new scaffolding strategies or studies on cellular behavior. For example, researchers utilized inkjet printing to modify substrates with patterns of DNA.[184] An inkjet printer deposited complementary DNA onto DNA- polyethylene glycol (PEG) -phospholipid modified substrate surface. These printed patterns offered high resolution renderings capable of precise and accurate immobilization of cells. Inkjet printing can also be utilized to pattern droplets of other bioactive molecules, such as peptides to induce cell adhesion and migration. One such study utilized CGRDS for cell adhesion and CWQPPRARI for promoting cell migration.[185] Surfaces patterned with these peptides demonstrated improved

endothelialization compared to unmodified surfaces by guiding endothelial cell adhesion and expansion.

These technologies, of course, are not limited to 2D patterning of vasculature structures, either, or thermal inkjet heads. Other techniques may incorporate vascular cells within hydrogel materials and subsequently deposit these hydrogel spheroids containing cells. This method may require subsequent fusion of cell-containing particles. In these methods, living cells

are directly deposited as droplets instead of being seeded onto preexisting scaffold structures as demonstrated in Figure 3.2.

One predominant method for 3D inkjet/drop dispensing methods of bioprinting involves the use of a biopaper (composed of a biocompatible gel, such as collagen) onto which bioink (multicellular spheroids) are printed. This method also takes advantage of the self assembly phenomena demonstrated by the multicellular spheroids as they are cultured into tissue constructs. Bioink

Figure 3.2 Deposition of cellular spheroids to form vessel. Spheres are printed, spheroid-by-spheroid, by layer. After multicellular spheroids are deposited, natural fusion of the aggregates through culturing will produce a complete tissue construct.

printing can be a rapid method to produce accurate, viable tissues, though the biopaper is a critical component for predicting success of the graft. The concentration of polymer in the biopaper must be carefully tuned for proper attachment and adaptation of the cells within the bioink.

The process of dispensing vascular structures, both acellular and cellular, may introduce a number of limitations. These processes may limit print resolution due to hardware and material constraints. The material choice in these processes is often limited by the constraints provided by a biological environment. For bioprinting of cells, materials are often restricted to hydrogels that have mechanical properties on their own that may be unsuitable for withstanding the natural hemodynamic forces in blood vessels. However, researchers are making progress in meeting these mechanical requirements. Pataky et al demonstrated the 3D printing of alginate hydrogel bioinks into vessel-like structures with diameters of roughly 90 µm.[186] Vessel structures were formed through the stacking of alginate beads. The group demonstrated that these vessels could withstand pressures up to 100 mBar before rupturing, whereas the group estimated relevant physiological pressures of 1 mBar to 20 mBar would be necessary. Polyurethanes can also be inkjet printed with more appropriate mechanical properties, but also do not directly incorporate the printing of cells. One group developed a pH sensitive, biodegradable polyurethane suitable for fabricating scaffolds via inkjet printing.[187] While the group did not specifically design the material for vessel printing, they demonstrated some of the steps necessary for developing a material intended

for cardiovascular implants. Cytocompatibility was tested by assessing the viability of fibroblasts and platelet adhesion of the printed scaffolds was assessed using fresh pig blood. The group was able to tune the materials by including a chain extender, N,N-bis(2-hyroxyethyl)-2-aminoethane-sulfonic acid (BES) to ensure that the tensile strength and elongation of the material could be improved and tuned for applications, such as vascular graft printing. In fact, including BES in the polyurethane formulation decreased platelet attachment compared to polyurethane scaffolds with BES. Cells must be seeded after graft fabrication instead of during the process. Particular methods of inkjet or deposition printing may introduce additional problems. For instance, bioink on biopaper printing requires removal of the biopaper from the fused tissue construct which in itself can be quite challenging.

Inkjet printing may also introduce significant cell damage and compromise cell viability. Cells also are unable to be printed in high densities due to the orifice diameter that may encourage cell sedimentation and aggregation.[182,188] Droplet fusion is also critical to vessel structural integrity. If fusion and shape of the droplets cannot be controlled precisely, structural integrity of the vessel may be comprised. This may prevent vessels from allowing blood perfusion or may result in more catastrophic problems, such as vessel rupture. In the design and consideration of deposition printing techniques, it is important to consider aspects of vascular cell behavior. For example, Fleming et al demonstrated the concept of vascular spheroid fusion.[189] Vascular spheroids, consisting of a SMC outter layer and EC inner

layer with a central lumen, fused to form elongated structures within collagen hydrogels. Spheroids adjacent to each other fused to form a single lumen. In these spheroids, ECs and SMCs self-assembled within combined spheroids to reform a single outer layer of SMCs and an inner layer of ECs with an in empty inner lumen. Utilizing the organization of multicellular constructs may offer tremendous impact on vessel bioprinting.

To aid in the production of heterogenous constructs, research utilizing multihead inkjet-based bioprinting has enabled the printing of multiple cell types organized within a construct. Heterogeneity may be determined by cell density or through the use of varying cell types. In these heterogenous constructs, vascular cell types can be incorporated to promote the vascularization of the bulk artificial organ construct. For example, one group designed an inkjet drop-on-demand system that was capable of printing a pattern construct consisting of three different cell types: human amniotic fluid-derived stem cells (hAFSCs), SMCs, and bovine aortic ECs.[190] To provide a scaffold for these cells, an alginate-collagen mixture provided layer-by-layer substrate support. The substrate was immersed in a $CaCl_2$ crosslinking solution between each printed layer of cells to ensure each preceding layer was bonded to the next. The printed construct supported the viability and vascularization of the 3D constructs *in vivo*. In another application of inkjet printing with a bio-ink, researchers printed multicellular spheroids of cardiac cells and ECs onto a bio-paper made of collagen and supplemented with VEGF.[191] (2008) The cell spheroids fused together over a considerable period

of time, much like droplets of liquid, to aid in the self-assembly of these 3D printed constructs. Constructs with ECs demonstrated the formation of conduits, indicative of vascularization, whereas constructs printed without ECs demonstrated no such structures.

3.3.2 Laser Printing

Laser-assisted technologies are another method of vessel printing developed in recent years. Barron et al introduce biological laser printing (BioLP) as an extension of matrix assisted pulsed laser evaporation direct write (MAPLE DW).[192,193] Originally, MAPLE DW was developed for the fabrication of electronics systems on a micron-scale which Barron et al adapted to deposit biological material while avoiding any direct interaction between the laser and the biological material. This is accomplished by the inclusion of a laser absorbing interlayer between the laser pulse and the biological materials. Material is transferred from a fluid biolayer onto a substrate. Thus, laser bioprinters require three main components[194]: (1) a pulsed laser source, (2) a target from which the biomaterial is printed, and (3) a substrate for printed material deposition. In BioLP, cells suspended in the target biomaterial are transferred to a collector slide via laser energy. These laser pulses create bubbles and the formation of the bubbles cause shock waves that propel the cells toward the collector substrate, in the process illustrated by Figure 3.3. This technique also offers high speed of fabrication, high efficiency, and low volume transfers. Adapting BioLP technology, Guillomet et al. developed a high-throughput workstation relevant to vascular bioprinting.[195] In their

adaptation of BioLP, they utilize concepts of bubble dynamics driven droplet ejection, enabling micrometer resolution. Guillomet et al. printed endothelial cells encapsulated in sodium alginate solutions and were able to print consistent droplets with five to seven cells per droplet.[195] Importantly, their methods utilized a lower glycerol concentration compared to other laser
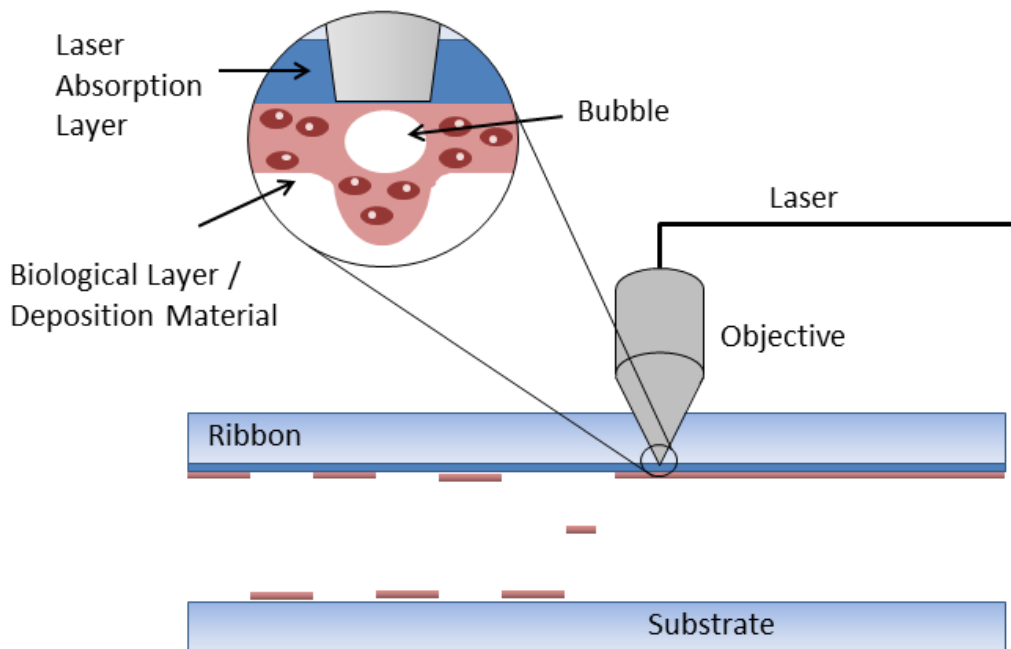
Figure 3.3 Schematic of general laser printing used to deposit patterned biological material containing vascular cells onto a substrate.

printing techniques utilizing cell. Previous studies show that glycerol concentrations of 10% v/v or higher may compromise cell viability.

Laser printing and patterning of vascular cells and structures can be affected by the viscosity of the deposition material, laser energy, pulse frequency, and laser printing speed.[196] Fabrication using laser systems benefits from high resolution which enables precise control of cell patterning.

Individual cells can be printed within 5.6 ± 2.5 µm of the intended pattern.[197] Such precision has not yet been demonstrated in other bioprinting techniques for the fabrication of vessels. However, laser printing must overcome the current limitations of printing true 3D structures, the need for photo-crosslinkable biomaterials, lengthy fabrication times, laser shock induced cell deformation, interactions of cells with light, and random settling of cells within the precursor solution.[165]

While 2D printing of these of laser printing has been largely successful, more recent work has translated 2D patterns of vascular cells into the fabrication of functional, 3D structures of vascular cells. In laser-induced forward transfer (LIFT) application, Gaebel et al laser printed a cardiac patch utilizing HUVECs and MSCs.[198] The cells were patterned to induce cardiac regeneration and their coculturing demonstrated increased vessel formation in infarcted hearts with the printed patches. Laser printing can be adapted to enable the printing of heterogenous 3D patterns onto a basemement membrane gel.[192] In one study, researchers demonstrated the use of this technique to print cocultured cells in the formation of branching/stemming structures.[199] These structures consisted of both human umbilical vein ECs (HUVECs) and human umbilical vein SMCs (HUVSMCs). HUVECs were deposited first to allow time for lumen formation. Following this period, the researchers utilized the BioLP method again to deposit HUVSMCs on and around the initial lumen structure formed by the HUVECS. The two cell populations appeared to interact to promote a vessel network; HUVSMCs limited HUVEC migration and

growth beyond the designated vessel pattern, and the cells appeared to form

cell-cell junctions necessary for vascular homeostasis.
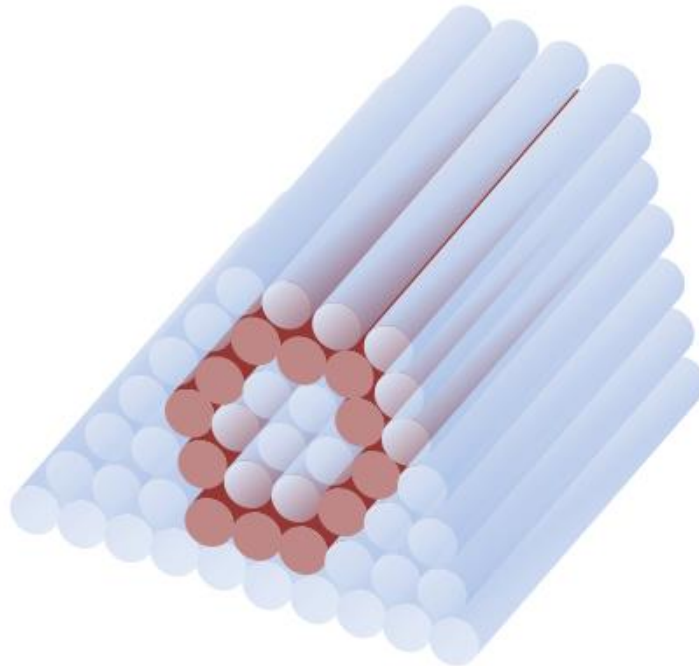
Figure 3.4 Demonstration of filaments organized via extrusion to bioprint blood vessels. Blue filaments represent acellular, support filaments that will be dissolved away. Red filaments represent cell-laden filaments that will form the tissue construct.

3.3.3 Extrusion Based Cell-Laden Hydrogel Deposition

The basic premise of extrusion based bioprinting relies on the extrusion

of continuous filaments. These filaments may consist of a combination of

biomaterials and/or cells. This process combines a fluid-dispensing system for

extrusion with a three-axis motor control system for printing.[165] The three-

axis control system enables precise deposition of filaments into a 3D construct.

In the filament tube printing methodology for vessels, grafts might be

fabricated by using acellular filaments to provide a structural platform for the

deposition of cell-containing filaments in a tube shape. To maintain the inner

lumen of the cell-containing vessel, acellular tubes may also be deposited within the inner lumen of the designated vessel, as shown in Figure 3.4. Cell viability in extrusion based system can easily be influenced by nozzle geometry, dispensing pressure, material flow rate, and material concentration.[200]

Bioprinted blood vessels can be fabricated more rapidly utilizing extrusion based methodologies compared to other methodologies outlined here. In addition, the deposition of cylindrical filaments can provide more reliable mechanical integrity to vessel structures.[201] Still, this technique suffers from some disadvantages that may be inhibitive toward current vessel bioprinting. For example, materials able to be used in extrusion based systems are limited. [201] In addition, resolution is much lower in these applications. Such a disadvantage may be inhibitive due to the micro-scale resolution and precision necessary for capillary-sized vessels fabricated for microvasculature networks. Similar to inkjet printing of vessels in some manners, nozzle pressure, nozzle diameter, and loaded cell density may affect shear stress experienced by cells during the printing process.[202] If shear stress is too high, cell viability suffers and may decrease the likelihood of successful viable vessel formation. The hydrogels traditionally used in these approaches are intrinsically weak. Their ability to withstand high pressure and mechanical loading may suffer, which can lead to vessel failure. The type of layer-by-layer fabrication used in filament extrusion fabrication may introduce its own host of issues. As with other modes of fabrication, there are constraints on the materials that can be used. Inherent to the nature of filament extrusion models, resolution and minimum

vessel diameters may also be markedly reduced compared to other methods of printing. Filaments extruded in a layer-by-layer fashion also may introduce seams and structural inconsistencies or artifacts that prevent high resolution and accurate rendering of the initial computer model.

Filament stacking models have been used to bioprint vessel-like structures relying on an agarose filament support and cellularized PEG hydrogel filaments.[203] The materials developed by this group enabled higher cell density suspensions. Two four-armed PEG derivatives were synthesized for their unique properties. These multi-armed PEGs possess a compact and symmetrical core. After converting the multi-armed PEGs into acrylate derivatives, tetra-acrylate derivatives (TetraPACs), the hydrogels could be used to co-crosslink thiolated hyaluronic acid and gelatin derivates, allowing the materials to be used in extrudable hydrogel printing. These modified TetraPAcs demonstrated equivalent or superior cell growth and proliferation support compared to polyethylene glycol-diacrylate (PEGDA) -crosslinked gels, in addition to demonstrating a higher shear storage modulus. This system was used to print NIH 3T3 cells in hydrogel macrofilaments organized in tubular constructs with internal diameters of 500 µm. Cells demonstrated viability for up to 4 weeks, supporting the use of this technique and these materials for potential use in blood vessel bioprinting.

Among the first studies to test 3D fiber deposition scaffold with heteregenous cell populations *in vivo*, Fedorovich et al used cell-laded extrusion fabrication to fabricate a scaffold containing regions of either endothelial

progenitor cell (EPCs) or mesenchymal stem cells (MSCs).[204] Fedorovich et al used a 3D fiber extrusion system called the Bioscaffolder. Using this bioprinting system, the group printed heterogeneously organized constructs with both osteo- and endothelial progenitor cells. As predicted, the cells differentiated heterogeneously within the construct. Perfusable blood vessels were formed in EPC-laden areas and bone tissue formed in areas laden with multipotent stromal stem cells.

Using a cell-laded hydrogel extrusion, researchers, focused on the computer modelling aspect of bioprinting macroscale blood vessels, demonstrated a hybrid printing technique for a human aorta.[205] Computer algorithms were developed. Overall, the general strategy to print these macroscale vessels was to use printed cell aggregates surrounded by support hydrogels to impart mechanical strength. To tackle the challenges of various structures that researchers may wish to bioprint, two different strategies were developed and utilized: cake-like supports and zig-zag patterning. Cake-like supports are formed by bioprinting a structure that supports itself in lay-by-layer printing. Each layer is printed in a series of long cylinder tubes dispensed by the bioprinter. Each of these cylinders is printed in a circular structure, so that the bioprinter is essentially printing cylinders made of the hoops. These cylinders support the next layer of prints by offsetting cylinder printing by the diameter of the support material. This enables each cylinder to be supported by two cylinders beneath it, suitable for hollow structures, such as an aorta. Alternatively, more complex structures can be formed using the group's so-

called zig-zag patterning approach.[205] While the cellular-component of the vessel is still dispensed in filaments forming hoops, the support material is printed in straight cylinders. Each subsequent layer is dispensed at a 90° degree angle from the last. In addition, the hoops that make up the vascular structure are dispensed in a curved formation to form a zig-zag pattern when viewed from a transverse cross section. Thus, each successive layer is supported by the lower layers and from the inner curves.

3.3.4 Stereolithography and Digital Light Processing

Stereolithography and digital light processing (DLP) utilizes a photosensitive printing resin for scaffold fabrication. The resin is irradiated, with either ultraviolet or visible light, through the bottom of a reservoir tray. One entire layer is irradiated at time, curing thin sheets of the resin. After a layer is cured, the scaffolds are repositioned by the machine to create a void between the bottom of the reservoir and the cured sections of the scaffold. This void is refilled by resin and the next layer is cured. Layer by layer, this process is repeated until vascular scaffold fabrication is complete. This type of fabrication process is used in a variety of other applications and has not been utilized for cellular vessel bioprinting; rather, current technologies limit vessel bioprinting to acellular structures that may serve as scaffolds for vessel tissue growth.

For stereolithographic blood vessel printing, material choice and development is a crucial aspect as it encompasses several of the requirements necessary for successful vascular graft or blood vessel fabrication. Fabrication

with such materials is limited in stereolithography due to the photo-polymerization requirements. These materials may affect mechanical properties, biocompatibility, host integration, and prosthetic adaptation. However, to address these issues, stereolithography enables the tuning of the material resin used to produce the vessels. One group demonstrated the successful development and tuning of a urethane based photoelastomer suitable for vascular tissue regeneration.[206] By using a urethane acrylate (UA) based polymer, the group could take advantage of additive manufacturing via photopolymerization. Such photoelastomer mechanical properties can also be mechanically tuned via the inclusion of reactive diluents. This particular study formulate a working printing resin using 30% wt UA and 70% wt 2-hydroxethyl acrylate (HEA). Printing with such materials could be achieved with DLP additive manufacturing and yielded fabricated scaffolds with mechanical properties similar to natural blood vessels. Researchers utilized printed patterning approach in an early technique to create capillary networks.[207] The pattern substrates were created with optical lithography. Following pattern printing, endothelial cells were cultured on the patterned surfaces. The cultured cells were then transferred to extracellular matrix and subsequently formed tubular structures. These micro-scale tubes could be transplanted into mice and function as capillary-like networks.

3.3.5 Syringe-Based Bioprinting

Vessels may also be printed utilized a syringe based bioprinting system. A syringe pump controls the flow of cell-laden alginate solution through a

coaxial nozzle system. The alginate solution crosslinks when it intersects with the flow of the crosslinking solution, the two solutions meeting at the outlet of the co-axial nozzle. Vessels formed using this technique may possess mechanical properties inadequate for hemodynamic mechanical forces. For instance, Yu et al demonstrated this technique with cartilage progenitor cells to study cell viability and functionality in vessel-like tubular channels.[208] The maximum tensile stress was 5.65 ± 1.78 kPa and the Young's moduls was 5.91 ± 1.12 kPa. With the technique, though, the group could print tubular cell-laden tubular channels with inner diameters of 135 ± 13 µm.

Choosing the appropriate technique

Depending on the application, each vessel bioprinting method offers distinct advantages and disadvantages. If mechanical properties after printing are crucial, stereolithography or inkjet printing of materials like polyurethane would be necessary. High resolution for vessel structures that necessitate detailed printing is based can be attained with lithography and laser based approaches. Stereolithography, spheroid deposition, filament extrusion, and syringe based printing appear to be suitable for the fabrication of larger vascular structures, as well. Of course, stereolithography is the only printing technique that currently does not support direct inclusion of cellular components during vessel printing. Less resolution is attained with prints, especially with filament extrusion and spheroid deposition of vessel components. Examples of relevant factors in making these choices can be seen in Table 3.1.

Table 3.1 Overview of various direct vessel printing methodologies and relevant properties

Printing Method	Direct cell incorporation?	Resolution	Materials
Inkjet	Yes	Tens to hundreds of microns	Cell solutions, proteins, Hydrogels, Polyurethanes
Spheroid Deposition	Yes	Hundreds of microns	Cell aggregates, Hydrogels
Laser-Based	Yes	~Five microns	Proteins, cell solutions, hydrogels
Filament Extrusion	Yes	Hundreds of microns	Hydrogels
Stereolithography	No	Tens of microns	Polyurethane, photoelastomers, acrylates
Syringe-Based	Yes	~One hundred microns	Hydrogel

3.4 Hybrid Vessel and Graft Fabrication

Another group sought to develop a method of producing scaffold-free, perfusable vascular grafts.[166] In this procedure, cells were pelleted into multicellular spheroids and the multicellular spheroids were subsequently used as the bioink. The bioink pellets were printed onto previously extruded agarose rods. These agarose rods served as a mold to support the layer-by-layer deposition of the multicellular spheroids into various tubular conduit branching patterns. These spheroids fused together to form continuous vessels if left cultured over 5-7 days. Using this technique, the group demonstrated bioprinted vessels could be printed in varying layers. For example, the inner lumen histology and immunohistochemistry confirmed that they successfully

bioprinted layers of fused multi-cellular spheroids organized with a SMC inner layer and a fibroblast outer layer. The group further demonstrated the potential of these cells by utilizing perfusion bioreactor to culture the conduits and demonstrate vascular maturity.

In fact, researchers have combined other methods of scaffold fabrication with bioprinting methodologies for the fabrication of vascular scaffolds. One group constructed electrospun vascular grafts made from polylactide (PLLA) and heparin.[209] After electrospinning, the grafts underwent fused deposition modeling to apply a single coil of polycaprolactone (PCL) around the tube graft. The authors of the study claimed that the inner electrospun layer enables the incorporation of a drug delivery system with a microenvironment conducive to endothelialization. The fused deposition modeling (FDM) outer layer bolsters the mechanical strength of the fabricated vessel.

Another hybrid approach utilizes the combined techniques of two-photon polymerization (2PP) and LIFT.[210] Introducing these novel approaches in a unique strategy, 2PP was used to photocrosslink acrylated PEG hydrogels. The 3D scaffolds produced by 2PP then undergo LIFT to introduce cell seeding. The group observed that the LIFT technique imparted no deleterious effects onto the deposited cells. Using 2PP, the group fabricated porous, hexagonal rings of PEGDa. Subsequently, LIFT was used to guide the seeding of SMCs and ECs.

Besides combining printing and fabrication techniques, Xu et al recently demonstrated simultaneous printing and transfection of endothelial cells.[211] It has been demonstrated that the printing process, specifically the application

of electric field or hydrodynamic pressures influences cell permeability.[212] Altered cell permeability enables the introduction of macromolecules into cells. To take advantage of this phenomenon, Xu et al incorporated green fluorescent proteins encapsulated in plasmids which were coprinted with aortic ECs. Through a variety of experiments, they showed that plasmid concentration, catridge model, and plasmid size influence gene transfection efficiency. Transfection was shown to be achieved simultaneously with the printing of ECs.

3.5 Casting

As an alternative to direct fabrication of the scaffold or blood vessels, another popular methodology is cast fabrication of blood vessels and scaffolds. The general methodology relies on computer generation of a casting model or mold. The vessel or vascular network can be 3D printed and subsequently used as a mold for casting a polymeric scaffold or used as a substrate for cellular growth and tissue formation. Thus, like many of the direct printing of vessels and vascular structures, the cast scaffolds may or may not directly incorporate living cells and tissues.

In one acellular method, Sodian et. al demonstrated the fabrication of a DLP-produced cast for a patient-specific aortic arch scaffold.[213] They demonstrated the proposed technique of obtaining an MRI for a patient and modeling the defect (in this case an isthmus stenosis). After defining the defect, they reconstructed a model of a corrected vascular structure by reconstructing

a nonstenotic aorta. The reconstructed, corrected model was fabricated via stereolithography and a vascular scaffold consisting of polyglycolide (PGA) and poly-4-hydroxybutyrate was cast onto the model vasculature to produce a scaffold ready for tissue engineering and suitable for implantation. This approach could potentially take advantage of a variety of materials suitable for cardiovascular applications. In addition, the cast scaffolds may or may not take advantage of cell seeding before implantation.

In a casting approach incorporating live tissue, Miller et al printed 3D filament networks of carbohydrate glass for the casting of functional vascular networks.[214] Carbohydrate glass serves as biocompatible, sacrificial material for the fabrication of printed vascular networks. The printed networks provided a substrate for the growth of cells and development of living vascular networks, at which the point the carbohydrate glass structure was dissolved. This resulted in a perfusable, functional vascular tissue network based on the original sacrificial template model. However, in order to secure the cells within the lattice structure, cells were suspended in an ECM prepolymer that was infused into the glass networks. The glass networks were also coated with a layer of poly(D-lactide-co-glycolide) before casting the ECM to prevent any disruption to the ECM crosslinking process and osmotic damage to the suspended cells. With the coating in place, the cells suspended in ECM prepolymer could be conveyed throughout the structure.

3.6 Post-Printing

Many of the challenges presented in various blood vessel printing strategies necessitate the maturation of the included or seeded cells into functional tissues. Many researchers assert that accelerated tissue maturation is necessary for these printed vessels to achieve the functional and biomechanical properties necessary for implantation.[215] Some of these challenges have been explored via material solutions, such as rapid polymerization and increased hydrogel stiffness. However, altering the materials in such a manner can negatively affect tissue fusion.[216] One potential innovation is that of an irrigation dripping, tripled fusion bioreactor that has removable porous mini-tubes. This design proposes three individual circuits.[217] One is used for maintaining a wet, physiological environment around the construct, the second enables media perfusion through the branched vasculature tree, and the third enables temporal perfusion. There are a variety of bioreactors that have been developed in the fabrication of tissue engineered vascular grafts that can simulate the biological environment necessary for tissue development.[218–220] These technologies primarily focus on the maturation of non-bioprinted tissues, but could be adapted to support structures post-printing. Continued research into platforms to support and accelerate vessel maturation is necessary for improving the applicability of bioprinted vessels. Of course, this will also necessitate the use of non-destructive techniques to monitor the maturation of the printed tissues.

To address some of these challenges, researchers are integrating other imaging and culturing technologies into the printing process to gauge and support tissue maturation within printed vessels. One group designed a system of hydrogel and cell printing utilizing a custom-tailored flow chamber for this purpose.[221] Several layers of collagen were printed and subsequently allowed time for gelation. Then, gelatin containing HUVECs were deposited in a straight line across the collagen layers. Following the deposition of the cell/gelatin mixture, collagen was again printed in layers to fill the rest of the flow chamber. After printing, the gelatin within the cell/gelatin mixture liquefied, allowing the cells to adhere to the collagen layers that now served as the surface of the channel. Media flow through the channel could then be established. The cells demonstrated high viability in the patterned tubes and were used to investigate the functionality of a mesoscopic fluorescence molecular tomography of the vessel constructs, enabling observations of fluid flow and fluorescent-labeled cells with high sensitivity and accuracy. Another group documented the production methodology utilized by *BioCell Printing*.[222] The entire system is a self-contained method of 3D fabrication involving four zones, as shown in Figure 3.5. In Zone 1, a multi-head printer dispenses the scaffold, which is then sterilized in Zone 2. Cells are seeded on the scaffolds in Zone 3 using another dispenser and finally cultured in Zone 4. This self-contained methodology may reduce the risk of contamination, while providing a translatable platform for clinical application of bioprinted vessels and vasculture trees incorporated into artificial organs.
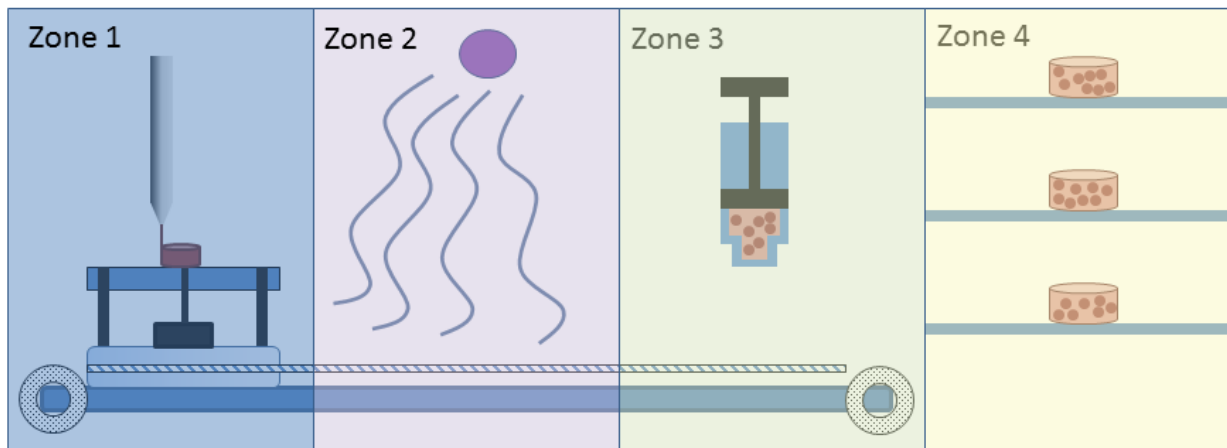
Figure 3.5 Basic schematic of the *BioCell Printer*, demonstrating a self-contained process of fabrication that can be used to incorporate vascularization, from printed scaffold to post-printing culturing of deposited tissues. Zone 1, scaffolds are printed. Zone 2, scaffolds are sterilized. Zone 3, cells are deposited. Zone 4, constructs are cultured for tissue maturation.

3.7 Conclusion and Future Trends

Emerging technologies in blood vessel printing will continue to provide potential solutions for the development of vascular graft applications and the vascularization of artificial organs. The continued integration of printing with blood vessel tissue engineering is still very much a work in progress but may offer enormous advantages in the form of custom-tailored vascular grafts and networks that could enable the biofabrication of more complex artificial organs. Vascularization of tissue engineered constructs will likely remain one of the predominant challenges in tissue engineering of artificial organs for clinical applications. While much work has focused on the materials and cellular

components of bioprinted vessels, there must be a focus on the process of bioprinting as a whole. For example, future work will necessitate more sophisticated vasculature modeling tools to help researchers, engineers, and clinicians design the appropriate anatomical models for integration within an artificial organ. Researchers must also consider the integral role of post-printing vessels. Current technology dictates the extended culture of cells to reach maturation appropriate for implantation. Self-contained printing and post-printing processes like that of the *BioCell Printing* system may be an indicator of the future direction of vessel printing.[222] As always, healthy endothelialization of printed vessels has, and will, remain a primary objective of vessel bioprinting due to the endothelial layer's intimate and crucial role in the success of any blood-material contacting artificial organ or graft. Challenges aside, the bioprinting of blood vessels continues to rapidly evolve, unlocking an emerging technology that may significantly impact the cardiovascular and artificial organ fabrication aspects of tissue engineering and biofabrication in a dramatic way.

Chapter 4: Solvent-Cast Fabrication of a Biodegradable Vascular Graft[3]

4.1 Introduction

Vascular grafts are integral to treating aneurysms, vascular reconstruction, congenital cardiovascular disease, and organ transplantation.[24] While autografts may be used as a gold standard, vessel availability may be limited by existing disease conditions or prior surgeries.[223,224] Investigation of potential synthetic grafts have largely supported the application of poly(ethylene terephthalate) (PET) and expanded poly(tetrafluorethylene) (ePTFE) grafts in large-diameter (>6mm) applications.[19] However, this same success has not been replicated in small diameter (<6mm) applications, more often resulting in graft failure due to stenosis.[19]

Tissue engineering approaches offer a potential solution to these challenges. Biodegradable small-diameter vascular grafts have been extensively researched for their controllable mechanical properties and promotion of native tissue remodeling. Such grafts have been constructed from biological and synthetic materials. Still, small-diameter vascular grafts have experienced a myriad of complications ranging from thrombus formation, aneurysms, intimal hyperplasia, calcium deposition, and noncompliance leading to low patency

---

[3] Adapted from: Melchiorri AJ, Hibino N, Brandes ZR, Jonas RA, and Fisher JP. Development and assessment of a biodegradable solvent cast polyester fabric small-diameter vascular graft. Journal of Biomedical Materials Research Part A. 2014 June; 102(6): 1972-1981.

rates and graft failure.[23,24,225] Biodegradable grafts may be replaced by native cells and extracellular matrix, allowing tissue remodeling to ensure biological and mechanical properties are consistent with native blood vessels to reduce long-term complications associated with vascular grafts.

Tailoring of small-diameter vascular graft mechanical properties is critical to achieving reduced complications. For example, the high elastic moduli of ePTFE and PET prevent these materials from deforming under pulsatile pressures like native blood vessels, disturbing normal blood flow and leading to complications that result in reduced patency.[226,227] A leading hypothesis suggests that a mismatch in the mechanical characteristics of the graft and native tissue can lead to disturbances within the mechanical environment resulting in a vessel remodeling response.[228,229] Much like healthy vessels respond to alterations in pressure and flow, tissues within and around the vascular graft may respond to mechanical disturbances, gradually causing an increase in vessel wall thickness.[230,231] This occurs in an effort to reestablish a baseline circumferential stress and can lead to stenosis. Thus, it is necessary to carefully match native vessel mechanical properties and diameters when designing a small-diameter vascular graft.

Additionally, the vascular graft material must elicit minimal inflammatory and thrombogenic response, while supporting cell attachment. Inflammation and thrombosis are added complications associated with small-diameter vascular grafts. Such conditions may lead to intimal hyperplasia and occlusion, leading to reduced graft patency.[31] Establishment of an

endothelial layer can also play a crucial role in regulating inflammation, thrombosis, permeability, and fibronlysis.[28,29] Thus, a vascular graft must be biocompatible with endothelial cells and promote cell attachment and proliferation to prevent thrombosis and ensure long-term biocompatibility.

Our aim was to utilize readily available components to reduce the time necessary to fabricate custom vascular grafts. We adapted a methodology introduced by Roh et al that can be potentially applied to any polyester sheet, allowing simple customization of scaffold dimensions through varying the component dimensions of a cylinder solvent casting system.[232] The first human trial evaluating tissue engineered vascular grafts fabricated in such a manner were implanted in 25 pediatric patients(median patient age 5.5 years) with single ventricle anomalies.[233,234] While the pure poly(lactic acid) (PLA) and poly(glycolic acid) (PGA) grafts used were generally successful, late-term (> 6 mo.) results indicated a 16% failure rate due to stenosis.

Utilizing these procedures, we hope to expedite the clinical availability of biodegradable vascular grafts with favorable mechanical properties and tissue-material interactions. We chose to explore the 90:10 copolymer poly(glycolic-co-lactic) acid (PGLA) sealed with a poly(DL-lactide-co-caprolactone) (P(CL/LA)) solution. As previously discussed, mechanical properties of vascular grafts can have a significant impact on preventing or causing reduced patency, or stenosis, in grafts. The purpose of this study was to determine the mechanical properties and biological compatibility of a small-diameter (~1 mm) PGLA-P(CL/LA) vascular graft. In addition, we investigated the effect of varying

P(CL/LA) concentrations within the sealant solution used for graft fabrication to adjust mechanical properties. We hypothesize that such grafts should have mechanical properties comparable to native vessels, while providing balanced degradation rates conducive to healthy neotissue formation *in vivo*.

4.2 Materials and Methods
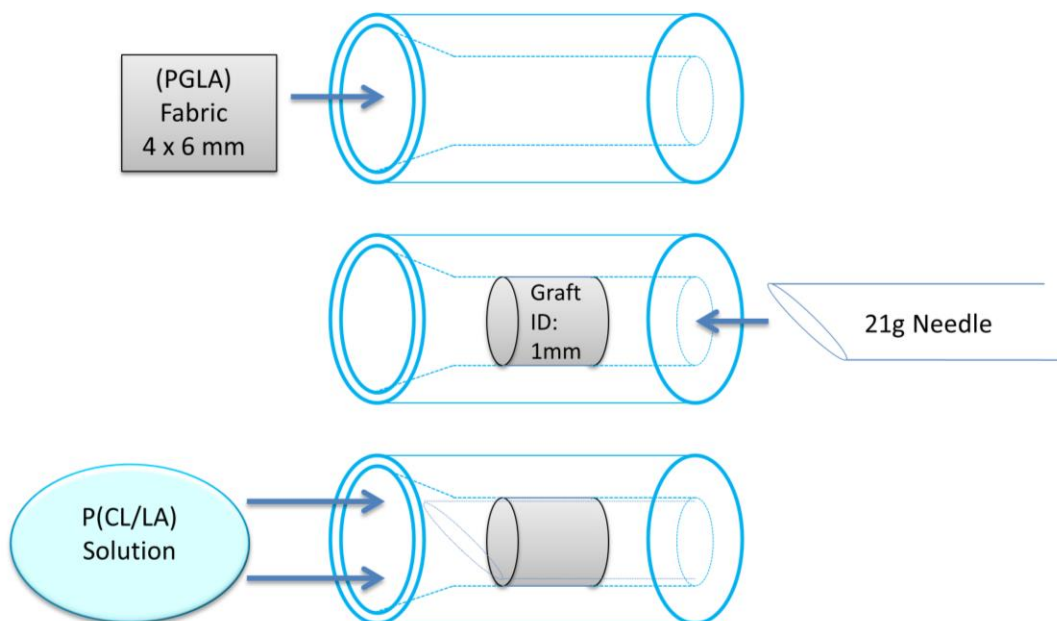
Figure 4.1 Diagram illustrating the method of graft fabrication.

4.2.1 Graft Fabrication

The method of graft fabrication was based on a previously reported methodology.[232] A non-woven 90:10 copolymer BIOFELT made of poly(glyocolic-co-lactic acid) (PGLA) of ~0.300 mm thickness was used to provide the structure for the graft (Biomedical Structures, Warwick, RI). Figure 4.1 provides a schematic of the fabrication process. Felt sections were cut to shape (6.0 mm x 4.0 mm) and inserted into a polypropylene tube with an inner

lumen diameter of 1.4 mm to form a tube shape. The polypropylene tube had a graduated taper to assist in graft insertion and rolling. A 21 g stainless steel needle was inserted in the inner lumen of the rolled felt and tube to maintain the patency of the graft during fabrication. A 40:60 copolymer sealant solution of P(CL/LA) (Sigma-Aldrich, St. Louis, MO) was dissolved in 1,4-dioxane at 10% and 15% w/v ratios. This sealant solution was then deposited into the polypropylene inner lumen to saturate the PGLA felt to seal and connect the seam of the rolled felt section. The sealant solution was allowed to penetrate the felt for 5 minutes before freezing the system at -20° C for 30 min. Sealed tubes then underwent freeze-drying for 24 h to eliminate the 1,4-dioxanes solvent from the system. After complete drying, the grafts were removed from the tubes and stored at -20° C for further use. To confirm lumen diameter and wall thickness, grafts (n=5) were cut into sections 1 mm in length and imaged on a Hitachi SU-70 scanning electron microscope (SEM) (Tokyo, Japan).

4.2.2 Mechanical Characterization

All tensiometry was performed using an INSTRON 5560 tensiometer with a 50 N load cell (Instron, Norwood, MA).

For tensile strength testing, samples were cut along the sealed seam after fabrication for tensile testing and secured in screw-action grips. Measurements were performed using a 10 mm/min crosshead speed for tensile strength and elastic modulus (n = 5). Elastic modulus was determined from the initial 10% of the stress-strain curve slope. Graft sections were elongated until failure.

Suture retention strength was measured by passing a 5-0 prolene suture approximately 1 mm from the end of the graft (n=5). The opposite end of the graft was secured in a stationary screw-action clamp and the suture was pulled out at a constant rate of 120 mm/min until graft failure.

Burst pressure was approximated using LaPlace's Law for blood vessels. $P = \frac{UTS * t}{r}$ where P = internal pressure, UTS = ultimate tensile strength in the circumferential direction, t = wall thickness, and r = radius. Grafts were cut to 0.5 mm sections and placed on metal hooks on the tensiometer (n=15). The tubular graft sections were stretched at a rate of 1 mm/min until failure and the tensile strength was used in calculating approximate burst pressure strengths.

4.2.3 Degradation Assessment

To assess the effects of biodegradation and resorption on the mechanical properties of the graft, grafts were immersed in a phosphate buffer saline (PBS) solution at 37º C in a benchtop shaker at 60 RPM. Grafts (n=5) were assessed at 1, 3, 7, 14, 21, 28, 42, 56, and 70 days of immersion. Dry mass of the grafts was recorded by removing the grafts from the PBS solution and allowing them to dry at room temperature until mass readings were stable over time. Elastic modulus and tensile strength were assessed as previously described for each time point, until time points at which graft integrity due to degradation prohibited accurate tensile testing.

4.2.4 In Vitro Cell Adhesion and Proliferation

Human endothelial vein cells (HUVECs) were used for cell adhesion and proliferation assessments on the grafts (Lonza, Basel, Switzerland). Cells were cultured in endothelial basal media (EBM) supplemented with EGM SingleQuot Kit Supplements and Growth Factors (Lonza, Basel, Switzerland). After fabrication, grafts were cut down the seam and flattened to fit ninety-six-well plates (Falcon, BD Labware, Franklin Lakes, NJ). All grafts were sterilized via UV light exposure for 1 hr before cell culture assays.

For cell adhesion, HUVEC cells were seeded at 5×10^3 cells per well (n = 4). Cultures were placed in an incubator at 37° C for 1.5 hrs. After incubation, grafts were thoroughly washed with PBS to remove any unattached cells. Live/Dead staining was performed to identify cells and wells were imaged under a fluorescent filter via a microscope. Attached cells were counted to determine HUVEC adhesion to the grafts. Cell counts were normalized to cells attached to tissue culture polystyrene (TCPS).

For cell proliferation, HUVECs were similarly seeded at 5×10^3 cells per well (n=4) and cultured in an incubator at 37° C. Seeded grafts underwent Live/Dead staining at 1, 3, and 7 days after initial cell seeding. Again, attached cells were counted via microscopy to determine HUVEC populations on the graft.

4.2.5 In Vivo Functionality

In order to assess early *in vivo* functionality, PGLA-P(CL/LA) vascular grafts sealed with 10% P(CL/LA) (n=2) and 15% P(CL/LA) (n=2) were implanted

as inferior vena cava (IVC) interposition grafts in 8 week old female severe combined immunodeficiency beige (SCID/bg) mice (20-30 g) using microsurgical technique. Mice were anesthetized, placed in the supine position, and an abdominal midline incision was made. The IVC was exposed, cross-clamped, and excised. Grafts 3 mm in length were inserted and secured using a 10-0 nylon suture for the proximal and distal anastomoses. Mice were recovered from surgery and maintained without anti-platelet or anti-coagulation therapies.

Two weeks after the procedure, anesthetized mice were sacrificed. Grafts were excised and fixed in 10% neutral buffered formalin and embedded in OCT (Optimal Cutting Temperature) compound for frozen sectioning. Sections were stained with H&E stain. Graft luminal diameter was measured on histological specimens using ImageJ software (Image Processing and Analysis in Java; National Institutes of Health, Bethesda, MD, USA). Smooth muscle cell infiltration was identified with rabbit-anti-human SMA (Dako, Glostrup, Denmark). Antibody binding was detected using a goat-anti-rabbit IgG-Alexa Fluor 568 (Invitrogen, Carlsbad, CA, USA) with subsequent 4′,6-diamidino-2-phenylindole nuclear counterstaining. NIH guidelines (or for non-U.S. residents similar national regulations) for the care and use of laboratory animals (NIH Publication #85-23 Rev. 1985) have been observed

4.2.6 Statistical analysis

Data were analyzed using ANOVA single factor analysis assuming normal data distribution with a confidence of 95% ($p < 0.05$). Standard deviation error bars are reported on each figure along with relevant statistical relationships.

4.3 Results

4.3.1 Graft Characteristics

Grafts fabricated with 10% w/v P(CL/LA) solution possessed an inner lumen diameter of 1.02 $\pm$ 0.15 cm and a wall thickness of 0.21 $\pm$ 0.02 cm. Grafts made with sealant solutions of 15% w/v P(CL/LA) yielded an inner lumen diameter of 1.01 $\pm$ 0.08 cm and a wall thickness of 0.18 $\pm$ 0.09 cm. Dimensions are shown and compared in Figure 4.2 and structural images can be observed in Figure 4.3.
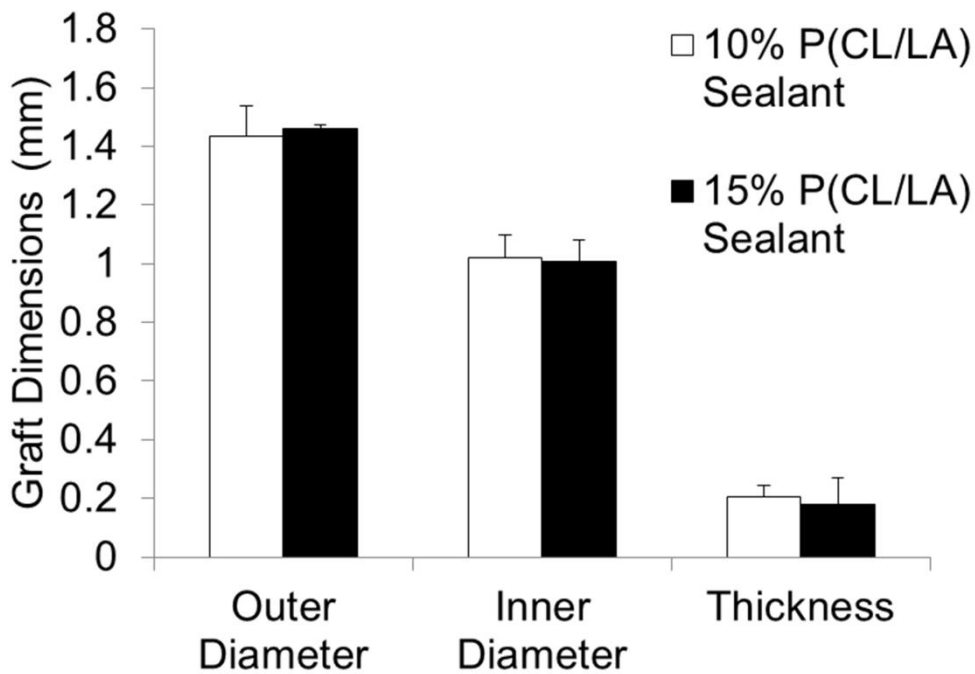
Figure 4.2 Dimensional data provided by SEM images of cross-sections cut from PGLA-P(CL/LA) grafts.

4.3.2 Mechanical Properties

Mechanical properties, including burst pressure, elastic modulus, and ultimate tensile strength were determined in order to ensure that grafts had the appropriate strength and elasticity to serve as vascular conduits. The ultimate tensile strength(UTS) of the grafts was found to be 2.93 $\pm$ 0.26 and 4.51 $\pm$ 0.97 MPa for 10% and 15% w/v P(CL/LA) solution sealed PGLA grafts, respectively. The elastic modulus for 10% P(CL/LA) sealed grafts was 17.73 $\pm$ 3.09 MPa and 15% P(CL/LA) sealed grafts was 26.90 $\pm$ 6.66 MPa. Ultimate tensile strength and elastic modulus before degradation can be observed in Figure 4.4 (A and B), respectively. Statistically significant differences were observed between the two graft groups.

After assessing circumferential tensile strength, burst pressure values were calculated. Graft cross sections appeared to tear first at the seam sealed by the P(CL/LA) solution. Burst pressures were approximated at 1002.17 $\pm$ 181.98 and 1321.66 $\pm$ 214.67 mmHg for 10% and 15% w/v P(CL/LA) solution sealed grafts. Results are shown in Figure 4.4 (C). 15% P(CL/LA) graft burst pressure were greater than 10% P(CL/LA) grafts, according to statistical significance.

Suture retention strength is crucial for the initial implantation of the grafts. Grafts sealed by 10% w/v P(CL/LA) sealed grafts were found to have a suture retention strength of 2.16 $\pm$ 0.37 N and 15% w/v P(CL/LA) sealed grafts

were 3.20 $\pm$ 0.577 N. Values for suture retention strength are shown in Figure

4.4 (D). Statistically significant differences were observed in suture retention

strength between 10% and 15% w/v P(CL/LA) sealed grafts.

Table 4.1 Mechanical properties of PGLA-P(CL/LA) grafts and human vessels commonly used in autologous transplants

Graft Type	Burst pressure (mmHg)	Modulus (MPa)	Ultimate tensile strength (MPa)	Suture retention strength (N)
PGLA w/ 10% P(CL/LA) sealant	1002.17 + 181.98	17.73 + 3.09	2.93 + 0.26	2.16 + 0.37 N
PGLA w/ 15% P(CL/LA) sealant	1321.66 + 214.67	26.90 + 6.67	4.51 + 0.97	3.20 + 0.577 N
Human saphenous vein[235–237]	1680-2273 mmHg	6.71 + 1.32	2.2 + 0.2	1.92 + 0.02 N
Human femoral artery[237–239]	2031-4225 mmHg	9-12	1-2	1.96 + 1.17 N
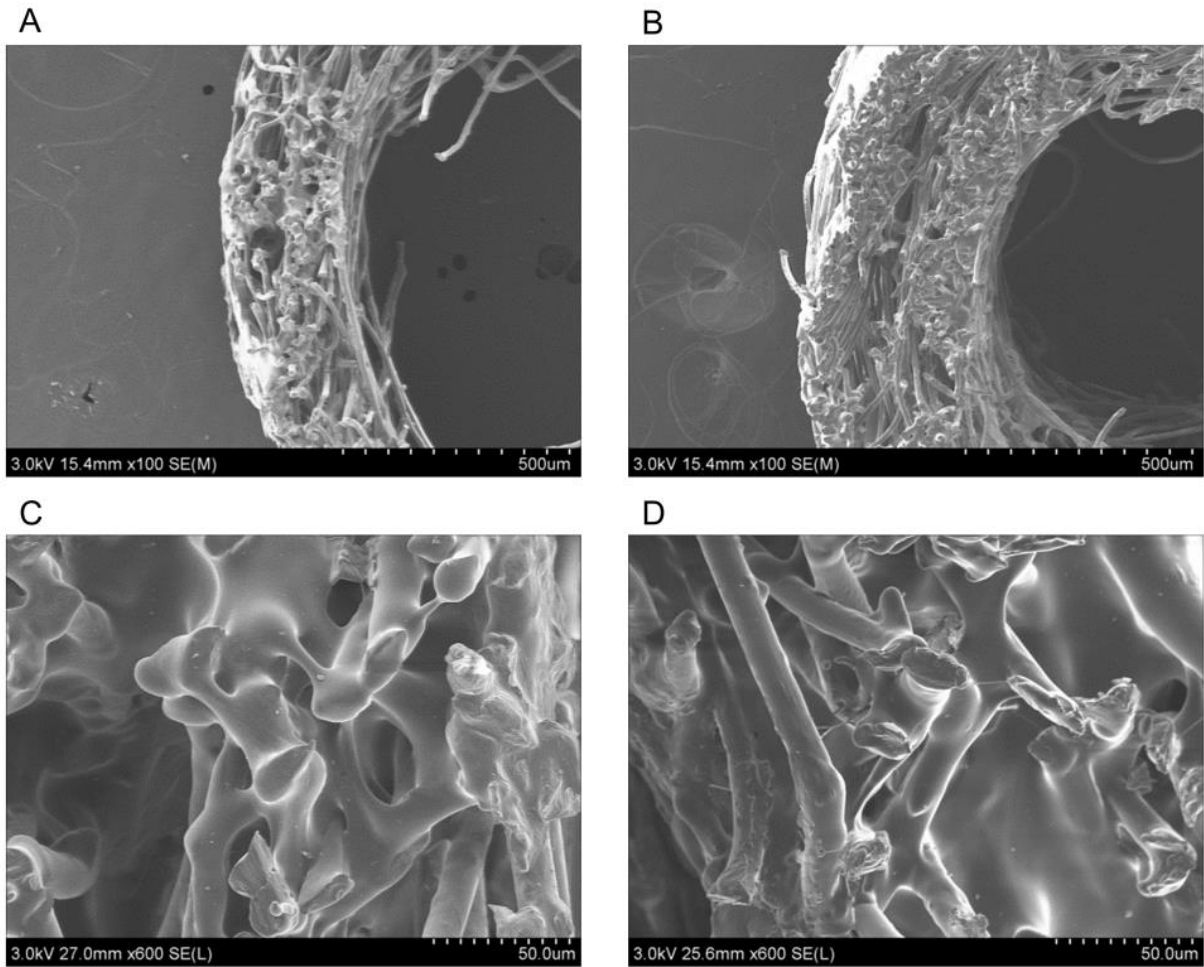
Figure 4.3 SEM images of vascular graft displaying structures formed by the PGLA sheet sealed with P(CL/LA). Grafts sealed with 10% (A and C) and 15% (B and D) P(CL/LA) solutions are shown.
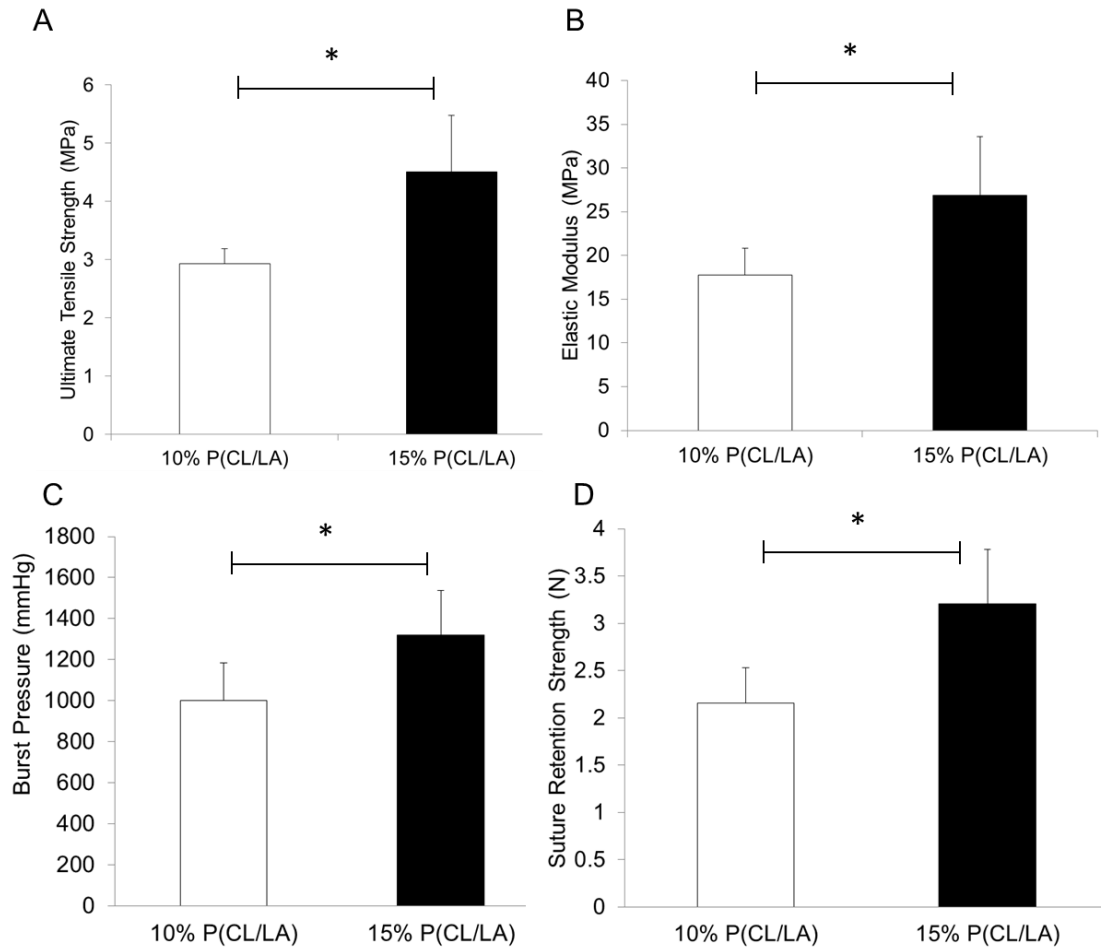
Figure 4.4 Comparison of mechanical properties, including (A) ultimate tensile strength, (B) elastic modulus, (C) burst pressure, and (D) suture retention strength of 10% and 15% P(CL/LA) solution sealed PGLA grafts. Statistically significant differences were observed between 10% and 15% P(CL/LA) grafts for each set of values. * : p < 0.05 between the two groups.

4.3.3 Degradation

Mass loss appeared minimal through the first two weeks of degradation. A significant decrease in mass was first observed after three weeks and continued steadily for the remainder of the observation period. Mass degradation is shown in (C). Throughout degradation, tensile strength was lost in both the 10% and 15% P(CL/LA) solution sealed grafts at a steady rate. Grafts appeared to retain only negligible UTS after three weeks, shown in Figure 4.5 (A). Additionally, the elastic modulus of the grafts decreased steadily over three weeks, though not as significantly as the UTS, as demonstrated in Figure 4.5 (B). Beside initial values, there were no statistically significant differences observed in the tensile strength or elastic modulus values between the 10% and 15% P(CL/LA) solution sealed grafts over the degradation period.
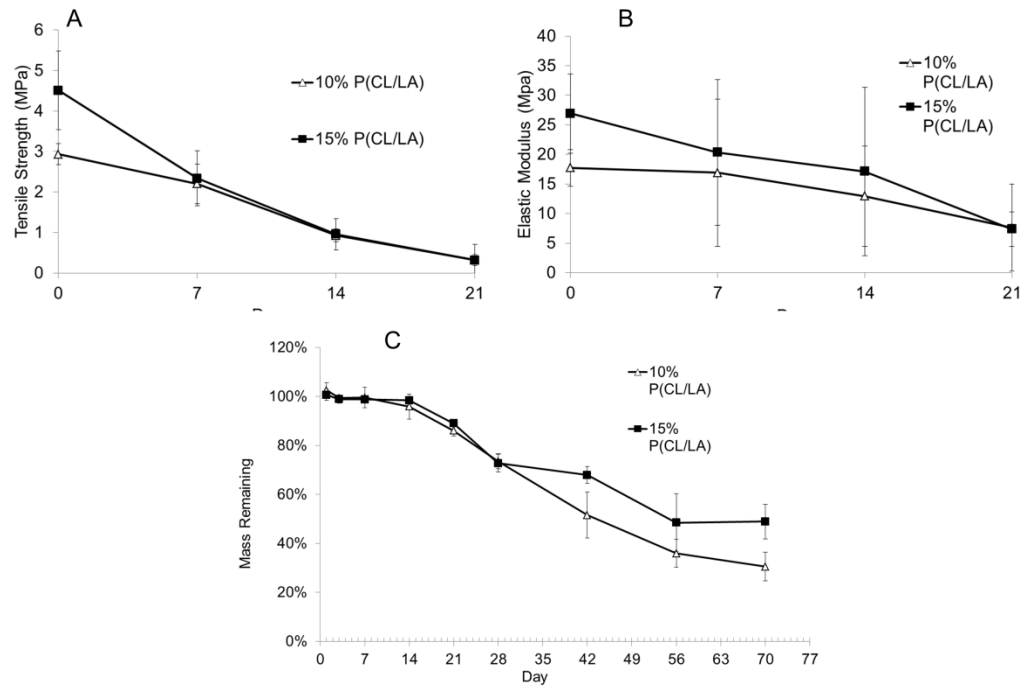
Figure 4.5 Comparison of mechanical properties during degradation between 10% and 15% P(CL/LA) solution sealed PGLA grafts. (A) Ultimate tensile strength and (B) elastic modulus values are shown. (C) Mass remaining of PGLA-P(CL/LA) grafts during degradation over 10 weeks.
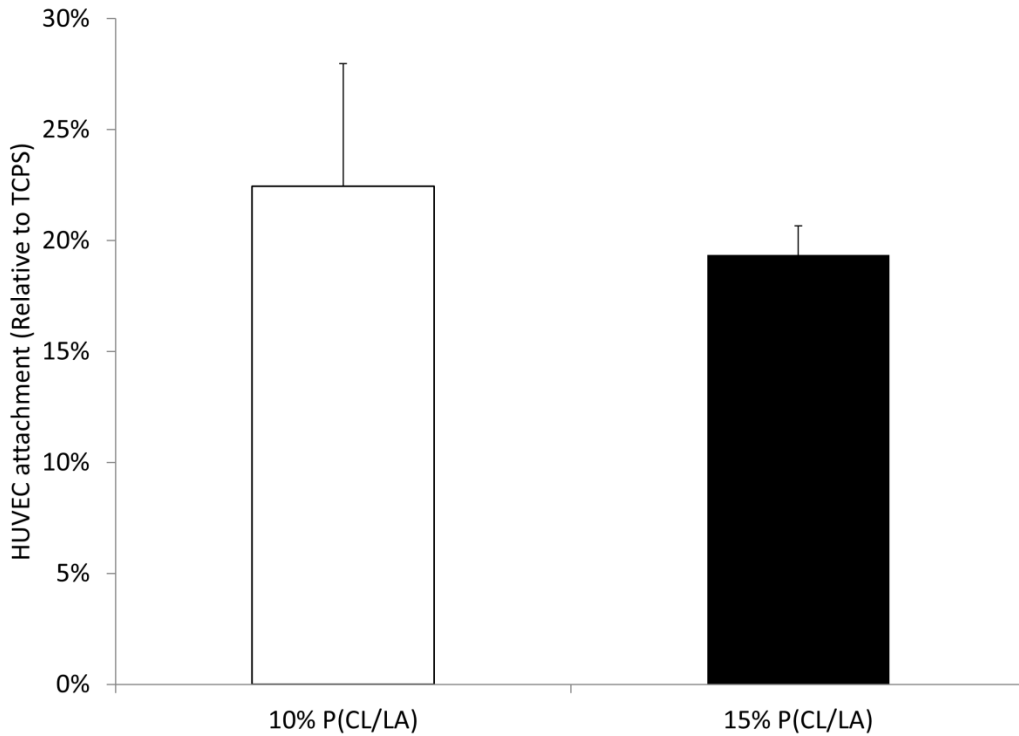
Figure 4.6 HUVEC attachment shown, normalized to TCPS. No statistically significant differences were observed between 10% and 15% P(CL/LA) solution sealed grafts.

4.3.4 Endothelial Cell Interactions

HUVEC attachment to the grafts 1.5 hrs after seeding was 22.44 $\pm$ 5.54% and 19.35 $\pm$ 1.32% for the 10% and 15% P(CL/LA) solution sealed grafts, respectively, when normalized to cell attachment on TCPS. Results are shown in Figure 4.6. Proliferation experiments showed expanding patches of HUVEC cell growth throughout the graft by day 7. HUVEC populations showed an increase in 10% and 15% P(CL/LA) grafts from day 1 to day 7 of 253.95 $\pm$

61.48% and 229.12 $\pm$ 54.44%, respectively. HUVEC attachment and

proliferation over 7 days is shown in Figure 4.7. While HUVEC attachment and

proliferation appeared slightly decreased in 15% P(CL/LA) grafts compared to

10%, no statistically significant differences were observed over the 7 day time

period. Both 10% and 15% P(CL/LA) grafts supported HUVEC attachment and
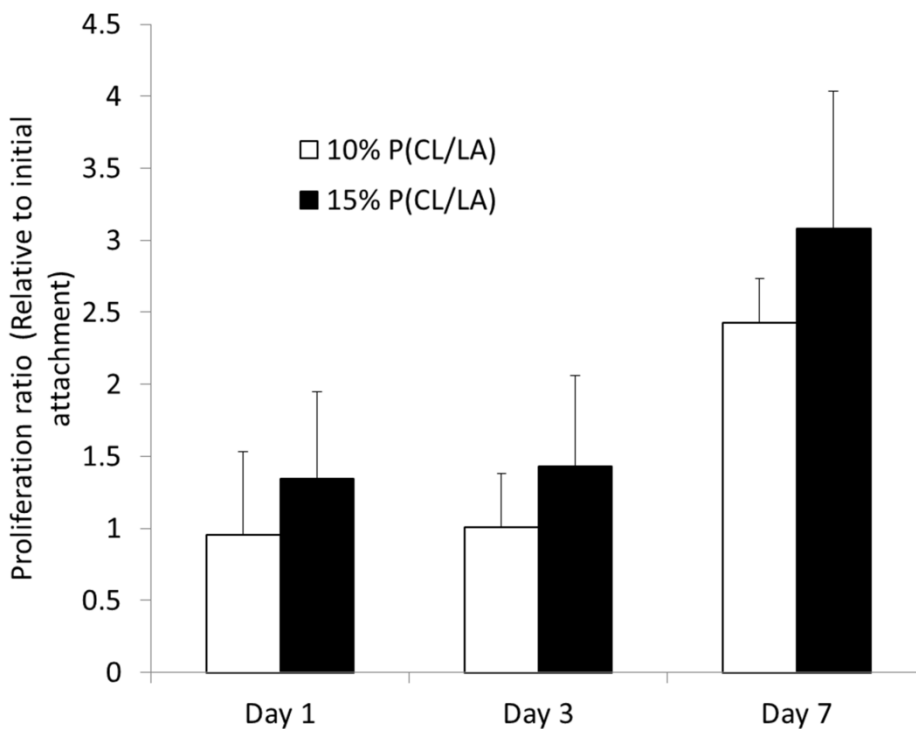
proliferation.

Figure 4.7. HUVEC proliferation on PGLA-P(CL/LA) grafts is observed over three timepoints. Grafts demonstrate HUVEC attachment and growth, with no statistical significance between 10% and 15% P(CL/LA) solution sealed PGLA grafts.

4.3.5 In Vivo Analysis

PGLA-P(CL/LA) grafts were successfully implanted as IVC interposition

grafts in SCID/bg mice. No evidence of thrombosis or graft aneurysm was

observed within the 2-week time point and grafts remained patent, as demonstrated by Figure 4.8 (A and B). Wall thickness appeared to be greater in the 15% P(CL/LA) solution sealed grafts (~1.16 mm) compared to 10% P(CL/LA) solution sealed grafts (~0.85 mm). The internal diameter of the PGLA-P(CL/LA) grafts was found to be ~1 mm. Grafts were infiltrated by cells and formation of extracellular matrix can be seen in Figure 4.8 (A and B). A thin monolayer of SMCs was observed on the luminal surface of the graft, indicating adequate porosity for cellular infiltration and neotissue formation. This early medial layer formation was observed in the grafts as evidenced in Figure 4.8 (C and D). All procedures involving animals were carried out in accordance with current institutional guidelines for the care and use of experimental animals.
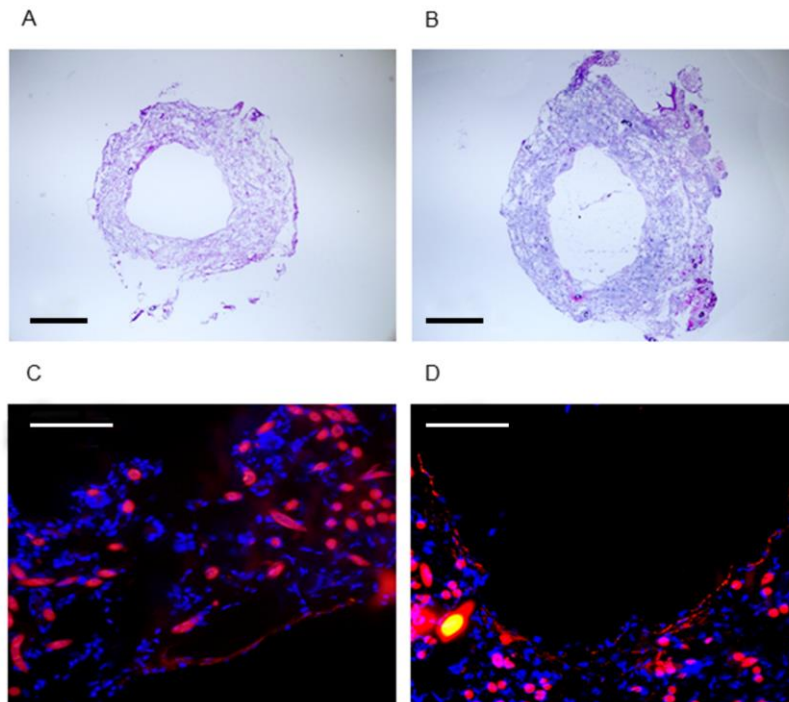
Figure 4.8 Neotissue formation shown by post-operative week 2. H&E stained (A) 10% and (B) 15% P(CL/LA) solution sealed grafts. SMCs can be observed infiltrating (C) 10% and (B) 15% P(CL/LA) solution sealed grafts. These cells are indicated by the small fluorescent red dots indicative of positive α-SMA staining along the inner lumen. Scale bars show 500 μm in (A) and (B); 100 μm in (C) and (D).

4.4 Discussion

The purpose of this study was to determine the characteristics of a small-diameter PGLA-P(CL/LA) vascular graft. We also investigated the effect of varying P(CL/LA) concentrations within the sealant solution used for graft fabrication. Through this analysis, we sought to determine if the PGLA copolymer grafts could offer a potential solution to stenosis, among other complications, experienced in other grafts fabricated in a similar manner.[233,240] We anticipated that the PGLA-based grafts would offer mechanical properties appropriately matched to native vascular properties, potentially offering graft performance favorably comparable to native blood vessels. Achieving these characteristics may reduce the mechanical disturbances presumably leading to intimal hyperplasia and graft stenosis.

PGLA-P(CL/LA) graft mechanical were comparable to native vessels commonly used in autologous transplantation procedures as determined by several prior studies. Previous studies have shown the ultimate tensile strength of native human femoral arteries to be 1-2 MPa and 2.2 ± 0.2 MPA for human saphenous veins.[236,238] The elastic modulus value was found to be 9-12 MPa for the human femoral artery and 6.71 ± 1.32 MPa for the human saphenous vein.[236,238] Burst pressure of a human saphenous vein was

1680-2273 mmHg and a human femoral artery was 2031-4225

mmHg.[235,237,239] The suture retention strength of a human saphenous

vein was found to be 1.92 ± 0.02 N and 1.96 ± 1.17 N for a human femoral

artery.[237] While values for the elastic modulus, ultimate tensile strength, and

suture retention strength compare favorably with the corresponding values in

native vessels, the calculated burst pressure of the PGLA-P(CL/LA) grafts is

weaker. Previous studies demonstrated that the seam of grafts fabricated with

this solvent cast method were observed to rupture first during burst pressure

testing.[232] Thus, the method utilized for circumferential tensile testing

ensured that the strength of the seam was tested. Tearing during testing often

occurred at the seam first. Qualitatively, this appeared to be the weakest

portion of the graft in the circumferential direction, resulting in the burst

pressures reported here. Despite this, grafts with similar burst pressure

strengths have been successfully implanted and maintained in animal

models.[241,242] The PGLA-P(CL/LA) grafts should be sufficiently strong

enough to allow for adequate vessel remodeling given the pilot *in vivo* test

success. The tensile strength of the PGLA-P(CL/LA) grafts decreased at a

relatively steady rate over 3 weeks, rather than experiencing a drastic decrease.

Initial mechanical analysis, combined with the *in vivo* assessments, suggests

that the degradation and change in mechanical properties may be adequate for

performance as a vascular graft.

Pilot *in vivo* studies demonstrated preliminary success of the PGLA-

P(CL/LA) grafts in a SCID/bg mouse model. The grafts were not seeded with

cells prior to implantation, but showed initial neotissue formation without stenosis. These preliminary animal procedures demonstrated the short-term biocompatibility of the grafts and implantability. Importantly, this mouse model also allows the implantation of grafts containing human vascular cells or components. While we did not seed our grafts with cells for this study, demonstrating the feasibility of graft implantation with the SCID/bg model will ensure future iterations with human biological or cellular components can be accurately assessed. The SCID/bg mouse model lacks an adaptive immune response, despite having a fully intact innate immune system. PGLA and PCL have not previously shown activation of the adaptive immune response.[243,244] Instead, these materials activate a foreign body response present in the innate immune system. Mechanical injury to the vessel incites the homing and adhesion of inflammatory cells into the intima.[245] This innate inflammatory response, present in this animal model, appears to play a crucial role in regulating endothelialization and intimal hyperplasia.[240,246–248] Prior studies have demonstrated the use of the SCID/bg mouse model for vascular grafting applications successfully.[240,249–252] Thus, the SCID/bg mouse appears to provide an adequate model for preliminary *in vivo* experiments.

In addition, a 2 wk time point was chosen to predict stenosis. A previous study utilizing similar surgical techniques and graft models recorded stenosis of grafts occurring at 2 weeks.[253] 2 weeks is a critical time to decide the fate of the graft. The group found that stenosis occurred via graft wall thickening,

as the luminal diameter of the grafts narrowed. The PGLA-P(CL/LA) grafts

maintained patency and inner lumen diameters at this time point and did not

exhibit the wall thickening documented by grafts experiencing stenosis in the

previous study.[253] According to our *in vitro* degradation tests, at 2 weeks, a

loss of tensile strength and elastic modulus were observed in the grafts.

However, the patency of the grafts *in vivo* suggested that tissue remodeling

after implantation prevented graft stenosis or graft aneurysm. The initial

modulus and UTS are also greater than values documented in native blood

vessels. According to *in vitro* degradation results, degradation of the grafts is

not only necessary for native tissue ingrowth, but also allows the PGLA-

P(CL/LA) grafts to better match mechanical properties of the native blood

vessels during remodeling. Biodegradation may have begun successfully as the

grafts integrated with extracellular matrix formation of vascular cells and

surrounding host tissue.

Overall, the PGLA-P(CL/LA) grafts appear to be a promising candidate for

small diameter vascular grafts due to their favorable mechanical properties,

degradation profiles, cytocompatibility, and pilot *in vivo* performance. This graft

demonstrates the flexibility of the needle/tube fabrication system described by

Roh et al to use alternative materials and custom dimensions for the graft.[232]

Besides physical customization of the graft, the PGLA-P(CL/LA) graft also offers

a solid platform for surface modification and functionalization. Both 10% and

15% P(CL/LA) grafts showed good biocompatibility and similar degradation

profiles. 10% P(CL/LA) grafts offer an elastic modulus more consistent with

native vessel values. In contrast, 15% P(CL/LA) grafts offer better burst pressure values and suture retention strength, benefiting early implantation procedures. The varied mechanical properties of these grafts would allow for customization of the graft system depending on the desired mechanical environment for graft implantation, such as carotid artery bypass versus peripheral artery disease. We are pursuing current studies to examine long-term (> 6 mo.) functionality of the grafts, including translation to a large animal model, and biofunctionalization via chemical surface modification to improve the *in situ* endothelialization of the PGLA-P(CL/LA) grafts.

4.5 Conclusion

We examined the performance of PGLA-P(CL/LA) vascular grafts with diameters of ~1mm. The grafts offered adequate mechanical properties, degradation profiles, and cytocompatibility. Preliminary animal studies demonstrated patency in the interposition grafts planted in the IVC. Early results from this study demonstrate the suitability of the PGLA-P(CL/LA) vascular graft as a platform for continued *in vivo* studies. While long-term animal studies will be necessary, these study provides early evidence that the PGLA-P(CL/LA) graft could be a candidate for future small-diameter vascular graft platforms.

Chapter 5: Contrasting *In Vivo* Endothelialization Strategies for Solvent-Cast Biodegradable Grafts[4]

5.1 Introduction

Cardiovascular disease is the leading cause of mortality worldwide.[1] To treat many of the conditions associated with cardiovascular disease, autologous vessels or synthetic grafts are often used. However, autologous vessels may be limited by existing conditions or previous surgeries.[223,224] In synthetic grafts, complications include lack of growth potential, calcification from secondary graft failure, increased susceptibility to infection, and increased risk for thromboembolic events and stenosis.[225,254] Tissue engineered vascular grafts (TEVGs) offer a potential strategy for overcoming these complications by providing a biodegradable scaffold for the autologous cells to attach, proliferate, and provide physiologic functionality. A scaffold that enables and encourages healthy vascular tissue growth while degrading over time would eliminate many of the complications associated with permanent, synthetic grafts. However, a primary mode of failure of small-diameter (<6 mm) TEVGs is graft stenosis due to neointimal hyperplasia and thrombosis.[23,25,231,254–256] Thus, a successful TEVG must prevent thrombosis and intimal hyperplasia. Since the endothelial layer of blood vessels is crucial for maintaining vascular homeostasis, prevention of intimal

---

[4] Adapted from: Melchiorri AJ, Hibino N, Yi T, Lee YU, Sugiura T, Tara S, Shinoka T, Breuer C, and Fisher JP. Contrasting biofuncationalization strategies for the enhanced endothelialization of biodegradable vascular grafts. Biomacromolecules. 2015 Jan; 16(2): 437-446.

hyperplasia, and thrombogenesis, the establishment of an endothelial cell (EC) monolayer that adequately covers the inner lumen of a TEVG is crucial to the graft's long-term success.[38,225,257] Rapid establishment of such a layer may alleviate the current challenges associated with biodegradable vascular grafts.

Establishing a monolayer of ECs on a TEVG can be accomplished via cell seeding and culturing before implantation. Grafts with a precultured endothelium before implantation perform well *in vivo* and demonstrate reduced complications traditionally associated with small-diameter vascular grafts.[258–261] However, cell seeding of these grafts can be time consuming, expensive, and clinically difficult.[262]

In an effort to expedite endothelialization and eliminate the challenges associated with cell seeding, researchers have investigated a variety of *in situ* endothelialization strategies.[38,257] These strategies have largely focused on recruiting and promoting the attachment and proliferation of ECs and endothelial progenitor cells (EPCs) on the inner lumen of grafts after implantation. The exact role of EPCs in endothelialization is still under debate, but both early and late EPCs show positive effects on *in vivo* endothelialization of vascular prosthetics.[75,155,156] Early EPCs may secrete angiogenic cytokines to support other EPCs and ECs, while late EPCs possess the potential for proliferation and EC colony formation.[52,75] While identification methods for EPCs should still be standardized, a common marker of EPCs is CD34.

To take advantage of the *in situ* endothelialization potential of ECs and EPCs, we focus on two strategies of vascular graft modification: (1) antibody immobilization and (2) growth factor loading. Antibody immobilization strategies primarily function to improve cell attachment to graft surfaces, while vascular endothelial growth factor (VEGF) loading and subsequent elution may induce cell mobilization into the blood along with migration from neighboring tissues. A variety of specific and non-specific molecules have been investigated to induce cell capture and attachment. One such biofunctional molecule, an antibody against CD34 (CD34Ab), has been used to induce endothelialization of permanent vascular stents through the increased attachment of both ECs and EPCs.[70,263,264] Including such an antibody may aid in the recruitment and attachment of neighboring ECs and EPCs. However, CD34$^+$ vascular cells represent a small percentage of cells in circulation.[75]

To increase the available numbers of EPCs in circulation, it may be necessary to introduce a mobilizing factor. For example, VEGF may increase the fraction of EPCs in circulation.[265] In addition, bound VEGF may influence EPC differentiation into mature EC-like phenotypes, while increasing the migration and proliferation of ECs.[150,266–268] Besides its influence on EPCs, diffusion of VEGF may also induce the migration and proliferation of resident ECs from mature vessels across anastomotic sites.[94,269] VEGF has been successfully delivered via scaffolds utilizing specific binding motifs present in heparin.[270–272] Crosslinked heparin also protects the bioactivity of bound proteins, which may increase the efficacy of VEGF delivery.[273] For

example, heparin molecules crosslinked to a polycaprolactone scaffold mediated VEGF loading and diffusion to successfully promote increased angiogenesis over unmodified PCL scaffolds[271]. In addition, heparin has antithrombotic properties conducive to minimizing thrombosis associated with the implantation of small-diameter vascular grafts, especially in localized dosages.[274]

We sought to expedite and improve the endothelialization of a biodegradable small-diameter vascular graft by assessing two coating strategies that utilized heparin-crosslinked surfaces to either load VEGF or immobilize CD34Ab. By utilizing these biomolecules, we were particularly interested in studying which strategy was more conducive to the endothelialization of these biodegradable polymeric grafts. We examined whether an initial burst release of VEGF or surfaces modified with CD34Ab would lead to more efficient and effective endothelialization of heparin-crosslinked vascular grafts. The effects of modified graft surfaces were characterized and tested by examining HUVEC and EPC attachment and proliferation in cell culture assays and an *in vivo* mouse model to assess endothelialization.
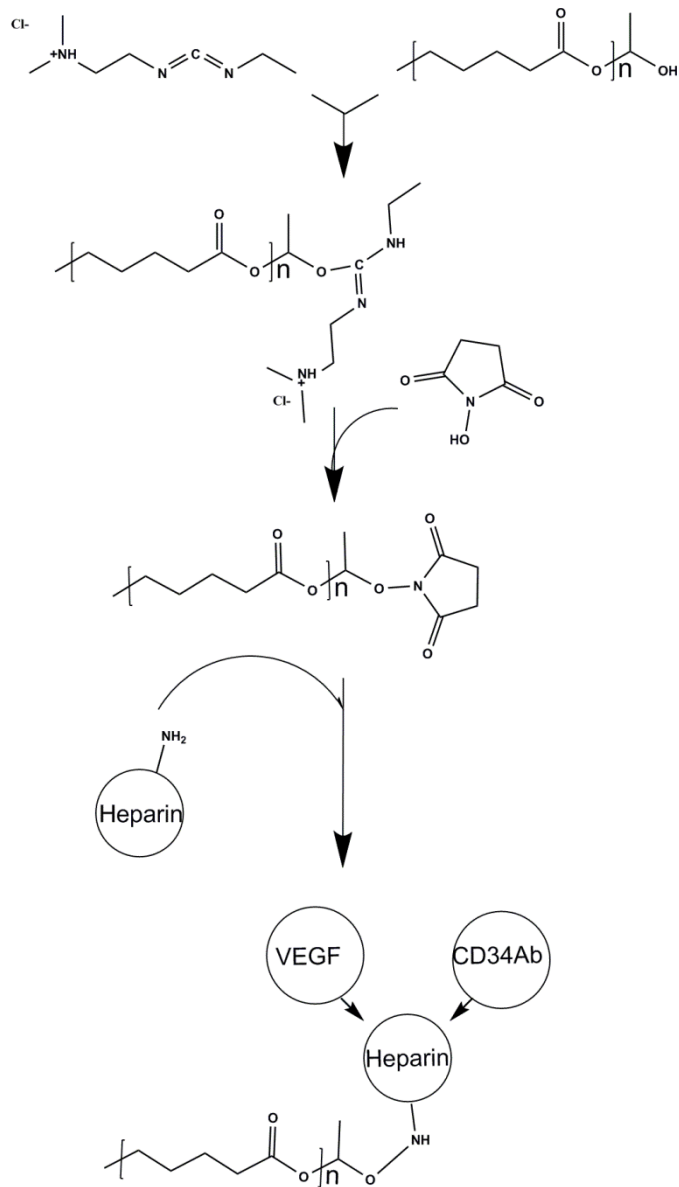
Figure 5.1 Graft Modification Scheme. EDC chemistry reaction for the crosslinking of heparin and subsequent loading and immobilization of VEGF and antibodies against CD34.

5.2 Materials and Methods

5.2.1 Graft Fabrication

The method of fabrication utilizes a solvent-casting technique described and characterized in previous studies.[232,275] Briefly, 6.00 x 4.00 mm sections were cut from a 90:10 poly(glycolic-co-lactic acid) (PGLA) for *in vitro* assays and poly(glycolic acid) (PGA) polymer BIOFELT (Biomedical Structures, Warwick, RI) for *in vivo* tests. The PGLA sections were inserted into a polypropylene tube with an inner lumen diameter of 1.4 mm and a 21-g stainless steel needle was inserted into the opposite end of the tube to maintain the patency of the inner lumen of the graft. Then, a 40:60 copolymer poly(caprolactone-co-DL-lactic acid) (PCLLA) solution of 15% w/v in 1,4-dioxane was deposited into the polypropylene tubes to saturate the PGLA or PGA felt. Grafts were subsequently frozen at -20° C for 30 min, followed by freeze-drying for 24 h to eliminate excess 1,4-dioxane solvent. After complete drying, grafts were stored at -20° C until used.

5.2.2 Graft Modification Procedures

Modified grafts utilized heparin cross-linking to immobilize VEGF or CD34Ab. We assessed the initial loading and retention of VEGF and CD34Ab on heparin crosslinked surfaces.

5.2.2.1 Heparin Crosslinking

Heparin crosslinking and quantification was adapted from a previously published method[271]. Crosslinking chemistry is demonstrated in Figure 5.1. Before crosslinking, scaffolds were immersed in 0.05 M MES buffer (pH = 5.55) for 15 minutes. Scaffolds were subsequently submerged in a solution of 0.5 M

ethyl-3-(3-dimethylaminopropyl)-carbodiimide) (EDC), 0.5 M N-

hydroxysuccinimide (NHS), and 1% w/v heparin in MES buffer. After

incubation for 14 hours, scaffolds were washed with distilled water to remove

excess byproducts.

5.2.2.2 VEGF Loading

A sterile solution of VEGF was prepared in PBS at a concentration of 500

ng/ml, according to previously published methods[125]. Scaffolds were

incubated in the VEGF solution for 1 hour, in sterile conditions, at room

temperature. Following incubation, grafts underwent eight 5 min washes in

sterile-filtered PBS solution to remove unbound VEGF.

5.2.2.3 CD34 Antibody Immobilization

For CD34Ab coating, heparin cross-linked grafts were immersed in 10

μg/mL solutions of primary antibody against CD34 in PBS overnight at 4° C in

the dark. Grafts were then washed 3 times with PBS.

5.2.3 Surface Modification Characterization

5.2.3.1 Scanning Electron Microscopy

The topographies of the modified and unmodified grafts were visualized

by a scanning electron microscope (SEM; Hitachi, Tokyo, Japan). Grafts (n=5)

were cut into sections 1 mm in length and fixed with 2% gluteraldehyde and

underwent subsequent serial dehydration in ethanol. Samples were then

allowed to dry and were subsequently mounted and sputter coated with carbon

before SEM examination.

5.2.3.2 Toluidine Blue Staining Assay

Cross-linked heparin was confirmed via a toluidine blue stain assay. A 0.0005% (w/v) toluidine blue zinc chloride double salt solution was prepared in 0.001 N hydrochloric acid with 0.02% (w/v) sodium chloride. Heparin crosslinked and unmodified scaffolds were incubated in the toluidine solution overnight at room temperature. A deep purple hue on the surface of scaffolds indicated the presence of heparin, while unmodified scaffolds remained white.

5.2.3.3 VEGF ELISA

To quantify VEGF attachment and release, a human VEGF ELISA kit (Sigma) was used according to manufacturer instructions. Briefly, standard VEGF curves were created according to manufacturer instructions and added to a 96-well plate coated with capturing antibodies (human VEGF-A). Samples for bound VEGF quantification were placed in the wells of a 96-well plate and served as the binding substrate for incubation with the 200 µl biotinylated anti-human VEGF detection antibody (100 ng/ml). Next, 200 µl of streptavidin-horse radish-peroxidase solution was added to each well and the plates were incubated for 45 minutes at room temperature. Following this, 100 µl of tetramethylbenzidine (TMB) solution was added and plates were subsequently incubated for 30 min in the dark at room temperature. The reaction was stopped by adding 50 µl of 2N H_2SO_4 "Stop" solution. The optical density (OD) of the resulting solutions was measured using a SpectraMax M5 plate reader at 450 nm with a reference wavelength of 650 nm. Values of VEGF immobilized on scaffolds were calculated from the standard curve. For VEGF release,

scaffolds with bound VEGF were incubated in PBS at 37º C with 65 rpm shaking. The PBS was collected at 1 h, 4 h, 24 h, and 40 h and replaced with fresh PBS. VEGF released into the solution was quantified using the previously described ELISA methods. In addition, non-specific binding of VEGF was assessed by incubating VEGF with graft surfaces as described, except no crosslinking of heparin was performed.

5.2.3.3 CD34 Ab Fluorescence Assay and ELISA

To confirm antibody immobilization, antibody-modified and unmodified scaffolds were incubated at room temperature with 1% bovine serum albumin solution for 30 min at room temperature to prevent non-specific binding. Scaffolds were then washed 3 times with PBS and a secondary anti-goat IgG antibody conjugated with FITC was added at 10 µg/mL in PBS. Scaffolds were again washed 3 times with PBS. Successful antibody immobilization could be observed using fluorescent microscopy. To quantify antibody attachment, a Goat IgG ELISA kit (Alpha Diagnostic International, San Antonio, TX) was used. The procedure followed manufacturer instructions, substituting CD34 antibodies instead of the IgG standards included with the kit. In addition, non-specific binding of CD34Ab was assessed by incubating CD34Ab with graft surfaces as described, except no crosslinking of heparin was performed.

5.2.4 In Vitro Adhesion and Proliferation

In vitro cell culture assays were used to assess initial cell attachment and metabolic activity over time to assess differences between CD34Ab- and VEGF-modified grafts compared to controls in 96-well tissue culture plates.

5.2.4.1 Human Umbilical Cord Vein Endothelial Cells (HUVEC)

HUVEC were obtained and cultured according to manufacturer's instructions (Lonza, Basel, Switzerland). Grafts were cut to fit 96-well tissue culture plate and placed in the bottom of the wells. Culture plates with CD34Ab-immobilized, heparinized control and unmodified control grafts were sterilized under ultraviolet (UV) irradiation for 1 hr. Grafts intended for VEGF-modification were UV irradiated before loading with sterile solution VEGF. Cells were seeded in the wells at a density of 5×10^4 cells/well and incubated at 37° C. To measure cell metabolic activity, an XTT assay was performed at 1.5 hrs, 1 day, 3 days, and 7 days after initial cell seeding. At each of these time points, cells also underwent Live/Dead staining and were counted via microscopy. Cell attachment numbers were defined by the total number of cells still adhered to graft surfaces after washing. Attachment percentage was calculated by comparison with the total cell numbers seeded on grafts which was normalized to total cells attached to separate tissue culture polystyrene (TCPS) controls. Fold change in cell populations was calculated by dividing the final cell population count (Day 7 time point) by the initial attachment number (1.5 hrs after seeding).

5.2.4.2 Endothelial Progenitor Cells (EPC)

Human EPCs were obtained and cultured according to the manufacturer's instructions (CelProgen, San Pedro, CA). Methods for assessment were identical to HUVEC assays.

5.2.4.3 XTT Assay

XTT assays were performed according to the manufacturer protocols (Roche Diagnostics, Indianapolis, IN). In summary, each cell-containing well of the 96-well plates was washed with PBS. 50 µl of XTT labeling mixture was added, along with 50 µl of culture medium. The plate was incubated at 37° C for 4 hours. Following incubation, the supernatant was transferred to a new plate. Absorbance of the supernatant was measured at 450 nm, with a 650 nm reference.

5.2.4.4 Real-time Polymerase Chain Reaction

HUVECs and EPCs were cultured separately in 6-well plates on grafts without modifications, with heparinization, with VEGF, or with CD34Ab (n=3). Cells were seeded at a density of 3×10^5 cells/well to ensure adequate RNA content for PCR analysis. RNA was extracted with an RNeasy kit (Qiagen, Dusseldorf, Germany) at 1, 3, and 7 days to be compared with initial RNA content isolated from cell samples immediately before seeding. Real-time PCR analysis was performed using a SYBR Green One-Step RT-PCR Kit (Qiagen). Reference numbers for primers are: eNOS (NM_000603), VEGF (NM_001025366), and GAPDH (NM_001256799). The results were analyzed using the comparative threshold cycle method and normalized with GAPDH as an endogenous reference, and reported as relative values ($\Delta\Delta$CT) to those of control.

5.2.5 In Vivo Implantation

All animal procedures were approved by the Nationwide Children's Hospital Institutional Animal Care and Use Committee. An *in vivo* trial was

performed in a manner adapted from a previous experiment we performed[275]. Briefly, grafts (1 mm in diameter and 3 mm in length) were implanted in female mice 6-8 wks of age as inferior vena cava (IVC) interpositional grafts using microsurgical technique. Grafts with VEGF- (n=10) or CD34Ab-modified surfaces (n=10), and unmodified surfaces (n=10) were used. All grafts, after modification, were UV irradiated to sterilize them onsite before implantation. Mice were anesthetized, placed in the supine position, and an abdominal midline incision was made. The IVC was exposed, cross-clamped, and excised. Grafts were implanted using a 10-0 nylon suture for the proximal and distal anastomoses. Mice were recovered from surgery and maintained without antiplatelet or anticoagulation therapies.

Two weeks after the procedure, mice were anesthetized and sacrificed. After excision, grafts were fixed in 4% para-formaldehyde and embedded in paraffin for histology, or embedded in optimal cutting temperature (OCT) compound (Tissue-Tek; Sakura Finetek, Torrance, CA, USA) for gene assay. Five micron thick sections were then stained with hematoxlyin and eosin (H&E) stain. Endothelial cells were identified with rabbit anti-CD31 (Abcam, MA, USA). Antibody binding was detected using biotinylated secondary antibodies, followed by binding of streptavidin-HRP. Color development was performed by a chromogenic reaction with 3,3-diaminobenzidine (Vector, CA, USA). Graft inner and outer diameters were measured using ImageJ software calculated from perimeter measurements. Nuclei were counterstained with hematoxylin. Explanted grafts frozen in OTC compound were sectioned into twenty 30 μm

sections using a Leica CM 1950 cryostat (Leica biosystems, Wetzlar, Germany). Excess OCT compound was removed by centrifugation in PBS. Total RNA was extracted and purified using the RNeasy mini kit (Qiagen) according to the manufacturer instructions. Reverse transcription was performed using High Capacity RNA-to-cDNA Kit (Applied Biosystems, CA, USA). All reagents and instrumentation for gene expression analysis were obtained from Applied Biosystems. Quantitative polymerase chain reaction (qPCR) was performed with a Step One Plus Real-Time PCR System using the TaqMan Universal PCR Master Mix Kit. Reference numbers for primers are: eNOS (Mm00435217_ml), VEGF (Mm01281449_m1), and HPRT (HPRT; Mm00446968_m1). The results were analyzed using the comparative threshold cycle method and normalized with HPRT as an endogenous reference, and reported as relative values ($\Delta\Delta$CT) to those of control. NIH guidelines for the care and use of laboratory animals (NIH publication #85-23 Rev. 1985) have been observed.

5.2.6 Statistical Analysis

Data were analyzed using analysis of variance single factor analysis with Student's *t*-test or ANOVA assuming normal data distribution with a confidence of 95% ($p < 0.05$). Standard deviation error bars are reported on each figure along with relevant statistical relationships.

5.3 Results

5.3.1 Quantitative Assessment of Immobilized CD34 Antibodies and VEGF

The morphology of the grafts was analyzed via SEM images because biomaterial interactions can be influenced by nanometer-scale surface features[106,276]. Figure 5.2 displays the acellular graft surfaces after the VEGF and CD34Ab modifications. While the surface features of the experimental groups appear rougher than the control grafts, there is not a discernible visible difference between surface patterns on each of the modified surfaces. The process of heparinization of graft surfaces appears to introduce round grain formations onto the material. Heparin attachment was confirmed via toluidine blue assay. CD34Ab attachment was confirmed via secondary FITC-Ab attachment and ELISA. ELISA was also used to confirm successful VEGF attachment.

First analyzing loading efficiency of VEGF, ELISA results demonstrated that VEGF modifications produced 3.08 ± 0.33% VEGF loading efficiency. CD34Ab loading efficiency was 23.57 ± 0.62%. The elution rates of the VEGF from the heparin-crosslinked TEVG surfaces can be seen in Figure 5.3. In 24 hours, 28.0 ± 2.9% of the VEGF remained on the VEGF-modified surfaces. CD34Ab retention after 24 hours showed 99.3 ± 0.20% of the antibody remained on CD34Ab-modified surfaces. Non-specific adsorption of biofunctional molecules was also determined. After incubating biofunctional molecules without heparin/EDC crosslinking and subsequent thorough

washing only 1.56 ± 0.47% of the antibody was still adsorbed. In comparison, 34.08 ± 16.64 % of total VEGF was found to be non-specifically adsorbed.
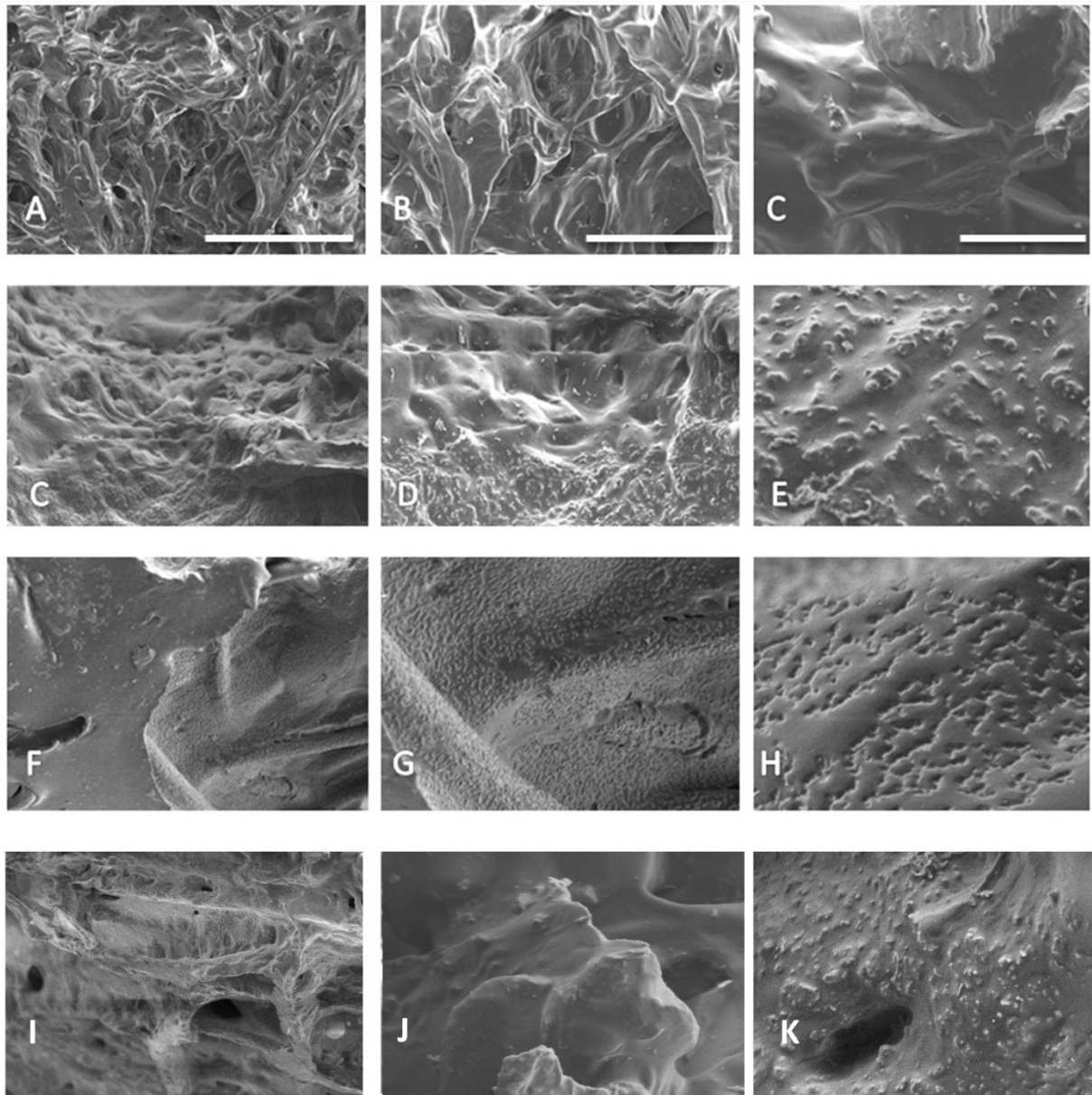
Figure 5.2 Graft surfaces before and after modification. Control (A-C), CD34Ab-modified (C-E), VEGF-modified (F-H), and heparin-only (I-K) are shown. Scale bars represent 100 µm (A,C,F,I), 40 µm (B,D,G,J), and 10 µm (C,E,H,K), respectively.
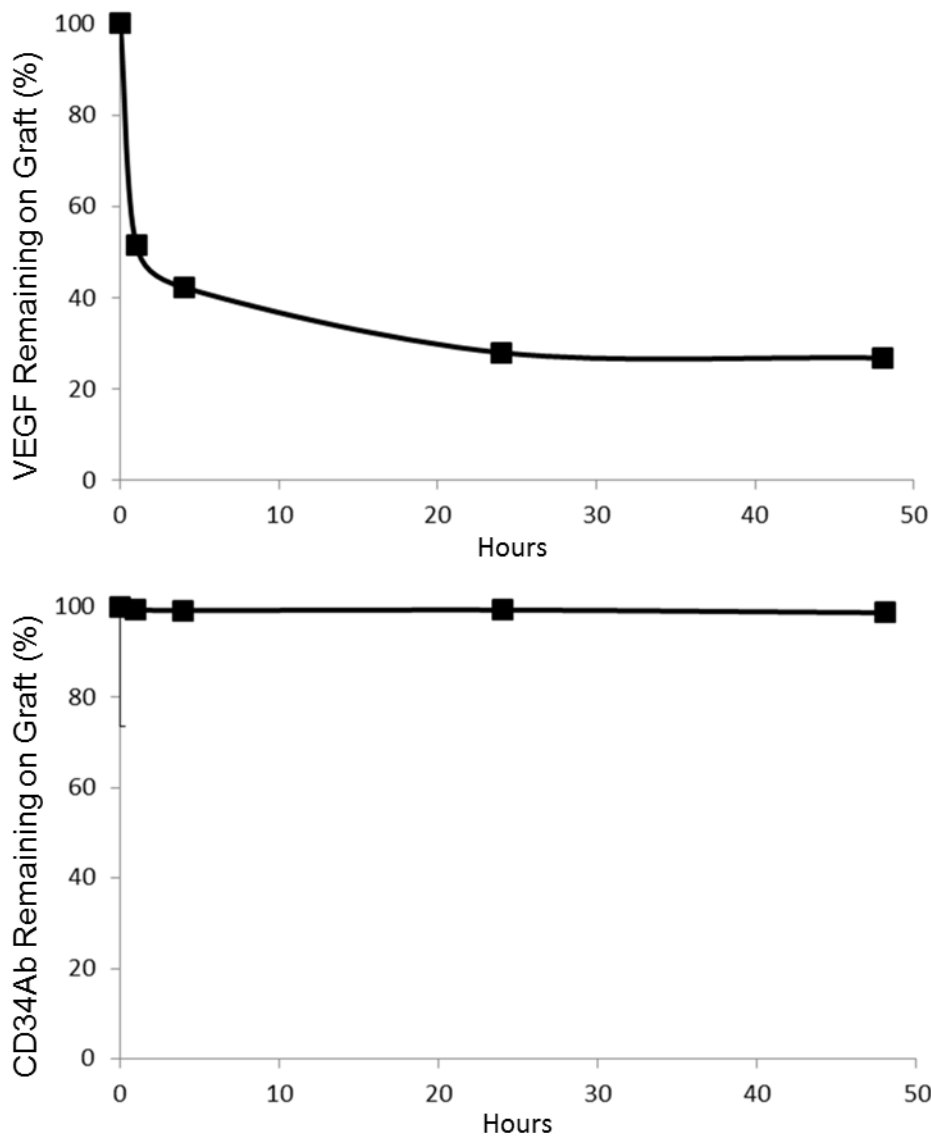
Figure 5.3 Persistence of biomolecules on graft surface. (A) VEGF and (B) CD34Ab percent of initially loaded molecules remaining on TEVGs over various timepoints. Grafts were incubated in PBS at 37°C, undergoing gentle shaking to investigate burst release of loaded biofunctional molecules within the first 48 hrs. n=3 for all time points.

5.3.2 EC and EPC Response to Modified TEVG Surfaces

Total metabolic activity of HUVECs and EPCs results are shown in Figure

5.4. CD34Ab-modified grafts demonstrated a statistically significant increase of

total HUVEC metabolic activity over control grafts on day 3, although there was no difference between CD34Ab- and VEGF-modified grafts ($p < 0.05$). Otherwise, there was no discernable difference between total metabolic activity of HUVEC populations over the 7 days on the modified and unmodified grafts. For total EPC metabolic activity, both CD34Ab-modified grafts demonstrated an increase over unmodified control and VEGF-modified TEVG surfaces at days 0 and 1 after initial cell seeding. At 7 days, only VEGF-modified grafts demonstrated a significant increase of total EPC metabolic activity compared to the control, although there was no difference between VEGF- and CD34Ab-modified grafts. Total metabolic activity of attached cells experienced no differences between heparin-only and unmodified controls, except on day 3 when total HUVEC metabolic activity was decreased on heparin-only grafts compared to unmodified controls.

CD34Ab-coated grafts demonstrated higher initial HUVEC and EPC attachment than control and VEGF-modified grafts. Both VEGF- and CD34Ab-modified grafts demonstrated a greater HUVEC population than the unmodified controls at day 1. On day 3, EPCs demonstrated greater cell numbers on CD34Ab grafts than the control. Additionally, CD34Ab-modified surfaces demonstrated a greater EPC population than both VEGF-modified and unmodified control grafts on day 7. Heparin-only controls demonstrated no differences than controls, other than a decrease in attached HUVEC populations on day 1. Figure 5.5 displays all Live/Dead counting results. Table 5.1 summarizes the initial attachment of cells to various graft surfaces and

Table 5.2 displays the proliferation of total cell populations attached to cell

grafts after 7 days.

Table 5.1. Initial attachment percentage of cells on graft surfaces normalized to tissue culture polystyrene. * Indicates statistical significance compared to control graft surfaces ($p < 0.05$).

Graft-Type	HUVEC	EPC
Control	21.34 ± 10.24	28.06 ± 11.33
Heparin Only	22.24 ± 8.98	33.17 ± 6.50
VEGF	28.23 ± 7.32	41.07 ± 6.74
CD34Ab	40.69 ± 10.69*	53.51 ± 17.32*

Table 5.2 Fold change of cells over 7 days.

Graft-Type	HUVEC (Fold Change)	EPC (Fold Change)
Control	4.00 ± 1.93	5.22 ± 2.41
Heparin Only	4.13 ± 1.76	5.33 ± 1.11
VEGF	4.39 ± 0.50	5.23 ± 0.79
CD34Ab	2.98 ± 0.61	7.02 ± 1.43
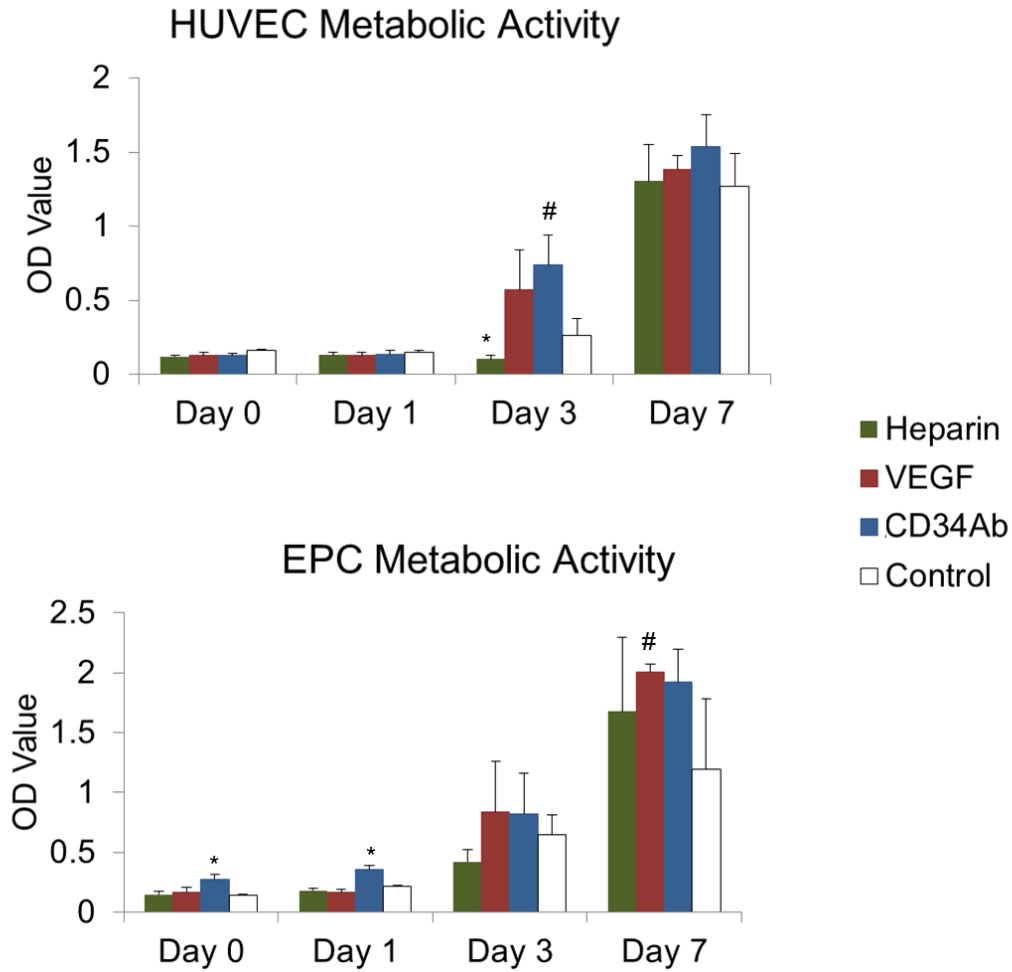
Figure 5.4 Total metabolic response to heparin-only, VEGF, and CD34Ab Modified Grafts. (Top) HUVEC metabolic activity measured via relative absorbance of XTT media. (Bottom) EPC metabolic activity measured via relative absorbance of XTT media. Please note that n = 4; * represents statistical significance compared to all other groups within the time point, # represents statistical significance compared to the unmodified control of that time point, & represents statistical significance compared to the heparin-only control of that time point ($p < 0.05$).
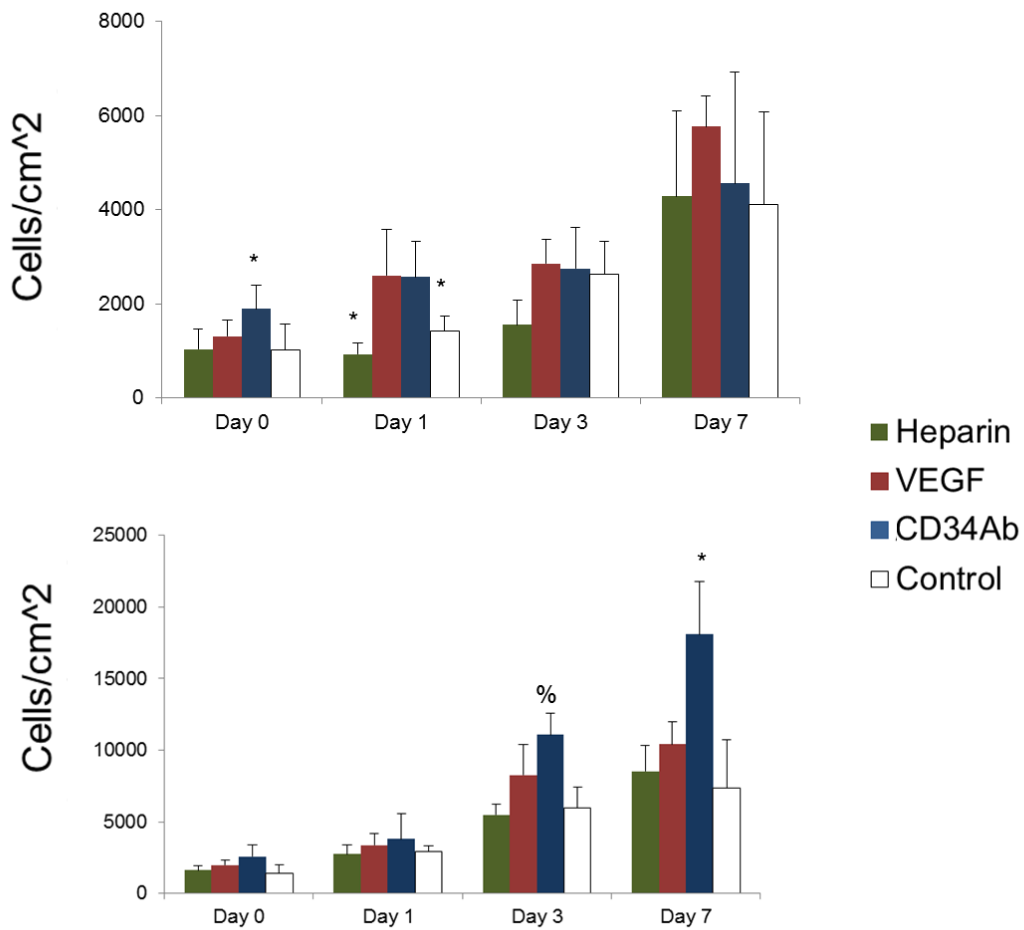
Figure 5.5 Cell attachment and proliferation on heparin-only, VEGF, and CD34Ab Modified Grafts. (Top) HUVEC population counted via Live/Dead. (Bottom) HUVEC population counted via Live/Dead. Please note that n = 4; * represents statistical significance compared to all other groups within the time point, %represents statistical significance compared to the heparin-only and unmodified control of that time point ($p < 0.05$).
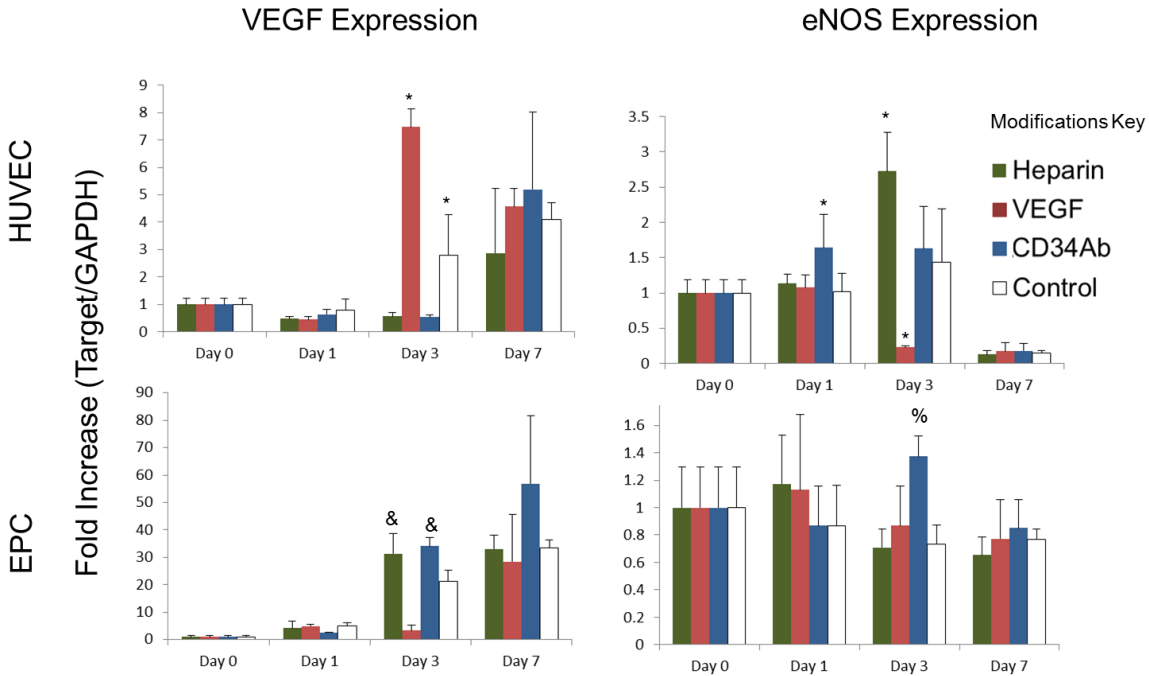
Figure 5.6 mRNA Expression of Cells on heparin-only, VEGF, and CD34Ab Modified Grafts. (Top) HUVEC mRNA expression of VEGF (Left) and eNOS (Right). (Bottom) EPC mRNA expression of VEGF (Left) and eNOS (Right). Please note that n = 3; * represents statistical significance compared to all other groups within the time point, & represents statistical significance compared to the VEGF and unmodified control of that time point , % represents statistical significance compared to the heparin-only and unmodified control of that time point ($p < 0.05$).

According to PCR results as summarized in Figure 5.6, HUVECs attached to CD34Ab grafts expressed an increased mRNA fold change in eNOS genes compared to other groups on day 1. On day 3, HUVECs on VEGF-modified grafts produced the most significantly increased fold change in VEGF gene expression compared to other grafts, while eNOS gene expression was

114

significantly reduced. In addition, on day 3, both heparin-only and CD34Ab grafts demonstrated higher fold change in VEGF expression of attached EPCs compared to VEGF-modified and unmodified grafts. EPCs attached to CD34Ab grafts also demonstrated significantly higher expression of eNOS on day 3. There were no significant differences between graft surfaces on day 7.

5.3.3 In Vivo Assessment of Modified Grafts

All modified grafts demonstrated a larger inner lumen diameter compared to control grafts after two weeks of implantation. Luminal cross-sectioned examples of retrieved grafts can be seen in Figure 5.7. Overall, grafts modified with CD34Ab resulted in a greater inner lumen diameter after two weeks of implantation compared to unmodified grafts and VEGF-modified grafts. Both VEGF- and CD34Ab-modified grafts retained larger inner diameters compared to controls. CD34Ab-modified grafts also demonstrated greater outer diameter compared to unmodified control grafts. In addition, antibody-modified grafts maintained a smaller wall thickness compared to VEGF-modified and unmodified grafts. Wall thicknesses are compared in Table 5.3. Similarly, qPCR analysis of explanted CD34Ab modified grafts demonstrated significantly higher gene expression of eNOS compared to control. VEGF grafts were not significantly different in terms of eNOS expression compared to explanted control graft samples. The three groups, when compared, did not demonstrate any significantly different levels of VEGF gene expression. Results are summarized and compared in Figure 5.8. CD31 staining (a marker for endothelial cells) demonstrated the formation of an

endothelium in modified grafts, as shown in Figure 5.9. Endothelial formation was especially prominent in grafts modified with CD34Ab.
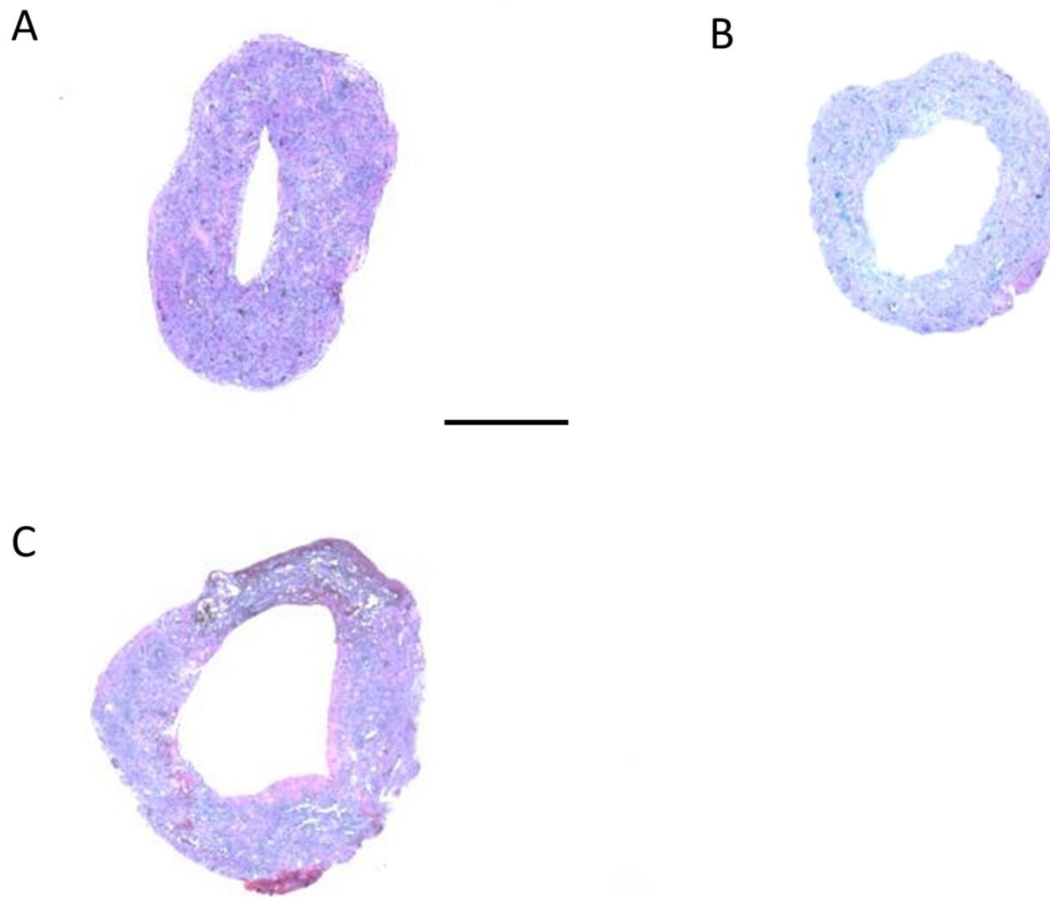
Figure 5.7 Cross sectional of TEVGs after implantation. (A) Control, (B) VEGF, and (C) CD34Ab. These representative cross sections demonstrate the visible difference in reduced diameter of the control (A) compared to the modified grafts (B and C) 2 weeks after implantation, as well as the tissue and extracellular matrix formation within the grafts. Scale bar represents 500 μm.
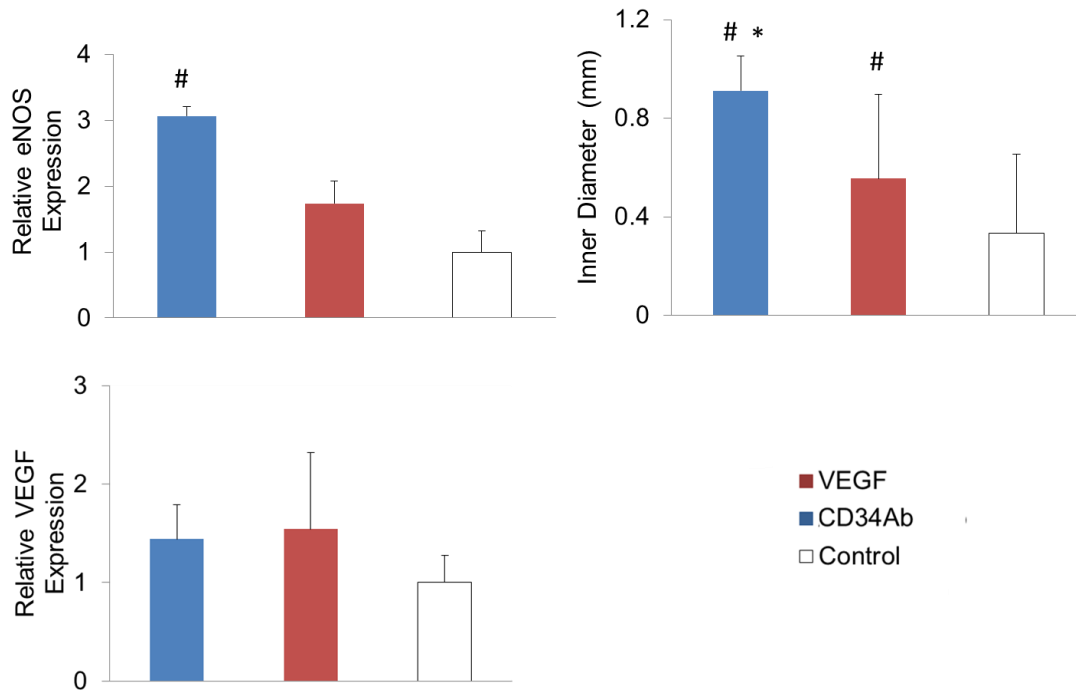
Figure 5.8 Biochemical and physical analysis of TEVGs. (Left) Relative eNOS expression of explanted samples. CD34Ab grafts resulted in increased eNOS expression in explanted tissues compared to explanted
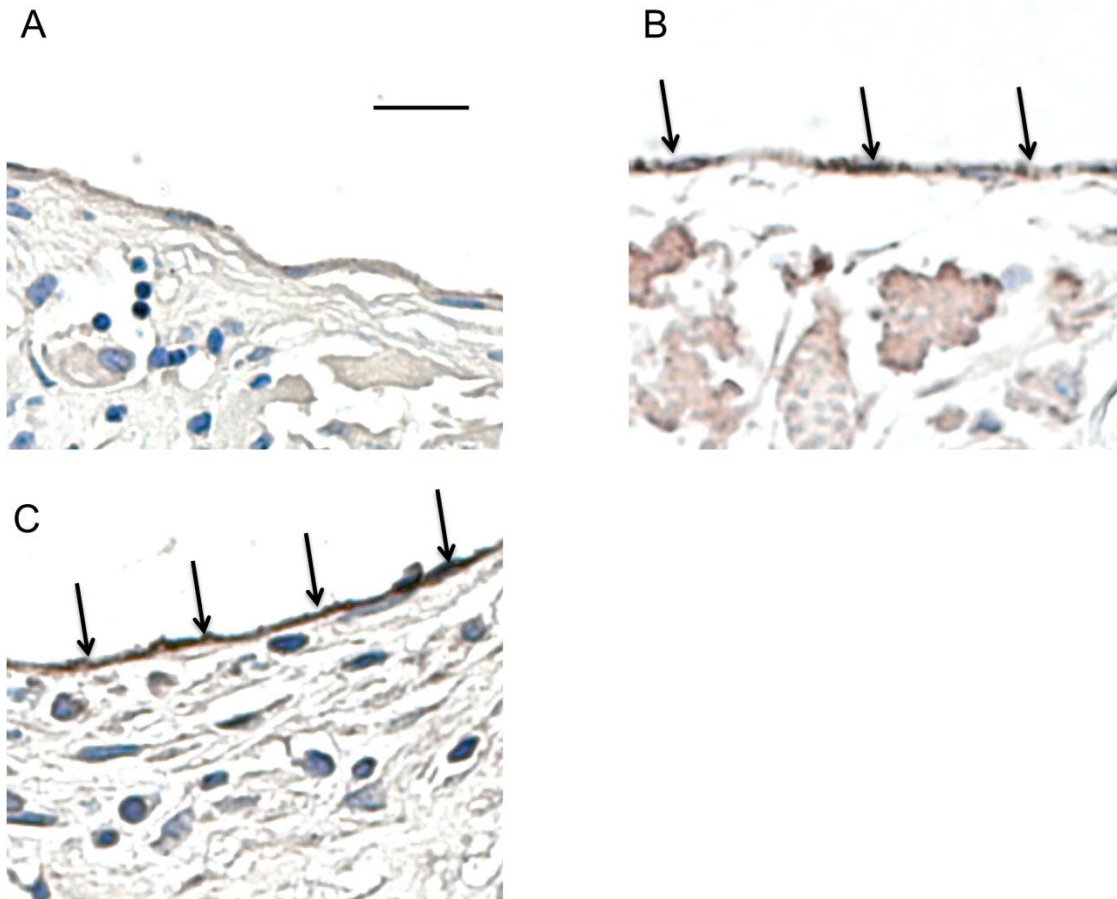
Figure 5.9 Endothelial Cell Staining of TEGVs. CD31 staining showing dark brown in images (indicated by arrows) of areas with endothelium formation and CD31 expression shown in (A) unmodified grafts and (B) VEGF, and (C) CD34Ab modified grafts after 2 weeks of implantation in a mouse model. CD34Ab demonstrated increased more uniform CD31 staining. Scale bar represents 20 µm.

Table 5.3 Approximate wall thickness of grafts implanted within mice after 2 weeks. * Indicates statistical significance compared to control graft surfaces ($p < 0.05$).

	CD34Ab	VEGF	Control
Approximate Wall Thicknesses (mm)	0.512 ± 0.182*	0.574 ± 0.391	0.537 ± 0.232

5.4 Discussion

The objective of this work was to contrast two strategies intended to improve the enhancement of vascular graft endothelialization. Specifically, we sought to determine if a burst release of VEGF from the graft surface or immobilized CD34Ab would result in enhanced endothelialization.

Through the quantification of VEGF and CD34 antibodies bound to the grafts, we were able to determine the loading efficiency and retention over time of these molecules on our biodegradable grafts. We found that VEGF experienced a burst release profile as expected from previous research.[271] In addition, lower VEGF loading compared to CD34Ab loading was expected based on these studies. It is possible that the highly-specific heparin-binding domains of VEGF limits loading due to the specific orientation and presentation of binding sites presented by heparin.[277] Because of these heparin-binding domains of VEGF, elution rates of VEGF from crosslinked heparin molecules in our study are similar to those that have been observed in other studies.[271,278,279] In contrast to the VEGF elution, CD34Ab concentrations did not significantly change over time, with minimal non-specific adsorption and nearly all bound antibodies retained, indicating the

antibodies are more permanently immobilized to the graft surface. This trend has been observed in similar research studies that hypothesize antibodies could be covalently linked due to aminolysis following EDC chemistry or may experience strong protein-protein interactions (such as van der Waals, hydrogen bonding, hydrophilic interactions, and electrostatic interactions, etc.).[65,71–73,280] Another cause of the immediate elution of VEGF is the larger percentage of non-specifically bound VEGF compared to CD34Ab (34.08 ± 16.64% vs. 1.56 ± 0.47%).

Through our *in vitro* studies, we found that modifications of grafts produced a noticeable change in micro-scale graft topography. Such topographical roughness may influence cell attachment, as demonstrated in previous studies. However, to demonstrate whether or not heparinization alone (and the resulting addition of roughness) caused increased cell attachment compared to our unmodified control, we assessed cell populations attached to our grafts. Heparinized grafts, without the addition of VEGF or CD34Ab, displayed no differences in cell attachment compared to unmodified, control grafts. Total metabolic activity of cells attached to such grafts were no different than control grafts either. In fact, after 1 day, total attached HUVECs numbered less than those on unmodified grafts and after 3 days, total metabolic activity of HUVECs was decreased compared to controls. Conversely, HUVECs attached to such grafts expressed increased gene levels of eNOS and EPCs attached to these grafts expressed increased levels of VEGF on day 3,

both compared to unmodified controls. Ultimately, the proliferation of cells on these grafts appeared no different than unmodified controls.

Our previous studies demonstrated that the small-diameter TEVG modified here possessed mechanical properties similar to native vessels and could be successfully implanted into a mouse model.[232,275] Previous research has also indicated that two weeks is sufficient to predict vessel remodeling and demonstrate whether or not intimal hyperplasia will occur.[253] Using a two week time point to determine acute endothelialization response, we modified our biodegradable polyester grafts and implanted them within mice. Though *in vivo* VEGF expression of tissues forming within the grafts was not statistically different between the groups, functionalized grafts demonstrated greater inner lumen diameter. Retention of inner lumen diameter at two weeks is a significant indication of lowered stenosis risks.[247] Functionalized grafts also demonstrated endothelial cell activity through expression of CD31. CD31, an endothelial cell marker, was evident in both of the biofunctionalized graft groups, and staining for CD31 demonstrated good endothelial cell coverage of the inner lumen of the grafts. However, only CD34Ab modified grafts demonstrated greater expression of eNOS compared to control grafts. CD34Ab grafts also demonstrated better retention of reduced wall thickness. These results may be related to the *in vitro* observation that CD34Ab grafts demonstrated significantly higher HUVEC and EPC attachment. Higher initial cell attachment may result in earlier formation of healthy endothelium which leads to less wall thickening and restenosis while

maintaining inner lumen diameter within an *in vivo* environment.[72,170,281]

Interestingly, the effects of the modified grafts, at least in this experimental

design, provided only transient or temporary advantages over control grafts *in vitro*. The most consistent results were in the initial attachment of cells to the

antibody modified grafts. Combining this with the performance of CD34Ab

grafts *in vivo* potentially provides further support to the idea that expedited cell

attachment may be one of the most important factors in improving *in situ*

endothelialization

VEGF concentrations as little as 10 ng/ml can affect EC migration and

proliferation.[269] Given the small volume of media (200 µl) and the relatively

large surface area (0.3165 cm^2) of the wells of the 96-well plate, this threshold

is easily attainable *in vitro* according to ELISA results. VEGF loading density

onto biodegradable grafts was approximated to be 12.92 ± 2.42 ng/cm^2 and,

subsequently, ensured VEGF concentrations of greater than 10 ng/ml *in vitro*.

Once implanted, the burst release of VEGF may have offered only acute

benefits, leading to observably less endothelialization compared to CD34Ab

grafts. Still, tissue formed on VEGF modified grafts did demonstrate increased

CD31 expression when compared to the unmodified, control grafts. Such

effects may be due to the recruitment and mobilization of ECs from neighboring

tissues according to other studies.[94,279] In fact, previous studies

demonstrate that the endothelialization of unmodified implanted grafts is

primarily due to migration of ECs over the anastomotic sites.[156] Thus, VEGF

may have acted locally to increase the mobilization of ECs from neighboring

tissues to impart increased endothelialization over unmodified grafts rather than providing any systemic mobilization of EPCs.

CD34Ab have been shown to been a potent recruitment tool to increase both EC and EPC attachment, especially on permanent stents.[70,72,73,282] While there are other CD34+ cells in whole blood circulation, previous research demonstrated that CD34Ab effectively induced attachment of CD34+ EPCs at significantly higher rates than CD34+ hematopoietic stem cell populations, ostensibly due to higher antigen presentation.[283,284] Our results supported the efficacy of CD34Ab recruitment in endothelial-like cell attachment to graft substrate and subsequent endothelial function. Such endothelial formation and function may have contributed to the thinner wall thickness of antibody-modified grafts, which may be indicative of reduced risk of restenosis. In conjunction with the results presented here, modification of biodegradable heparin-crosslinked vascular grafts with CD34Ab, with or without other biofunctional molecules, may be a promising strategy for expediting and increasing graft surface endothelialization.

Overall, modified grafts demonstrated trends in great inner lumen diameter retention and eNOS expression, which is crucial for vascular homeostasis and can be used as an indicator for healthy endothelial function. Healthy endothelial formation was further confirmed through the staining of CD31 expression within the inner lumen of the explanted grafts, especially evident in those grafts modified with CD34Ab.

5.5 Conclusions

The goal of this study was to determine if biofunctionalization of biodegradable vascular grafts could improve overall graft endothelialization and subsequently reduce stenosis after implantation. Biodegradable polyester vascular grafts were functionalized via a unique strategy of heparin-crosslinking to immobilize CD34Ab or VEGF. Although *in vitro* data provided support only for transient increased endothelial activity or cell attachment, modified graft surfaces elicited better endothelial and endothelial-like cell attachment *in vivo.* It appears that heparin-crosslinked biodegradable polymer grafts modified with CD34Ab modestly outperformed VEGF-modified grafts and significantly outperformed control grafts. Modified grafts promoted neotissue formation without major complications like thrombosis or stenosis. The performance of the modified, biodegradable vascular grafts appears to be a promising improvement to the *in situ* endothelialization of synthetic vascular grafts for tissue engineering.

Chapter 6: *In Vitro* Endothelization via Endothelial Progenitor Cell Seeding and Maturation in a Bioreactor System[5]

6.1 Introduction

The most significant challenge in vascular tissue engineering is the development of small-diameter grafts with antithrombotic properties and high patency. Numerous attempts have been made to improve the patency and success of these grafts with inner diameters of less than 6 mm.[34,257] The reduced patency is generally caused by thrombosis and intimal hyperplasia, and the prevailing notion is that the early establishment of a healthy endothelium can reduce the risk of these issues.[254] One approach to expediting the growth of a functional endothelium is the seeding of cells on a vascular graft prior to implantation. In order to support cells seeded *in vitro*, a variety of cell types, materials, fabrication techniques, and bioreactors have been used to provide the mechanical and biological environment for the development of tissue engineered vascular grafts (TEVGs).[285–289] In this study we focus on seeding, proliferating, and differentiating endothelial progenitor cells (EPCs) on a biodegradable vascular graft within a tubular perfusion system (TPS) bioreactor.

Several strategies exist for the extraction and isolation of native endothelial cells (ECs) from autologous vessels.[36] However, the clinical

---

[5] Adapted from: Melchiorri AJ, Kimerer LK, and Fisher JP. In vitro endothelialization via endothelial progenitor cell seeding and maturation in a bioreactor system. (In prep)

application of these techniques is made challenging by the limited number of available ECs and limited proliferative potential of mature ECs, along with donor site morbidity associated with EC harvest. In contrast, studies have shown EPCs have improved proliferative potential. Methods of isolation and large-scale expansion of these cells have also been developed.[290] EPCs have been implicated in the repair and function of the endothelium, and the harvest of these cells is less invasive than that of ECs. Thus, these cells may prove to be a promising candidate for the seeding of vascular grafts before implantation.[291]

An integral component to the development of a mature endothelium is biomechanical stimuli. Such mechanical forces applied by blood flow can affect vascular remodeling, homeostasis, and disease.[229] As one example, shear stress provides vital input toward the proliferation and maturation of vessel-related cells such as ECs and smooth muscles cells.[139,287] More recently, investigations into EPCs show differentiation of progenitor cells into EC-like cells with the influence of arterial shear stress conditions.[140,141,150,292,293] Fluid flow through TEVGs can be simulated in systems like TPS bioreactors which can offer distinct advantages over static culture conditions, including providing cell waste removal, nutrient delivery, and mechanical stimuli.[294–297]

In this study, we demonstrate a methodology for the fabrication, seeding, and subsequent culture of TEVGs utilizing off-the-self products, demonstrated in Figure 6.1. The vascular graft and bioreactor are both constructed of

commercially available components which allows for the easy manufacture, repeatability, and modification of this total TEVG preparation system. For the scaffold portion of this work, we used a solvent-cast, poly(glycolic acid) (PGA)-based felt graft with a poly(DL-caprolactone-*co*-lactic acid) solution characterized in a previous study.[275] The graft is mechanically compatible with vascular tissues, porous, biodegradable, and demonstrated good cell adhesion and infiltration when implanted in a mouse model. This scaffold platform was chosen for its ease of production and modification.[298] The next component of the TEVG preparation system is the TPS bioreactor. Like the scaffold, all the materials and parts are commercially available and we've previously demonstrated the successful application of the TPS bioreactor in the development and support of various tissue engineering constructs.[294,299–301] In contrast to work showing the differentiation of EPCs in arterial shear stress environments, we chose to demonstrate cell seeding and differentiation in venous shear stress conditions given the lack of available TEVGs for venous conditions and their application in conditions such as congenital heart disease. Finally, for the biological component, we used EPCs for cell seeding.

The objective of this study was to determine if this off-the-shelf TEVG preparation system would demonstrate successful neotissue formation and endothelial formation of EPCs within the biodegradable scaffolds in comparison with grafts seeded and cultured in a static environment. In addition, we explored the application of low flow rate conditions to simulate the effects of

the venous environment on EPC differentiation. Any component of the

bioreactor may easily be switched out with off-the-shelf components to

accommodate vascular grafts of varying sizes and shapes. Likewise, the

bioreactor system could be used with virtually any vascular graft and cell type.
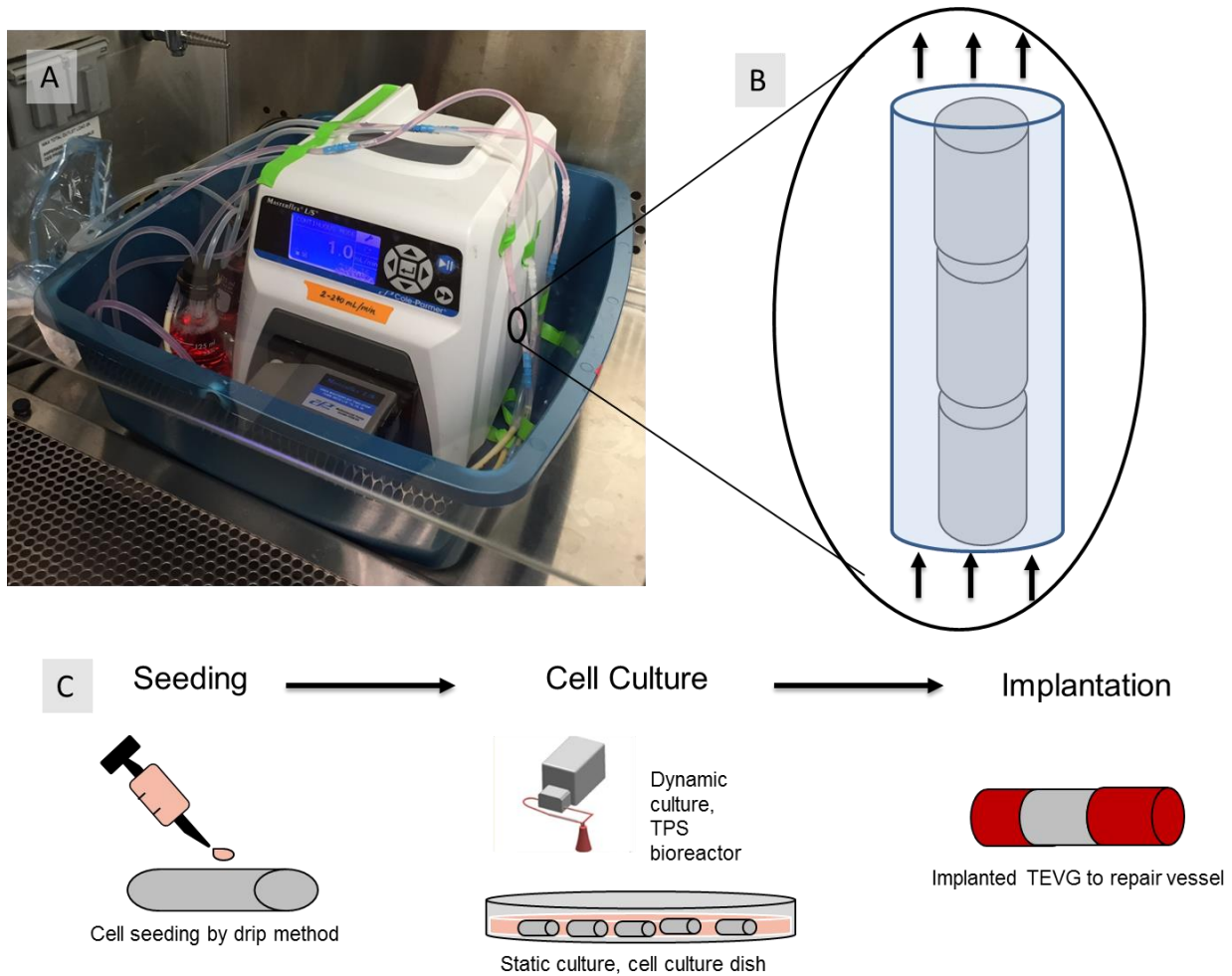
Figure 6.1 Schematic of seeding and culture process. A) The TPS bioreactor set up shortly after vascular grafts and media were introduced. B) TEVGs seeded with EPCs placed in perfusion flow chambers. C) Proposed process utilizing seeding, culturing, and eventual implantation.

6.2 Methods

6.2.1 Vascular Graft Fabrication

Grafts were fabricated according to previous studies.[232,275] Rectangular sections of 6.00 x 4.00 mm were cut from a poly(glycolic acid) (PGA) polymer BIOFELT (Biomedical Structures, Warwick, RI). These sections were then inserted into a polypropylene tube with an inner lumen diameter of 1.4 mmg. To maintain the patency of the inner lumen during the solvent-casting procedure, a 21 g stainless steel needle was inserted into the opposite end of the tube. A 40:60 copolymer poly(caprolactine-*co*-DL-lactic acid) (PCLLA) solution 15% w/v in 1,4-dioxane was then deposited into the tubes and saturated the PGA scaffold. Saturated grafts were then frozen at -20° C for 30 min and subsequently freeze-dried for 24 h. Afterwards grafts were stored at -20° C until used.

6.2.2 Bioreactor Design

The bioreactor systems consists of a design adapted from a previously described methodology.[301] Briefly, an L/S multichannel pump system (Cole Palmer, Vernon Hills, IL) was used to drive flow (2 mL/min) through a tubing circuit. The flow rate was chosen based on previous data regarding EPC differentiation into EC-like cells. Such a flow rate mimics physiologically relevant venous wall shear stresses of 0.6 dynes/cm^2. Pharmed BPT tubing (Cole Palmer, Vernon Hills, IL) was used for the portion of the circuit passing through the pump. All other tubing was comprised of platinum-cured silicone and was joined by silver ion-lined microbial resistant tubing connecters. (Cole

Palmer). The growth chamber where grafts were placed consisted of platinum-cured silicone tubing with an inner diameter of 3.2 mm and a wall thickness of 0.8 mm. After the tubing and components were autoclaved, they were assembled inside a laminar flow hood. Each growth circuit was packed with 15 consecutive, cell-seeded grafts. Following loading and assembly, the bioreactors were placed in a cell culture incubator at 37° C and 5% CO_2. Cell media was loaded into separate 125 mL Erlenmeyer flasks for each tubing circuit and topped with rubber stoppers. Media within the flasks was replaced with fresh media every 3 days.

6.2.3 EPC Culture

EPCs were purchased from Celprogen (Torrance, CA). Cells were cultured in polystyrene flasks prior to seeding, and media was changed every 3 days. Human Endothelial Progenitor Cell Complete Growth Media w/ Serum and Antibiotics (Celrogen) was used.

6.2.4 EPC Seeding

Cells were trypsinized, pelleted, and resuspended in fresh media at 1.0 x 10^7 cells/ml. Grafts were placed on untreated tissue culture dishes. For each graft, 100 µl of cell suspension was pipetted through it. Excess solution was pipetted 4 additional times to ensure graft saturation. Grafts were then incubated for 30 min at 37° C and 5% CO_2 to ensure cell attachment. Excess media was then washed off with PBS. Seeded grafts were either placed in a 34.8 mm diameter tissue culture plate for static conditions (n=5) or they were

loaded into the growth chamber of a tubing circuit for continuous flow

bioreactor conditions (n=5).

6.2.5 DNA Quantification

Cell pellets were isolated from grafts via trypsinization. Pellets were then

resuspended in PBS, and the DNA was isolated using a DNeasy Tissue Kit

(Qiagen, Valencia, CA). Standard manufacturer protocols were followed.

Subsequent quantification of double stranded DNA was accomplished with a

Quant-iT Picogreen dsDNA Assay Kit (Invitrogen, Waltham, MA). After 5 min

incubation in the dark with the PicoGreen dsDNA reagent (n=3 for each group

in each time point), fluorescence was measured using an M5 SpectraMax plate

reader (Molecular Devices, Sunnyvale, CA) using an excitation of 480 nm and

emission of 520 nm.

6.2.6 Quantitative Reverse Transcriptase Polymerase Chain Reaction (qRT-PCR)

Cell pellets were isolated from vascular grafts, and RNA was

subsequently extracted via an RNeasy Mini Plus Kit (Qiagen, Venlo,

Netherlands). Reverse transcription of the isolated RNA and subsequent

reactions were performed using a QuantiTect SYBR Green RT-PCR Kit (Qiagen).

Quantitect primer assays targeted expression of CD34 (Quantitect primer assay

ID: HS_cd34_1_SG), CD31 (HS_PECAM1_1_SG), von Willebrand's Factor (vWF,

HS_VWF_1_SG), vascular endothelial growth factor (VEGF, HS_VEGFA_1_SG),

and nitric oxide synthase 3 (NOS3, HS_NOS3_1_SG). Results were then

analyzed using the comparative threshold cycle method and normalized using

GAPDH as an endogenous reference. Relative values ($\Delta\Delta$CT) to those of control are reported.

6.2.7 Histological Analysis

Grafts were removed from the bioreactor or static culture dishes at 3, 7, and 14 days after cell seeding. Samples were subsequently fixed in 4% paraformaldehyde and embedded in paraffin. The embedded grafts were then sectioned at 5 µm thickness. Samples were stained with hematoxylin and eosin (H&E) stain or underwent immunohistochemical staining to detect CD31 antigens via a rabbit anti-CD31, CD34 via a mouse anti-CD34, or von Willebrand Factor (vWF) via a mouse anti-vWF antibody (Abcam, MA). The resulting antibody binding was detected through a biotinylated secondary antibody along with subsequent binding of streptavidin-HRP. A DAB Chromogen Kit (Invitrogen, Carlsbad, CA) was used for color development.

6.2.8 Statistical Analysis

Data were analyzed using analysis of variance single factor analysis with Student's *t*-Test or ANOVA assuming normal data distribution with a confidence of 95% ($p < 0.05$). Standard deviation errors bars are reported on each figure along with relevant statistical relationships.

6.3 Results

Initial cell seeding of a solution containing 5×10^5 cells resulted in an average of $2.43 \pm 0.64 \times 10^4$ cells/graft, resulting in a seeding efficiency of 4.85 ± 1.30 %. EPC populations cultured in static achieved a total fold change of

7.63 ± 2.20 after 7 days and 3.34 ± 0.62 after 14 days. EPC populations

increased 25.67 ± 3.86 fold after 7 days and 37.16 ± 3.04 after 14 days. Total

EPCs attached to dynamically cultured TEVGs achieved a population of 9.01 x

10^5 ± 0.81 x 10^5 cells after 14 days in contrast to a total population of 0.74 x

10^5 ± 0. 15 x 10^5 cells on statically cultured cells. These observations were

further supported by DNA quantification. Picogreen assays yielded a total DNA

concentration of 1026.74 ± 83.26 ng/ml for dynamically cultured TEVGs at 14

days and 145.19 ± 4.01 ng/ml in statically cultured TEVGs. Overall,

dynamically cultured TEVGs demonstrated a significant increase in long-term

proliferation of EPCs, shown through cell and DNA quantification of cells

attached to grafts as shown in Figure 6.2.
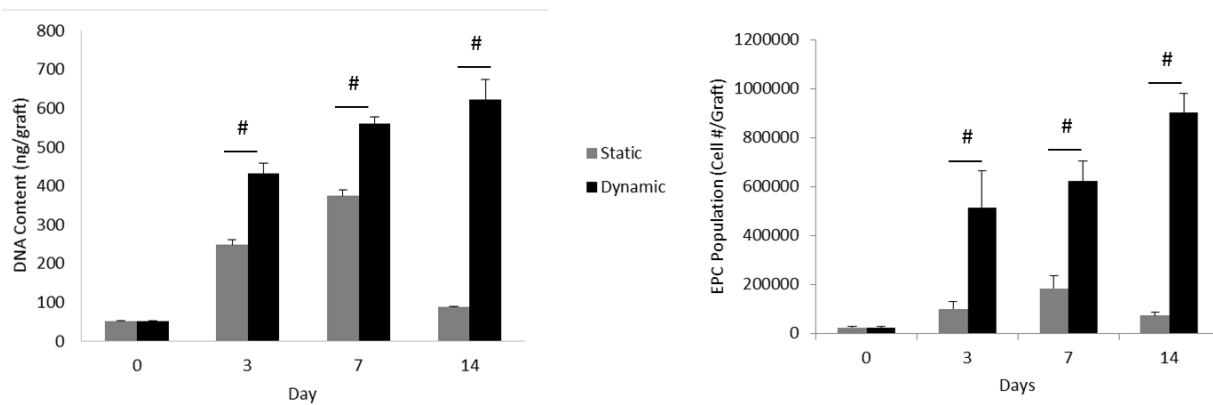
Figure 6.2 DNA quantification and EPC population evaluation on static and dynamic grafts. # represents statistical significance compared to all other groups within the time point (p < 0.05).

Relative mRNA expression was analyzed by comparing the fold increase

of markers related to endothelial function and phenotype. Fold increase was

evaluated by quantifying mRNA expression of dynamically and statically

cultured TEVGs at various time points compared to EPCs after initial seeding. Results are summarized in Figure 6.3. NOS3 expression was shown to increase over time compared to initial grafts, although there was not a statistically significant difference between dynamic and static EPC populations. On the other hand, both VEGF and vWF expression demonstrated increases by Day 14 when comparing dynamically cultured TEVGs to statically cultured TEVGs. Both static and dynamic populations exhibited increased CD31 expression after Days 3, 7, and 14 compared to EPCs after initial seeding. While dynamically cultured TEVGs demonstrated decreased CD34 expression on Day 14 compared to statically cultured samples, statically cultured TEVGs demonstrated decreased CD34 expression on Days 3 and 7. CD34 expression in dynamically cultured TEVGs decreased from Day 3 to Day 14. In contrast, CD34 expression in statically cultured TEVGs increased from Day 3 to Day 14.
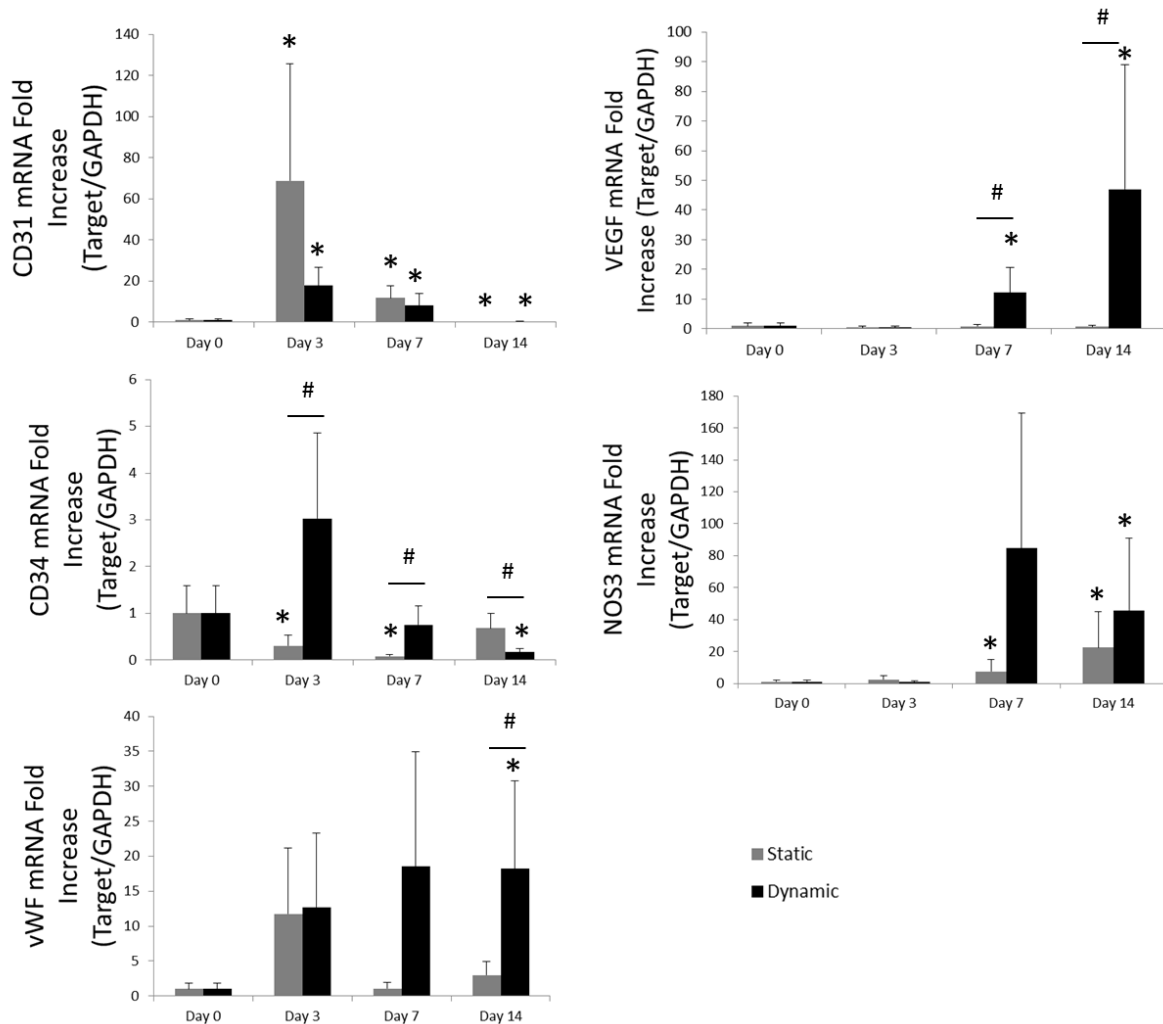
Figure 6.3 PCR results. mRNA fold increases are presented over 14 days of culturing either in static or dynamic culture. * represents statistical significance compared to initial (Day 0), # represents statistical significance compared to all other groups within the time point (p < 0.05).

Histological staining and immunohistochemistry provided insight into the effects of culturing on EPC-based tissue formation within the TEVGs. H&E stains in Fig 6.4 demonstrate more thorough distribution of EPCs throughout TEVG cross sections in dynamically cultured samples. In contrast, statically cultured TEVGs demonstrated less distributed EPC populations and sparser

tissue formation. Immunohistochemistry results showed expression of

endothelial markers, CD31 and vWF, along with EPC marker CD34 in Fig 6.5.
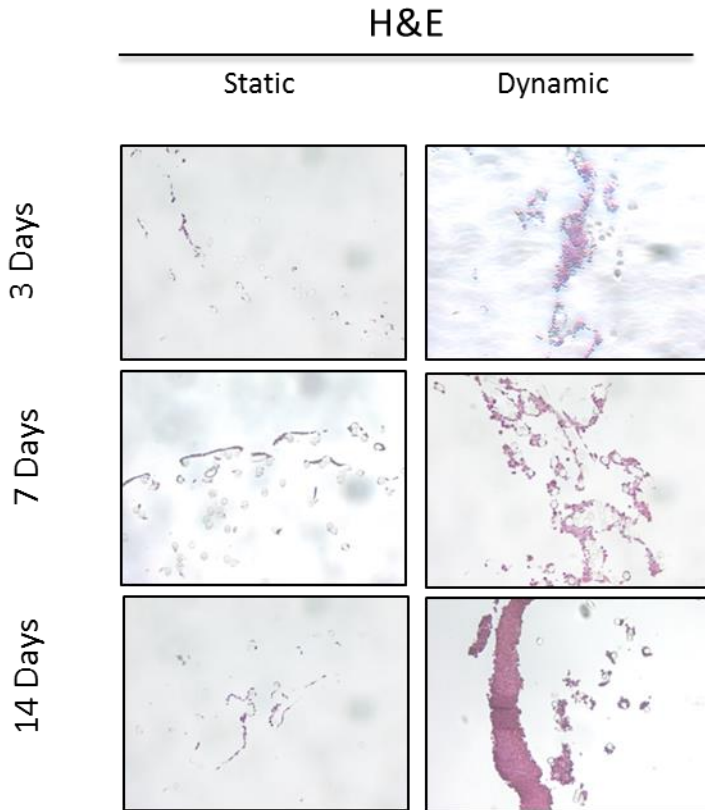
Figure 6.4 H&E staining to demonstrate tissue formation within cross-sectional cuts of grafts cultured in static or dynamic cultures. Pink staining demonstrates tissue and extracellular matrix formation within the calls of cultured grafts. Images suggest denser tissue formation in dynamic cultures.
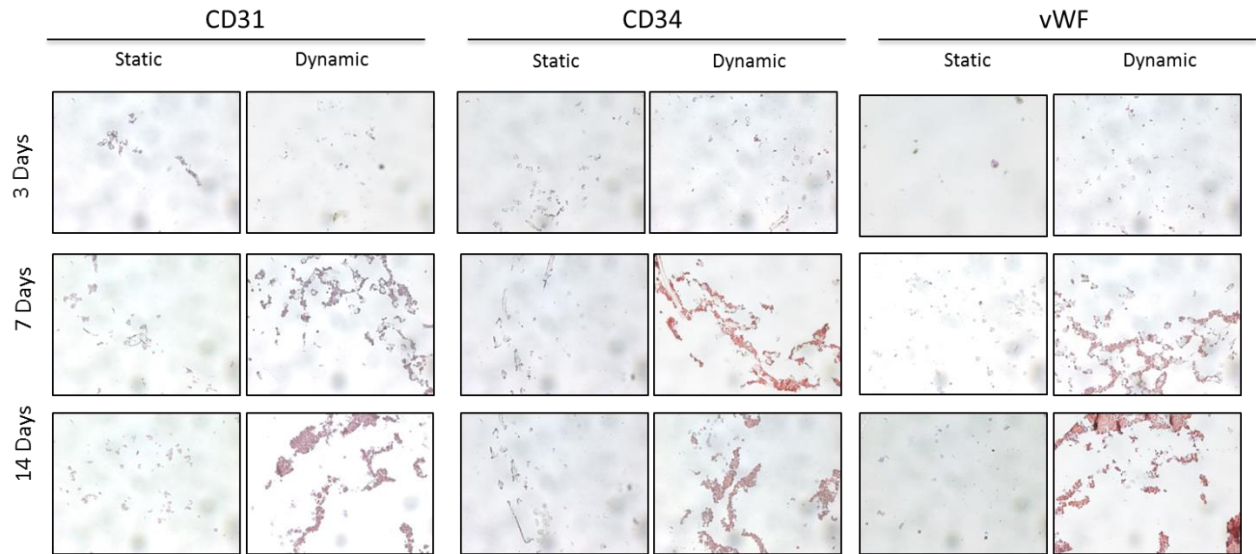
Figure 6.5 Immunohistochemical staining to demonstrate tissue formation and marker expression within cross-sectional cuts of grafts cultured in static or dynamic cultures.

6.4 Discussion

EPCs provide a promising cell type for the seeding of TEVGs. However, like other cell types, expansion time and differentiation may be limited *in vitro*. We sought to determine if we could improve the proliferation and function of EPCs seeded on an established TEVG platform through the culturing of these grafts in a TPS bioreactor system. In addition, we used the TPS bioreactor to apply low level shear stress to the TEVGs to simulate venous conditions.

A low flow rate was chosen for several reasons. First, we hoped to establish an appropriate bioreactor setup to culture grafts suitable for the venous system. Much research focuses on the arterial environment for TEVG applications, but there are more limited vascular graft materials available for venous system. Thus, we hoped to determine the effects of shear stresses

experienced by the endothelium in conditions similar to the venous system. Second, it has been shown that a low flow rate supports better cell adhesion on graft surfaces during *in vitro* culture.[302] Prolonged adhesion is crucial to cell proliferation and eventual endothelialization of a TEVG.

Overall, our results indicated dynamically cultured TEVGs in a low shear stress environment provide a robust platform for cell population growth and function compared to a static environment. The marked increase in cell number and DNA content in dynamically cultured grafts demonstrates the TPS bioreactor's superiority over static culture conditions in improving cell proliferation and population growth. PCR results also demonstrated the efficacy of dynamically cultured EPC-seeded TEVGs in terms of endothelial function, which is critical to vascular homeostasis and health. This includes the expression of molecules such as nitric oxide (eNOS), indicated by NOS3 expression. This protective enzyme contributes to the inhibition of platelet aggregation and adhesion, which mediates inflammation and thrombosis.[303] In addition, VEGF is an essential growth factor for ECs. VEGF, which may also be mediated by eNOS, can induce EC migration and proliferation, aiding the formation of a healthy endothelium.[304,305] Dynamically cultured TEVGs seeded with EPCs demonstrated improved VEGF and NOS3 expression over statically cultured TEVGs. Thus, dynamically cultured EPCs may not only provide better neotissue formation over TEVGs through proliferation, but may also provide a more functional endothelium than statically cultured grafts immediately upon implantation. The presence of functional EPCs expressing

such markers may also mediate the normal growth of vascular smooth muscle cells within the graft, effectively preventing or reducing issues of intimal hyperplasia.[306] Importantly, dynamically cultured TEVGs also expressed increased functional endothelial markers, vWF and NOS3, compared to statically cultured EPCs as demonstrated by PCR results, and immunohistochemistry seemed to support these findings. The benefit of culturing EPC-seeded TEVGs in a TPS bioreactor is quite clear.

However, several challenges remain to be solved. This particular method of initial cell seeding led to low rates of initial cell attachment. The physical method of seeding may be improved to enhance cell retention on grafts. Alternatively, techniques to improve cell adhesion to biomaterials have been employed to improve EPC attachment to vascular graft materials. These include modifications such as heparin-coated scaffolds, VEGF, antibodies, and various peptides.[298,302,306,307] Such modifications may improve initial cell seeding, which in turn may expedite *in vitro* endothelialization and tissue formation on bioreactor cultured TEVGs. This may enable a complete endothelial layer to form in a matter of weeks. In addition, there is still some controversy on the role of EPCs and the role of specific subsets of these cells.[308] For example, outgrowth endothelial cells (OECs) may express markers more consistent with mature ECs compared to endothelial colony forming cells (ECFCs).[289,309] In this study, bone-marrow derived EPCs isolated from peripheral blood expressing CD34, VEGFR-2, and CD133 were used. Other subsets of EPCs may perform differently in the low shear stress

environment we exposed the EPC-seeded TEVGs to. Still, the TEVG and TPS bioreactor setups are amenable to multiple cell types and may foster the endothelialization of grafts utilizing various subtypes of EPCs.

6.5 Conclusion

In this study, we successfully demonstrated the enhanced proliferation, infiltration, and differentiation of EPCs into endothelial-like cells seeded on TEVGs and cultured in a dynamic TPS bioreactor system utilizing low shear stresses akin to the venous system. This platform provides an elegant and effective method of enhancing endothelialization through the use of a readily available cell-type to seed small-diameter TEVGs prior to implantation, which may drastically reduce complications such as intimal hyperplasia and thrombosis. Further optimization and development of this platform may offer an off-the-shelf clinical solution to improve implanted TEVG patency.

Chapter 7: 3D Printed Biodegradable Polymeric Vascular Grafts[6]

7.1 Introduction

The most common form of birth defect worldwide is congenital heart disease (CHD).[310] Treating CHD presents unique complications. For example, specific defects may present uniquely in different patients due to anatomical differences. Proper design and adaptation of implanted grafts to correct these defects is crucial because graft orientation and shape is integral to successful CHD surgical outcomes.[11,12] In addition, current grafts used in these procedures suffer from progressive obstruction, infection, increased risk of thromboembolitic complications, a lack of growth potential, poor long-term durability, and calcification.[4–8] Graft failure is expected in 70-100% of cases in 10-15 years.

To address the challenges of growth potential, host-tissue integration, and anatomical differences, 3D printing patient-specific grafts offers tremendous opportunity in tissue engineering. A biodegradable, tissue-engineered graft would eliminate the chronic effects of permanent, synthetic grafts used today. In addition, 3D printing may enable better customization to address the orientation and shape issues related to CHD surgical outcomes. Yet there are many limitations to overcome. Current bioprinting efforts have enabled the fabrication of biologically functional blood vessels.[203,208] But

---

these vessels are more suited for vascularization of larger tissues due to material and size constraints, along with insufficient mechanical properties for larger-scale vessels unless they've been extensively cultured to allow for tissue maturation. Previous studies have also examined the use of fabricating grafts utilizing solvent-cast molding processes, but 3D printing the graft directly can reduce the steps necessary to construct a scaffold.[249,275] An earlier study documented the development of a printable polyurethane that may be suitable for vascular materials and another described the printing of combined 3D printing and electrospinning technique,[187,311] but none to our knowledge have demonstrated *in vivo* functionality of a fully 3D printed non-cellular vascular graft. Our study presents the development and application of a platform for the fully 3D printed fabrication of non-cellular biodegradable scaffolds for vascular tissue engineering demonstrated *in vivo*. Such a platform may eventually enable the production of more complex structures customized for experimental studies or clinical applications by incorporating customized macroscale geometry—like vessel bifurcations and curves—with controlled microscale architecture—like porosity and surface roughness, which we have successfully incorporated using this technique for bone tissue engineering.[312]

We examine techniques and materials developed for the 3D printing of vascular tissue engineering scaffolds utilizing poly(propylene fumarate) (PPF) and demonstrate its efficacy in the mouse venous system. For this study, we focused on a venous graft model because there are no ideal commercially

available synthetic biomaterials for the repair or reconstruction of vessels in venous circulation. PPF is a biocompatible and biodegradable polyester that contains a carbon-carbon double bond along its backbone.[313] This enables crosslinking between polymer chains. Such crosslinking can be initiated via photoinitiators. Due to this photocrosslinkability and its biocompatibility, PPF is a prime candidate for 3D fabrication techniques such as digital light stereolithography (DLP) (as depicted in Figure 7.1a) to construct functional, tissue-engineering scaffolds. DLP has long been a proven method of 3D printing of constructs for such scaffolds, including those constructed of PPF.[314–320] The overall process is demonstrated in Figure 7.1b. As we are focused on CHD, this represents a relatively simple case of coarctation of the aorta. Images of the aorta are first obtained via MRI or CT and segmented for analysis. A custom graft is designed to fit the specific curvature of this patient's anatomy and subsequently can be tested both for fit and fluid dynamics before eventual 3D fabrication of the customized implant.

7.2 Methods

7.2.1 Resin Formulation

Polypropylene fumarate (PPF) was synthesized as previously described.[321] The reaction was continued until the desired molecular weight, 1200 Da, was achieved and confirmed via gel permeation chromatography (GPC). To enable printing with the synthesized PPF, DEF was added to the PPF to achieve a weight ratio of 5:4 PPF:DEF. Before adding the DEF to the PPF,

photoininitiators and photoinhibitors were dissolved in the DEF under

continuous mixing at room temperature for 1 h. The photoinitiator, bis(2,4,6-

trimethylbenzoyl) phenylphosphine oxide (BAPO, Ciba Specialty Chemical,

Tarrytown, NY), was added at 1% w/w. To control excess cross-linking, 0.2%

w/w α-tocopherol (Vitamin E, Sigma Aldrich, St. Louis, MO) and 1% w/w

hydroxyl-methoxybenzophenone (BAPO, Sigma) were used.

7.2.2 Graft Fabrication

    All scaffolds and test objects were designed using SolidWorks (Dassault

Systemes SolidWorks Corp., Waltham, MA) and fabricated using an

EnvisionTEC Perfactory P4 with Enhanced Resolution Module (EnvisionTEC,

Detroit, MI). The mode of fabrication was UV light digital stereolithography to

cure individual 50 µm layers of resin at 50 s exposure with a brightness of 275

mW/dm^2. For mechanical characterization of the printed material, dogbone

films were printed vertically with a thickness of 0.30 mm, an effective length of

7.0 mm, and a width of 2.0 mm. These were printed in the same direction and

with the same defect density as grafts printed for *in vivo* implantation. Due to

size and dimensional constraints of mouse models and the desire for producing

replicable results, instead of custom grafts for each mouse, uniform vascular

grafts were printed. Vascular grafts printed for degradation studies and *in vivo*

studies (also printed vertically) had lengths of 6.0 mm, inner diameters of 1

mm, and a wall thickness of 0.15 mm. Discs for *in vitro* studies were printed

with diameters of 6.3 mm and thicknesses of 0.2 mm. Grafts and other printed

objects were subsequently exposed to extra UV light via the Otoflash lamp

(EnvisionTec). Grafts exposed to 100 flashes of the Otoflash lamp are labeled UV100, 500 flashes are UV500, and 2000 flashes are UV2000.

7.2.3 Mechanical Characterization

All tensiometry was performed with an INSTRON 5560 tensiometer using a 50 N load cell (Instron, Norwood, MA) on printed dogbone shapes with a 10 mm/min crosshead speed to assess ultimate tensile strength and elastic modulus. Printed samples were elongated until failure. Circumferential tensile strength was assessed to estimate burst pressure values using LaPlace's Law for blood vessels. P=(UTS x t)/r, where P = internal pressure, UTS = ultimate tensile strength in the circumferential direction, t = wall thickness, and r = radius. To perform these tests, 3D printed cylindrical grafts were cut to 0.5 mm sections and placed on metal hooks on the tensiometer (n=5). These sections were stretched at a rate of 1 mm/min until failure.

7.2.4 Degradation Assessment

To assess the effects of biodegradation, cylindrical vascular grafts and dogbone structures were used. Initial mass of each printed sample was obtained before placing them in glass scintillation vials. Each vial was filled with 5 mL of 0.01 M, pH 7.4 phosphate buffered saline (PBS) and the samples were placed on a shaker table at 75 rpm and 37º C. At each time point (days 0, 1, 7, 14, 28, 56, and 112), samples were evaluated for change in mass. Tensile testing was also performed on the dogbone-shaped printed films to assess changes in elastic modulus and ultimate tensile strength, as described in the section entitled Mechanical Characterization.

7.2.5 In Vitro *Cell Attachment and Proliferation*

To assess relevant vascular cell type compatibilities with printed graft materials, human endothelial vein cells (HUVECs) and human umbilical vein smooth muscle cells (HUSMCs) were seeded and cultured to measure cell adhesion and proliferation on the printed graft samples (Lonza, Basel, Switzerland). PPF resin discs were printed with a diameter of 6.3 mm and a thickness of 200 µm to fit in the wells of a ninety-six-well plate cell cultures. Printed samples were sterilized via UV light exposure for 1 h before cell culture assays.

To assess initial cell adhesion, cells were seeded at 5×10^3 cells per well (n=4). This was performed with HUVECs and HUSMCs, separately. Cell culture plates were then incubated at 37°C for 1 hr. After incubations, non-adherent cells were removed with thorough washing using sterile PBS. Live/Dead staining was then used to identify attached, live cell populations on the cultured printed discs. Images were obtained under a fluorescent filter via a microscope. ImageJ (National Institutes of Health, Bethesda, Maryland). Cell count adhesion percentages were normalized to the control, tissue culture polystyrene (TCPS).

To assess cell proliferation, HUVECs and HUSMCs were cultured separately (n=4) and cultured at 37° C. Printed discs seeded with cells were thoroughly washed with sterile PBS and stained using a Live/Dead assay at 1, 3, and 7 days after initial seeding. A fluorescent filter and microscope were

used to capture images of the discs and cells were subsequently counted with ImageJ.

7.2.6 Animal Model

The *in vivo* procedure described here was adapted from our previous work.[275] Cylindrical grafts (1 mm in diameter and 3 mm in length) were printed underwent ethylene oxide sterilization. 8-10 week old female C.B-17 SCID/bg mice weighing 18-30g (Taconic) were used for all graft implantations in the current study. While the long-term goal of this technology is to address more complex anatomical structural corrections, the animal model selected for this initial platform assessment was chosen for its uniformity between test subjects and test subject implantation sites to provide statistically relevant results and assessments on tissue-material interactions. Implantations were performed in the inferior vena cava (IVC) of mice due to the IVC's straight and similar geometry between test subjects (~1.0 mm inner diameter and ~3.0 mm length). Thus, there was little, if any, anatomical variation between surgical sites chosen for this initial animal study using 3D printed vascular graft technology. All animals received humane care following the National Institutes of Health Guide for the Care and Use of Laboratory Animals, and the Institutional Animal Care and Use Committee at Nationwide Children's Hospital (Columbus, OH) approved all animal procedures described.

7.2.7 Graft Implantation

3D printed vascular grafts (inner diameter: 1.0 mm, wall thickness: 0.5 mm, length: 3.0 mm) were implanted as inferior vena cava (IVC) interposition

grafts in 24 C.B-17 SCID/bg mice following previously described aseptic microsurgical methods.[232] Briefly, mice were administered a pre-anesthetic analgesic of ketoprofen (5mg/kg) then anesthetized with an intraperitoneal injection of ketamine (100mg/kg) and xylazine (10mg/kg). A midline incision was made, the abdominal organs eviscerated, and the IVC exposed. The IVC was bluntly dissected from the abdominal aorta. Vascular scaffolds were placed as interposition grafts (end-to-end anastomoses) using a running 10-0 nylon suture. After confirming a patent anastomoses and hemostasis, the abdominal organs were returned to the abdominal cavity and the peritoneum closed with a running 6-0 prolene suture. Animals received routine post-operative care and did not receive anticoagulation or anti-platelet therapy over the course of observation. Animals were humanely sacrificed at either 3 or 6 months (n=6 per graft type, per time point) and grafts explanted for further analysis.

7.2.8 Graft Ultrasound Monitoring

High frequency Doppler ultrasonography (Vevo Visualsonics 770, Visualsonics, Toronto, ON, Canada) was used to monitor graft implants at the 3 and 6 month time points. Mice were anesthetized with 1.5% inhaled isoflurane (1.0 L/min). Lumen diameter was determined with B-mode images using Image J software (National Institutes of Health, Bethesda, MD) and patency was determined with color Doppler in the graft lumen.

7.2.9 Histomorphometry

Grafts were perfusion fixed with 10% (vol/vol) formalin, explanted, stored overnight at 4°C, and embedded in paraffin following previously established methods.[232] Sections (5 µm thick) were stained with hematoxylin and eosin (H&E) and visualized with light field microscopy (Axio Imager.A2, Zeiss, Jena, Germany). Photomicrographs were analyzed with Image J software (National Institutes of Health, Bethesda, MD) to determine graft lumen diameter and wall thickness. Lumen diameter was calculated as: lumen perimeter ÷ π and wall thickness was calculated as: (adventitia diameter – lumen diameter) ÷ 2.

7.2.10 Immunohistochemistry

To characterize vascular neotissue in 3D printed vascular scaffolds at 3 and 6 months post-implantation, sections were deparaffinized, rehydrated, and blocked for endogenous peroxidase activity (0.3% H_2O_2 in MeOH) and nonspecific background staining (Background Sniper, Biocare Medical, Concord, CA). Antigens were retrieved using the citrate buffer method (pH 6.0, 90°C). Primary antibodies used were: anti-CD31 (1:50, Ab28364, Abcam, Cambridge, MA), anti-α-Smooth Muscle Actin (1:500, M0851, Dako, Carpinteria, CA), anti-F4/80 (1:1000, MCA437R, AbD Serotec, Kidlington, Oxford, UK), anti-MMP-2 (1:200, Ab37150, Abcam, Cambridge, MA), anti-MMP-9 (1:200, Ab38898, Abcam, Cambridge, MA), anti-Collagen I (1:250, Ab292, Abcam, Cambridge, MA) and anti-Collagen III (1:250, Ab7778, Abcam, Cambridge, MA). After primary antibody incubation, binding was detected with species appropriate biotinylated secondary antibodies (Dako, Carpinteria, CA),

incubation with Horseradish Peroxidase (HRP) Streptavidin (Dako, Carpinteria, CA) and chromogenic detection with 3,3-diaminobenzidine (Vector Laboratories, Burlingame, CA). Nuclei were identified with a hematoxylin counterstain (Gill's Formula, Vector Laboratories, Burlingame, CA). Slides were then dehydrated, mounted, and visualized with light field microscopy (Axio Imager.A2, Zeiss, Jena, Germany).

7.2.11 Scanning Electron Microscopy (SEM)

To confirm intimal tissue and endothelialization, selected graft explants were processed for SEM. Tissue samples were perfusion fixed with 10% Formalin before explant, washed with PBS, then dehydrated to 100% EtOH. Samples were then dried with hexamethyldisilazane (Sigma Aldrich, St. Louis, MO) mounted, and gold sputter coated. SEM images were obtained with a Hitachi S-4800 Scanning Electron Microscope at 5.0 kV.

7.2.12 RNA Extraction and Reverse Transcription Quantitative Polymerase Chain Reaction (RT-qPCR)

Upon sacrifice, graft explants were flushed with PBS and embedded in OCT Compound (Tissue Tek, Sakura Finetek, Torrance, CA). Frozen tissue blocks were sliced (30 µm thick sections) on a CM1950 cryostat (Leica Biosystems, Buffalo Grove, IL). Sections were washed in PBS to remove OCT Compound, and Total RNA was extracted using the Ambion® PARIS™ system following manufacturer's instructions (Life Technologies, Thermo Fisher Scientific, Waltham, MA). Reverse transcription was performed using the High Capacity RNA-to-cDNA Kit (Applied Biosystems, Foster City, CA) following manufacturer's instructions in order to obtain complimentary DNA for the

quantitative PCR assay. PCR was performed with the Step One Plus Real-Time PCR System using the TaqMan Universal PCR Master Mix Kit (Applied Biosystems, Foster City, CA) per the manufacturer's protocol. Total reaction volume was 20 µL: 10 µL TaqMan Fast Advanced Master Mix (2x), 1 µL Taqman Gene Expression Assay (20x), 7 µL nuclease free H_2O, 2 µL cDNA. Reference numbers for primers used are: Pecam1 (Mm01242584_m1), Itgam (Mm00434455_m1), Mmp2 (Mm00439498_m1), Mmp9 (Mm00442991_m1), Acta2 (Mm00725412_s1), Nos3 (Mm00435217_m1), Hprt (Mm00446968_m1), Colla1 (Mm00801666_g1), Col3a1 (Mm01254476_m1). Gene expression assays were used in duplicate and values were analyzed using the comparative threshold cycle method and normalized to the expression of the endogenous reference gene HPRT. Results are reported as relative values ($\Delta\Delta$CT) to the mean gene expression of C.B-17 SCID/bg IVC (n=3).

7.2.13 Statistical Analysis

Data were analyzed using analysis of variance single factor analysis with Student's *t*-test or ANOVA assuming normal data distribution with a confidence of 95% ($p < 0.05$). Standard deviation error bars are reported on each figure along with relevant statistical relationships.

7.3 Results and Discussion

To ensure the viability of PPF grafts for vascular applications, we first performed mechanical testing on 3D printed dogbones (Figure 7.2a). Most current methodologies of printing do not directly produce devices with

adequate mechanical strength.[186,322] Bioprinting strategies necessitate cell seeding and culturing to develop tissue-based grafts with adequate strength to be viable once implanted. Still, few non-cellular vascular graft printing strategies have been pursued that demonstrate the mechanical properties shown immediately after fabrication by the PPF-based grafts. Mechanical properties of the 3D printed structure relied largely on the amount of post-printing exposure to ultraviolet (UV) radiation via an Otoflash lamp, which increased polymer crosslinking. Each flash of the Otoflash emits ~11 J. Thus, 100 flashes yields ~1100 J (UV100), 500 flashes yields ~5500 J (UV500), and 2000 flashes yields ~22,000 J (UV2000) of energy over the broad spectrum of UV light radiated by the lamp. Results of tensile testing can be observed in Figure 7.2b and 7.2c. With 100 flashes of the UV lamp, 3D printed PPF samples demonstrated an ultimate tensile strength (UTS) of 1.48 ± 0.88 MPa and an elastic modulus of 8.79 ± 3.28 MPa; 500 flashes yielded samples with an UTS of 2.06 ± 1.28 MPa and an elastic modulus of 11.32 ± 2.82 MPa; and 2000 flashes yielded an UTS of 10.97 ± 3.28 MPa and an elastic modulus of 19.74 ± 3.17 MPa. Additionally, UV100 grafts demonstrated an estimated burst pressure of 5037.22 ± 2108.09 mmHg, UV500 demonstrated 7175.97 ± 2148.76 mmHg, and UV2000 demonstrated 17658.53 ± 6210.77 mmHg, all well beyond physiologic environmental conditions and burst pressure of native blood vessels (saphenous vein, 1599 ± 877 mmHg, and internal mammary artery, 3196 ± 1264 mmHg) .[235,237,239,323] The printed grafts demonstrated initial mechanical properties comparable to native vessels used

in grafting procedures and appropriate for use as venous scaffolds.[237,324]

In terms of mechanical properties, there were no statistically significant

differences between UV100 and UV500 grafts, although UV2000 grafts

exhibited mechanical properties beyond those demonstrated by cardiovascular

tissues and thus were not used for *in vivo* studies due to this drastic

mechanical incompatibility. Such incompatibilities are known to contribute to

patency issues such as intimal hyperplasia.[325]
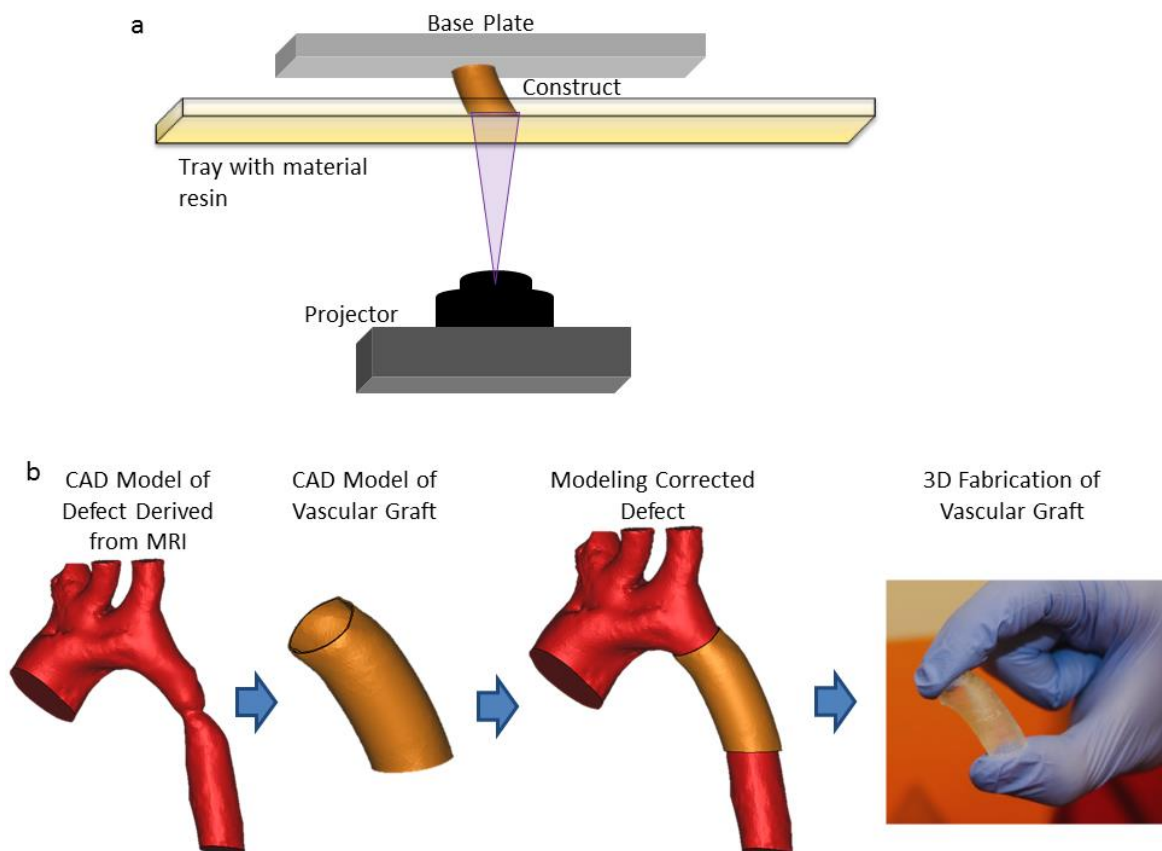
Figure 7.1 Method for 3D Printing Shape Specific Vascular Grafts. (a) Digital light processing (DLP) stereolithography of PPF, where the PPF-based material resin is first placed within a light transparent tray. Next, a projector emits a precise image onto the bottom of the resin tray. A single layer of the construct is cured at once, before the construct (attached to the base plate), is moved vertically to allow for curing of the next layer. (b) Design and fabrication process of 3D printed graft to treat a coarctation of the aorta. Images obtained via medical imaging technologies such as MRI or CT are segmented and used to create a 3D computer model. A customized vascular graft can then be created via CAD software, and subsequently assessed with the segmented model of the defect. Once the graft design has been finalized, it can be 3D printed
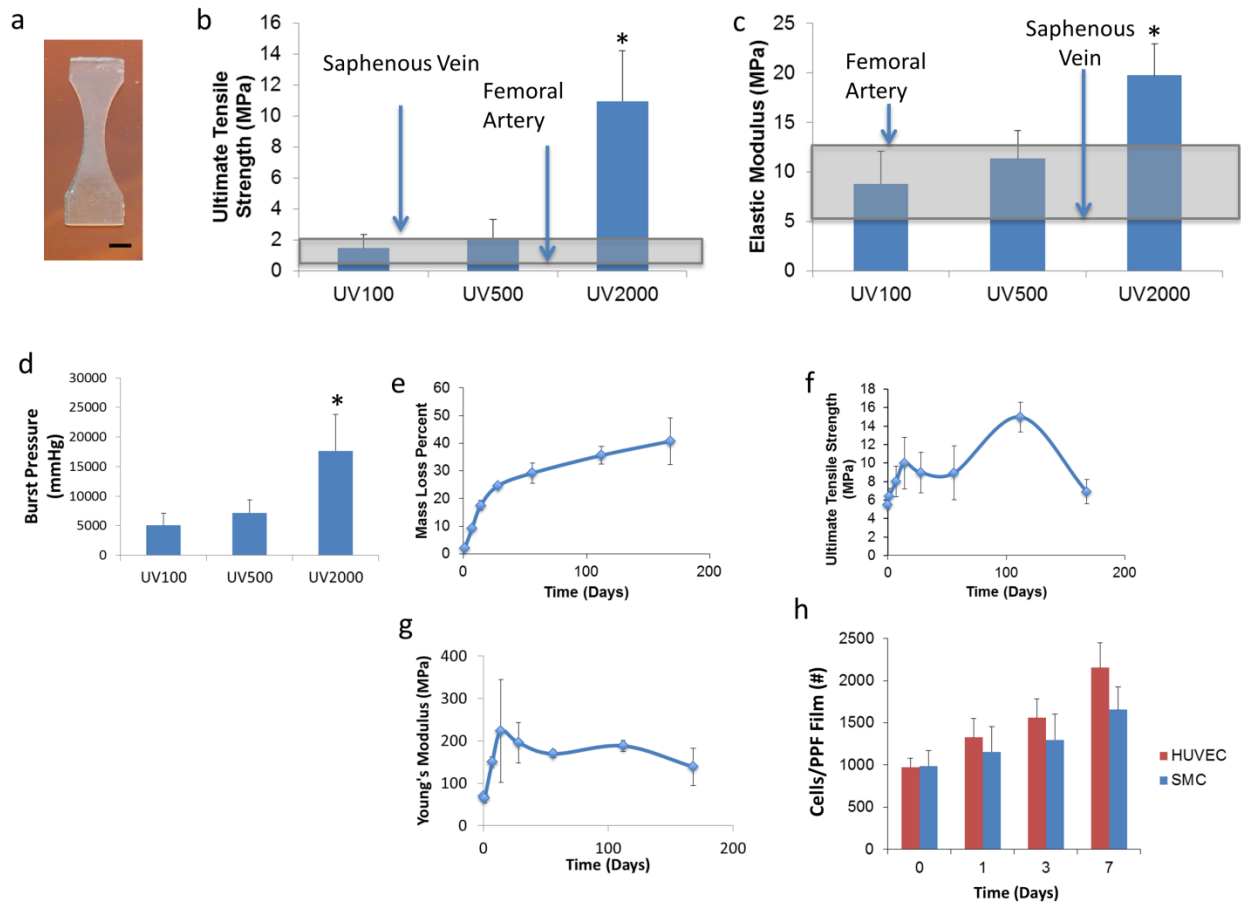
Figure 7.2 Mechanical Characterization of 3D Printed PPF Material. (a) An image of the dogbone shape 3D printed PPF used for mechanical studies; scale bar is 2.0 mm. (b and c) Mechanical properties of 3D printed grafts exposed to UV light post-printing via the Otoflash curing device. These properties are compared with the saphenous vein and femoral artery, where the shaded gray box highlights the range of mechanical properties found in such autologous tissue implants. (d) Burst pressure estimates based upon circumferential tensile tests. (e to g) In vitro degradation of 3D printed grafts over 6 months. (e) Mass loss over time. (f and g) Change in ultimate tensile strength and Young's modulus, respectively, over time. (h) Growth of HUVEC and SMC populations on 3D printed substrates in cell culture. *Represents statistical significance between groups ($p < 0.05$).

Since PPF is biodegradable, it is crucial to assess the effects of degradation on graft mechanical properties to predict long-term mechanical support once implanted. After 6 months of *in vitro* degradation (Figure 7.2e to

7.2g), printed grafts experienced a 40.76 ± 8.37 % decrease in mass. The UTS, Figure 7.2f, of these printed materials increased over time, peaking at 4 months of degradation, after which it returned to values comparable to the initial UTS. The elastic modulus of the grafts appeared to increase initially before slowly decreasing as shown in Figure 7.2g.

These properties were generally maintained throughout the duration of our 6 month degradation study, despite the mass loss of the scaffold. We hypothesize that the increase in strength during degradation, evidenced by the changes in elastic modulus and UTS, may have been caused by a combination of two phenomena. First, during the printing process, the PPF chains may not be uniformly, fully crosslinked. In addition, free radicals may have been entrapped within highly crosslinked networks portions, only to be released during degradation and heating (in this case, from room temperature to a simulated physiological environment at37° C).[326] This may result in the ongoing, long-term crosslinking of polymer chains well after the scaffolds were initially printed. In addition, we believe that as smaller chains degrade, there may be reduced steric hindrance between the larger chains. This enables increased crosslinking and entanglement between these chains, which may increase the elastic modulus and UTS of the scaffolds.

Before implantation of the grafts, we also assessed the viability of relevant vascular cell types. Human umbilical vein cells (HUVECs) and human umbilical vein smooth muscle cells (HUSMCs) were seeded on 3D printed PPF surfaces to assess initial attachment. 19.5 ± 2.1 % of seeded HUVECs and 19.8

± 3.7 % of seeded HUSMCs successfully attached. As shown in Figure 7.2h, over 7 days HUVECs experienced a 1.91 ± 0.66 fold increase in total population, and HUSMCs demonstrated a 1.29 ± 0.70 fold increase in total population. This established cell viability on the 3D printed surfaces.

Once implanted in mice, non-cellular 3D printed PPF scaffolds demonstrated their functionality as venous interposition grafts (Figure 7.3a-f). Mouse IVCs were chosen as implantation sites due to the minimal, if any, geometric variation between test subjects. This provided a simple initial *in vivo* platform in which anatomical differences between test subjects were minimized so that biocompatibility results could be better analyzed. Given the relatively controlled geometry between test subjects, straight, tubular grafts were used. This aided in experimental replicability and enabled statistical analysis of the grafts and provided a proof of concept for the use of 3D printed polymers as a vascular material. Future large animal studies will be necessary to demonstrate the customization of grafts for more complicated vasculature. We were particularly interested in studying whether the UV100 or UV500 grafts performed any differently *in vivo* due to slight differences in mechanical properties. No significant differences existed between the two graft groups (n=6). All grafts demonstrated no thrombosis, graft aneurysm, or stenosis at any time over the 6 month implantation experiment. Additionally, grafts remained patent throughout the experiment. Histological morphometry of paraffin embedded sections demonstrated no significant difference in graft thickness between time points, suggesting minimal to no restenosis.

Confirming this, lumen diameters (Figure 3k) obtained from ultrasound images over the 6 month time course are shown in Figure 7.3l-o. Color Doppler ultrasound confirmed graft patency in all animals of both groups. Lumen diameters measured from B-mode images suggest that the inner diameter of both graft types did not significantly change over the course of implantation.
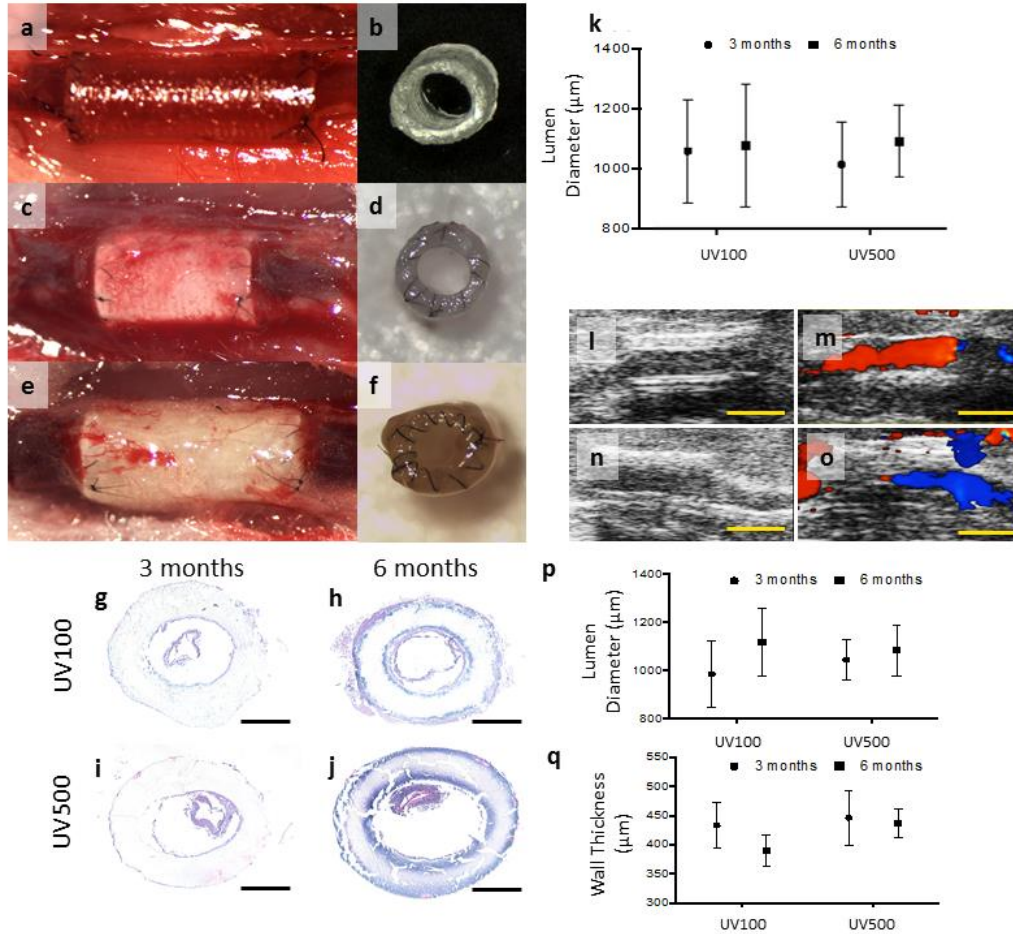
Figure 3: 3D Printed PPF Vascular Graft During 6 Months of Implantation in a Mouse Model. (a and b) 3D printed graft at the time of implantation, (c and d) 3 months after implantation, and (e and f) 6 months after implantation. No thrombosis or stenosis was observed upon gross examination at the time of explantation in either graft type. (k) Lumen diameters obtained from ultrasound images over the 6 month time course. (l and m) Representative B-Mode image and color Doppler image, respectively, of UV100 graft at 6 months. (n and o) Representative B-Mode image and color Doppler image, respectively, of UV500 graft at 6 months. Color Doppler ultrasound confirmed graft patency in all animals of both groups; scale bars are 2.0 mm. Histological section of implanted graft, with H&E staining of (g and h) UV100 and (i and j) UV500 at (g and i) 3 months and (h and j) 6 months after implantation. Of note, detachment of intimal layer was an artificial effect created during the slicing of the histological section. Although no cellular infiltration was observed at either time point, graft degradation is evident at 6 months and UV500 grafts appear saturated with eosinophilic serum proteins; scale bars are 500 μm. (p) Lumen diameter and (q) wall thickness over the time course of observation.
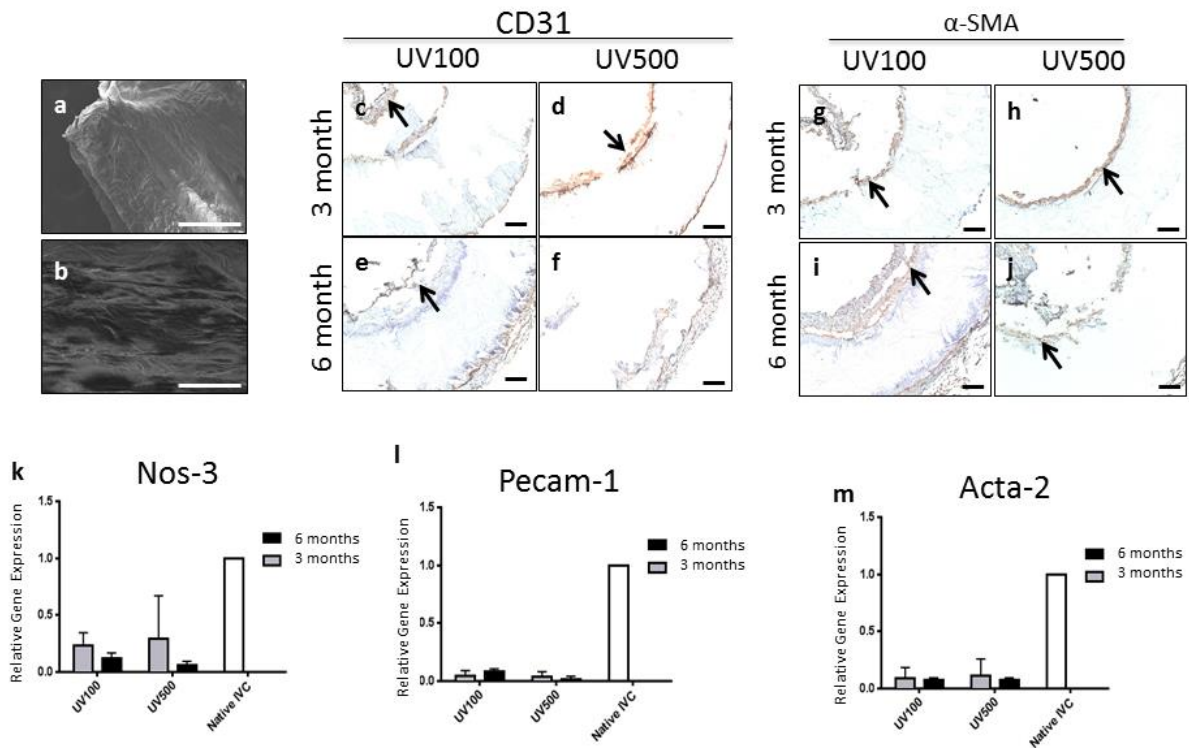
Figure 7.4 Endothelialization of 3D Printed Graft. SEM imaging of (a) UV100 and (b) UV500 grafts illustrate an intact endothelial monolayer in both groups confirmed a confluent attached endothelial monolayer; scale bars are 500 μm. CD31 staining of (c and e) UV100 and (d and f) UV500 graft walls to identify endothelial cells at the (c and d) 3 month and (e and f) 6 month time points demonstrates an endothelial monolayer, although there is detachment of the endothelial cell layer visible due to the histological preparation process. CD31 stained cells indicated by arrows. RT-qPCR for (k) NOS-3 and (l) Pecam-1 expression in tissues adhered to grafts compared to native IVC. Vascular smooth muscle cell proliferation in the 3D printed graft is shown with α-SMA staining of (g and i) UV100 and (h and j) UV500 sections at the (g and h) 3 month and (i and j) 6 month time points. α-SMA stained cells are indicated by arrows; scale bars are 100 μm. RT-qPCR for (m) Acta-2 indicates Acta-2 expression and smooth muscle cell proliferation,

H&E staining of explanted graft sections are shown in Figure 7.3g-j. Of note, detachment of the intimal layer was an artificial effect created during tissue slicing. Neotissue formation was mainly found along the inner lumen and exterior of the graft, while lumen diameter and wall thickness were

maintained throughout the experiment (Figure 7.3p-q). Most importantly, endothelialization of the grafts was observed. SEM imaging illustrated an intact endothelial monolayer in both groups (Figure 7.4a-b), confirming a confluent attached endothelial monolayer. Endothelial cells (CD-31 staining) and SMC (α-SMA staining) proliferation could be observed along graft surfaces as seen in Figure 7.4a-j. This was observed even without the aid of cell-seeding or the addition of biofunctional molecules to promote cell attachment and growth. Still, minimal cellular infiltration within the graft was observed at any time point. To improve this in future work, because degradation occurred slowly in the current platform, porous features may be incorporated into the 3D printed structure that could induce cell infiltration before and during bulk degradation. This may further enable the 3D printed grafts to perform more similarly to native vessels by enabling more thorough neotissue infiltration, formation, and function.

In assessing tissue functionality, NOS-3 and PECAM-1 gene expression (Figure 7.4k-l) was lower in the 3D printed graft tissues compared to native IVCs. While less endothelial functionality was present in grafts when compared to native IVC according to qt-PCR results, positive expression of eNOS in both groups suggests active vascular tissue repair and remodeling processes. This may also be one reason for the low incidence of thrombosis observed in the present study. NOS-3 is an important regulator of SMC proliferation, as well. However, NOS-3 levels expressed by ECs on the grafts may have decreased at 6 months due to the limited growth of SMCs within the graft. To identify SMCs,

α-SMA staining of explanted graft sections was observed and can be seen in Figure 7.4g to 7.4j. SMC layers can be observed in both groups, although the limited porosity of the 3D printed graft prevents more robust SMC formation of a medial layer. RT-qPCR for Acta-2 indicated that Acta-2 expression and SMC proliferation occurred within neotissues formed on grafts, although they were markedly lower than that of the native IVC over the 6 month time course (Figure 7.4m), which may again relate to the constrained formation of a medial layer due to lack of graft porosity in these experimental models. Our previous work has demonstrated more thorough and uniform infiltration of cells within grafts in as little as two weeks when TEVGs contained higher porosity.[275,298] Porosity may be better achieved either through the use of 3D printers with higher printing resolutions, enabling the fabrication of smaller microarchitectural features, or the use of standard porosity introduction techniques such as porogen leaching.

Vascular remodeling processes underway in the 3D printed grafts was also demonstrated with the secretion of matrix metalloproteases (MMP) and macrophage attachment, a crucial step in graft and tissue formation.[253] To identify macrophages and secreted matrix MMP activity, stains were performed for F4/80, MMP-2, and MMP-9 as seen in Figure 7.5a-l. Corresponding RT-qPCR for confirmed gene expression of Itgam, MMP-2, and MMP-9. Extended inflammation, as evidenced by F4/80 positive cells and relatively high expression of Itgam in both groups over the course of 6 months (Figure 7.5m-o), suggests that implanted scaffolds from both groups elicited a continued

foreign body response. Concomitant with macrophage attachment to scaffolds was significant secretion of matrix MMP, highlighting the degree of extended inflammation and tissue remodeling processes underway. Extended inflammation suggests that implanted scaffolds elicited a continued foreign body response. Such a persistent response may result in tissue calcification.[327–329] This may be avoided through improvement and modulation of the degradation rate of the current PPF vascular graft printing materials and the graft design by altering the molecular weight of the PPF polymer and introducing more surface features to increase surface area. Still, eventual degradation of the grafts may completely eliminate the inflammatory response, in contrast to permanent synthetic grafts currently used in CHD surgeries.
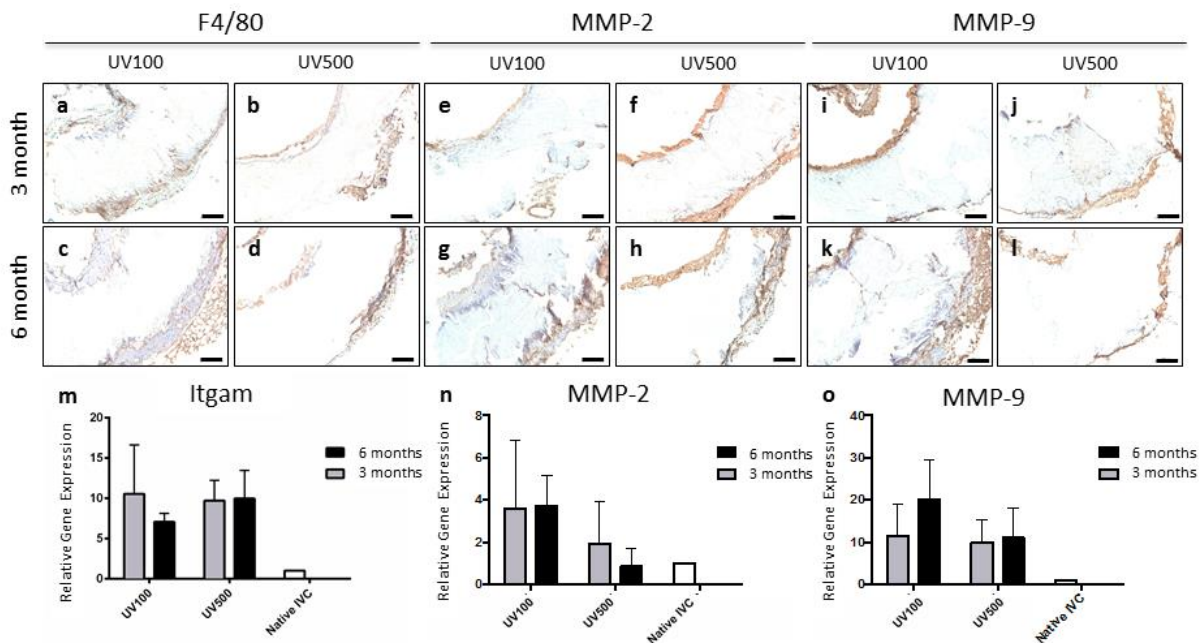
Figure 7.5. Inflammation and Extracellular Matrix Remodeling in 3D Printed Graft. (a to d) F4/80, (e to h) MMP-2, and (i to l) MMP-9 staining of (a, c, e, g, i, k) UV100 and (b, d, f, h, j, l) UV500 sections to identify macrophages and secreted matrix MMP activity at the (a, b, e, f, i, j) 3 month and (c, d, g, h, k, l) 6 month time points; scale bars are 100 μm. RT-qPCR for (m) Itgam, (n) MMP-2, and (o) MMP-9 confirm positive staining observed in tissue samples.
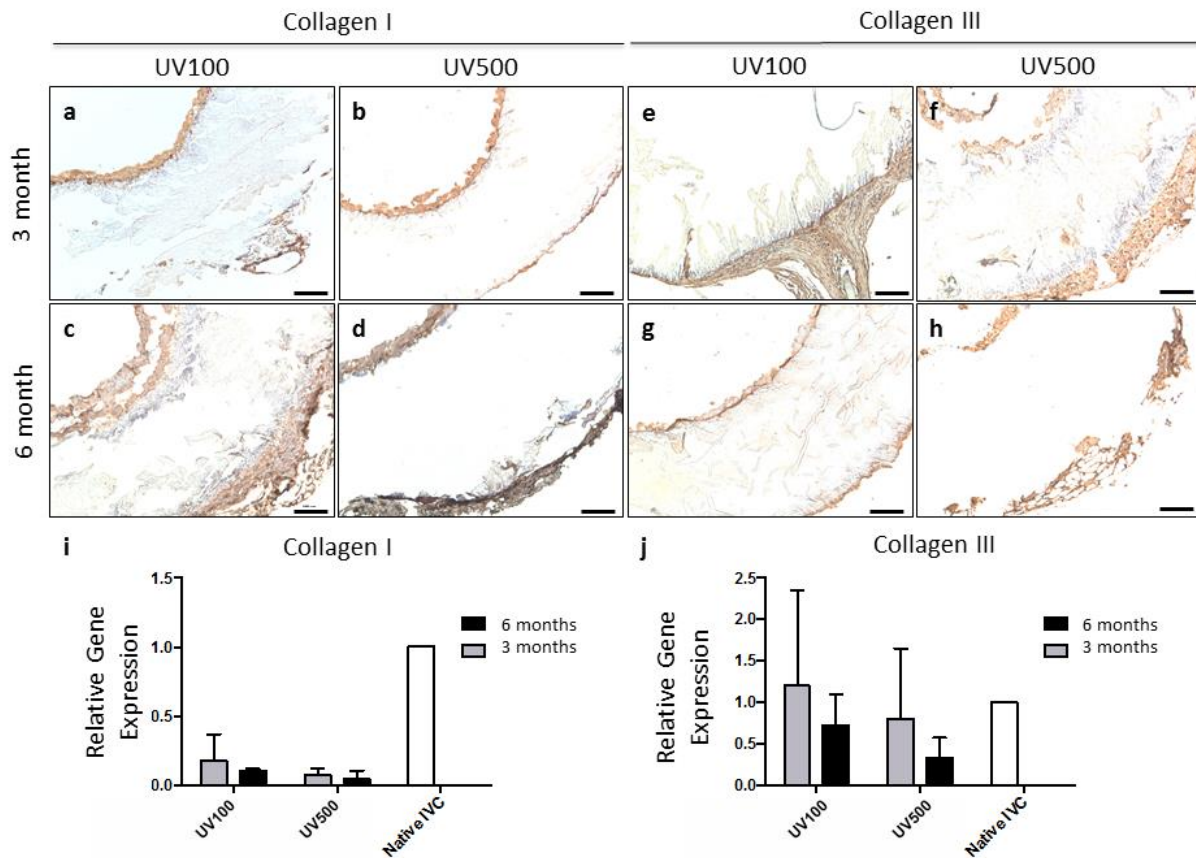
Figure 7.6 ECM Deposition in 3D Printed Graft. (a to d) Collagen I and (e to h) collagen III staining of (a, c, e, g) UV100 and (b, d, f, h) UV500 sections to identify matrix deposition and remodeling at the (a, b, e, f) 3 month and (c, d, g, h) 6 month time points, illustrating that vascular neotissue in both groups was collagen-rich and active ECM turnover occurred in these constructs over 6 months. RT-qPCR of frozen graft explants for (i) collagen I and (j) collagen III was lower or similar to native IVC; scale bars are 100 μm.

Additional evidence of tissue formation was demonstrated by collagen deposition and ECM remodeling. Immunostaining to identify collagen deposition remodeling at the 3 month and 6 month time points illustrates that vascular neotissue in both groups was collagen-rich and active ECM turnover occurred in these constructs over 6 months as seen in Figure 7.6a-h. While

Collagen I expression appeared reduced compared to native IVC (Figure 7.6i), gene expression of Collagen III appeared similar to that of native IVC at 3 months (Figure 7.6j). Early (3 month) expression of Collagen III is a common observation in graft implants and suggests active ECM deposition, tissue remodeling, and immature neotissue. However, the lack of Collagen I expression at later time points could be attributed to either the extended inflammation and high MMP activity (Figure 7.5n-o) or a reduced influence of mechanobiological and biomechanical stimuli on infiltrating cells and deposited ECM due to the slow degradation rate of the 3D printed polymer scaffold.

7.4 Conclusion

To conclude, we examined and present here a novel method of 3D printing biodegradable materials for vascular tissue engineering. Overall this graft fabrication strategy enabled the printing of scaffolds with inner diameters of 1 mm and wall thicknesses of 150 μm which sustained patency and functionality over 6 months of implantation in the venous system of mice. The scaffolds and materials we designed and analyzed possessed adequate mechanical properties and were capable of supporting vascular tissue growth both *in vitro* and *in vivo*. Implantation of the 3D printed grafts within mice demonstrated the suturability and long-term efficacy of the scaffolds up to 6 months after surgery, demonstrating that the 3D printed polymer resin can be a suitable vascular material. Future efforts in this arena will incorporate more complex microarchitectural features along with patient-specific macroscale

geometries. This material and technique provides a powerful platform that can be expanded upon for the study and development of customized vascular tissue engineering scaffolds utilizing 3D printing technologies.

Chapter 8: Comparison of Poly(Propylene Fumarate) and Poly(Propylene Fumarate-*co*-Caprolactone) Vascular Grafts[7]

8.1 Introduction

The most common birth defect in the world is congenital heart disease, and severe cases require extensive surgery using permanent vascular grafts. However, the gold-standard grafts come from premade sizes that do not allow for the long-term growth of patients. To minimize complications associated with permanent synthetic grafts, researchers are turning to biodegradable tissue engineering scaffolds. These strategies are especially attractive when coupled with 3D printing technologies to fabricate custom-tailored vascular grafts.
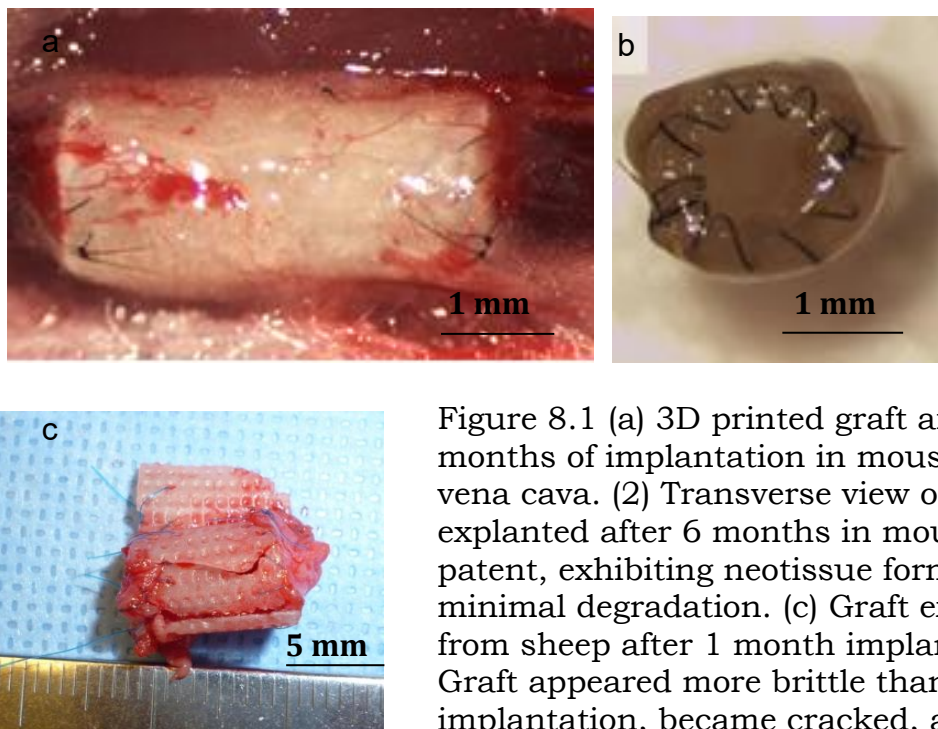
Figure 8.1 (a) 3D printed graft after 6 months of implantation in mouse inferior vena cava. (2) Transverse view of graft, explanted after 6 months in mouse. Still patent, exhibiting neotissue formation, but minimal degradation. (c) Graft explanted from sheep after 1 month implantation. Graft appeared more brittle than at time of implantation, became cracked, and exhibited signs of stenosis.

Previously, we investigated 3D printable biodegradable poly(propylene fumarate) (PPF) grafts. Examples are shown in Figure 8.1. These grafts supported cell viability and exhibited mechanical properties similar to native blood vessels. We implanted the grafts in the inferior vena cava of mice. Grafts remained patent after 6 months, although degradation appeared minimal. The grafts were next implanted in the carotid arteries and veins of sheep. While they functioned in the carotid vein, grafts failed in the arterial environment due to fracturing and restenosis

To mitigate these issues, we investigated altering our 3D printing resin by utilizing copolymers to help adjust the mechanical properties of grafts printed from our polymers. Several different copolymers of PPF have previously been studied to alter the polymer's intrinsic properties. Polymers such as poly(ethylene glycol), hyaluronic acid, and polycaprolactone have been incorporated or copolymerized with PPF and PPF-based constructs.[330–333] We chose to examine a PPF and poly(caprolactone) (PCL) copolymer, with chemical structures demonstrated in Figure 8.2. We hypothesized that the addition of PCL components (which do not contain crosslinkable carbon-carbon double bonds) would decrease crosslinking between polymer chains and thus decrease stiffness and increase degradation rates with higher feed ratios of PCL during copolymer synthesis.

By incorporating different feed ratios of PCL into a poly(propylene fumarate-*co*-caprolactone)-based printing resin, we aimed to adjust the mechanical properties and degradation characteristics of our 3D printing resin

and compare these results with that of a PPF-only resin we previously investigated.
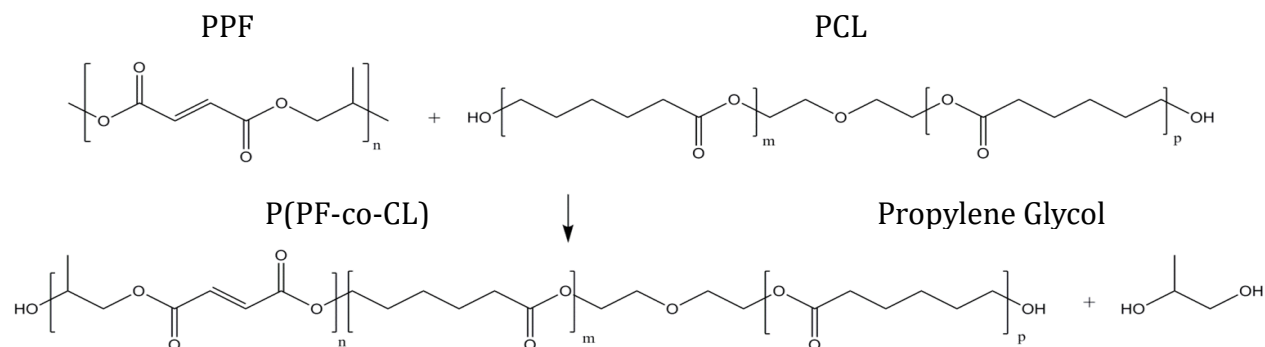
Figure 8.2 Chemical structures of PPC and PCL before copolymerization. Following copolymerization reaction, P(PF-co-CL) and byproduct, propylene glycol, are produced.

8.2 Methods

8.2.1 Material Synthesis and Preparation

Poly(propylene fumarate-co-caprolactone) (P(PF-co-CL) was synthesized in the laboratory according to previously documented methodologies.[321,334] Briefly, 1,2-propane diol and diethyl fumarate (DEF) were mixed in a three-neck flask with a catalyst, zinc chloride, and a crosslinking inhibitor, hydroquinone. The fumaric diester was first obtained by maintain the reaction at 150° C for four hours. Byproducts ethanol and excess 1,2-propane diol were removed. The resulting intermediate was transesterified under vacuum until a molecular weight (Mn) of ~1200 was achieved. Following polymerication of the PPF block, different feed ratios of polycaprolactone diols (Mn ~2000) (Sigma) were added. Feed ratio refers to mass PCL added during synthesis in relationship to the total mass (TM) of DEF and PCL components (theoretical

PCL composition in the final copolymer). The following ratios were used: 0.3 PCL:TM, 0.5 PCL:TM, and 0.7 PCL:TM. A catalyst, 0.2 g of antimony trioxide, was added to the three-neck flask and the polymers were mixed under nitrogen at 100° C for 30 min. The reaction temperature was then gradually raised to 160° C under vacuum and copolymerization was allowed to take place for 5 hrs. The resulting copolymer was purified with distilled water and saturated brine. Sodium sulfate was then used to remove the organic phase, followed by vacuum filtration. Following dissolving the copolymer in methylene chloride, the P(PF-*co*-CL) was obtained by rotary evaporation, precipitated in ether, and then underwent rotary evaporation again. The copolymer was then diluted with DEF at a 4:5 mass ratio (DEF:P(PF-co-CL)) to reduce viscosity of the 3D printing resin. Photoinhibitors, α-tocopherol and HMB (Sigma), were added to control diffusive crosslinking. A photoinitiator, bis(2,4,6-trimethylbenzoyl) phenylphosphine oxide (BAPO, Ciba Specialty Chemical, Tarrytown, NY) was added at 1% w/w

8.2.2 Sample Fabrication

3D models were constructed via Solidworks (Dassault Systèmes SolidWorks Corp, Waltham, MA) and printed via an EnvisionTec Perfactory 4 (Dearborn, MI). The mode of fabrication was UV light digital stereolithography to cure individual 50 µm layers of resin at 50 s exposure with a brightness of 275 mW/dm^2. Dogbone shapes were printed for mechanical characterization with a thickness of 0.30 mm, an effective length of 7.0 mm, and a width of 2.0 mm. For mass degradation studies, vascular grafts similar to our previous

studies were fabricated with lengths of 6.0 mm, inner diameters of 1.0 mm, and a wall thickenss of 0.15 mm. For cell culture assays, discs were printed with 6.3 mm diameters and thicknesses of 0.2 mm. Grafts were then exposed to 100 flashes of an Otoflash lamp (EnvisiontTec) to complete post-process crosslinking of the samples.

8.2.3 Mechanical Testing

Tensile testing assessed ultimate tensile strength (UTS) and elastic modulus. Tensiometry was performed with an INSTRON 5560 tensiometer using a 50 N load cell (Instron) with a crosshead spead of 10 mm/min. Printed samples were elongated until failure.

8.2.4 Degradation

Mass was recorded over time to assess grafts that were immersed in a PBS environment at 37° C. Mass was evaluated at each time point (days 0, 7, 14, 28, 56).

8.2.5 X-ray Photoelectron Spectroscopy (XPS) Analysis

Prior to analysis, all samples were rinsed in deionized water to remove buffer salts. The Kratos Axis Ultra delay-line detector (DLD) instrument in hybrid mode using a monochromatic Al K$\alpha_{1,2}$ x-ray source ($h\nu$ = 1486.6 eV) was used (Kratos Analytical Ltd, Manchester, UK). The axis of the analyzer lens was oriented at 0° from the surface normal to capture the emitted photoelectrons. Elemental composition of the surface was obtained from a survey scan covering 0 eV to 1300 eV using a pass energy of 160 eV with an energy resolution of 1 eV. High-resolution spectra of the C_{1s} regions (278 eV to 298 eV) were acquired

using a pass energy of 40 eV with an energy resolution of 0.1 eV. 3 survey scans and 1 high resolution scan were performed on each sample. Energy scales were calibrated by normalizing the large CH_x peak in the C_{1s} region to 285.0 eV and a linear background was subtracted for all peak quantifications. The peak areas were normalized by the manufacturer supplied sensitivity factors.

8.2.6 Time-of-Flight Secondary Ion Mass Spectrometry (ToF-SIMS) Analysis

ToF-SIMS experiments were performed using an Iontof IV (Iontof GmbH, Münster, Germany) instrument equipped with a 15 keV Bi_3^+ analysis source and an 8 keV Ar^+ sputter source, both oriented at an incidence angle of 45°. Bi_3^+ in the high-current bunched mode (high resolution mode) was rastered within a 500 μm × 500 μm area to acquire mass spectra in both positive and negative polarities. Spectra were calibrated to CH_3^+, $C_3H_4^+$, $C_3H_7O^+$, and $C_7H_3^+$ peaks for positive polarity, and CH^-, C_2H^-, C_3H^-, and C_4H^- peaks for negative polarity. Images of 2 mm × 2 mm were also acquired in the large scan analysis mode to visualize the distribution and homogeneity of the protein coverage on the surface. The ion dose density used was 2.1×10^{10} ions/cm^2, well under the static limit of 10^{12} ions/cm^2 where only 1% of the sample surface is consumed.

8.2.7 Cell Attachment and Proliferation

HUVECs (Lonza) were seeded on 3D printed discs placed in 96 well plated to determine potential cytotoxicity of the printed copolymers in comparison with printed PPF. 5×10^3 cells were deposited on each sample, one sample per well. Cell culture plates were then incubated for 1.5 hrs at 37° C to

assess initial attachment. After incubation, non-adherent cells were removed through sterile PBS washing. Live/Dead staining was used to identify living cell populations and images were obtained using a fluorescent filter via a light microscope. All cell counts were normalized to a PPF control. To assess short-term proliferation, seeded HUVECs were also washed, stained, and imaged at 1 and 4 days after initial seeding.

8.3 Results

Copolymers of PPF and PCL were synthesized based on three different PCL feed ratios during initial synthesis to create P(PF-*co*-CL). Molecular weight (Mn) of the resulting copolymers is show in in Table 8.1. All three copolymers were able to be incorporated in 3D printing resins and yielded successfully printed samples for all prior studies.

Table 8.1 PCL feed ratio during synthesis and resulting copolymer molecular weight (Mn)

PCL feed ratio	P(PF-*co*-CL) mol wt (Da)
0.30	6395
0.50	6593
0.70	6602

Tensiometry was used to determine the UTS and elastic moduli of dogbone samples printed with the various polymers. Printing with a feed ratio of 0.3 resulted in samples with an UTS of 16.65 ± 1.48 MPa and an elastic modulus of 175.00 ± 19.50 MPa, 0.5 resulted in samples with an UTS of 2.01 ± 0.33 MPa and an elastic modulus of 6.28 ± 1.03 MPa, and 0.7 resulted in

samples with an UTS of 13.38 ± 1.75 MPa and an elastic modulus of 90.94 ±

14.98. Results are shown in Figure 8.3. Results demonstrated statistically

significant differences between all samples. Mass degradation of grafts (Figure

8.4) exhibited a 15.52 ± 0.83 % loss after eight weeks in 0.30 PCL:PPF samples,

28.87 ± 3.77 % loss in 0.5 PCL:PPF samples, and 18.11 ± 0.35 % loss in 0.7

PCL:PPF samples.
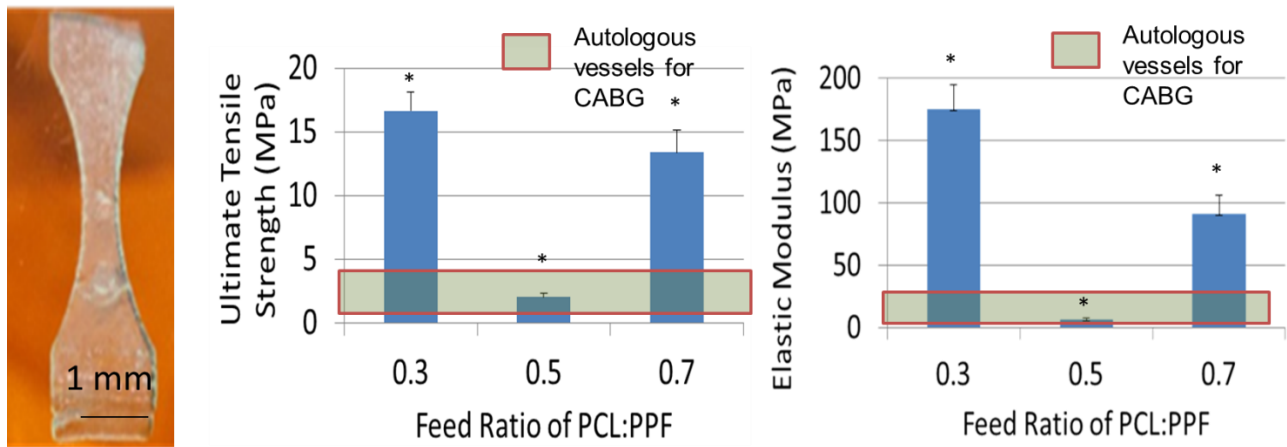
Figure 8.3 Mechanical properties of printed samples compared to native vessels used as autologous implants according to the literature sources.[235,236,238,239,275] * represents statistical significance between groups (p<0.05).

ToF-SIMS was used to identify the molecular fragments of the polymers,

and if possible, discriminate which fragments are originating from which

polymer type. This way, comparing the intensities of the fragments could reveal

concentration differences. To facilitate the identification of fragments from

spectra that contain millions of peaks, a multivariate statistical analysis called

principal components analysis (PCA) was performed. The process quickly

identified peaks in the spectra that corresponded with a specific type of

polymer, and illustrated that the intensity varies linearly with the feed ratio. For example in the negative spectrum, principal component 2 identified a collection of peaks from PPF (shown in Figure 8.5) whose intensities varied rather linearly with concentration. Intensity of peaks identified by PCA demonstrated decreasing intensity as concentrations of PCL increased as shown in Figure 8.6.

Table 8.2 XPS survey scan results demonstrate the surface elemental composition (atomic %) of the four samples, and high resolution C 1s scan results show the quantitative composition of the C-C bond at a binding energy of 285 eV, C-O bond at a binding energy of 287 eV, and C=O bond at a binding energy of 289 eV. High resolution C 1s scans revealed that the atomic composition of C-O and C=O decreased linearly with the PCL feed ratio (Figure 8.7).

In Figure 8.8 and 8.9, samples from Live/Dead assays can be seen. PPF was used as a control due to its previously demonstrated cell compatibility.[335] There were no statistically significant differences between any of the P(PF-*co*-CL)-based samples compared to the 3D printed PPF samples throughout the duration of the experiment.
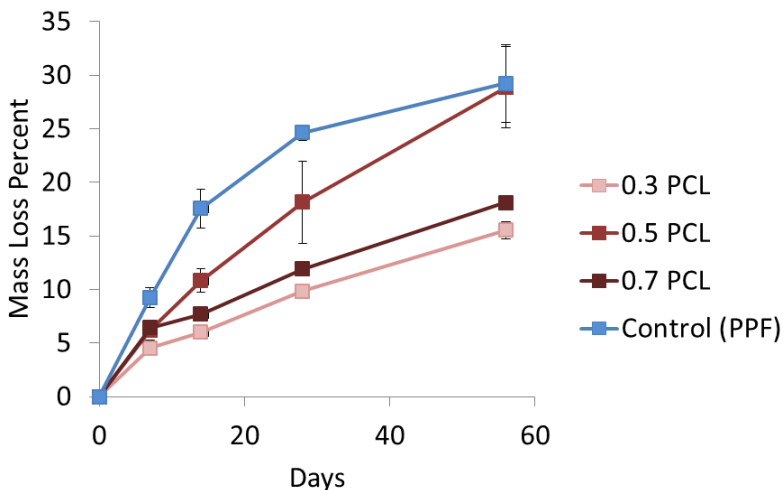
Figure 8.4 Graft degradation observed over 8 weeks. A feed ratio of 0.5 PCL:PPF yielded grafts that degraded most similarly to control PPF grafts. However, 0.3 and 0.5 PCL:PPF grafts degraded at a significantly slower rate, contrasting with our original hypothesis.
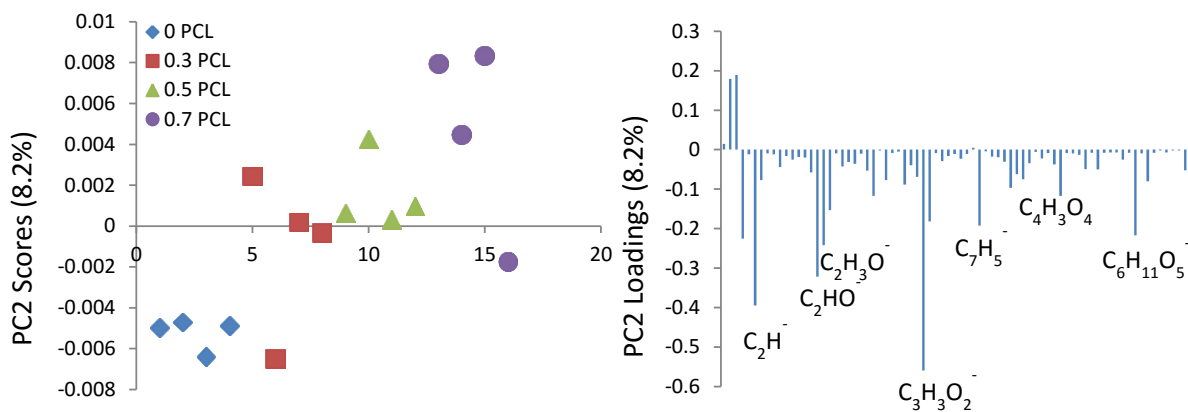
Figure 8.5 Scores and loadings plots from principal component 2 (which represented 8.2% of the variance), showing the variables (peaks) that are responsible for the trend seen in the scores plot. It was found that the intensities of these variables corresponded more with higher PPF concentrations.
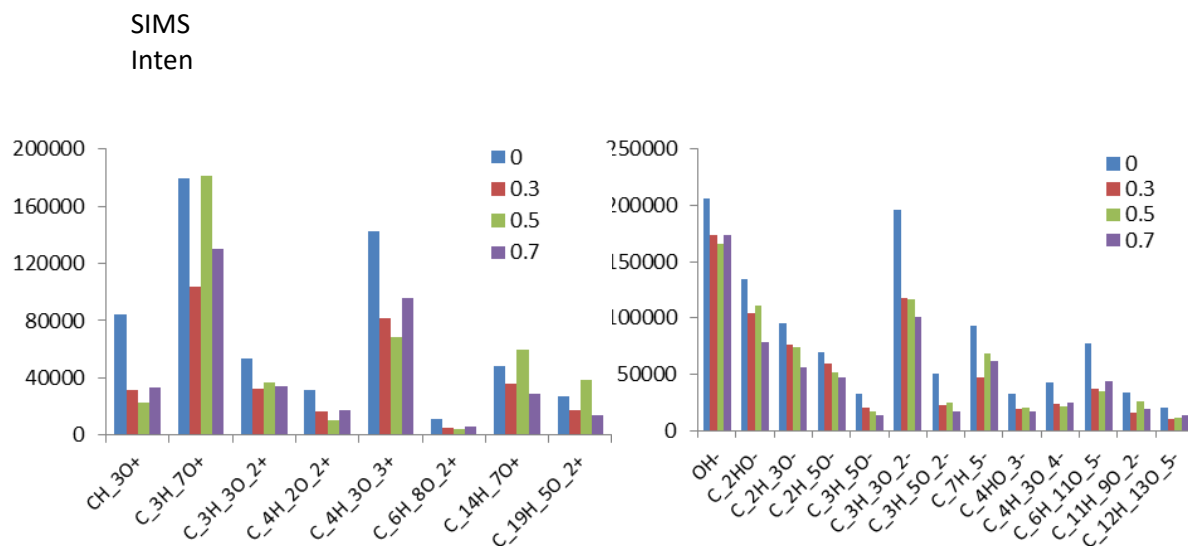
SIMS
Inten

Figure 8.6 ToF-SIMS results showing the raw intensities of the peaks identified using PCA for both positive (left) and negative (right) polarities.

Table 8.2 XPS survey scan results.

	C 1s	O 1s		C-C	C-O	C=O
(1) Pure PPF	70.1 ± 0.2	29.9 ± 0.2		40.1 ± 0.1	34.0 ± 0.0	25.9 ± 0.1
(2) 0.3 PCL/PPF	71.4 ± 0.3	28.6 ± 0.3		46.0 ± 0.2	30.3 ± 0.1	23.7 ± 0.1
(3) 0.5 PCL/PPF	72.3 ± 0.1	27.7 ± 0.1		51.0 ± 1.1	27.4 ± 0.5	21.6 ± 0.6
(4) 0.7 PCL/PPF	72.6 ± 0.3	27.4 ± 0.3		53.5 ± 0.4	25.8 ± 0.3	20.7 ± 0.2
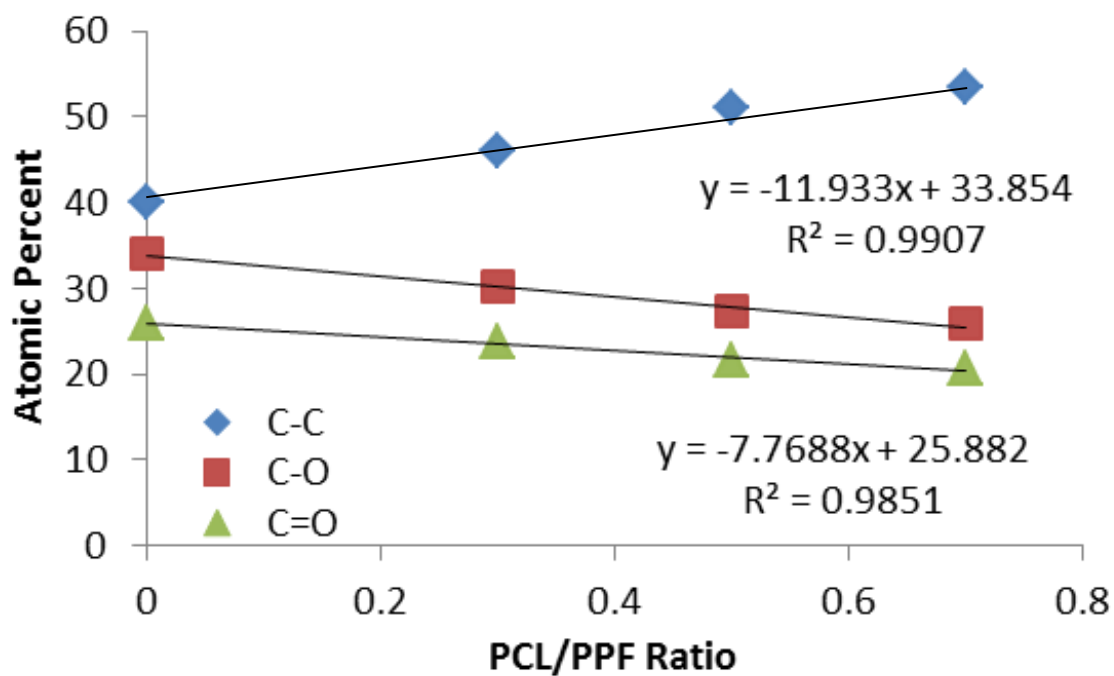
Figure 8.7 Relative concentration of C 1s species plotted as a function of PCL/PPF ratio.
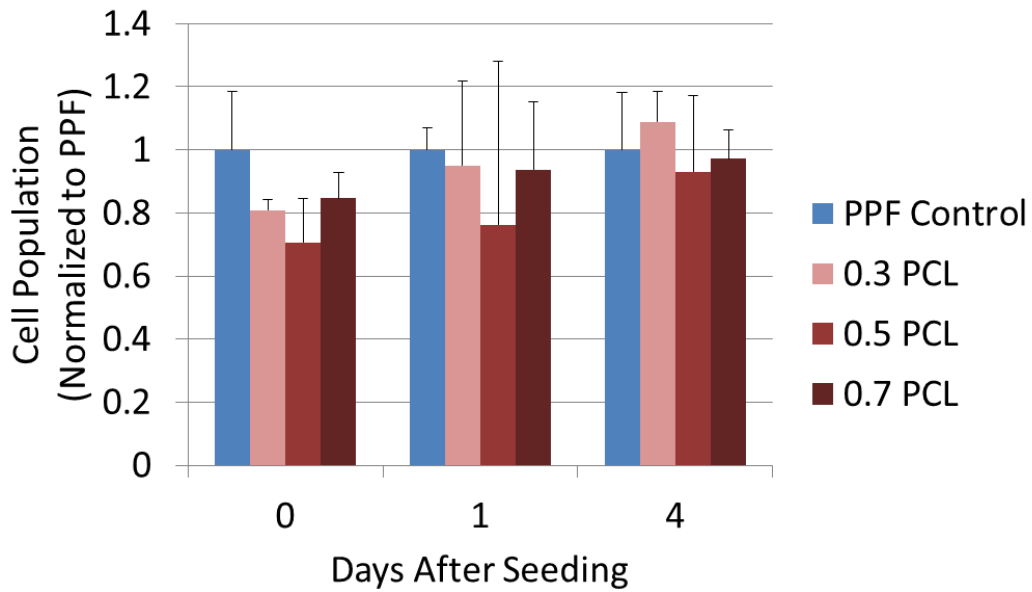
Figure 8.8 Cell populations compared to control PPF (a documented biocompatible material) at each time point. No significant differences in cell populations were observed over time, with copolymers performing similarly to PPF alone.
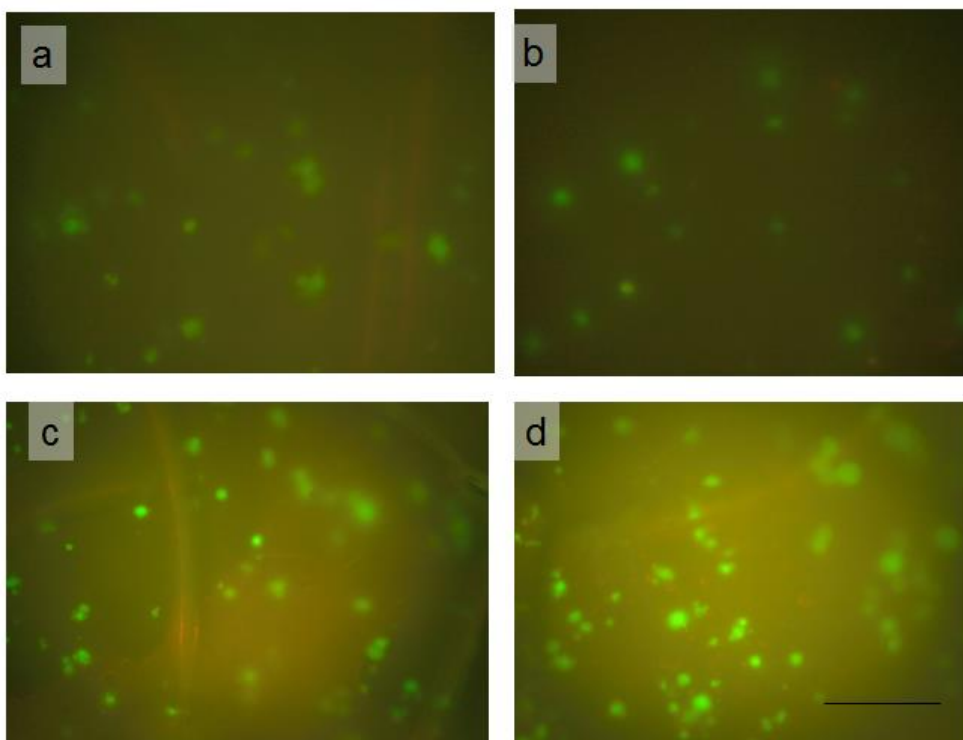
Figure 8.9 Live/Dead images of HUVECs after initial attachment on grafts with PCL feed ratio of (a) 0.3, (b) 0.5, and (c) 0.7. (d) Control PPF. Note autofluorescence of PPF and P(PF-*co*-CL) is an imaging artifact. Scale bar = 200 μm.

8.4 Discussion

Copolymers offer the ability to modulate material properties through varying the ratios of included polymers. PCL, a well-characterized biomaterial, is normally uncrosslinkable, but has been cleared by the FDA for a variety of biomedical uses.[336] When polymerized with PPF, the PPF components enable crosslinking between polymer strands. Previous reports document the crosslinking of P(PF-*co*-CL) through thermal and photocrosslinking.[332,337] We aimed to employ this photocrosslinkable polymer blend into our established 3D printing platform for the fabrication of vascular grafts. By adjusting the

ratio of included PCL diols, we hoped to determine if one of these blends demonstrated mechanical properties consistent with native blood vessels while increasing the degradation rate of our 3D printed grafts.

The majority of the elements present in the material were carbon and oxygen, with a few samples containing silicon from siloxanes (not shown), a common surface contaminant. Monomers of PPF have a C:O ratio of 7:4, but the measured ratio is closer to 7:3 meaning that a large amount of adventitious carbon is likely present on these films. Moreover, with the monomers of PCL having a ratio of 3:1, the 0.5 PCL feed ratio mixture should have a ratio of 7:3, which is reasonably close to the measured ratio of 8:3. Even with the presence of adventitious carbon, the trend is reflective of the actual composition of the polymer mixture. Overall, the decreasing oxygen concentration can be used as an indicator to determine the composition of the mixture. In addition to oxygen, it was found that species of carbon can be used to determine the composition. Figure 8.7 supported the composition of C-O and C=O groups decreased linearly with PCL/PPF, which supports the notion that more PCL is indeed included within block copolymers with increased feed ratios of PCL. Comparing the intensities of the peaks identified by PCA gave an interesting result wherein the majority of the peaks showed a decreasing intensity of these peaks as the concentration of PCL increased (Figure 8.6). The same procedure was performed for positive polarity spectra, with the comparison of the intensities shown in the figure. The trends for the positive peaks were not as convincing, most likely due to the presence of siloxanes on the surface which can

significantly attenuate the peak intensities from charge competition. Since fragments of siloxanes rarely carry negative charges, it turned out that the negative spectra were better at showing this trend in concentration since the ionization efficiency of the polymer fragment ions were was relatively unaffected. However, in summary, ToF-SIMs and XPS both demonstrated copolymer chemical makeups consistent with theoretical predictions based on PCL feed ratios during P(PF-*co*-CL) synthesis.

From our studies, we found certain polymer blends may exhibit sufficient mechanical properties compared to the properties of native vessels, which may alleviate mechanical failure issues demonstrated in earlier PPF-only grafts. Mechanical properties of 3D printed samples were tunable by adjusting the ratio of included PCL, leading to elastic moduli ranging from 6.3–175.0 MPa and UTSs of 2.0–16.6 MPa. However, we did observe an unexpected trend in the copolymer degradation and mechanical strength profiles. Copolymers synthesized with a 0.3 PCL and 0.7 PCL feed ratio produced 3D printed samples with both UTS and elastic moduli well above the document values associated with native blood vessels used in arterial bypass graft procedures. In contrast, 0.5 PCL feed ratios yielded synthesized polymers that, when printed, resulted in samples within the accepted mechanical property range of native vessels.

We hypothesize there may be a couple of phenomena at work: 1.) In the case of 0.3 PCL, the sheer number of available crosslinkable groups in the PPF contributes to high crosslinking and thus higher mechanical strength and

longer degradation times. In such a case, the 0.5 PCL copolymer would benefit from increased flexibility of the polymer backbone due to the increased feed ratio of PCL diols, effectively decreasing the elastic modulus and stiffness.[338] 2.) In the case of 0.7 PCL, there may be increased crosslinking between polymers compared to 0.5 PCL. This may be due to decreased cyclic reactions (intra-polymer crosslinking instead of inter-polymer crosslinking). Such a phenomenon may occur in a polymer with less available C-C double bonds in each polymer strand; this creates a situation in which there is a higher likelihood of inter-polymer crosslinking and thus stronger, more crosslinked polymer networks.

Related to this, increased mechanical properties may be associated with crystallinity. Prior studies demonstrated that P(PF-*co*-CL) is amorphous when PCL compositions are less than 70%.[332] In general, crystalline polymers tend to be much stiffer, which may explain the drastic increase in elastic modulus and UTS of the 0.7 PCL blend compared to the 0.5 PCL blend which may yet be an amorphous polymer. Crystallinity may also affect degradation rates. A previous study describes the morphology of the P(PF-*co*-CL) copolymers with lower feed ratios as reminiscent of PGLA blends.[332] This copolymer has a higher degradation rate than both its individual component polymers. Yet even the blends of P(PF-*co*-CL) with amorphous morphologies (0.3, 0.5) did not result in significantly increased degradation rates compared to PPF alone.

Despite the differences in mechanical properties and degradation rates between the copolymer blends, *in vitro* cell studies demonstrated less variation

between copolymers. Still, HUVECs did not display the spread-out morphology indicative of normal EC cobblestone morphology. This may be due to the highly hydrophobic nature of the P(PF-co-CL) which does not favor cell attachment and proliferation.[337] If these copolymers were to be used for vascular materials, further surface modification, as previously described, may be necessary to reduce the hydrophobicity and enable better cell attachment by promoting normal EC morphology.[339] Cytotoxicity assays indicated no statistically significant difference between PPF and any of the P(PF-*co*-CL) materials in regards to cell viability, showing the biocompatibility of these printing resins are similar. It is also well-known that surface properties such as mechanical properties, topography, and substrate chemistry may influence cell proliferation, adhesion, function, and differentiation.[340–343] Thus, the research presented here offers numerous benefits to studying cellular interactions with biomaterials. 3D printing may be used to control topography of substrates and copolymers maybe used to precisely control mechanical properties. Overall, this copolymer provides a novel, tunable platform for the study of 3D printed tissue engineering scaffolds.

8.5 Conclusion

In this study, we have shown that block copolymers of P(PF-*co*-CL) can be readily synthesized, processed into a 3D printable resin, and used in the 3D printing of biodegradable scaffolds. While we found that two of these copolymers based on synthesis feed ratios of 0.3 and 0.7 PCL:PPF may be

unsuitable as a vascular material, results indicated that scaffolds printed using resins based off a 0.5 PCL feed ratio copolymer may serve as a mechanically compatible vascular graft material. Still, all three copolymers demonstrated cytocompatibility on par with PPF alone, demonstrated that tuning of 3D printable PPF copolymers may be a promising strategy in the development of new 3D printable scaffolds and other tissue engineering applications.

Chapter 9: Biofunctional Modifications of 3D Printed Vascular Grafts[8]

9.1 Introduction
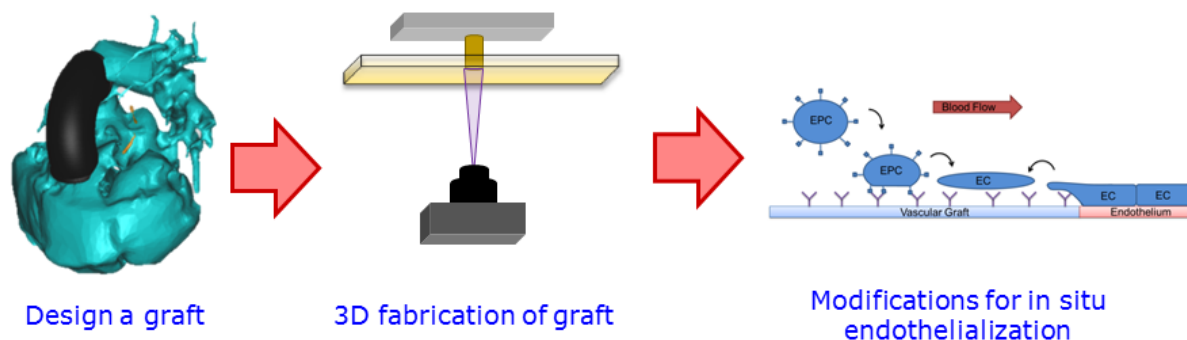
Figure 9.1 3D printing and modification paradigm for the fabrication of patient-specific grafts that are modified to improve neotissue formation.

Congenital heart disease (CHD) is the most common birth defect worldwide and is the leading cause of congenital defect-related death.[310] CHD may present in drastically different geometries between patients. To address the unique challenges of addressing each patient's anatomy, custom fabricated grafts offer the advantage of patient-specific geometry and orientation.[11,12] The development of 3D printable vascular grafts may address this need for custom graft shapes. However, one of the most important

contributors to a vascular graft's success upon implantation is the establishment of a healthy endothelium.[31,231,246] A confluent layer on endothelial cells along the lumen of the graft greatly reduces deleterious side effects such as thrombosis and intimal hyperplasia which result in reduced patency and restricted blood flow. Establishment of a healthy and active endothelium is crucial to all vascular grafts' success, including 3D printable vascular grafts.

A variety of strategies and techniques have been used to enhance the endothelialization of vascular grafts once implanted.[339] Strategies ranging from the introduction of controlled porosity to microarchitectural features to the chemical attachment of biofunctional proteins and other molecules have been pursued. These chemical modifications utilizing biofunctional molecules may be accomplished through the use of reactive chemistries involving the covalent binding of amines.[271,344,345] We have previously demonstrated the benefit of using one of these techniques, EDC-mediated heparin-crosslinking, to immobilize vascular endothelial growth factor (VEGF) and CD34 antibodies (CD34Ab) to the surface of biodegradable polyester vascular grafts.[298] This strategy proved successful in improving the functional endothelialization of implanted vascular grafts compared to unmodified controls.

In this study, we hoped to determine whether these same techniques could be utilized in 3D printed vascular grafts. Again, we propose to use acellular techniques to reduce the regulatory, time, and labor burden for the inclusion of cells in our 3D printed grafts. The overall methodology, as

demonstrated in Figure 9.1, would follow three general steps: 1) Design a custom graft based on medical imaging, 2) 3D print the computer designed graft, and 3) chemically modify the 3D-printed graft with select biofunctional molecules, such as those shown in Figure 9.2. We examine the effects of immobilizing various concentrations of VEGF and CD34Ab on 3D printed PPF grafts on both HUVEC and EPC populations. We use these results to determine strategies of biofunctionalization that best encourage cell attachment, in the hopes that this will improve *in situ* endothelialization of the 3D-printed vascular grafts.
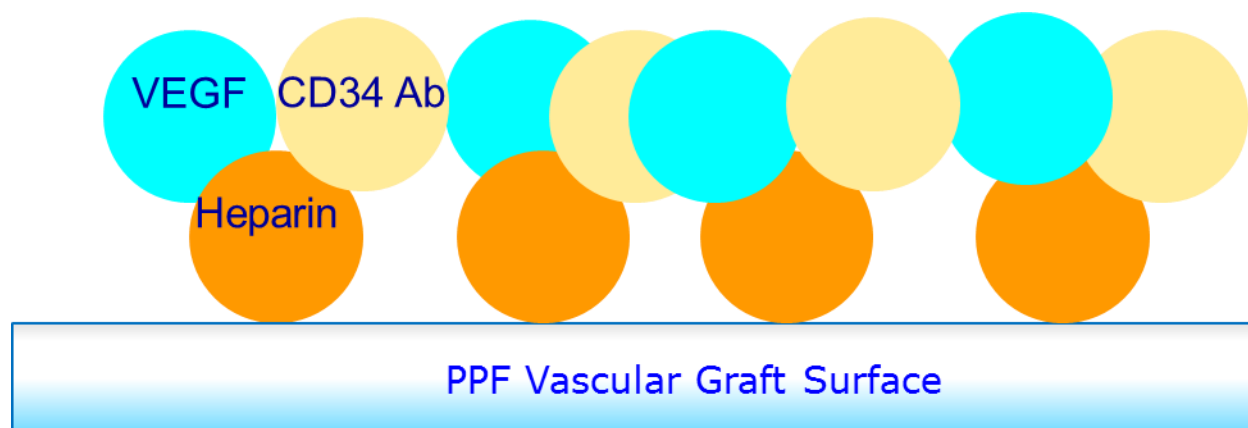
Figure 9.2 Proposed method of biofunctionalization. Heparin, VEGF, and CD34Ab were chosen for their roles in EPC and EC recruitment, attachment, and coagulation regulation.

9.2 Methods

9.2.1 Material synthesis

Polypropylene fumarate (PPF) was synthesized and used in a printing resin as previously described.[321] The reaction was allowed to continue until the PPF reached the desired molecular weight of 1200 Da. This was confirmed

through gel permeation chromatography (GPC). Diethyl fumarate (DEF) was added to the PPF at a weight ratio of 5:4 PPF:DEF to make the printing resin viscosity amenable to 3D printing. Photoininitiators and photoinhibitors were also dissolved in the DEF prior to mixing with PPF under continuous mixing at room temperature for 1 h. These components aid in the resolution of printed objects. To control excess cross-linking, 0.2% w/w α-tocopherol (Vitamin E, Sigma Aldrich, St. Louis, MO) and 1% w/w hydroxyl-methoxybenzophenone (HMB, Sigma) was used. The photoinitiator, bis(2,4,6-trimethylbenzoyl) phenylphosphine oxide (BAPO, Ciba Specialty Chemical, Tarrytown, NY), was added at 1% w/w.

9.2.2 Graft and Sample Fabrication

Films and samples for modification, characterization, and cell attachment purposes were printed using an EnvisionTEC Perfatory P4 with Enhanced Resolution Module (EnvisionTEC, Detroit, MI). This technique utilized UV light digital stereolithography to cure individual 50 μm layers of printing resin at 50 s exposure with a brightness of 275 mW/dm^2. Films of 1 cm x 1 cm were printed for the purpose of XPS and ToF-SIMS characterization, and discs with a diameter of 6.3 mm and a thickness of 0.2 mm were printed for *in vitro* cell studies.

9.2.3 Graft Modification

Heparin crosslinking and quantification was adapted from a previously published method.[271] All grafts were modified with heparin (Hep) alone, VEGF added to Hep, CD34Ab added to Hep, or a combination of VEGF and

CD34Ab (CD34Ab+VEGF) added to Hep-modified grafts. Before crosslinking, scaffolds were immersed in 0.05 M MES buffer (pH = 5.55) for 15 minutes. Scaffolds were subsequently submerged in a solution of 0.5 M ethyl-3-(3-dimethylaminopropyl)-carbodiimide (EDC), 0.5 M N-hydroxysuccinimide (NHS), and 1% w/v heparin in MES buffer. After incubation for 14 hours, scaffolds were washed with distilled water to remove excess byproducts. A sterile solution of VEGF was prepared in PBS at a concentration of 0, 10, 100, or 1000 ng/ml, according to previously published methods[125]. Scaffolds were incubated in the VEGF solution for 1 hour, in sterile conditions, at room temperature. Following incubation, grafts underwent eight 5 min washes in sterile-filtered PBS solution to remove unbound VEGF. For CD34Ab coating, heparin cross-linked grafts were immersed in 0.1, 1.0, and 10.0 µg/mL solutions of primary antibody against CD34 in PBS overnight at 4º C in the dark. Grafts were then washed 3 times with PBS.

9.2.4 Modification Quantification

To quantify VEGF attachment and release, a human VEGF ELISA kit (Sigma) was used according to manufacturer instructions. Briefly, standard VEGF curves were created according to manufacturer instructions and added to a 96-well plate coated with capturing antibodies (human VEGF-A). Samples for bound VEGF quantification were placed in the wells of a 96-well plate and served as the binding substrate for incubation with the 200 µl biotinylated anti-human VEGF detection antibody (100 ng/ml). Next, 200 µl of streptavidin-horse radish-peroxidase solution was added to each well and the plates were

incubated for 45 minutes at room temperature. Following this, 100 µl of tetramethylbenzidine (TMB) solution was added and plates were subsequently incubated for 30 min in the dark at room temperature. The reaction was stopped by adding 50 µl of 2N H_2SO_4 "Stop" solution. The optical density (OD) of the resulting solutions was measured using a SpectraMax M5 plate reader at 450 nm with a reference wavelength of 650 nm. Values of VEGF immobilized on scaffolds were calculated from the standard curve. For VEGF release, scaffolds with bound VEGF were incubated in PBS at 37° C with 65 rpm shaking. The PBS was collected at 1 h, 4 h, 24 h, and 40 h and replaced with fresh PBS. VEGF released into the solution was quantified using the previously described ELISA methods.

To confirm antibody immobilization, antibody-modified and unmodified scaffolds were incubated at room temperature with 1% bovine serum albumin solution for 30 min at room temperature to prevent non-specific binding. Scaffolds were then washed 3 times with PBS and a secondary anti-goat IgG antibody conjugated with FITC was added at 10 µg/mL in PBS. Scaffolds were again washed 3 times with PBS. Successful antibody immobilization could be observed using fluorescent microscopy. To quantify antibody attachment, a Goat IgG ELISA kit (Alpha Diagnostic International, San Antonio, TX) was used. The procedure followed manufacturer instructions, substituting CD34Ab instead of the IgG standards included with the kit. In addition, non-specific binding of CD34Ab was assessed by incubating CD34Ab with graft surfaces as described, except no crosslinking of heparin was performed.

9.2.5 X-ray Photoelectron Spectroscopy (XPS) Analysis

Prior to analysis, all samples were rinsed in deionized water to remove buffer salts. The Kratos Axis Ultra delay-line detector (DLD) instrument in hybrid mode using a monochromatic Al $K\alpha_{1,2}$ x-ray source (hv = 1486.6 eV) was used (Kratos Analytical Ltd, Manchester, UK). The axis of the analyzer lens was oriented at 0° from the surface normal to capture the emitted photoelectrons. Elemental composition of the surface was obtained from a survey scan covering 0 eV to 1300 eV using a pass energy of 40 eV with an energy resolution of 0.5 eV. High-resolution spectra of In_{3d} (eV to eV), P_{2p} (120 eV to 140 eV), and C_{1s} regions (278 eV to 298 eV) were acquired using a pass energy of 40 eV with an energy resolution of 0.1 eV. At least 3 scans were performed on each sample. Energy scales were calibrated by normalizing the large CH_x peak in the C_{1s} region to 285.0 eV and a linear background was subtracted for all peak quantifications. The peak areas were normalized by the manufacturer supplied sensitivity factors.

9.2.6 Time-of-Flight Secondary Ion Mass Spectrometry (ToF-SIMS) analysis

ToF-SIMS experiments were performed using an Iontof IV (Iontof GmbH, Münster, Germany) instrument equipped with a 25 keV Bi_3^+ analysis source and an 8 keV Ar^+ sputter source, both oriented at an incidence angle of 45° to the surface normal. For analysis, Bi_3^+ in the high-current bunched mode was rastered within a 150 μm × 150 μm area to acquire mass spectra in both positive and negative polarities. Spectra were calibrated to CH_3^+, $C_3H_4^+$, $C_3H_7O^+$, and $C_7H_3^+$ peaks for positive polarity, and CH^-, C_2H^-, C_3H^-, and C_4H^-

peaks for negative polarity. Images of 2 mm × 2 mm were also acquired in the large scan analysis mode to visualize the distribution and homogeneity of the protein coverage on the surface.

9.2.7 Cell Attachment and Proliferation

   In vitro cell culture assays were used to assess initial cell attachment and metabolic activity over time to assess differences between CD34Ab- and VEGF-modified grafts compared to controls in 96-well tissue culture plates. HUVECs were obtained and cultured according to manufacturer's instructions (Lonza, Basel, Switzerland). Scaffolds were printed to fit 96-well tissue culture plate and placed in the bottom of the wells. Culture plates with CD34Ab-immobilized, heparinized control and unmodified control grafts were sterilized under ultraviolet (UV) irradiation for 1 hr. Grafts intended for VEGF-modification were UV irradiated before loading with sterile solution VEGF. Cells were seeded in the wells at a density of 5×10^4 cells/well and incubated at 37° C. To measure cell metabolic activity, an XTT assay was performed at 1.5 hrs, 1 day, and 3 days after initial cell seeding. At each of these time points, cells also underwent Live/Dead staining and were counted via microscopy. Cell attachment numbers were defined by the total number of cells still adhered to graft surfaces after washing. Fold change in cell populations was calculated by dividing the final cell population count (Day 3 time point) by the initial attachment number (1.5 hrs after seeding). Human endothelial progenitor cells (EPCs) were obtained and cultured manufacturer's instructions (CelProgen, San Pedro, CA). Methods for assessment were identical to HUVEC assays.

9.2.8 Statistical Analysis

Data were analyzed using analysis of variance single factor analysis with Student's *t*-test or ANOVA assuming normal data distribution with a confidence of 95% ($p < 0.05$). Standard deviation error bars are reported on each figure along with relevant statistical relationships.

9.3 Results

The success of heparinization was confirmed through the dark blue color change associated with the toluidine blue assay demonstrated on heparinized printed PPF grafts as shown in Figure 9.3. In addition, FITC-conjugated antibody attachment (Figure 9.3) and ELISA results confirmed the attachment of CD34Ab (Figure 9.4). VEGF immobilization was confirmed via ELISA in Figure 9.5.

according to the
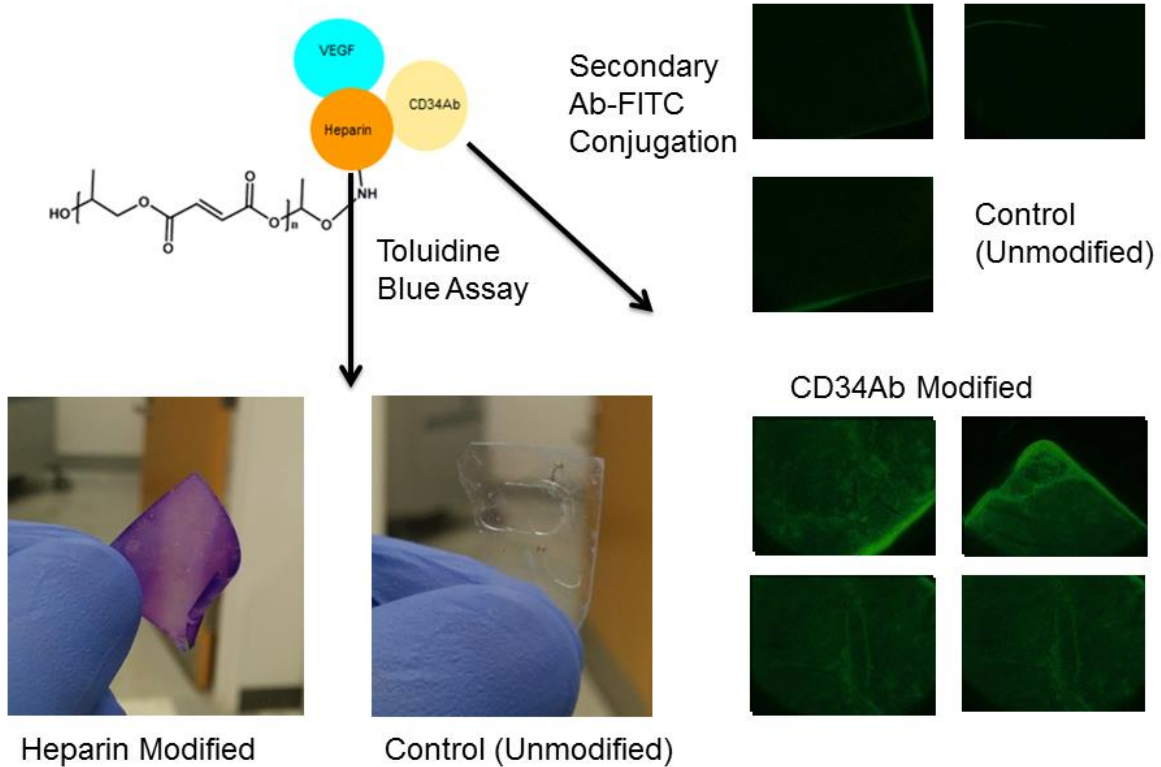
Figure 9.3 Verification of heparin modification as demonstrated by toluidine blue assay and CD34Ab attachment via a FITC-conjugated anti-goat antibody. (CD34Ab contains goat IgG)

Loading capabilities of various concentrations of VEGF are shown in Figure 9.5. While incubating PPF films in a VEGF solution of 10 ng/ml demonstrated lower concentrations of attached VEGF, there was no significant difference between VEGF attachment on films incubated in VEGF solutions of 100 and 1000 ng/ml. Likewise, these results corresponded to the attachment of HUVECs to the modified surfaces. No significant differences were found

between HUVEC attachment on films incubated in 0 and 10 ng/ml VEGF

solutions. However, both 100 and 1000 ng/ml VEGF solutions resulted in

increased attachment of HUVECs. EPCs experienced no statistically significant

differences between films incubated with various levels of VEGF.

In Figure 9.4, results of incubating PPF films in various concentrations of

CD34Ab can be seen. A significant increase in the concentration of attached

antibody was demonstrated in vascular grafts incubated with 1.0 or 10.0 µg/ml

compared to films incubated in 0.0 or 0.1 µg/ml of CD34Ab. In addition, films

incubated in 10.0 µg/ml exhibited greatly increased concentrations of

antibodies compared to films incubated in 1.0 µg/ml CD34Ab. Both HUVECs

and EPCs demonstrated greater fractions of attached cells on PPF films

incubated with 1.0 and 10.0 µg/ml of CD34Ab.
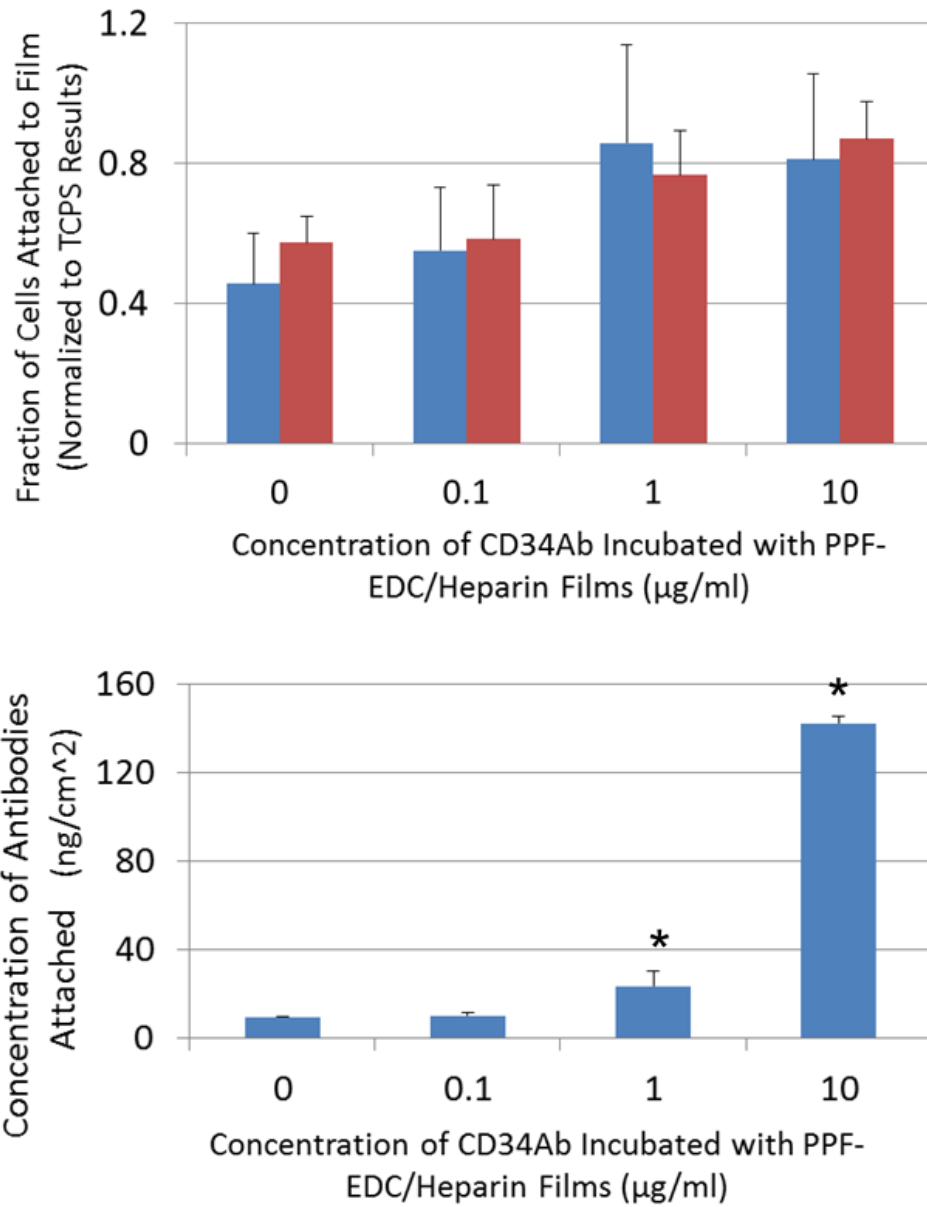
Figure 9.4 Fraction of cells attached to CD34Ab-modified grafts, and concentrations of CD34Ab relative to solutions 3D printed samples were incubated in. * represents statistical significance between groups (p<0.05)
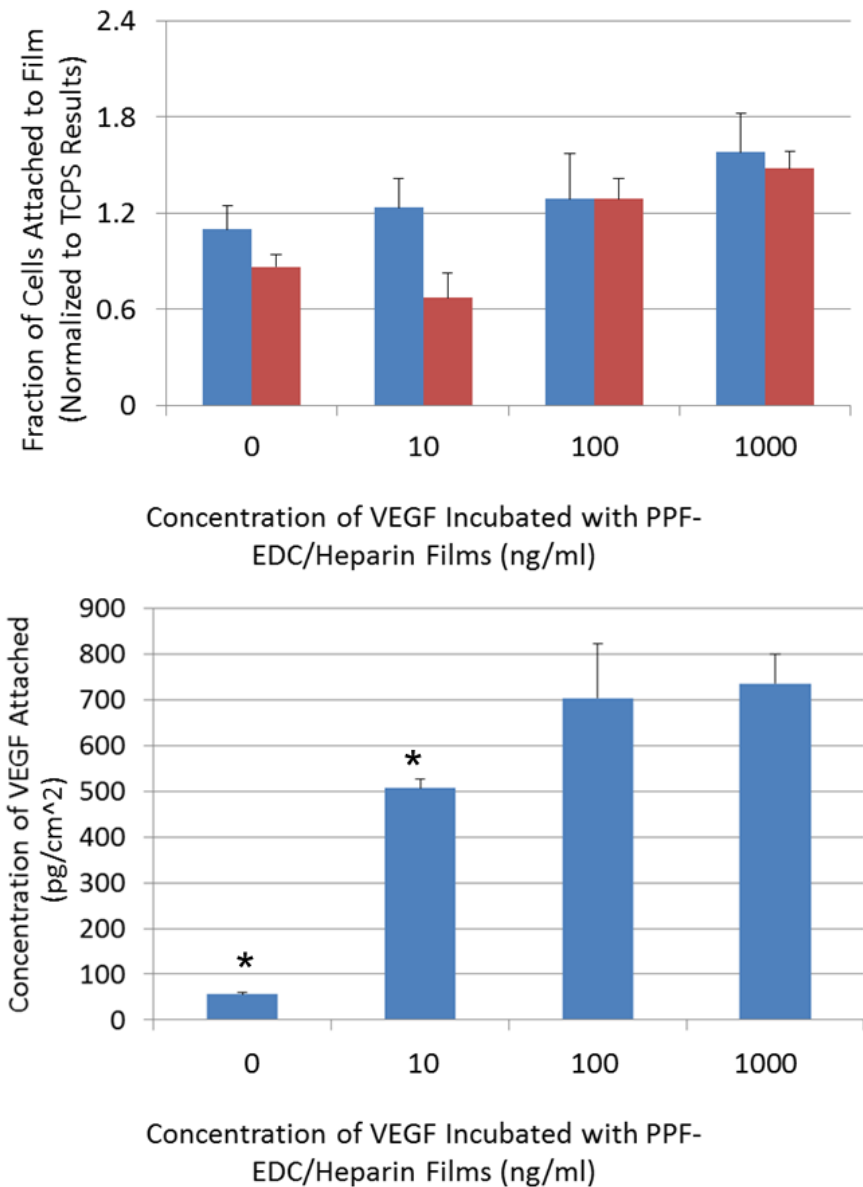
Figure 9.5 Fraction of cells attached to VEGF-modified grafts, and concentrations of VEGF relative to solutions 3D printed samples were incubated in. * represents statistical significance between groups (p<0.05)

From these results, subsequent experiments utilized 100 ng/ml VEGF incubations and 10 μg/ml CD34Ab incubations for graft modifications.

Table 9.1 shows the XPS survey scan results. The majority of the elements are carbon and oxygen, followed by nitrogen/sulfur from proteins, sodium from buffers, and silicon from siloxane.

Table 9.1 Survey scan showing the elemental composition (%) of the five surfaces

	C 1s	N 1s	O 1s	Si 2p*	S 2p	Na 1s
(1) Control	69.1	0.2	30.1	0.6	-	-
(2) Hep	66.5	8.6	24.0	0.1	0.2	0.5
(3) CD34Ab	65.0	13.6	20.5	0.3	0.4	0.3
(4) VEGF	65.9	11.5	21.7	0.3	0.4	0.3
(5) CD34Ab+VEGF	65.0	15.4	18.7	0.3	0.3	0.3

* the source of Si is from siloxanes, a common contaminant in plastic vials, bottles, tubes, etc.

Table 9.2 High resolution C 1s scans showing the fraction of oxidized C (%).

	C-C	C-O	C=O
(1) Control	40.6	34.1	25.3
(2) Hep	67.3	3.6	29.1
(3) CD34Ab	62.2	5.8	32.0
(4) VEGF	65.3	3.7	31.0
(5) CD34Ab+VEGF	60.1	5.3	34.6

The high resolution scans of C 1s lines shows the chemical composition of the carbon species. For the control, roughly 34 % of the carbon is in the form of an ether and 25 % as a carbonyl group. Table 9.2 shows results of C 1s scans.

ToF-SIMS analysis of protein films is difficult due mostly to two factors: the absence of large secondary ion fragments that could identify the amino acid (due to ion-induced fragmentation); and the interpretation of the varying concentration of amino acid fragments to determine a protein's identity. There are characteristic fragments that correspond to each of the 20 amino acids (see Table 9.3); however, since most proteins contain the same 20 amino acids, ToF-SIMS data from adsorbed proteins cannot be easily differentiated based on the presence or absence of unique peaks. To overcome this problem, a multivariate analysis technique called principal components analysis (PCA) has been used to facilitate the identification process. The technique can reveal

differences between each mass spectra (scores) by comparing the relative intensities of each of the amino acid fragments shown in Table 3 (loadings).

Table 9.3 Summary of the most intense fragment peaks observed in the positive spectra of poly(amino acids). Only the top three most intense peaks, if more than one, were included per amino acid for brevity. For a full list, consult previous studies.[346]

Ala	44.05 (C_2H_6N), 143.08 ($C_6H_{11}N_2O_2$)
Arg	43.03 (CH_3N_2), 73.09 ($C_4H_{11}N$), 100 ($C_4H_{10}N_3$)
Asn	70.03 (C_3H_4NO), 87.06 ($C_3H_7N_2O$), 88.04 ($C_3H_6NO_2$)
Asp	88.04 ($C_3H_6NO_2$)
Cys	45.01 (CHS)
Gln	84.04 (C_4H_6NO)
Glu	84.04 (C_4H_6NO), 102 ($C_4H_8NO_2$)
Gly	30.03 (CH_4N)
His	81.05 ($C_4H_5N_2$), 82.05 ($C_4H_6N_2$), 110.07 ($C_5H_8N_3$)
Ile	86.10 ($C_5H_{12}N$)
Leu	86.10 ($C_5H_{12}N$)
Lys	84.08 ($C_5H_{10}N$)
Met	61.01 (C_2H_5S)
Phe	120.08 ($C_8H_{10}N$), 131.05 (C_9H_7O)
Pro	68.05 (C_4H_6N), 70.07 (C_4H_8N)
Ser	60.04 (C_2H_6NO), 71.01 ($C_3H_3O_2$)
Thr	69.06 (C_4H_5O), 74.06 (C_3H_8NO)
Trp	130.07 (C_9H_8N), 159.09 ($C_{10}H_{11}N_2$), 170.06 ($C_{11}H_8NO$)
Tyr	107.05 (C_7H_7O), 136.08 ($C_8H_{10}NO$)
Val	72.08 ($C_4H_{10}N$), 83.05 (C_5H_7O)

Figure 9.6 shows the scores and loadings plots comparing the relative intensities of the 20 amino acids among the samples with surface modifications. The largest variation in the data was shown as principal component 1 (PC1), and the second largest variation is shown as PC2. The first principal component (PC1 along the x-axis) in the scores plot (Figure 9.6a) showed the separation of VEGF samples from Heparin samples and CD34Ab samples from VEGF samples. Large scan images of the surfaces were acquired to visualize the distribution of the CH_4N^+ fragment as shown in Figure 9.7.
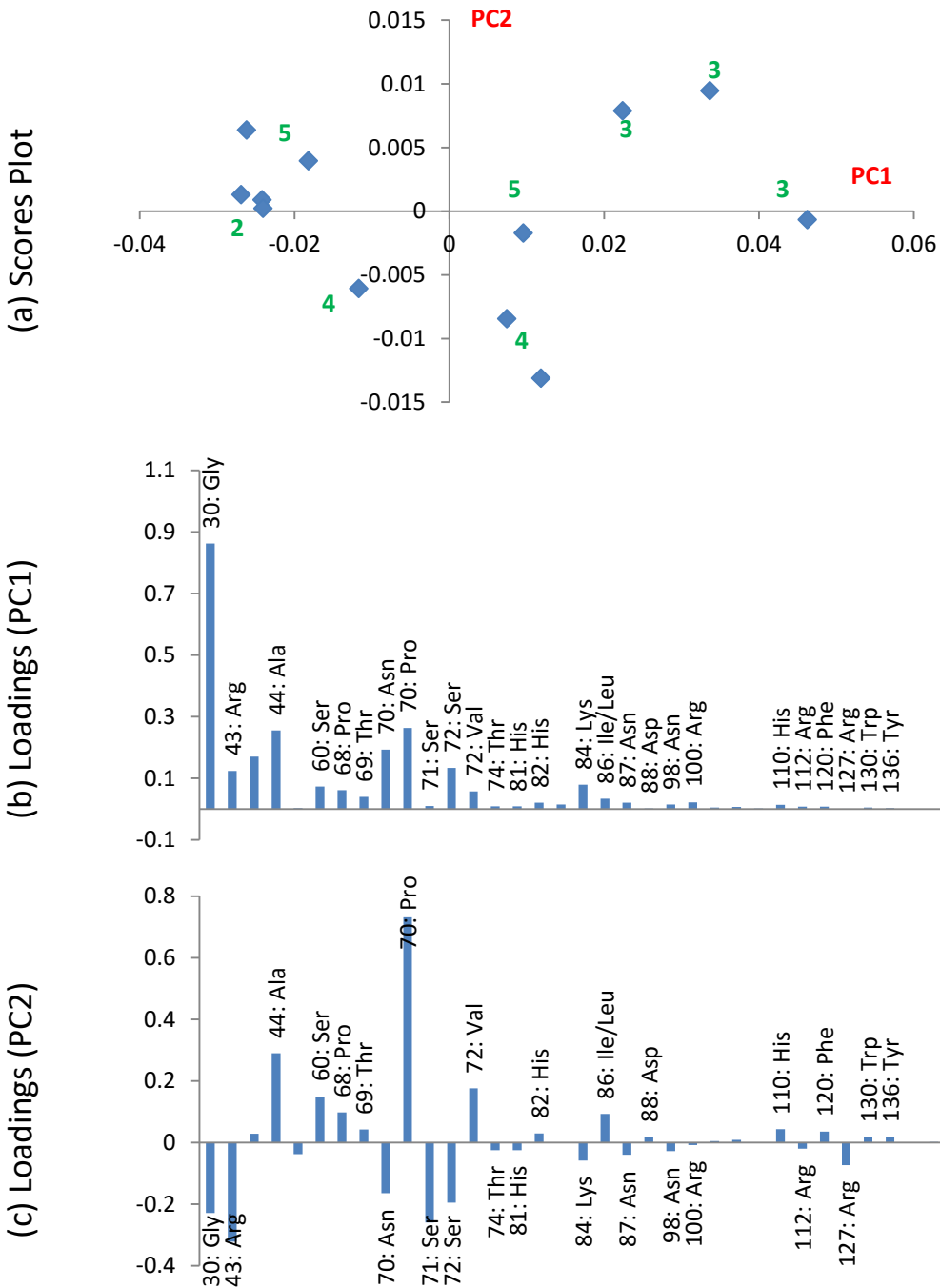
Figure 9.6 PCA scores and loadings plots generated from the ToF-SIMS analysis of samples 2 (Hep), 3 (CD34Ab), 4 (VEGF), and 5 (CD34Ab+VEGF). The separation of the samples in the scores plot (a) is due to the varying concentration of amino acid fragments seen in their respective loadings plots (b) and (c). In (a), the first principal component is on the x-axis and second principal component is on the y-axis.
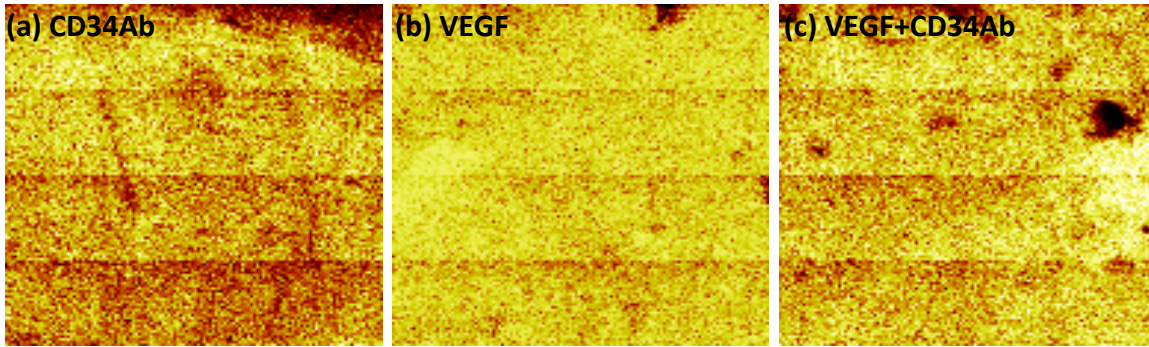
Figure 9.7 2 mm × 2mm ToF-SIMS large scan images of the surfaces of samples with CD34Ab, VEGF, and VEGF+CD34Ab generated from stitching twenty 500 μm × 500 μm images. The images show the distribution of the CH4N+ fragment within this area (lighter color denotes higher intensity). Due to charging from non-flat dielectric surfaces, each ToF-SIMS image had attenuated signals around the scan area, generating dark lines seen in the images above.
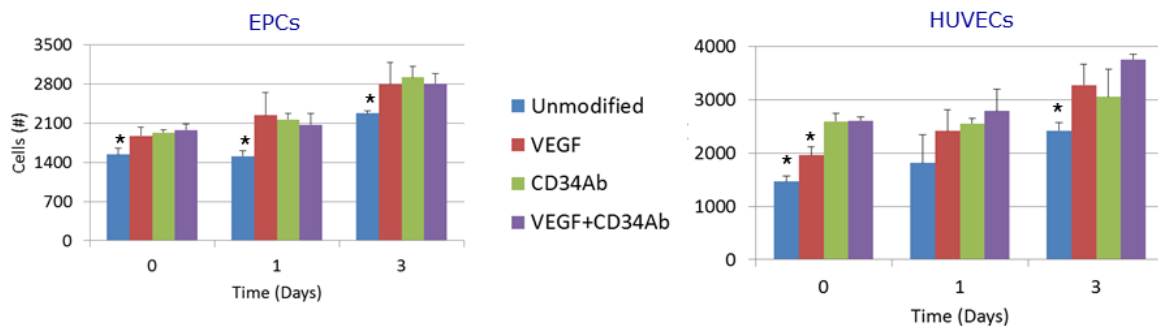
Figure 9.8 Cell populations (EPC and HUVEC) on the surface of unmodified and modified 3D printed PPF substrates.

As shown in Fig 9.8, all grafts modified with VEGF, CD34Ab, or a combination (VEGF+CD34Ab) experienced greater initial attachment of both HUVECs and EPCs. Greater populations of EPCs were present on all modified grafts after 1 and 3 days of incubation. HUVECs demonstrated greater

populations on all modified grafts compared to unmodified controls after 3 days of incubation. Table 9.4 shows the total fold change in HUVEC and EPC populations on modified 3D-printed PPF films.

Table 9.4. Fold change of EPC and HUVEC populations on various 3D printed PPF films.

Cell Type	Unmodified	VEGF	CD34Ab	VEGF+CD34Ab
EPC	1.48 ± 0.11	1.50 ± 0.24	1.51 ± 0.11	1.42 ± 0.12
HUVEC	1.65 ± 0.16	1.67 ± 0.22	1.18 ± 0.21	1.44 ± 0.06

9.4 Discussion

In this study, we aimed to show that chemical modifications known to improve the endothelialization of vascular grafts could be applied toward 3D printed vascular materials. The results presented here demonstrate the successful modification of these printed samples.

Interestingly, in our previous studies, the crosslinking of heparin through EDC-NHS chemistry was presumably accomplished through the presence of carboxylic acid groups in the PGA and PLA components of the vascular graft.[298] However, PPF contains no such functional group. Yet the results presented here demonstrate the successful immobilization of heparin, VEGF, and CD34Ab to 3D printed PPF films. It is hypothesized that a couple of phenomena may allow for this type of chemical modification. First, given the acidic environment of the MES buffer, degradation of the PPF films may occur,

resulting in the presence of fumaric acid, which may be involved in the EDC crosslinking of heparin. As an alternative hypothesis, the EDC-NHS reaction may incite crosslinking between the heparin molecules. These larger complexes may then adhere to the surface of the PPF via non-covalent interactions such as hydrogen bonding, hydrophilic interactions, electrostatic interactions, etc.[65,71–73,280] Though the exact method of heparin, VEGF, and CD34Ab immobilization remains uncertain, the ELISA results demonstrate the PPF films were successfully modified.

Further analysis via XPS and ToF-SIMS confirms these findings. Referring to Table 9.1, the increase in nitrogen shows that there is adsorption of proteins or nitrogen-containing molecules on the printed PPF films, indicating successful adsorption events. On average, heparin is seen to contribute roughly 8% of nitrogen to the surface, CD34Ab roughly 13%, and VEGF roughly 3%. Larger nitrogen values usually indicate a thicker adsorption layer or adsorption of larger protein structures, and thus it can be seen a thicker layer of CD34Ab is present on grafts which corresponds to ELISA results.

In Figure 9.6, comparison of PC2 (y-axis in Figure 9.6a) showed that CD34Ab-modified films and CD34Ab+VEGF-modified films demonstrated differences in amino acid composition relative to VEGF films. According to the PC2 loadings plot in Figure 9.6c, CD34Ab and CD34Ab+VEGF corresponded with higher relative concentrations of amino acids with hydrophobic side chains. Hydrophobic amino acids, such as alanine, valine, isoleucine/leucine,

phenylalanine, and tryptophan, were seen to correspond with CD34Ab- and CD34Ab+VEGF-modified films, which could indicate the presence of the variable domain of the antibody. Since the information depth of ToF-SIMS is 2 nm to 3 nm, the detection of the variable domain would indicate that the antibodies are oriented upright on the surface, which is potentially more favorable to providing available binding sites to HUVECs and EPCs. On the other hand, VEGF-modified films were seen to correspond with amino acids side chains that are either charged or polar, such as arginine which is present in VEGF.[347]

As shown in the PC1 loadings plot (Figure 9.6b), separation between samples was due to a progressively higher relative concentrations of all amino fragments for VEGF-modified films relative to heparin-only, and for CD34Ab-modified films relative to VEGF-modified films (positive loadings corresponds with amino acid fragments in the positive scores, and vice versa). This meets our expectations since heparin does not have amino acids and VEGF-modified films have less amino acid content than CD34Ab-modified films due to lower loading rates. This also signifies the combinatorial coating (VEGF+CD34Ab) had less protein content than VEGF-modified films at the locations analyzed, indicating a patchy coverage of CD34Ab on the surface. However, since XPS results indicated that VEGF+CD34Ab samples had the highest nitrogen content, the PCA results most likely indicate a deposition of contaminants on the surface which is attenuating the protein signal. Figure 9.7 displays ToF-SIMS images for VEGF, CD34Ab, and VEGF+CD34Ab samples, showing the

distribution of the CH_4N^+ fragment within a 2 mm × 2mm area. Comparison with images of CD34Ab and VEGF samples show that the surface of VEGF+CD34Ab samples exhibit patches of dark circles that indicates the presence of large island structures (hundreds of microns) on the surface. These structures are attenuating the protein signal underneath. Also, the darker images of CD34Ab and VEGF+CD34Ab samples relative to VEGF samples could mean that the coverage of antibodies may be patchy. Despite this potential lack of uniformity, attachment of cells on modified grafts were still enhanced compared to unmodified 3D-printed samples.

While much remains to be characterized on a molecular level, this study demonstrates the expansion of the 3D-printed vascular graft platform we previously developed. Still, the application of VEGF and CD34Ab grafts appear promising. VEGF has been shown to aid in the recruitment and mobilization of ECs, which is a primary method of natural graft endothelialization.[156,279] CD34Abs have shown to be a potent and well-utilized EC and EPC recruitment tool.[73,263,282] However, the methods demonstrated here are not restricted to the functionalization of 3D printed constructs with solely CD34Ab and VEGF. Other molecules, such as functional peptide groups, growth factors, or antibodies, may be incorporated with the heparin crosslinking process. This means both existing and new modification strategies may easily be integrated into our 3D printing vascular graft platform to greatly improve *in vivo* outcomes through improved endothelialization or functionality.

9.5 Conclusion

The goal of this study was to determine if biofuncationalization methods could be used with 3D-printed biodegradable vascular grafts. We demonstrated successful modification of 3D-printed vascular materials with functional molecules, CD34Ab and VEGF, which have been previously shown to effectively encourage functional endothelialization *in situ*. Such findings demonstrate the robustness of the 3D-printed platform we've developed and exhibit the potential for customization and further modification of printed vascular materials to drastically improve experimental and clinical applications of our 3D-printed vascular graft platform.

Chapter 10: Summary and Future Directions

10.1 Summary

In this work we demonstrated the fabrication, modification, and application of synthetic polymeric materials for vascular graft applications. The overall goal was to develop strategies for patient-specific vascular grafts that could be used to treat CHD. Current methods of treating CHD rely on permanent synthetic grafts without growth potential or biofunctional properties. It is thought that a tissue-engineering approach to designing patient-specific grafts could drastically improve long-term outcomes of treating CHD while minimizing acute and chronic side effects of current treatments. We focused on two main research subjects: 1) The study of endothelialization phenomena as it relates to an established vascular graft platform (solvent-cast vascular grafts), and 2) the development of a novel method of vascular graft fabrication (3D printed grafts).

The first research area involved the establishment of a solvent-cast graft fabrication method along with two different strategies to improve neotissue formation within the grafts. We demonstrated the development and characterization of PGLA-based electrospun mesh scaffolds for use as vascular grafts. These scaffolds possessed adequate mechanical properties comparable to native vessels used in small-diameter applications, and they supported levels of cellular attachment and proliferation comparable to other vascular graft applications in the literature. Preliminary animal studies also demonstrated that these grafts maintained patency when implanted as an IVC

conduit in mice and supported cellular infiltration. To improve these initial results, we studied two methods of expedited endothelialization based on different biological phenomena. First, we used interactions between cells and biomolecules by immobilizing CD34Ab and VEGF to our graft surfaces. These modified grafts appeared to support better cellular attachment and function compared to unmodified grafts, as documented by cell quantification, PCR, histology, and immunohistochemistry results both *in vitro* and *in vivo* as an IVC conduit in mice. Second, we utilized mechanical stress relationships between cells and their environment. Specifically, we focused on the effects of low shear stresses (of the venous system) on EPC proliferation, function, and differentiation. We demonstrated the functional differences of EPCs experiencing these low shear stresses in a TPS bioreactor system compared to statically cultured EPCs. This system not only provides a method to study the effects of various stresses on TEVGs, but it also provides a readily available system to seed, expand, and prime cells on a TEVG for implantation.

The second research area involved the development of a 3D printable material for the fabrication of patient-specific vascular grafts. Like in the first research area, the first step in this one was the establishment of the initial materials and fabrication method platform. To achieve this, we developed a novel 3D printing resin based on PPF. After many iterations on this initial resin, we developed a candidate resin that resulted in 3D printed samples with mechanical properties similar to those of native blood vessels commonly used in vessel transplant procedures. The 3D printed vascular grafts also proved to

be biocompatible *in vitro* and *in vivo* in a mouse IVC model. Neotissue formation was observed within the lumen of the vascular graft and patency was retained in all the implanted grafts. In order to improve functional tissue growth, we later examined the attachment and immobilization of functional biomolecules, VEGF and CD34Ab, to 3D printed graft surfaces. The heparin-based EDC/NHS chemistry used in our previous studies proved to successfully foster the loading of these molecules. In addition, we assessed the feasibility of 3D printed a copolymer P(PF-*co*-CL) to modulate the mechanical and degradation properties of our 3D printing resin. While we successfully showed these copolymers could be 3D printed and mechanically tested, we found only one of the tested copolymers to potentially be suitable for vascular graft materials. However, the biofunctionalization and copolymer printing studies demonstrate the versatility of the 3D printing PPF platform. The ability to fine-tune the 3D printing and post-printing processes enables a wide array of vascular technologies to benefit from the fabrication of these patient-specific implantable materials.

New applications, avenues of research, and capabilities of these two platforms are discussed below.

10.2 Future Directions

The *in vivo* studies throughout this work have centered on application in the venous system. This provides an integral model for the development of grafts suitable for CHD, but cardiovascular defects comprise a wide array of

environmental and mechanical conditions besides those present in the venous system. While Chapter 7 demonstrates the basic functionality and effectiveness of the 3D printed vascular material platform, more studies investigating more complex shapes need to be completed to truly realize the benefits of 3D printed vascular grafts. This may include the study of aortic grafts to provide a different mechanical environment for the assessment of these grafts as well. In addition, robust computational fluid dynamic and *in vivo* studies comparing generic and patient-specific vascular grafts would greatly bolster the significance of this new platform of fabrication.

Degradation rates of the 3D printed grafts are also relatively slow. As shown in Chapter 7, after 6 months only ~ 40 % of the graft has degraded. Copolymers may, as presented in Chapter 8, may be one way to control the degradation of these grafts. However, according to our work, polycaprolactone diols (Mn ~2000) did not significantly increase degradation rates of the 3D printed grafts and, in fact, two feed ratios of the polymer decreased degradation rates. These studies still demonstrate that copolymers can easily be substituted into the 3D printed resin and warrant further examination.

In addition, increased porosity of 3D printed grafts is necessary to encourage cellular infiltration. Improved 3D printing hardware with better resolution may allow for the inclusion of pores small enough for cellular infiltration while preventing "bleeding." But such technologies do not yet exist in the 3D printing platforms presented here. Instead, it may be necessary to

use traditional pore inclusion processes, such as porogen leaching, to improve cellular infiltration within the bulk geometry of 3D printed graft structures.

Both in the 3D printed and the solvent-cast polymeric felt graft studies, we examined strategies to capture EPCs. There is still much debate on the exact role of EPCs and their subpopulations within endothelialization and vascular homeostasis. The surface modifications presented here in Chapters 5 and 9 focused on CD34$^+$ EPCs, which is a rather generic population of circulating cells. As subpopulations are better characterized, such as ECFCs, it may be more advantageous to alter the surface modification of the graft materials presented here to better target those specific cells. In addition, determining the optimal EPC subpopulation for expediting and improving endothelialization of grafts may drastically improve the cell seeding process demonstrated in Chapter 6. In fact, various cell culturing techniques are already being developed to isolate specific EPC subpopulations, which may aid in providing a reliable cell source for preseeding of vascular grafts.

While much developmental research should be done on both the 3D printing and solvent-cast vascular grafts, regulatory and manufacturing concerns should be considered for the eventual clinical translation of these technologies. Similar solvent-cast polymeric grafts have already been utilized in clinical studies, which demonstrates the promise of the technologies presented in Chapters 4, 5, and 6. In contrast, the 3D printing technologies presented in Chapters 7, 8, and 9 require substantially more developmental work prior to meeting regulatory challenges, including optimizing degradation rates,

identifying appropriate copolymers, and demonstrating the success of this technology in more complex conditions. In addition, PPF has not been previously used in an FDA cleared or approved device, which may increase the burden of proof necessary for premarket approval. Fortunately, the FDA has been proactive about addressing 3D printing biotechnology and has already cleared some 3D printed, implantable materials, proving that 3D printing will have an important place in the future of clinical work.

The research presented in this thesis, along with future developments, would result in improved strategies to fabricate patient-specific vascular grafts. These strategies could dramatically improve patient outcomes, reduce the number of surgeries associated with CDH, and enable the widespread use of TEVGs for clinical applications.

Chapter 11: Contributions

My research has resulted in 8 publications published or in press, along with 3 publications in the preparation and submission process. The 3D printing portion of this research has resulted 2 invention disclosures, 2 provisionary patents, and 1 full patent application. This work has also been awarded the University of Maryland Life Science Invention of the Year in 2014 and a business plan utilizing the technology won 1st place at the Bioscience Day Professor Venture Fair. This work was also awarded Most Likely to be Publicly Funded at the University of Maryland Nanocenter's NanoDay and a Society for Biomaterials STAR Honorable Mention. Over the course of my research, I was supported by a National Science Foundation Graduate Research Fellowship, an American Heart Association Predoctoral Fellowship, a Warren G. Citrin Engineering Graduate Student Fellowship, and a Fischell Fellowship from the University of Maryland. Our work is the first of its kind in the 3D printing of acellular, mechanically compatible vascular grafts consisting of biomaterials with documented biocompatibility and biodegradability. This research requires much further development, but we believe we have contributed a crucial stepping stone toward the discovery and development of future clinical applications based on this novel technology.

Chapter 12: References

1. Lloyd-Jones D, Adams RJ, Brown TM, Carnethon M, Dai S, De Simone G, et al. Heart disease and stroke statistics--2010 update: a report from the American Heart Association. Circulation. 2010;121(7):e46–215.

2. Pierpont ME, Basson CT, Benson DW, Gelb BD, Giglia TM, Goldmuntz E, et al. Genetic Basis for Congenital Heart Defects : Current Knowledge A Scientific Statement From the American Heart Association Congenital Cardiac Defects Committee , Council on Cardiovascular. Circulation. 2007;115(23):3015–38.

3. Samanek M, Slavik Z, Krejcir M. Annual and seasonal variations in the prevalence of congenital cardiac malformations in live-born infants. Cardiol. Young. 1992;2(02):152–7.

4. Dearani JA, Danielson GK, Puga FJ, Schaff H V, Warnes CA, Driscoll D, et al. Late follow-up of 1095 patients undergoing operation for complex congenital heart disease utilizing pulmonary ventricle to pulmonary artery conduits. Ann. Thorac. Surg. 2003;75(2):399–410.

5. Petrossian E, Reddy VM, McElhinney DB, Akkersdijk GP, Moore P, Parry AJ, et al. Early results of the extracardiac conduit Fontan operation. J. Thorac. Cardiovasc. Surg. 1999;177(4):688–96.

6. Stark J. The use of valved conduits in pediatric cardiac surgery. Pediatr. Cardiol. 1998;86:II150–3.

7. Cleveland DC, Williams WG, Razzouk AJ, Trusler GA, Rebeyka IM, Duffy L, et al. Failure of cryopreserved homograft valved conduits in the pulmonary circulation. Circulation. 1992;86(5):II150–I153.

8. Jonas RA, Freed MD, Mayer JE, Castaneda AR. Long-term follow-up of patients with synthetic right heart conduits. Circulation. 1995;72(3(2)):II77–I83.

9. Hoffman JIE, Kaplan S. Incidence of congenital heart disease. J. Am. Coll. Cardiol. 2002;285(20):1890–900.

10. Bermudez CA, Dearani JA, Puga FJ, Schaff H V, Warnes CA, O'Leary PW, et al. Late results of the peel operation for replacement of failing extracardiac conduits. Ann. Thorac. Surg. 2004;77(3):881–7.

11. Whitehead KK, Sundareswaran KS, Parks WJ, Harris MA, Yoganathan AP, Fogel MA. Blood flow distribution in a large series of patients having the Fontan operation: a cardiac magnetic resonance velocity mapping study. J. Thorac. Cardiovasc. Surg. 2009;138(1):96–102.

12. Frommelt PC, Mitchell ME, Lamers LJ, Jaquiss RDB, Tweddell JS, Mussatto KA. Coarctectomy combined with an interdigitating arch reconstruction results in a lower incidence of recurrent arch obstruction after the Norwood procedure than coarctectomy alone. J. Thorac. Cardiovasc. Surg. 2012;143(5):1098–102.

13. Sorensen TS, Korperich H, Greil GF, Eichhorn J, Barth P, Meyer H, et al. Operator-independent isotropic three-dimensional magnetic resonance imaging for morphology in congenital heart disease: a validation study. Circulation. 2004;110(2):163–9.

14. Haramati LB, Glickstein JS, Issenberg HJ, Haramati N, Crooke G a. MR imaging and CT of vascular anomalies and connections in patients with congenital heart disease: significance in surgical planning. Radiographics. 2002;22(2):337–9.

15. Sodian R, Weber S, Markert M, Loeff M, Lueth T, Weis FC, et al. Pediatric cardiac transplantation: three-dimensional printing of anatomic models for surgical planning of heart transplantation in patients with univentricular heart. J. Thorac. Cardiovasc. Surg. 2008;136(4):1098–9.

16. Giovinco N a, Dunn SP, Dowling L, Smith C, Trowell L, Ruch J a, et al. A novel combination of printed 3-dimensional anatomic templates and computer-assisted surgical simulation for virtual preoperative planning in Charcot foot reconstruction. J. Foot Ankle Surg. 2012;51(3):387–93.

17. Schmauss D, Schmitz C, Bigdeli AK, Weber S, Gerber N, Beiras-Fernandez A, et al. Three-dimensional printing of models for preoperative planning and simulation of transcatheter valve replacement. Ann. Thorac. Surg. 2012;93(2):e31–3.

18. World Health Organization. World Health Statistics 2012. Geneva; 2012.

19. Abbott WM, Callow A, Moore W, Rutherford R, Veith F, Weinberg S. Evaluation and performance standards for arterial prostheses. J. Vasc. Surg. 1993;17(4):746–56.

20. Budd JS, Allen KE, Hartley G, Bell PRF. The effect of preformed confluent endothelial cell monolayers on the patency and thrombogenicity of small calibre vascular grafts. Eur. J. Vasc. Surg. 1991;5(4):397–405.

21. Pasic M, Müller-Glauser W, Von Segesser LK, Lachat M, Mihaljevic T, Turina MI. Superior late patency of small-diameter Dacron grafts seeded with omental microvascular cells: an experimental study. Ann. Thorac. Surg. 1994;58(3):677–84.

22. Demiri EC, Iordanidis SL, Mantinaos CF. Experimental use of prosthetic grafts in microvascular surgery. Handchirurgie, Mikrochirurgie, Plast. Chir. Organ der Deutschsprachigen Arbeitsgemeinschaft fur Handchirurgie Organ der Deutschsprachigen Arbeitsgemeinschaft fur Mikrochirurgie der Peripher. Nerven und Gefasse Organ der V. 1999;31(2):102–6.

23. Zilla P, Bezuidenhout D, Human P. Prosthetic vascular grafts: wrong models, wrong questions and no healing. Biomaterials. 2007;28(34):5009–27.

24. Wang X, Lin P, Yao Q, Chen C. Development of small-diameter vascular grafts. World J. Surg. 2007;31(4):682–9.

25. Nieponice A, Soletti L, Guan J, Hong Y, Gharaibeh B, Maul TM, et al. In vivo assessment of a tissue-engineered vascular graft combining a biodegradable elastomeric scaffold and muscle-derived stem cells in a rat model. Tissue Eng. Part A. 2010;16(4):1215–23.

26. McAllister TN, Maruszewski M, Garrido S a, Wystrychowski W, Dusserre N, Marini A, et al. Effectiveness of haemodialysis access with an autologous tissue-engineered vascular graft: a multicentre cohort study. Lancet. 2009;373(9673):1440–6.

27. Kakisis JD, Liapis CD, Breuer C, Sumpio BE. Artificial blood vessel: the Holy Grail of peripheral vascular surgery. J. Vasc. Surg. Off. Publ. Soc. Vasc. Surg. Int. Soc. Cardiovasc. Surg. North Am. Chapter. 2005;41(2):349–54.

28. Rubanyi GM. The role of endothelium in cardiovascular homeostasis and diseases. J. Cardiovasc. Pharmacol. 1993;22(Suppl. 4):S1–14.

29. Van Hinsbergh VWM. The endothelium: vascular control of haemostasis. Eur. J. Obstet. Gynecol. Reprod. Biol. 2001;95(2):198–201.

30. Pearson JD. Endothelial cell function and thrombosis. Best Pract. Res. Clin. Haematol. 1999;12(3):329–41.

31. Patel SD, Waltham M, Wadoodi A, Burnand KG, Smith A. The role of endothelial cells and their progenitors in intimal hyperplasia. Ther. Adv. Cardiovasc. Dis. 2010;4(2):129–41.

32. Naito Y, Williams-Fritze M, Duncan DR, Church SN, Hibino N, Madri J a, et al. Characterization of the natural history of extracellular matrix production in tissue-engineered vascular grafts during neovessel formation. Cells. Tissues. Organs. 2012;195(1-2):60–72.

33. Zarbiv G, Sc M, Sarig U, Karram T, Hoffman A, Machluf M, et al. Porcine small diameter arterial extracellular matrix supports endothelium formation and media remodeling forming a promising vascular engineered biograft. Tissue Eng Part A. 2012;18(3-4):411–22.

34. Schmedlen RH, Elbjeirami WM, Gobin AS, West JL. Tissue engineered small-diameter vascular grafts. Clin. Plast. Surg. 2003;30(4):507–17.

35. Berglund JD, Galis ZS. Designer blood vessels and therapeutic revascularization. Br. J. Pharmacol. 2003;140(4):627–36.

36. Jain RK, Au P, Tam J, Duda DG, Fukumura D. Engineering vascularized tissue. Nat. Biotechnol. 2005;23(7):821–3.

37. Avci-Adali M, Ziemer G, Wendel HP. Induction of EPC homing on biofunctionalized vascular grafts for rapid in vivo self-endothelialization-- a review of current strategies. Biotechnol. Adv. 2010;28(1):119–29.

38. de Mel A, Jell G, Stevens MM, Seifalian AM. Biofunctionalization of biomaterials for accelerated in situ endothelialization: a review. Biomacromolecules. 2008;9(11):2969–79.

39. Berger K, Sauvage LR, Rao AM, Wood SJ. Healing of arterial prostheses in man: its incompleteness. Ann. Surg. 1972;175(1):118–27.

40. Pasquinelli G, Freyrie A, Preda P, Curti T, D'Addato M, Laschi R. Healing of prosthetic arterial grafts. Scanning Microsc. 1990;4(2):351–62.

41. Clowes AW, Kirkman TR, Reidy MA. Mechanisms of arterial graft healing. Rapid transmural capillary ingrowth provides a source of intimal endothelium and smooth muscle in porous PTFE prostheses. Am. J. Pathol. 1986;123(2):220–30.

42. Asahara T, Murohara T, Sullivan A, Silver M, van der Zee R, Li T, et al. Isolation of Putative Progenitor Endothelial Cells for Angiogenesis. Science (80-.). 1997;275(5302):964–6.

43. Takahashi T, Kalka C, Masuda H, Chen D, Silver M, Kearney M, et al. Ischemia- and cytokine-induced mobilization of bone marrow-derived endothelial progenitor cells for neovascularization. Nat. Med. 1999;5(4):434–8.

44. Rafii S, Lyden D. Therapeutic stem and progenitor cell transplantation for organ vascularization and regeneration. Nat. Med. 2003;9(6):702–12.

45. Crosby JR, Kaminski WE, Schatteman G, Martin PJ, Raines EW, Seifert RA, et al. Endothelial cells of hematopoietic origin make a significant contribution to adult blood vessel formation. Circ. Res. 2000;87(9):728–30.

46. Ladhoff J, Fleischer B, Hara Y, Volk H-D, Seifert M. Immune privilege of endothelial cells differentiated from endothelial progenitor cells. Cardiovasc. Res. 2010;88(1):121–9.

47. Shi Q, Rafii S, Wu MH, Wijelath ES, Yu C, Ishida A, et al. Evidence for circulating bone marrow-derived endothelial cells. Blood. 1998;92(2):362–7.

48. Lee SP, Youn SW, Cho HJ, Li L, Kim TY, Yook HS, et al. Integrin-linked kinase, a hypoxia-responsive molecule, controls postnatal vasculogenesis by recruitment of endothelial progenitor cells to ischemic tissue. Circulation. 2006;114(2):150–9.

49. Oh IY, Yoon CH, Hur J, Kim JH, Kim TY, Lee CS, et al. Involvement of E-selectin in recruitment of endothelial progenitor cells and angiogenesis in ischemic muscle. Blood. 2007;110(12):3891–9.

50. Schmidt D, Breymann C, Weber A, Guenter CI, Neuenschwander S, Zund G, et al. Umbilical cord blood derived endothelial progenitor cells for tissue engineering of vascular grafts. Ann. Thorac. Surg. 2004;78(6):2094–8.

51. Lin Y, Weisdorf DJ, Solovey A, Hebbel RP. Origins of circulating endothelial cells and endothelial outgrowth from blood. J. Clin. Invest. 2000;105(1):71–7.

52. Hirschi KK, Ingram D a, Yoder MC. Assessing identity, phenotype, and fate of endothelial progenitor cells. Arterioscler. Thromb. Vasc. Biol. 2008;28(9):1584–95.

53. Yoon C-H, Hur J, Park K-W, Kim J-H, Lee C-S, Oh I-Y, et al. Synergistic neovascularization by mixed transplantation of early endothelial progenitor cells and late outgrowth endothelial cells: the role of angiogenic cytokines and matrix metalloproteinases. Circulation. 2005;112(11):1618–27.

54. Reed DM, Foldes G, Hardling SE, Mitchell JA. Stem cell derived endothelial cells for cardiovascular disease; a therapeutic perspective. Br. J. Clin. Pharmacol. 2013;75(4):897–906.

55. Urbich C, Aicher A, Heeschen C, Dernbach E, Hofmann WK, Zeiher AM, et al. Soluble factors released by endothelial progenitor cells promote

migration of endothelial cells and cardiac resident progenitor cells. J. Mol. Cell. Cardiol. 2005;39(5):733–42.

56.   Aicher A, Zeiher AM, Dimmeler S. Mobilizing endothelial progenitor cells. Hypertension. 2005;45(3):321–5.

57.   Edlund U, Sauter T, Albertsson A-C. Covalent VEGF protein immobilization on resorbable polymeric surfaces. Polym. Adv. Technol. 2011;22(1):166–71.

58.   De Visscher G, Mesure L, Meuris B, Ivanova A. Improved endothelialization and reduced thrombosis by coating a synthetic vascular graft with fibronectin and stem cell homing factor SDF-1α. Acta Biomater. 2011;8(3):1330–8.

59.   Zhou M, Liu Z, Li K, Qiao W, Jiang X, Ran F, et al. Beneficial effects of granulocyte-colony stimulating factor on small-diameter heparin immobilized decellularized vascular graft. J. Biomed. Mater. Res. Part A. 2010;95(2):600–10.

60.   Zeng W, Yuan W, Li L, Mi J, Xu S, Wen C, et al. The promotion of endothelial progenitor cells recruitment by nerve growth factors in tissue-engineered blood vessels. Biomaterials. 2010;31(7):1636–45.

61.   Zeng W, Wen C, Wu Y, Li L, Zhou Z, Mi J, et al. The use of BDNF to enhance the patency rate of small-diameter tissue-engineered blood vessels through stem cell homing mechanisms. Biomaterials. 2012;33(2):473–84.

62.   Baumann L, Prokoph S, Gabriel C, Freudenberg U, Werner C, Beck-Sickinger AG. A novel, biased-like SDF-1 derivative acts synergistically with starPEG-based heparin hydrogels and improves eEPC migration in vitro. J. Control. Release. 2012;162(1):68–75.

63.   Gong XB, Li YQ, Gao QC, Cheng B Bin, Shen BR, Yan ZQ, et al. Adhesion behavior of endothelial progenitor cells to endothelial cells in simple shear flow. Acta Mech. Sin. 2011;27(6):1071–80.

64.   Ciraci E, Della Bella S, Salvucci O, Rofani C, Segarra M, Bason C, et al.

Adult human circulating CD34-Lin-CD45-CD133- cells can differentiate into hematopoietic and endothelial cells. Blood. 2011;119(8):2105–15.

65.   Zhang M, Wang Z, Wang Z, Feng S, Xu H, Zhao Q, et al. Immobilization of anti-CD31 antibody on electrospun poly(ε -caprolactone) scaffolds through hydrophobins for specific adhesion of endothelial cells. Colloids Surfaces B Biointerfaces. 2011;85(1):32–9.

66.   Markway BD, McCarty OJT, Marzec UM, Courtman DW, Hanson SR, Hinds MT. Capture of flowing endothelial cells using surface-immobilized anti-kinase insert domain receptor antibody. Tissue Eng. Part C Methods. 2008;14(2):97–105.

67.   Muller WA, Ratti CM, McDonnell SL, Cohn ZA. A human endothelial cell-restricted, externally disposed plasmalemmal protein enriched in intercellular junctions. J. Exp. Med. 1989;170(2):399–414.

68.   Stockinger H, Gadd SJ, Eher R, Majdic O, Schreiber W, Kasinrerk W, et al. Molecular characterization and functional analysis of the leukocyte surface protein CD31. J. Immunol. 1990;145(11):3889–97.

69.   Tanaka Y, Albelda SM, Horgan KJ, Van Seventer GA, Shimizu Y, Newman W, et al. CD31 expressed on distinctive T cell subsets is a preferential amplifier of beta 1 integrin-mediated adhesion. J. Exp. Med. 1992;176(1):245–53.

70.   Nakazawa G, Granada JF, Alviar CL, Tellez A, Kaluza GL, Guilhermier MY, et al. Anti-CD34 antibodies immobilized on the surface of sirolimus-eluting stents enhance stent endothelialization. JACC Cardiovasc. Interv. 2010;3(1):68–75.

71.   Lin Q, Ding X, Qiu F, Song X, Fu G, Ji J. In situ endothelialization of intravascular stents coated with an anti-CD34 antibody functionalized heparin-collagen multilayer. Biomaterials. 2010;31(14):4017–25.

72.   Chen J, Cao J, Wang J, Maitz MF, Guo L, Zhao Y, et al. Biofunctionalization of titanium with PEG and anti-CD34 for hemocompatibility and stimulated endothelialization. J. Colloid Interface Sci. 2012;368(1):636–47.

73.   Yin M, Yuan Y, Liu C, Wang J. Combinatorial coating of adhesive polypeptide and anti-CD34 antibody for improved endothelial cell adhesion and proliferation. J. Mater. Sci. Mater. Med. 2009;20(7):1513–23.

74.   Yeh ETH, Zhang S, Wu HD, Körbling M, Willerson JT, Estrov Z. Transdifferentiation of human peripheral blood CD34+-enriched cell population into cardiomyocytes, endothelial cells, and smooth muscle cells in vivo. Circulation. 2003;108(17):2070–3.

75.   Pearson JD. Endothelial progenitor cells - hype or hope? J. Thromb. Haemost. 2009;7(2):255–62.

76.   Kawahara D, Matsuda T. Hydrodynamic shear-stress-dependent retention of endothelial and endothelial progenitor cells adhered to vascular endothelial growth factor-fixed surfaces. J. Biomed. Mater. Res. Part B Appl. Biomater. 2012;100(5):1218–28.

77.   Yoon M, Hwang HJ, Kim JH. Immobilization of antibodies on the self-assembled monolayer by antigen-binding site protection and immobilization kinetic control. J. Biomed. Sci. Eng. 2011;04(04):242–7.

78.   Shmanai V V, Nikolayeva TA, Vinokurova LG, Litoshka AA. Oriented antibody immobilization to polystyrene macrocarriers for immunoassay modified with hydrazide derivatives of poly(meth)acrylic acid. BMC Biotechnol. 2001;1:4.

79.   Caiado F, Dias S. Endothelial progenitor cells and integrins: adhesive needs. Fibrogenesis Tissue Repair. 2012;5:4.

80.   Iivanainen E, Kähäri V-M, Heino J, Elenius K. Endothelial cell-matrix interactions. Microsc. Res. Tech. 2003;60(1):13–22.

81.   Short SM, Talbott GA, Juliano RL. Integrin-mediated signaling events in human endothelial cells. Brugge J, editor. Mol. Biol. Cell. 1998;9(8):1969–80.

82.   Zhang X, Groopman JE, Wang JF. Extracellular matrix regulates endothelial functions through interaction of VEGFR-3 and integrin

alpha5beta1. J. Cell. Physiol. 2005;202(1):205–14.

83. Williams SK, Kleinert LB, Patula-Steinbrenner V. Accelerated neovascularization and endothelialization of vascular grafts promoted by covalently bound laminin type 1. J. Biomed. Mater. Res. Part A. 2011;99(1):67–73.

84. Hersel U, Dahmen C, Kessler H. RGD modified polymers: biomaterials for stimulated cell adhesion and beyond. Biomaterials. 2003;24(24):4385–415.

85. Blit PH, McClung WG, Brash JL, Woodhouse K a, Santerre JP. Platelet inhibition and endothelial cell adhesion on elastin-like polypeptide surface modified materials. Biomaterials. 2011;32(25):5790–800.

86. Behjati M, Kazemi M, Hashemi M, Zarkesh-Esfahanai SH, Bahrami E, Hashemi-Beni B, et al. Double-chimera proteins to enhance recruitment of endothelial cells and their progenitor cells. Int. J. Cardiol. 2012;167(5):1560–9.

87. Zheng W, Wang Z, Song L, Zhao Q, Zhang J, Li D, et al. Endothelialization and patency of RGD-functionalized vascular grafts in a rabbit carotid artery model. Biomaterials. 2012;33(10):2880–91.

88. Wang Z, Wang H, Zheng W, Zhang J, Zhao Q, Wang S, et al. Highly stable surface modifications of poly(3-caprolactone) (PCL) films by molecular self-assembly to promote cells adhesion and proliferation. Chem. Commun. 2011;47(31):8901–3.

89. Kuwabara F, Narita Y, Yamawaki-Ogata A, Kanie K, Kato R, Satake M, et al. Novel Small-Caliber Vascular Grafts With Trimeric Peptide for Acceleration of Endothelialization. Ann. Thorac. Surg. 2011;93(1):156–63.

90. Kanie K, Narita Y, Zhao Y, Kuwabara F, Satake M, Honda S, et al. Collagen type IV-specific tripeptides for selective adhesion of endothelial and smooth muscle cells. Biotechnol. Bioeng. 2012;109(7):1808–16.

91. Kato R, Kaga C, Kunimatsu M, Kobayashi T, Honda H. Peptide array-based interaction assay of solid-bound peptides and anchorage-

dependant cells and its effectiveness in cell-adhesive peptide design. J. Biosci. Bioeng. 2006;101(6):485–95.

92.   Wang J, Liu C, Lu X, Yin M. Co-polypeptides of 3,4-dihydroxyphenylalanine and L-lysine to mimic marine adhesive protein. Biomaterials. 2007;28(23):3456–68.

93.   Ku SH, Park CB. Human endothelial cell growth on mussel-inspired nanofiber scaffold for vascular tissue engineering. Biomaterials. 2010;31(36):9431–7.

94.   Shin YM, Lee Y Bin, Kim SJ, Kang JK, Park J-C, Jang W, et al. Mussel-inspired immobilization of vascular endothelial cell growth factor (VEGF) for enhanced endothelialization of vascular grafts. Biomacromolecules. 2012;13(7):2020–8.

95.   Roach P, Eglin D, Rohde K, Perry CC. Modern biomaterials: a review - bulk properties and implications of surface modifications. Journals Mater. Sci. Mater. Med. 2007;18(7):1263–77.

96.   Simon C, Palmaz JC, Sprague E a. Influence of topography on endothelialization of stents: clues for new designs. J. Long. Term. Eff. Med. Implants. 2000;10(1-2):143–51.

97.   Miller DC, Thapa A, Haberstroh KM, Webster TJ. Endothelial and vascular smooth muscle cell function on poly(lactic-co-glycolic acid) with nano-structured surface features. Biomaterials. 2004;25(1):53–61.

98.   Hubbi ME, Ahn EH, Downey J, Afzal J, Kim DH, Rey S, et al. Matrix Rigidity Controls Endothelial Differentiation and Morphogenesis of Cardiac Precursors. Sci. Signal. 2012;5(227):ra41–ra41.

99.   Vaz CM, van Tuijl S, Bouten CVC, Baaijens FPT. Design of scaffolds for blood vessel tissue engineering using a multi-layering electrospinning technique. Acta Biomater. 2005;1(5):575–82.

100. Baker BM, Mauck RL. The effect of nanofiber alignment on the maturation of engineered meniscus constructs. Biomaterials. 2007;28(11):1967–77.

101. Kurpinski KT, Stephenson JT, Janairo RRR, Lee H, Li S. The effect of fiber alignment and heparin coating on cell infiltration into nanofibrous PLLA scaffolds. Biomaterials. 2010;31(13):3536–42.

102. Shalumon KT, Sreerekha PR, Sathish D, Tamura H, Nair S V, Chennazhi KP, et al. Hierarchically designed electrospun tubular scaffolds for cardiovascular applications. J. Biomed. Nanotechnol. 2011;7(5):609–20.

103. Du F, Zhao W, Zhang M, Mao H, Kong D, Yang J. The synergistic effect of aligned nanofibers and hyaluronic acid modification on endothelial cell behavior for vascular tissue engineering. J. Nanosci. Nanotechnol. 2011;11(8):6718–25.

104. Chung TW, Liu DZ, Wang SY, Wang SS. Enhancement of the growth of human endothelial cells by surface roughness at nanometer scale. Biomaterials. 2003;24(25):4655–61.

105. Miller DC, Haberstroh KM, Webster TJ. PLGA nanometer surface features manipulate fibronectin interactions for improved vascular cell adhesion. J Biomed Mater Res A. 2007;81(3):678–84.

106. Ranjan A, Webster TJ. Increased endothelial cell adhesion and elongation on micron-patterned nano-rough poly(dimethylsiloxane) films. Nanotechnology. 2009;20(30):305102.

107. Dickinson LE, Rand DR, Tsao J, Eberle W, Gerecht S. Endothelial cell responses to micropillar substrates of varying dimensions and stiffness. J. Bomedical Mater. Res. Part A. 2012;100(6):1457–66.

108. Van Der Lei B, Wildevuur CR. From a synthetic, microporous, compliant, biodegradable small-caliber vascular graft to a new artery. Thorac. Cardiovasc. Surg. 1989;37(6):337–47.

109. Salem AK, Stevens R, Pearson RG, Davies MC, Tendler SJB, Roberts CJ, et al. Interactions of 3T3 fibroblasts and endothelial cells with defined pore features. J. Biomed. Mater. Res. 2002;61(2):212–7.

110. Zhang Z, Wang Z, Liu S, Kodama M. Pore size, tissue ingrowth, and

endothelialization of small-diameter microporous polyurethane vascular prostheses. Biomaterials. 2004;25(1):177–87.

111. Maheshwari G, Brown G, Lauffenburger DA, Wells A, Griffith LG. Cell adhesion and motility depend on nanoscale RGD clustering. J. Cell Sci. 2000;113(10):1677–86.

112. Koo LY, Irvine DJ, Mayes AM, Lauffenburger DA, Griffith LG. Co-regulation of cell adhesion by nanoscale RGD organization and mechanical stimulus. J. Cell Sci. 2002;115(Pt 7):1423–33.

113. Huang J, Grater S V, Corbellini F, Rinck S, Bock E, Kemkemer R, et al. Impact of order and disorder in RGD nanopatterns on cell adhesion. Nano Lett. 2009;9(3):1111–6.

114. Le Saux G, Magenau A, Böcking T, Gaus K, Gooding JJ. The relative importance of topography and RGD ligand density for endothelial cell adhesion. PLoS One. 2011;6(7):e21869.

115. Vartanian KB, Kirkpatrick SJ, McCarty OJT, Vu TQ, Hanson SR, Hinds MT. Distinct extracellular matrix microenvironments of progenitor and carotid endothelial cells. J. Biomed. Mater. Res. Part A. 2009;91(2):528–39.

116. Dickinson LE, Moura ME, Gerecht S. Guiding endothelial progenitor cell tube formation using patterned fibronectin surfaces. Soft Matter. 2010;6(20):5109.

117. Ito Y, Hasuda H, Terai H, Kitajima T. Culture of human umbilical vein endothelial cells on immobilized vascular endothelial growth factor. J. Biomed. Mater. Res. Part A. 2005;74(4):659–65.

118. Wang R, Yang Y, Qin M, Wang L, Yu L, Shao B, et al. Biocompatible hydrophilic modifications of poly(dimethylsiloxane) using self-assembled hydrophobins. Chem. Mater. 2007;19(13):3227–31.

119. Bilewicz R, Witomski J, Van Der Heyden A, Tagu D, Palin B, Rogalska E. Modification of electrodes with self-assembled hydrophobin layers. J. Phys. Chem. B. 2001;105(40):9772–7.

120. Corvis Y, Walcarius A, Rink R, Mrabet NT, Rogalska E. Preparing catalytic surfaces for sensing applications by immobilizing enzymes via hydrophobin layers. Anal. Chem. 2005;77(6):1622–30.

121. Hou S, Li X, Li X, Feng X. Coating of hydrophobins on three-dimensional electrospun poly(lactic-co-glycolic acid) scaffolds for cell adhesion. Biofabrication. 2009;1(3):035004.

122. Solouk A, Cousins BG, Mirzadeh H, Seifalian AM. Application of plasma surface modification techniques to improve hemocompatibility of vascular grafts: A review. Biotechnol. Appl. Biochem. 58(5):311–27.

123. Siow KS, Britcher L, Kumar S, Griesser HJ. Plasma methods for the generation of chemically reactive surfaces for biomolecule immobilization and cell colonization - a review. Plasma Process. Polym. 2006;3(6-7):392–418.

124. Liu H, Li X, Niu X, Zhou G, Li P, Fan Y. Improved hemocompatibility and endothelialization of vascular grafts by covalent immobilization of sulfated silk fibroin on poly(lactic-co-glycolic acid) scaffolds. Biomacromolecules. 2011;12(8):2914–24.

125. Wulf K, Teske M, Lo M, Luderer F, Schmitz K-P, Löbler M, et al. Surface functionalization of poly(ε-caprolactone) improves its biocompatibility as scaffold material for bioartificial vessel prostheses. J. Biomed. Res. Part B Appl. Biomater. 2011;98(1):89–100.

126. Sin D, Miao X, Liu G, Wei F, Chadwick G, Yan C, et al. Polyurethane (PU) scaffolds prepared by solvent casting/particulate leaching (SCPL) combined with centrifugation. Mater. Sci. Eng. C. 2010;30(1):78–85.

127. Wu H, Fan J, Chu CC, Wu J. Electrospinning of small diameter 3-D nanofibrous tubular scaffolds with controllable nanofiber orientations for vascular grafts. J. Mater. Sci. Mater. Med. 2010;21(12):3207–15.

128. Ziabari M, Mottaghitalab V, Haghi AK. A new approach for optimization of electrospun nanofiber formation process. Korean J. Chem. Eng. 2010;27(1):340–54.

129. Soliman S, Sant S, Nichol JW, Khabiry M, Traversa E, Khademhosseini A. Controlling the porosity of fibrous scaffolds by modulating the fiber diameter and packing density. J. Biomed. Mater. Res. Part A. 2011;96(3):566–74.

130. Fridrikh S V, Yu JH, Brenner MP, Rutledge GC. Controlling the Fiber Diameter during Electrospinning. Phys. Rev. Lett. 2003;90(14):144502.

131. Subbiah T, Bhat GS, Tock RW, Parameswaran S, Ramkumar SS. Electrospinning of nanofibers. J. Appl. Polym. Sci. 2005;96(2):557–69.

132. Lee JW, Ahn G, Kim JY, Cho D-W. Evaluating cell proliferation based on internal pore size and 3D scaffold architecture fabricated using solid freeform fabrication technology. J. Mater. Sci. Mater. Med. 2010;21(12):3195–205.

133. Zhang AP, Qu X, Soman P, Hribar KC, Lee JW, Chen S, et al. Rapid Fabrication of Complex 3D Extracellular Microenvironments by Dynamic Optical Projection Stereolithography. Adv. Mater. 2012;24(31):4266–70.

134. Baudis S, Nehl F, Ligon SC, Nigisch A, Bergmeister H, Bernhard D, et al. Elastomeric degradable biomaterials by photopolymerization-based CAD-CAM for vascular tissue engineering. Biomed. Mater. 2011;6(5):055003.

135. Pareta R a, Reising AB, Miller T, Storey D, Webster TJ. Increased endothelial cell adhesion on plasma modified nanostructured polymeric and metallic surfaces for vascular stent applications. Biotechnol. Bioeng. 2009;103(3):459–71.

136. Lu J, Khang D, Webster TJ. Greater endothelial cell responses on submicron and nanometer rough titanium surfaces. J. Biomed. Mater. Res. Part A. 2010;94(4):1042–9.

137. Desmet T, Morent R, De Geyter N, Leys C, Schacht E, Dubruel P. Nonthermal plasma technology as a versatile strategy for polymeric biomaterials surface modification: a review. Biomacromolecules. 2009;10(9):2351–78.

138. Xu H, Deshmukh R, Timmons R, Nguyen KT. Enhanced endothelialization on surface modified poly(L-lactic acid) substrates. Tissue Eng. Part A. 2011;17(5-6):865–76.

139. Ando J, Yamamoto K. Vascular mechanobiology: endothelial cell responses to fluid shear stress. Circ. J. 2009;73(11):1983–92.

140. Obi S, Yamamoto K, Shimizu N, Kumagaya S, Masumura T, Sokabe T, et al. Fluid shear stress induces arterial differentiation of endothelial progenitor cells. J. Appl. Physiol. 2009;106(1):203–11.

141. Obi S, Masuda H, Shizuno T, Sato A, Yamamoto K, Ando J, et al. Fluid shear stress induces differentiation of circulating phenotype endothelial progenitor cells. J. Appl. Physiol. 2012;303(6):C595–606.

142. Xiao Q, Kiechl S, Patel S, Oberhollenzer F, Weger S, Mayr A, et al. Endothelial progenitor cells, cardiovascular risk factors, cytokine levels and atherosclerosis – results from a large population-based study. Schmidt H, editor. PLoS One. 2007;2(10):e975.

143. De Falco E, Porcelli D, Torella AR, Straino S, Iachininoto MG, Orlandi A, et al. SDF-1 involvement in endothelial phenotype and ischemia-induced recruitment of bone marrow progenitor cells. Blood. 2004;104(12):3472–82.

144. Fong GH, Rossant J, Gertsenstein M, Breitman ML. Role of the Flt-1 receptor tyrosine kinase in regulating the assembly of vascular endothelium. Nature. 1995;376(6535):66–70.

145. Fong GH, Klingensmith J, Wood CR, Rossant J, Breitman ML. Regulation of flt-1 expression during mouse embryogenesis suggests a role in the establishment of vascular endothelium. Dev. Dyn. 1996;207(1):1–10.

146. Bahlmann FH, DeGroot K, Duckert T, Niemczyk E, Bahlmann E, Boehm SM, et al. Endothelial progenitor cell proliferation and differentiation is regulated by erythropoietin. Kidney Int. 2003;64(5):1648–52.

147. Li A, Dubey S, Varney ML, Dave BJ, Singh RK. IL-8 directly enhanced endothelial cell survival, proliferation, and matrix metalloproteinases

production and regulated angiogenesis. J. Immunol. 2003;170(6):3369–76.

148. Kermani P, Hempstead B. Brain-derived neurotrophic factor: a newly described mediator of angiogenesis. Trends Cardiovasc. Med. 2007;17(4):140–3.

149. Yamamoto K, Takahashi T, Asahara T, Ohura N, Sokabe T, Kamiya A, et al. Proliferation, differentiation, and tube formation by endothelial progenitor cells in response to shear stress. J. Appl. Physiol. 2003;95(5):2081–8.

150. Suzuki Y, Yamamoto K, Ando J, Matsumoto K, Matsuda T. Arterial shear stress augments the differentiation of endothelial progenitor cells adhered to VEGF-bound surfaces. Biochem. Biophys. Res. Commun. 2012;423(1):91–7.

151. Barsotti MC, Magera A, Armani C, Chiellini F, Felice F, Dinucci D, et al. Fibrin acts as biomimetic niche inducing both differentiation and stem cell marker expression of early human endothelial progenitor cells. Cell Prolif. 2011;44(1):33–48.

152. Ziebart T, Schnell A, Walter C, Kämmerer PW, Pabst A, Lehmann KM, et al. Interactions between endothelial progenitor cells (EPC) and titanium implant surfaces. Clin. Oral Investig. 2012;17(1):301–9.

153. Chai C, Leong KW. Biomaterials approach to expand and direct differentiation of stem cells. Mol. Ther. 2007;15(3):467–80.

154. Shi Z, Neoh KG, Kang ET, Poh CK, Wang W. Enhanced endothelial differentiation of adipose-derived stem cells by substrate nanotopography. J Tissue Eng Regen Med. 2012;8(1):50–8.

155. Yoder MC. Human endothelial progenitor cells. Cold Spring Harb. Perspect. Med. 2012;2(7):a006692.

156. Hagensen MK, Vanhoutte PM, Bentzon JF. Arterial endothelial cells: still the craftsmen of regenerated endothelium. Cardiovasc. Res. 2012;95(3):1–33.

157. Yoder MC. Defining human endothelial progenitor cells. J. Thromb. Haemostasisaemostasis. 2009;7(Suppl 1):49–52.

158. Motwani JG, Topol EJ. Aortocoronary saphenous vein graft disease: pathogenesis, predisposition, and prevention. Circulation. 1998;97(9):916–31.

159. Lytle BW, Loop FD, Cosgrove DM, Ratliff NB, Easley K, Taylor PC. Long-term (5 to 12 years) serial studies of internal mammary artery and saphenous vein coronary bypass grafts. J. Thorac. Cardiovasc. Surg. 1985;89(2):248–58.

160. Desai ND, Cohen EA, Naylor CD, Fremes SE. A randomized comparison of radial-artery and saphenous-vein coronary bypass grafts. N. Engl. J. Med. 2004;351(22):2302–9.

161. Muschler GF, Nakamoto C, Griffith LG. Engineering principles of clinical cell-based tissue engineering. J. Bone Joint Surg. Am. 2004;86-A(7):1541–58.

162. Zhang ZY, Teoh SH, Chong MSK, Lee ESM, Tan LG, Mattar CN, et al. Neo-vascularization and bone formation mediated by fetal mesenchymal stem cell tissue-engineered bone grafts in critical-size femoral defects. Biomaterials. 2010;31(4):608–20.

163. Askarinam A, James AW, Zara JN, Goyal R, Corselli M, Pan A, et al. Human perivascular stem cells show enhanced osteogenesis and vasculogenesis with Nel-like molecule I protein. Tissue Eng. Part A. 2013;19(11-12):1386–97.

164. Wang L, Fan H, Zhang Z-Y, Lou A-J, Pei G-X, Jiang S, et al. Osteogenesis and angiogenesis of tissue-engineered bone constructed by prevascularized β-tricalcium phosphate scaffold and mesenchymal stem cells. Biomaterials. 2010;31(36):9452–61.

165. Ozbolat IT, Yu Y. Bioprinting toward organ fabrication: challenges and future trends. IEEE Trans. Biomed. Eng. 2013;60(3):691–9.

166. Norotte C, Marga FS, Niklason LE, Forgacs G. Scaffold-free vascular tissue engineering using bioprinting. Biomaterials. 2009;30(30):5910–7.

167. Murohara T. Printing a tissue: a new engineering strategy for cardiovascular regeneration. Arterioscler. Thromb. Vasc. Biol. 2010;30(7):1277–8.

168. Visconti RP, Kasyanov V, Gentile C, Zhang J, Markwald RR, Mironov V. Towards organ printing: engineering an intra-organ branched vascular tree. Expert Opin. Biol. Ther. 2010;10(3):409–20.

169. Tanzi MC. Bioactive technologies for hemocompatibility. Expert Rev. Med. Devices. 2005;2(4):473–92.

170. Avci-Adali M, Stoll H, Wilhelm N, Perle N, Schlensak C, Wendel HP. In vivo tissue engineering: mimicry of homing factors for self-endothelialization of blood-contacting materials. Pathobiology. 2013;80(4):176–81.

171. Potter RF, Groom AC. Capillary diameter and geometry in cardiac and skeletal muscle studied by means of corrosion casts. Microvasc. Res. 1983;25(1):68–84.

172. Mathura KR, Vollebregt KC, Boer K, De Graaff JC, Ubbink DT, Ince C. Comparison of OPS imaging and conventional capillary microscopy to study the human microcirculation. J. Appl. Physiol. 2001;91(1):74–8.

173. Zhang WJ, Liu W, Cui L, Cao Y. Tissue engineering of blood vessel. J. Cell. Mol. Med. 2007;11(5):945–57.

174. Sarkar S, Schmitz-Rixen T, Hamilton G, Seifalian AM. Achieving the ideal properties for vascular bypass grafts using a tissue engineered approach: a review. Med. Biol. Eng. Comput. 2007;45(4):327–36.

175. Furchgott RF, Zawadzki J V. The obligatory role of endothelial cells in the relaxation of arterial smooth muscle by acetylcholine. Nature. 1980;288(5789):373–6.

176. Casscells W. Migration of smooth muscle and endothelial cells. Critical

events in restenosis. Circulation. 1992;86(3):723–9.

177. Cines DB, Pollak ES, Buck CA, Loscalzo J, Zimmerman GA, McEver RP, et al. Endothelial cells in physiology and in the pathophysiology of vascular disorders. Blood. 1998;91(10):3527–61.

178. Matsumoto T, Nagayama K. Tensile properties of vascular smooth muscle cells: Bridging vascular and cellular biomechanics. J. Biomech. 2012;45(5):745–55.

179. Marga F, Jakab K, Khatiwala C, Shepherd B, Dorfman S, Hubbard B, et al. Toward engineering functional organ modules by additive manufacturing. Biofabrication. 2012;4(2):022001.

180. Mondy WL, Cameron D, Timmermans J-P, De Clerck N, Sasov A, Casteleyn C, et al. Micro-CT of corrosion casts for use in the computer-aided design of microvasculature. Tissue Eng. Part C. Methods. 2009;15(4):729–38.

181. Mondy WL, Cameron D, Timmermans J-P, De Clerck N, Sasov A, Casteleyn C, et al. Computer-aided design of microvasculature systems for use in vascular scaffold production. Biofabrication. 2009;1(3):035002.

182. Cui X, Boland T. Human microvasculature fabrication using thermal inkjet printing technology. Biomaterials. 2009;30(31):6221–7.

183. Roth E a, Xu T, Das M, Gregory C, Hickman JJ, Boland T. Inkjet printing for high-throughput cell patterning. Biomaterials. 2004;25(17):3707–15.

184. Sakurai K, Teramura Y, Iwata H. Cells immobilized on patterns printed in DNA by an inkjet printer. Biomaterials. 2011;32(14):3596–602.

185. Boivin M-C, Chevallier P, Hoesli C a, Lagueux J, Bareille R, Rémy M, et al. Human saphenous vein endothelial cell adhesion and expansion on micropatterned polytetrafluoroethylene. J. Biomed. Mater. Res. A. 2013;101(3):694–703.

186. Pataky K, Braschler T, Negro A, Renaud P, Lutolf MP, Brugger J. Microdrop Printing of Hydrogel Bioinks into 3D Tissue-Like Geometries.

Adv. Mater. 2011;24(3):391–6.

187. Zhang C, Wen X, Vyavahare NR, Boland T. Synthesis and characterization of biodegradable elastomeric polyurethane scaffolds fabricated by the inkjet technique. Biomaterials. 2008;29(28):3781–91.

188. Xu T, Jin J, Gregory C, Hickman JJJJ, Boland T. Inkjet printing of viable mammalian cells. Biomaterials. 2005;26(1):93–9.

189. Fleming P a, Argraves WS, Gentile C, Neagu A, Forgacs G, Drake CJ. Fusion of uniluminal vascular spheroids: a model for assembly of blood vessels. Dev. Dyn. 2010;239(2):398–406.

190. Xu T, Zhao W, Zhu J-M, Albanna MZ, Yoo JJ, Atala A. Complex heterogeneous tissue constructs containing multiple cell types prepared by inkjet printing technology. Biomaterials. 2013;34(1):130–9.

191. Jakab K, Norotte C, Damon B, Marga F, Neagu A, Besch-Williford CL, et al. Tissue engineering by self-assembly of cells printed into topologically defined structures. Tissue Eng. Part A. 2008;14(3):413–21.

192. Barron JA, Wu P, Ladouceur HD, Ringeisen BR. Biological laser printing: a novel technique for creating heterogeneous 3-dimensional cell patterns. Biomed. Microdevices. 2004;6(2):139–47.

193. Barron JA, Spargo BJ, Ringeisen BR. Biological laser printing of three dimensional cellular structures. Appl. Phys. A. 2004;79(4-6):1027–30.

194. Ringeisen BR, Othon CM, Barron JA, Young D, Spargo BJ. Jet-based methods to print living cells. Biotechnol. J. 2006;1(9):930–48.

195. Guillemot F, Souquet a, Catros S, Guillotin B, Lopez J, Faucon M, et al. High-throughput laser printing of cells and biomaterials for tissue engineering. Acta Biomater. 2010;6(7):2494–500.

196. Ovsianikov A, Gruene M, Pflaum M, Koch L, Maiorana F, Wilhelmi M, et al. Laser printing of cells into 3D scaffolds. Biofabrication. 2010;2(1):014104.

197. Schiele NR, Chrisey DB, Corr DT. Gelatin-based laser direct-write technique for the precise spatial patterning of cells. Tissue Eng. Part C. Methods. 2011;17(3):289–98.

198. Gaebel R, Ma N, Liu J, Guan J, Koch L, Klopsch C, et al. Patterning human stem cells and endothelial cells with laser printing for cardiac regeneration. Biomaterials. 2011;32(35):9218–30.

199. Wu PK, Ringeisen BR. Development of human umbilical vein endothelial cell (HUVEC) and human umbilical vein smooth muscle cell (HUVSMC) branch/stem structures on hydrogel layers via biological laser printing (BioLP). Biofabrication. 2010;2(1):014111.

200. Nair K, Yan K, Sun W. A multilevel numerical model quantifying cell deformation in encapsulated alginate structures. J. Mech. Mater. Struct. 2007;2(6):1121–39.

201. Melchels FPW, Domingos MAN, Klein TJ, Malda J, Bartolo PJ, Hutmacher DW. Additive manufacturing of tissues and organs. Prog. Polym. Sci. 2012;37(8):1079–104.

202. Nair K, Gandhi M, Khalil S, Yan KC, Marcolongo M, Barbee K, et al. Characterization of cell viability during bioprinting processes. Biotechnol. J. 2009;4(8):1168–77.

203. Skardal A, Zhang J, Prestwich GD. Bioprinting vessel-like constructs using hyaluronan hydrogels crosslinked with tetrahedral polyethylene glycol tetracrylates. Biomaterials. 2010;31(24):6173–81.

204. Fedrovich NE, Wijnberg HM, Dhert WJA, Alblas J. Distinct Tissue Formation by Heterogeneous Printing of Osteo- and Endothelial Progenitor Cells. Tissue Eng Part A. 2011;17(15 and 16):2113–21.

205. Kucukgul C, Ozler B, Karakas HE, Gozuacik D, Koc B. 3D Hybrid Bioprinting of Macrovascular Structures. Procedia Eng. 2013;59:183–92.

206. Baudis S, Pulka T, Steyrer B, Wilhelm H, Weigel G, Stampfl J, et al. 3D printing of Urethane-based Photoelastomers for Vascular Tissue Regeneration. MRS Proc. 2010;1239:3–8.

207. Kobayashi A, Miyake H, Hattori H, Kuwana R, Hiruma Y, Nakahama K, et al. In vitro formation of capillary networks using optical lithographic techniques. Biochem. Biophys. Res. Commun. 2007;358(3):692–7.

208. Yu Y, Zhang Y, Martin J a, Ozbolat IT. Evaluation of cell viability and functionality in vessel-like bioprintable cell-laden tubular channels. J. Biomech. Eng. 2013;135(9):91011.

209. Centola M, Rainer a, Spadaccio C, De Porcellinis S, Genovese J a, Trombetta M. Combining electrospinning and fused deposition modeling for the fabrication of a hybrid vascular graft. Biofabrication. 2010;2(1):014102.

210. Ovsianikov a, Gruene M, Pflaum M, Koch L, Maiorana F, Wilhelmi M, et al. Laser printing of cells into 3D scaffolds. Biofabrication. 2010;2(1):014104.

211. Xu T, Rohozinski J, Zhao W, Moorefield EC, Atala A, Yoo JJ. Inkjet-mediated gene transfection into living cells combined with targeted delivery. Tissue Eng. Part A. 2009;15(1):95–101.

212. Wells DJ. Gene therapy progress and prospects: electroporation and other physical methods. Gene Ther. 2004;11(18):1363–9.

213. Sodian R, Fu P, Lueders C, Szymanski D, Fritsche C, Gutberlet M, et al. Tissue engineering of vascular conduits: fabrication of custom-made scaffolds using rapid prototyping techniques. Thorac. Cardiovasc. Surg. 2005;53(3):144–9.

214. Miller JS, Stevens KR, Yang MT, Baker BM, Nguyen D-HT, Cohen DM, et al. Rapid casting of patterned vascular networks for perfusable engineered three-dimensional tissues. Nat. Mater. 2012;11(9):768–74.

215. Mironov V, Kasyanov V, Markwald RR. Organ printing: from bioprinter to organ biofabrication line. Curr. Opin. Biotechnol. 2011;22(5):667–73.

216. Jakab K, Neagu A, Mironov V, Markwald RR, Forgacs G. Engineering biological structures of prescribed shape using self-assembling

multicellular systems. Proc. Natl. Acad. Sci. U. S. A. 2004;101(9):2864–9.

217. Mironov V, Kasyanov V, Drake C, Markwald RR. Organ printing: promises and challenges. Regen. Med. 2008;3(1):93–103.

218. Barron V, Lyons E, Stenson-Cox C, McHugh PE, Pandit A. Bioreactors for cardiovascular cell and tissue growth: a review. Ann. Biomed. Eng. 2003;31(9):1017–30.

219. Couet F, Meghezi S, Mantovani D. Fetal development, mechanobiology and optimal control processes can improve vascular tissue regeneration in bioreactors: An integrative review. Med. Eng. Phys. 2012;34(3):269–78.

220. Sodian R, Lemke T, Fritsche C, Hoerstrup SP, Fu P, Potapov E V, et al. Tissue-engineering bioreactors: a new combined cell-seeding and perfusion system for vascular tissue engineering. Tissue Eng. 2002;8(5):863–70.

221. Zhao L, Lee VK, Yoo S-S, Dai G, Intes X. The integration of 3-D cell printing and mesoscopic fluorescence molecular tomography of vascular constructs within thick hydrogel scaffolds. Biomaterials. 2012;33(21):5325–32.

222. Bartolo P, Domingos M, Gloria a., Ciurana J. BioCell Printing: Integrated automated assembly system for tissue engineering constructs. CIRP Ann. - Manuf. Technol. 2011;60(1):271–4.

223. Veith FJ, Moss CM, Sprayregen S, Montefusco C. Preoperative saphenous venography in arterial reconstructive surgery of the lower extremity. Surger. 1979;85(3):253–6.

224. Darling RC, Linton RF. Durability of femoropopliteal reconstructions. Surgery. 1972;123(4):472–9.

225. Chlupác J, Filová E, Bacáková L. Blood vessel replacement: 50 years of development and tissue engineering paradigms in vascular surgery. Physiol. Res. 2009;58(Suppl 2):S119–39.

226. Tai NR, Salacinski HJ, Edwards A, Hamilton G, Seifalian AM. Compliance

properties of conduits used in vascular reconstruction. Br. J. Surg. 2000;87(11):1516–24.

227. Reichert V, Addili F, Schmitz-Rixen T. Changes in biomechanical properties of biological and synthetic prostheses. Khirurgiia (Sofiia). 1997;(4):29–35.

228. Dzau VJ, Gibbons GH. Vascular remodeling: mechanisms and implications. J. Cardiovasc. Pharmacol. 1993;21(Suppl 1):S1–5.

229. Humphrey JD. Vascular adaptation and mechanical homeostasis at tissue, cellular, and sub-cellular levels. Cell Biochem. Biophys. 2008;50(2):53–78.

230. Yokota T, Ichikawa H, Matsumiya G, Kuratani T, Sakaguchi T, Iwai S, et al. In situ tissue regeneration using a novel tissue-engineered, small-caliber vascular graft without cell seeding. J. Thorac. Cardiovasc. Surg. 2008;136(4):900–7.

231. Haruguchi H, Teraoka S. Intimal hyperplasia and hemodynamic factors in arterial bypass and arteriovenous grafts: a review. J. Artif. Organs. 2003;6(4):227–35.

232. Roh JD, Nelson GN, Brennan MP, Mirensky TL, Yi T, Hazlett TF, et al. Small-diameter biodegradable scaffolds for functional vascular tissue engineering in the mouse model. Biomaterials. 2008;29(10):1454–63.

233. Hibino N, McGillicuddy E, Matsumura G, Ichihara Y, Naito Y, Breuer C, et al. Late-term results of tissue-engineered vascular grafts in humans. J. Thorac. Cardiovasc. Surg. 2010;139(2):431–6.

234. Shin'oka T, Matsumura G, Hibino N, Naito Y, Watanabe M, Konuma T, et al. Midterm clinical result of tissue-engineered vascular autografts seeded with autologous bone marrow cells. J. Thorac. Cardiovasc. Surg. 2005;129(6):1330–8.

235. Lamm P, Juchem G, Milz S, Schuffenhauer M, Reichart B. Autologous Endothelialized Vein Allograft: A Solution in the Search for Small-Caliber Grafts in Coronary Artery Bypass Graft Operations. Circulation.

2001;104(Supplement 1):I – 108 – I – 114.

236. Han DW, Park YH, Kim JK, Jung TG, Lee KY, Hyon SH, et al. Long-term preservation of human saphenous vein by green tea polyphenol under physiological conditions. Tissue Eng. 2005;11(7-8):1054–64.

237. L'Heureux N, Dusserre N, Konig G, Victor B, Keire P, Wight TN, et al. Human tissue-engineered blood vessels for adult arterial revascularization. Nat. Med. 2006;12(3):361–5.

238. Sell SA, McClure MJ, Barnes CP, Knapp DC, Walpoth BH, Simpson DG, et al. Electrospun polydioxanone-elastin blends: potential for bioresorbable vascular grafts. Biomed. Mater. 2006;1(2):72–80.

239. L'Heureux N, Pâquet S, Labbé R, Germain L, Auger FA. A completely biological tissue-engineered human blood vessel. FASEB J. 1998;12(1):47–56.

240. Roh JD, Sawh-Martinez R, Brennan MP, Jay SM, Devine L, Rao D a, et al. Tissue-engineered vascular grafts transform into mature blood vessels via an inflammation-mediated process of vascular remodeling. Proc. Natl. Acad. Sci. U. S. A. 2010;107(10):4669–74.

241. Ma N, Wang Z, Chen H, Sun Y, Hong H, Sun Q, et al. Development of the novel biotube inserting technique for acceleration of thick-walled autologous tissue-engineered vascular grafts fabrication. J. Mater. Sci. Mater. Med. 2011;22(4):1037–43.

242. Zhang L, Zhou J, Lu Q, Wei Y, Hu S. A novel small-diameter vascular graft : in vivo behavior of biodegradable three-layered tubular scaffolds. Biotechnol. Bioeng. 2008;99(4):1007–15.

243. Van Der Giessen WJ, Lincoff AM, Schwartz RS, Van Beusekom HM, Serruys PW, Holmes DR, et al. Marked inflammatory sequelae to implantation of biodegradable and nonbiodegradable polymers in porcine coronary arteries. Circulation. 1996;94(7):1690–7.

244. Athanasiou KA, Niederauer GG, Agrawal CM. Sterilization, toxicity, biocompatibility and clinical applications of polylactic acid/polyglycolic

acid copolymers. Biomaterials. 1996;17(2):93–102.

245. Hinokiyama K, Valen G, Tokuno S, Vedin JB, Vaage J. Vein graft harvesting induces inflammation and impairs vessel reactivity. Ann. Thorac. Surg. 2006;82(4):1458–64.

246. Inoue T, Croce K, Morooka T, Sakuma M, Node K, Simon DI. Vascular inflammation and repair: implications for re-endothelialization, restenosis, and stent thrombosis. JACC Cardiovasc. Interv. 2011;4(10):1057–66.

247. Hibino N, Yi T, Duncan DR, Rathore A, Dean E, Naito Y, et al. A critical role for macrophages in neovessel formation and the development of stenosis in tissue-engineered vascular grafts. FASEB J. . 2011;25(12):4253–63.

248. Zhu S, Malhotra A, Zhang L, Deng S, Zhang T, Freedman NJ, et al. Human umbilical cord blood endothelial progenitor cells decrease vein graft neointimal hyperplasia in SCID mice. Atherosclerosis. 2010;212(1):63–9.

249. Nelson GN, Mirensky T, Brennan MP, Roh JD, Yi T, Wang Y, et al. Functional small-diameter human tissue-engineered arterial grafts in an immunodeficient mouse model: preliminary findings. Arch. Surg. 2008;143(5):488–94.

250. Goyal A, Wang Y, Su H, Dobrucki LW, Brennan M, Fong P, et al. Development of a model system for preliminary evaluation of tissue-engineered vascular conduits. J. Pediatr. Surg. 2006;41(4):787–91.

251. Mirensky TL, Nelson GN, Brennan MP, Roh JD, Hibino N, Yi T, et al. Tissue-engineered arterial grafts: long-term results after implantation in a small animal model. J. Pediatr. Surg. 2009;44(6):1127–32; discussion 1132–3.

252. Zheng L, Gibson TF, Schechner JS, Pober JS, Bothwell ALM. Bcl-2 transduction protects human endothelial cell synthetic microvessel grafts from allogeneic T cells in vivo. J. Immunol. 2004;173(5):3020–6.

253. Hibino N, Yi T, Duncan DR, Rathore A, Dean E, Naito Y, et al. A critical role for macrophages in neovessel formation and the development of stenosis in tissue-engineered vascular grafts. FASEB J. 2011;25(12):4253–63.

254. Wang X, Lin P, Yao Q, Chen C. Development of small-diameter vascular grafts. World J. Surg. 2007;31(4):682–9.

255. Hibino N, McGillicuddy E, Matsumura G, Ichihara Y, Naito Y, Breuer C, et al. Late-term results of tissue-engineered vascular grafts in humans. J. Thorac. Cardiovasc. Surg. 2010;139(2):431–6, 436.e1–2.

256. Kannan RY, Salacinski HJ, Butler PE, Hamilton G, Seifalian AM. Current status of prosthetic bypass grafts: a review. J. Biomed. Mater. Res. B. Appl. Biomater. 2005;74(1):570–81.

257. Melchiorri AJ, Hibino N, Fisher JP. Strategies and Techniques to Enhance the In Situ Endothelialization of Small-Diameter Biodegradable Polymeric Vascular Grafts. Tissue Eng. Part B. 2013;19(4):292–307.

258. Jensen N, Lindblad B, Ljungberg J, Leide S, Bergqvist D. Early attachment of platelets, leukocytes, and fibrinogen in endothelial cell seeded Dacron grafts. Ann. Vasc. Surg. 1996;10(6):530–6.

259. Rupnick MA, Hubbard FA, Pratt K, Jarrell BE, Williams SK. Endothelialization of vascular prosthetic surfaces after seeding or sodding with human microvascular endothelial cells. J. Vasc. Surg. Off. Publ. Soc. Vasc. Surg. [and] Int. Soc. Cardiovasc. Surgery, North Am. Chapter. 1989;9(6):788–95.

260. Deutsch M, Meinhart J, Zilla P, Howanietz N, Gorlitzer M, Froeschl A, et al. Long-term experience in autologous in vitro endothelialization of infrainguinal ePTFE grafts. J. Vasc. Surg. Off. Publ. Soc. Vasc. Surg. [and] Int. Soc. Cardiovasc. Surgery, North Am. Chapter. 2009;49(2):352–62; discussion 362.

261. Bordenave L, Fernandez P, Rémy-Zolghadri M, Villars S, Daculsi R, Midy D. In vitro endothelialized ePTFE prostheses: clinical update 20 years after the first realization. Clin. Hemorheol. Microcirc. 2005;33(3):227–34.

262. Avci-Adali M, Perle N, Ziemer G, Wendel HP. Current concepts and new developments for autologous in vivo endothelialisation of biomaterials for intravascular applications. Eur. Cell. Mater. 2011;21:157–76.

263. Larsen K, Cheng C, Tempel D, Parker S, Yazdani S, den Dekker WK, et al. Capture of circulatory endothelial progenitor cells and accelerated re-endothelialization of a bio-engineered stent in human ex vivo shunt and rabbit denudation model. Eur. Heart J. 2012;33(1):120–8.

264. Aoki J, Serruys PW, Van Beusekom H, Ong ATL, McFadden EP, Sianos G, et al. Endothelial progenitor cell capture by stents coated with antibody against CD34: the HEALING-FIM (Healthy Endothelial Accelerated Lining Inhibits Neointimal Growth-First In Man) Registry. J. Am. Coll. Cardiol. 2005;45(10):1574–9.

265. Chavakis E, Dimmeler S. Homing of progenitor cells to ischemic tissues. Antioxid. Redox Signal. 2011;15(4):967–80.

266. Wang QR, Wang BH, Zhu WB, Huang YH, Li Y, Yan Q. An in vitro study of differentiation of hematopoietic cells to endothelial cells. Bone Marrow Res. 2011;2011:846096.

267. Shen YH, Shoichet MS, Radisic M. Vascular endothelial growth factor immobilized in collagen scaffold promotes penetration and proliferation of endothelial cells. Acta Biomater. 2008;4(3):477–89.

268. Neufeld G, Cohen T, Gengrinovitch S, Poltorak Z. Vascular endothelial growth factor (VEGF) and its receptors. FASEB J. 1999;13(1):9–22.

269. Morales-Ruiz M, Fulton D, Sowa G, Languino LR, Fujio Y, Walsh K, et al. Vascular endothelial growth factor-stimulated actin reorganization and migration of endothelial cells is regulated via the serine/threonine kinase Akt. Circ. Res. 2000;86(8):892–6.

270. Nillesen STM, Geutjes PJ, Wismans R, Schalkwijk J, Daamen WF, Van Kuppevelt TH. Increased angiogenesis and blood vessel maturation in acellular collagen-heparin scaffolds containing both FGF2 and VEGF. Biomaterials. 2007;28(6):1123–31.

271. Singh S, Wu BM, Dunn JC. The enhancement of VEGF-mediated angiogenesis by polycaprolactone scaffolds with surface cross-linked heparin. Biomaterials. 2011;32(8):2059–69.

272. Yao C, Markowicz M, Pallua N, Noah EM, Steffens G. The effect of cross-linking of collagen matrices on their angiogenic capability. Biomaterials. 2008;29(1):66–74.

273. Brandner B, Kurkela R, Vihko P, Kungl AJ. Investigating the effect of VEGF glycosylation on glycosaminoglycan binding and protein unfolding. Biochem. Biophys. Res. Commun. 2006;340(3):836–9.

274. Andresen DM, Barker JH, Hjortdal VE. Local heparin is superior to systemic heparin in preventing arterial thrombosis. Microsurgery. 2002;22(6):265–72.

275. Melchiorri AJ, Hibino N, Brandes ZR, Jonas R a, Fisher JP. Development and assessment of a biodegradable solvent cast polyester fabric small-diameter vascular graft. J. Biomed. Mater. Res. A. 2013;102(6):1972–81.

276. Carpenter J, Khang D, Webster TJ. Nanometer polymer surface features: the influence on surface energy, protein adsorption and endothelial cell adhesion. Nanotechnology. 2008;19(50):505103.

277. Krilleke D, Ng Y-SE, Shima DT. The heparin-binding domain confers diverse functions of VEGF-A in development and disease: a structure-function study. Biochem. Soc. Trans. 2009;37(Pt 6):1201–6.

278. Liu SLS, Chen JCJ, Chen CCC, Huang NHN. The nanofabrication of CD34 antibody-VEGF-heparin on titanium surface via layer-by-layer assembly for biofunctionalization. Nanoelectron. Conf. (INEC), 2010 3rd Int. 2010.

279. Zhou M, Liu Z, Wei Z, Liu C, Qiao T, Ran F, et al. Development and validation of small-diameter vascular tissue from a decellularized scaffold coated with heparin and vascular endothelial growth factor. Artif. Organs. 2009;33(3):230–9.

280. Liu S, Liu T, Chen J, Maitz M, Chen C, Huang N. Influence of a layer-by-

layer-assembled multilayer of anti-CD34 antibody, vascular endothelial growth factor, and heparin on the endothelialization and anticoagulation of titanium surface. J. Biomed. Mater. Res. A. 2013;101(4):1144–57.

281. Kong D, Melo LG, Mangi AA, Zhang L, Lopez-Ilasaca M, Perrella MA, et al. Enhanced Inhibition of Neointimal Hyperplasia by Genetically Engineered Endothelial Progenitor Cells. Circulation. 2004;109(14):1769–75.

282. Lin G, Finger E, Gutierrez-Ramos JC. Expression of CD34 in endothelial cells, hematopoietic progenitors and nervous cells in fetal and adult mouse tissues. Eur. J. Immunol. 1995;25(6):1508–16.

283. Hatch A, Hansmann G, Murthy SK. Engineered alginate hydrogels for effective microfluidic capture and release of endothelial progenitor cells from whole blood. Langmuir. 2011;27(7):4257–64.

284. Hansmann G, Plouffe BD, Hatch A, von Gise A, Sallmon H, Zamanian RT, et al. Design and validation of an endothelial progenitor cell capture chip and its application in patients with pulmonary arterial hypertension. J. Mol. Med. (Berl). 2011;89(10):971–83.

285. Tondreau MY, Laterreur V, Gauvin R, Vallières K, Bourget J-M, Lacroix D, et al. Mechanical properties of endothelialized fibroblast-derived vascular scaffolds stimulated in a bioreactor. Acta Biomater. 2015;18:176–85.

286. Ahn H, Ju YM, Takahashi H, Williams DF, Yoo JJ, Lee SJ, et al. Engineered small diameter vascular grafts by combining cell sheet engineering and electrospinning technology. Acta Biomater. 2015;16:14–22.

287. Mun CH, Jung Y, Kim SH, Kim HC, Kim SH. Effects of Pulsatile Bioreactor Culture on Vascular Smooth Muscle Cells Seeded on Electrospun Poly (lactide-co-ε-caprolactone) Scaffold. Artif. Organs. 2013;37(12):E168–78.

288. Bérard X, Rémy-Zolghadri M, Bourget C, Turner N, Bareille R, Daculsi R, et al. Capability of human umbilical cord blood progenitor-derived endothelial cells to form an efficient lining on a polyester vascular graft in vitro. Acta Biomater. 2009;5(4):1147–57.

289. Punshon G, Sales KM, Vara DS, Hamilton G, Seifalian a. M. Assessment of the potential of progenitor stem cells extracted from human peripheral blood for seeding a novel vascular graft material. Cell Prolif. 2008;41(2):321–35.

290. Hofmann NA, Reinisch A, Strunk D. Isolation and large scale expansion of adult human endothelial colony forming progenitor cells. J. Vis. Exp. 2009;(32):1524.

291. Glynn JJ, Hinds MT. Endothelial Outgrowth Cells: Function and Performance in Vascular Grafts. Tissue Eng Part B Rev. 2014;20(4):294–303.

292. Egorova AD, DeRuiter MC, De Boer HC, Van De Pas S, Gittenberger-De Groot AC, Van Zonneveld AJ, et al. Endothelial colony-forming cells show a mature transcriptional response to shear stress. Vitr. Cell. Dev. Biol. - Anim. 2012;48(1):21–9.

293. Ankeny RF, Ankeny CJ, Nerem RM, Jo H. Maturing EPCs into endothelial cells: may the force be with the EPCs. Focus on "Fluid shear stress induces differentiation of circulating phenotype endothelial progenitor cells." AJP Cell Physiol. 2012;303(6):C589–91.

294. Yeatts AB, Both SK, Yang W, Alghamdi HS, Yang F, Fisher JP, et al. In Vivo Bone Regeneration Using Tubular Perfusion System Bioreactor Cultured Nanofibrous Scaffolds. Tissue Eng. Part A. 2013;20(1-2):139–46.

295. Rotenberg MY, Ruvinov E, Armoza A, Cohen S. A multi-shear perfusion bioreactor for investigating shear stress effects in endothelial cell constructs. Lab Chip. 2012;12(15):2696–703.

296. Huang AH, Niklason LE. Engineering biological-based vascular grafts using a pulsatile bioreactor. J. Vis. Exp. 2011;(52):2646.

297. Liu Y, Teoh S, Chong M, Yeow C, Kamm R, Choolani M, et al. Contrasting Effects of Vasculogenic Induction Upon Biaxial Bioreactor Stimulation of Mesenchymal Stem Cells and Endothelial Progenitor Cells Cocultures in Three-Dimensional Scaffolds Under In Vitro and In Vivo Paradigms for Vascularized Bone Tissue Engine. Tissue Eng Part A. 2013;19(7-8):893–904.

298. Melchiorri AJ, Hibino N, Yi T, Lee YU, Sugiura T, Tara S, et al. Contrasting Biofunctionalization Strategies for the Enhanced Endothelialization of Biodegradable Vascular Grafts. Biomacromolecules. 2015;16(2):437–46.

299. Pisanti P, Yeatts AB, Cardea S, Fisher JP, Reverchon E. Tubular perfusion system culture of human mesenchymal stem cells on poly-L-lactic acid scaffolds produced using a supercritical carbon dioxide-assisted process. J. Biomed. Mater. Res. A. 2012;100(10):2563–72.

300. Yeatts AB, Geibel EM, Fears FF, Fisher JP. Human mesenchymal stem cell position within scaffolds influences cell fate during dynamic culture. Biotechnol. Bioeng. 2012;109(9):2381–91.

301. Yeatts AB, Fisher JP. Tubular perfusion system for the long-term dynamic culture of human mesenchymal stem cells. Tissue Eng. Part C. Methods. 2011;17(3):337–48.

302. Wang X, Cooper S. Adhesion of endothelial cells and endothelial progenitor cells on peptide-linked polymers in shear flow. Tissue Eng. Part A. 2013;19(9-10):1113–21.

303. Förstermann U, Münzel T. Endothelial nitric oxide synthase in vascular disease: From marvel to menace. Circulation. 2006;113(13):1708–14.

304. Cai J, Jiang WG, Ahmed A, Boulton M. Vascular endothelial growth factor-induced endothelial cell proliferation is regulated by interaction between VEGFR-2, SH-PTP1 and eNOS. Microvasc. Res. 2006;71(1):20–31.

305. Hutchings H, Ortega N, Plouët J. Extracellular matrix-bound vascular endothelial growth factor promotes endothelial cell adhesion, migration, and survival through integrin ligation. FASEB J. Off. Publ. Fed. Am. Soc. Exp. Biol. 2003;17(11):1520–2.

306. Zhou M, Liu Z, Liu C, Jiang X, Wei Z, Qiao W, et al. Tissue engineering of small-diameter vascular grafts by endothelial progenitor cells seeding heparin-coated decellularized scaffolds. J. Biomed. Mater. Res. - Part B

Appl. Biomater. 2012;100 B(1):111–20.

307. Chen X, Wang J, An Q, Li D, Liu P, Zhu W, et al. Electrospun poly(l-lactic acid-co-ε -caprolactone) fibers loaded with heparin and vascular endothelial growth factor to improve blood compatibility and endothelial progenitor cell proliferation. Colloids Surfaces B Biointerfaces. 2015;128:106–14.

308. Basile DP, Yoder MC. Circulating and tissue resident endothelial progenitor cells. J. Cell. Physiol. 2014;229(1):10–6.

309. Ingram DA, Mead LE, Tanaka H, Meade V, Fenoglio A, Mortell K, et al. Identification of a novel hierarchy of endothelial progenitor cells using human peripheral and umbilical cord blood. Blood. 2004;104(9):2752–60.

310. Go AS, Mozaffarian D, Roger VL, Benjamin EJ, Berry JD, Borden WB, et al. Heart disease and stroke statistics-2013 update: A Report from the American Heart Association. Circulation. 2013;127(1):e6–245.

311. Lee SJ, Heo DN, Park JS, Kwon SK, Lee JH, Lee JH, et al. Characterization and preparation of bio-tubular scaffolds for fabricating artificial vascular grafts by combining electrospinning and a 3D printing system. Phys. Chem. Chem. Phys. 2014;17(5):2996–9.

312. Wang MO, Vorwald CE, Dreher ML, Mott EJ, Cheng M-H, Cinar A, et al. Evaluating 3D-Printed Biomaterials as Scaffolds for Vascularized Bone Tissue Engineering. Adv. Mater. 2015;27(1):138–44.

313. Wang MO, Etheridge JM, Thompson J a, Vorwald CE, Dean D, Fisher JP. Evaluation of the in vitro cytotoxicity of cross-linked biomaterials. Biomacromolecules. 2013;14(5):1321–9.

314. Wallace J, Wang MO, Thompson P, Busso M, Belle V, Mammoser N, et al. Validating continuous digital light processing (cDLP) additive manufacturing accuracy and tissue engineering utility of a dye-initiator package. Biofabrication. 2013;6(1):015003.

315. Liska R, Schuster M, Inführ R, Turecek C, Fritscher C, Seidl B, et al. Photopolymers for rapid prototyping. J. Coatings Technol. Res.

2007;4(4):505–10.

316. Lee JW, Lan PX, Kim B, Lim G, Cho D-W. 3D scaffold fabrication with PPF/DEF using micro-stereolithography. Microelectron. Eng. 2007;84(5-8):1702–5.

317. Cooke MN, Fisher JP, Dean D, Rimnac C, Mikos AG. Use of stereolithography to manufacture critical-sized 3D biodegradable scaffolds for bone ingrowth. J. Biomed. Mater. Res. Part B Appl. Biomater. 2003;64(2):65–9.

318. Seck TM, Melchels FPW, Feijen J, Grijpma DW. Designed biodegradable hydrogel structures prepared by stereolithography using poly(ethylene glycol)/poly(D,L-lactide)-based resins. J. Control. Release. 2010;148(1):34–41.

319. Lee SJ, Kang HW, Park JK, Rhie JW, Hahn SK, Cho DW. Application of microstereolithography in the development of three-dimensional cartilage regeneration scaffolds. Biomed. Microdevices. 2008;10(2):233–41.

320. Wang MO, Piard C, Melchiorri AJ, Dreher M, Fisher J. Evaluating Changes in Structure and Cytotoxicity During In Vitro Degradation of 3D Printed Scaffolds. Tissue Eng. 2015;21(9-10):1642–53.

321. Kasper FK, Tanahashi K, Fisher JP, Mikos AG. Synthesis of poly(propylene fumarate). Nat. Protoc. 2009;4(4):518–25.

322. Billiet T, Vandenhaute M, Schelfhout J, Van Vlierberghe S, Dubruel P. A review of trends and limitations in hydrogel-rapid prototyping for tissue engineering. Biomaterials. 2012;33(26):6020–41.

323. Konig G, McAllister TN, Dusserre N, Garrido SA, Iyican C, Marini A, et al. Mechanical properties of completely autologous human tissue engineered blood vessels compared to human saphenous vein and mammary artery. Biomaterials. 2009;30(8):1542–50.

324. Sell S a, McClure MJ, Barnes CP, Knapp DC, Walpoth BH, Simpson DG, et al. Electrospun polydioxanone-elastin blends: potential for bioresorbable vascular grafts. Biomed. Mater. 2006;1(2):72–80.

325. Ballyk PD, Walsh C, Butany J, Ojha M. Compliance mismatch may promote graft-artery intimal hyperplasia by altering suture-line stresses. J. Biomech. 1998;31(3):229–37.

326. Timmer MD, Ambrose CG, Mikos AG. In vitro degradation of polymeric networks of poly(propylene fumarate) and the crosslinking macromer poly(propylene fumarate)-diacrylate. Biomaterials. 2003;24(4):571–7.

327. Abedin M, Tintut Y, Demer LL. Vascular calcification: Mechanisms and clinical ramifications. Arterioscler. Thromb. Vasc. Biol. 2004;24(7):1161–70.

328. Moe SM, Chen NX. Inflammation and vascular calcification. Blood Purif. 2005;23(1):64–71.

329. New SEP, Aikawa E. Cardiovascular calcification: an inflammatory disease. Circ. J. 2011;75(6):1305–13.

330. Suggs LJ, Shive MS, Garcia CA, Anderson JM, Mikos AG. In vitro cytotoxicity and in vivo biocompatibility of poly(propylene fumarate-co-ethylene glycol) hydrogels. J. Biomed. Mater. Res. 1999;46(1):22–32.

331. Jayabalan M. Studies on Poly (propylene fumarate-co-caprolactone diol) Thermoset Composites towards the Development of Biodegradable Bone Fixation Devices. Int J Biomater. 2009;2009:486710.

332. Wang S, Lu L, Gruetzmacher JA, Currier BL, Yaszemski MJ. A biodegradable and cross-linkable multiblock copolymer consisting of poly(propylene fumarate) and poly(ε-caprolactone): Synthesis, characterization, and physical properties. Macromolecules. 2005;38(17):7358–70.

333. Lee JW, Ahn G, Kim DS, Cho DW. Development of nano- and microscale composite 3D scaffolds using PPF/DEF-HA and micro-stereolithography. Microelectron. Eng. 2009;86(4-6):1465–7.

334. Wang S, Lu L, Gruetzmacher JA, Currier BL, Ã MJY. Synthesis and characterizations of biodegradable and crosslinkable poly (e-caprolactone

fumarate), poly (ethylene glycol fumarate), and their amphiphilic copolymer. Biomaterials. 2006;27:832–41.

335. Wang MO, Etheridge JM, Thompson JA, Vorwald CE, Dean D, Fisher JP. Evaluation of the in vitro cytotoxicity of cross-linked biomaterials. Biomacromolecules. 2013;14(5):1321–9.

336. Ng KW, Hutmacher DW, Schantz JT, Ng CS, Too HP, Lim TC, et al. Evaluation of ultra-thin poly(epsilon-caprolactone) films for tissue-engineered skin. Tissue Eng. 2001;7(4):441–55.

337. Wang S, Kempen DH, Simha NK, Lewis JL, Windebank AJ, Yaszemski MJ, et al. Photo-Cross-Linked Hybrid Polymer Networks Consisting of Poly (propylene fumarate) and Poly (caprolactone fumarate): Controlled Physical Properties and Regulated Bone and Nerve Cell Responses. Biomacromolecules. 2008;9(4):1229–41.

338. Odian G. Principles of Polymerization. 4th ed. Hoboken, NJ; 2004.

339. Melchiorri A. Strategies and Techniques to Enhance the In Situ Endothelialization of Small-Diameter Biodegradable Polymeric Vascular Grafts. Tissue Eng. Part B. 2013;19(4):292–307.

340. Kulangara K, Leong KW. Substrate topography shapes cell function. Soft Matter. 2009;5(21):4072.

341. Discher DE, Janmey P, Wang Y-L. Tissue cells feel and respond to the stiffness of their substrate. Science. 2005;310(5751):1139–43.

342. Yao X, Peng R, Ding J. Cell-material interactions revealed via material techniques of surface patterning. Adv. Mater. 2013;25(37):5257–86.

343. Llopis-Hernández V, Rico P, Ballester-Beltrán J, Moratal D, Salmerón-Sánchez M. Role of surface chemistry in protein remodeling at the cell-material interface. PLoS One. 2011;6(5).

344. Waite JH, Tanzer ML. Polyphenolic Substance of Mytilus edulis: Novel Adhesive Containing L-Dopa and Hydroxyproline. Science. 1981;212(4498):1038–40.

345. Yang Z, Wang J, Luo R, Maitz MF, Jing F, Sun H, et al. The covalent immobilization of heparin to pulsed-plasma polymeric allylamine films on 316L stainless steel and the resulting effects on hemocompatibility. Biomaterials. 2010;31(8):2072–83.

346. Lhoest JB, Wagner MS, Tidwell CD, Castner DG. Characterization of adsorbed protein films by time of flight secondary ion mass spectrometry. J. Biomed. Mater. Res. 2001;57(3):432–40.

347. Conn G, Bayne ML, Soderman DD, Kwok PW, Sullivan KA, Palisi TM, et al. Amino acid and cDNA sequences of a vascular endothelial cell mitogen that is homologous to platelet-derived growth factor. Proc. Natl. Acad. Sci. U. S. A. 1990;87(7):2628–32.